

This item was submitted to Loughborough's Institutional Repository (<https://dspace.lboro.ac.uk/>) by the author and is made available under the following Creative Commons Licence conditions.



CC creative commons
COMMONS DEED

Attribution-NonCommercial-NoDerivs 2.5

You are free:

- to copy, distribute, display, and perform the work

Under the following conditions:

 **Attribution.** You must attribute the work in the manner specified by the author or licensor.

 **Noncommercial.** You may not use this work for commercial purposes.

 **No Derivative Works.** You may not alter, transform, or build upon this work.

- For any reuse or distribution, you must make clear to others the license terms of this work.
- Any of these conditions can be waived if you get permission from the copyright holder.

Your fair use and other rights are in no way affected by the above.

This is a human-readable summary of the [Legal Code \(the full license\)](#).

[Disclaimer](#) 

For the full text of this licence, please go to:
<http://creativecommons.org/licenses/by-nc-nd/2.5/>

**A Doctoral Thesis submitted in partial fulfilment of the
requirements for the award of the degree of Doctor of
Philosophy in Chemical Engineering**

**Process analytical technology
based investigation of the
crystallization of pharmaceutical
polymorphs, salts and hydrates**

**by
Krystel Howard**

**Pharmaceutical Systems Engineering Group
Department of Chemical Engineering
Loughborough University
July 2011**

© by Krystel Howard (2011)

Abstract

Pharmaceutical industries aim for continuous improvement in the manufacturing process of producing medicines. Demands on the pharmaceutical industries are to produce quality products in a quick and cost effective way. Designing a robust crystallization process so as to produce quality crystals with the desired polymorphic form, morphology, size and size distribution, will contribute towards meeting these demands. The Food and Drug Administration regulating body encourages the development of quality by design (QbD) approaches, involving the use of process analytical technology (PAT) for the design of the crystallization process. This method enables the design of the crystallization process to be more flexible in terms of variation in operating conditions and process parameters so long as the quality of the product is maintained. The aim of this thesis work is to use QbD approaches involving the use of PAT tools and solid state analytical (SSA) techniques to increase process knowledge and understanding, which is required for the robust design of crystallization processes.

Discovery of all possible polymorphic forms of an active pharmaceutical ingredient (API) is important for the design of a robust crystallization process in which product quality is consistent during scale up and to prevent late stage failures. This thesis work shows the importance of using PAT tools and SSA techniques for monitoring polymorphic transformations and for the discovery of new polymorphic forms that have not yet been reported in the literature. A range of PAT tools including the FBRM, turbidity probe and ATR-UV/Vis spectrometer detected polymorphic transformations during both cooling and antisolvent crystallization experiments using the model system sodium benzoate in water and a propan-2-ol (IPA)/water mixture. Information obtained from a range of SSA techniques provided supporting evidence for the discovery of a new channel hydrate, channel solvate and an anhydrous form of sodium benzoate.

The problem of crusting (solid depositing on vessel walls) occurring within crystallization vessels has been investigated with the use of a combination of PAT tools and SSA techniques. The FBRM and turbidity probe detected a change occurring during the cooling crystallization process of *para*-amino benzoic acid (ABA) in ethyl acetate. Repeats of the experiments using the ATR-UV/Vis confirmed that the change

was due to crusting forming on vessel walls and not a polymorphic transformation. PAT tools also detected changes occurring during a pH controlled polymorphic cooling crystallization experiment (Chapter 9), which was subsequently confirmed by SSA methods to be due to the formation of a mixture of products and not a polymorphic transformation. This research work shows the importance of using a combination of PAT tools and SSA techniques for gaining a deeper understanding of the crystallization process and to prevent misinterpretation of results, saving both time and money. Also this research work highlights the need for improvement within industrial scale vessel design, such as vessels with variable jacket height, to prevent the problems of crusting. Robust MSZW measurements are obtained at laboratory scale using the model crystallization systems *para* and *meta*-ABA in water. PAT tools used include the FBRM and turbidity probe. The robust MSZW takes into consideration variation in process parameters including ramp rate, vessel size (1 mL and 1 L), agitator speed and type. This robust MSZW can be used for the design of scale up experiments (pilot plant and industrial scale), increasing the likelihood of producing a quality product. Nucleation orders used within crystallization models were determined from the MSZW measurements. Results showed that the nucleation order varied within different crystallization set-ups (vessel size and mixing conditions) using the model system *meta*-ABA in water. Therefore model-based design and scale-up of crystallization processes must be used carefully and more detailed mechanistic models, which take into consideration the effect of mixing need to be designed to improve the generality and applicability of crystallization models.

pH controlled polymorphic crystallization experiments were performed using the model systems *meta* and *para*-ABA in ethanol and water. A combination of 5 PAT tools were used in a single vessel to monitor the cooling crystallization process. PAT tools used include FBRM, ATR-UV/Vis, PVM, pH and a temperature probe. Various parameters including mixing conditions, solvent, pH of solution, strength and type of acid were varied to investigate the best conditions to produce salts. Results showed that careful selection of design parameters and salt selection is important for producing quality crystals of the desired morphology so as to prevent problems in downstream processing.

Table of Contents

List of Figures	viii
List of Tables	xix
List of symbols	xxi
List of Greek letters	xxiii
Abbreviations	xxiv
Acknowledgements	xxv
Chapter 1. Introduction	1
1.1 Background.....	1
1.2. Aims of current study	4
1.3. Contributions of the thesis	5
1.4. Structure of the thesis	6
Chapter 2. Literature review	9
2.1 Definition and detection of a crystal.....	9
2.2 Crystal systems and lattices	9
2.3 Phase equilibria and crystallization methods.....	12
2.3.1 Introduction.....	12
2.3.2 Phase rule.....	13
2.3.3 Phase diagrams	13
2.3.4 Crystallization methods	18
2.4 Nucleation.....	20
2.4.1 Introduction.....	20
2.4.2 Primary nucleation.....	21
2.4.3 Secondary nucleation.....	25
2.5 Polymorphism.....	27
2.5.1 Introduction.....	27
2.5.2 Classification of polymorphs	29
2.5.3 Thermodynamics of polymorphism.....	31
2.5.4 Polymorphic transformation and kinetics	35
2.5.6 Conclusion on polymorphism.....	39
2.6 Analytical methods for crystallization.....	39

2.6.1 Introduction.....	39
2.6.2 FBRM and its use with other PAT tools.....	41
2.6.3 Particle vision measurement (PVM) probe.....	44
2.6.4 ATR-UV/Vis spectroscopy.....	44
2.6.5 Introduction to solid state analysis (SSA).....	47
2.6.6 Microscopy	47
2.6.7 Differential scanning calorimetry (DSC).....	48
2.6.8 Thermal gravimetric analysis (TGA).....	51
2.6.9 Dynamic vapour sorption (DVS).....	52
2.6.10 X-ray powder diffraction (XRPD).....	52
2.6.11 Solid state spectroscopy techniques.....	55
2.6.12 Conclusions.....	56
2.4 Conclusions on literature survey.....	57
Chapter 3. Materials, experimental set-up and methodology	58
3.1 Introduction.....	58
3.2 Materials	58
3.3 Avantium Crystal 16 experiments and solubility measurements.....	59
MSZW measurements involved suspending PABA in water using 1 mL vials. The range of concentrations used is 10 to 35 mg/mL. A ramp rate of 0.5, 0.3 and 0.1 °C/min is used for each concentration value to obtain the clear (solubility) points and cloud (nucleation) points. The process is repeated using the isomer MABA using the concentration range of 12 to 28 mg/mL. Results are discussed within Chapter 7.....	60
3.4 Cooling crystallization experiments at scales of 250 mL, 750 mL and 1 L	60
3.4.1 Cooling crystallization of sodium benzoate in water.....	61
3.4.2 Cooling crystallization of PABA in ethyl acetate.....	62
3.4.3 Cooling crystallization of PABA/MABA in water for MSZW determination	63
3.4.4 pH controlled cooling crystallization experiments of PABA/MABA in ethanol.....	63
3.5 Antisolvent crystallization experiments.....	64
3.6 Salt precipitation and evaporation experiments	66
3.7 Summary of experiments performed within each Chapter	67
3.8 Solid state analysis of crystals	69
3.9 Conclusions.....	70

Chapter 4. PAT based investigation of the cooling crystallization of sodium benzoate hydrate	72
4.1 Introduction.....	72
4.2 Experiments performed.....	73
4.3 Solubility measurements	73
4.4 Monitoring of sodium benzoate hydrate formation using PAT tools	74
4.5 Evaluation of the formation of the new sodium benzoate hydrate using solid state analytical methods	77
4.6 Conclusions.....	86
Chapter 5. A PAT based investigation of the polymorphic transformations during the antisolvent crystallization of sodium benzoate from IPA/water mixture	87
5.1 Introduction.....	87
5.2 Experiments performed.....	88
5.3 PAT tools for the monitoring and detection of solvent mediated polymorphic transformation of sodium benzoate in water/IPA mixture.....	89
5.4 SSA for the detection of new forms of crystalline compound.....	96
5.4.1 Discovery of a new solvate form of sodium benzoate.....	97
5.4.2 Combined DSC and HSM for the detection of higher melting polymorphic forms of sodium benzoate.....	105
5.5. Conclusions.....	107
Chapter 6. Application of PAT tools for the identification of crusting problems within crystallization processes	108
6.1 Introduction.....	108
6.2 Experiments performed.....	109
6.3 Monitoring the cooling crystallization process of <i>para</i> -amino benzoic acid (PABA) from ethyl acetate using PAT tools	109
6.4 Identifying a common problem of crusting in crystallization vessels through the use of solid state analysis.....	114
6.5 Conclusions.....	119
Chapter 7. PAT used to examine the effect of mixing on the crystallization of pharmaceutical products	121
7.1 Introduction.....	121
7.2 Experiments performed.....	122

7.3 Variation in key parameters on the MSZW and nucleation kinetics for isomers of ABA	122
7.3.1 MSZW determination using different size vessels	123
7.3.2 MSZW determination using different agitator speeds and type	128
7.3.3 Evaluation of the effect of cooling rate on the MSZW and investigation of the variability of nucleation kinetics with different crystallization conditions	133
7.4 Robust MSZW region for the isomers of ABA	143
7.4.1 Variation in the MSZW between the three isomers of ABA.....	143
7.4.2 Robust MSZW region for PABA and MABA.....	145
7.5 Conclusions.....	148
Chapter 8. Crystallization and characterisation of salts of o, m, p-amino benzoic acid isomers	150
8.1 Introduction.....	150
8.2 Experiments performed.....	153
8.3 Acidic salts of PABA and MABA by cooling crystallization	153
8.3.1 Introduction.....	153
8.3.2 Solid state characterisation of the hydrochloric salt of MABA.....	154
8.3.3 Solid state characterisation of the hydrobromic salt of MABA.....	158
8.3.4 Solid state characterisation of the hydrobromic salt of PABA	164
8.3.5 Solid state characterisation on the hydrochloride salt of PABA	169
8.3.6 Structural comparison of the bromide and chloride salts of PABA	175
8.4 Acidic salts of PABA formed by precipitation.....	177
8.4.1 Introduction.....	177
8.4.2 Solid state characterisation of the sulphuric salt of PABA.....	177
8.4.3 Solid state characterisation of the phosphoric salt of PABA.....	182
8.5 Basic salts of PABA formed by evaporation	189
8.5.1 Introduction.....	189
8.5.2 Hydrated forms of the sodium salt of PABA.....	189
8.5.3 Hydrated forms of potassium salt of PABA	195
8.6 Conclusions.....	200
Chapter 9. pH controlled polymorphic crystallization.....	201
9.1 Introduction.....	201
9.2 Experiments performed.....	202

9.3 Evaluation of pH sensitivity and effect of solvent on the crystallization of MABA and the discovery of a new polymorphic form of MABA	202
9.4 Application of PVM for identifying the crystallization conditions of different forms of compounds of MABA	210
9.5 Evaluation of pH sensitivity and effect of solvent on the crystallization of PABA	212
9.6 Application of PAT tools for monitoring the pH mediated crystallization of mixtures of PABA and the HCl salt.....	218
9.7 Conclusions.....	223
Chapter 10. Conclusions and future work.....	224
10.1 Conclusions.....	224
10.2 Recommendation for future work.....	230
References.....	232
Appendix A. Avantium Crystal 16 equipment	250
Appendix B. Pictures of salt crystals produced within Chapter 8 of thesis.....	251
Appendix C. Turbidity (solubility) results for sodium benzoate in organic solvents	252
Appendix D. Solubility graphs for <i>para</i> - and <i>meta</i> -amino benzoic acid in water obtained from the Literature	254
Appendix E. TGA and DVS calculations on the molecular ratio of sodium benzoate in water and the sodium and potassium salts of PABA (see chapters 4, 5 and 8)....	255
Appendix F. Calculation on the concentration of sodium chloride in water during a pH controlled cooling crystallization experiment of PABA in water (See Figure 9.17 within Chapter 9)	257
Appendix G. Derivation of pH-solubility equations (This derivation can be obtained from Florence and Attwood, 1981) (see Chapter 8)	260
List of Publications	263

List of Figures

Figure 2.1. A single unit cell. Length of axes: a, b and c. Angles between the axes: α , β and γ (Myerson, 2002)	10
Figure 2.2. Various forms of space lattices	10
Figure 2.3. Phase diagram of concentration versus temperature showing the various regions within a crystallization process	16
Figure 2.4. Solubility curve for sucrose, citric acid and sodium chloride in water (Davey and Garaside, 2000)	18
Figure 2.5. A flow chart of the different forms of nucleation	20
Figure 2.6. Two possible paths for the formation of a critical size (stable) nucleus	21
Figure 2.7. Free energy diagram for nucleation explaining the existence of a ‘critical nucleus’ (Mullin, 2001)	23
Figure 2.8. Effect of the degree of supersaturation on the nucleation rate	24
Figure 2.9. Effect of the temperature on the critical size nucleus and the Gibbs free energy change of formation (Mullin, 2001).....	25
Figure 2.10. Schematic of (a) channel hydrate and (b) isolate hydrate	30
Figure 2.11. Phase diagrams for a compound containing two polymorphic forms (dimorphic) showing a monotropic and enantiotropic system.....	32
Figure 2.12. Activation energy barriers required to overcome for the formation of the two polymorphs (I and II) within a dimorphic system, where G_0 is the Gibbs free energy of the solute in a supersaturated solution, G_I is the Gibbs free energy of polymorph (I), G_{II} is the Gibbs free energy of polymorph (II), G_I^* is the energy required to form polymorph (I) and G_{II}^* is the energy required to form polymorph (II).	36
Figure 2.13. FRBM probe tip with laser beam (adapted from Greaves <i>et al.</i> , 2008)	41
Figure 2.14. Laser beam detection of many chord lengths for a single particle.....	42
Figure 2.15. Total internal reflection occurring within the ATR-UV/Vis probe (adapted from Billot <i>et al.</i> , 2010)	45
Figure 2.16. UV/Vis spectrum for sodium benzoate in water	46

Figure 2.17. Typical DSC plot of a polymorphic transition occurring within the solid state	49
Figure 2.18. Typical DSC plot of a polymorphic transition occurring from re-crystallization of the melt	50
Figure 2.19. Schematic view of an X-ray diffractometer	53
Figure 3.1. (a) Schematic of the set-up and (b) picture of the crystallization rig at LU for the cooling crystallization of sodium benzoate from water experiments	61
Figure 3.2. Schematic set up of the crystallization rig using (a) 4-pitched blade turbine with FBRM and ATR-UV/Vis (LU rig) and (b) 3-blade glass retreat curve agitator with FBRM and turbidity probes (AZ rig).....	62
Figure 3.3. Schematic of the crystallization rig for the pH controlled cooling crystallization experiments (AZ rig).....	64
Figure 3.4. Schematic set-up of the crystallization rig for (a) automated LabMax system with a 3-blade glass retreat curve agitator (AZ rig) and (b) laboratory rig with a 4-pitched blade turbine agitator (LU rig).....	65
Figure 3.5. Picture of the antisolvent crystallization rig set-up performed with a peristaltic pump (Loughborough University)	66
Figure 4.1. Solubility results for sodium benzoate in water obtained from (a) Crystal 16 unit (turbidity points) and (b) literature data (Stephen and Stephen, 1963) and gravimetric method	74
Figure 4.2. FBRM results for the cooling crystallization of sodium benzoate in water at different initial concentrations (C_0): (a) 1 L vessel and $C_0 = 466$ mg/mL; (b) 250 mL vessel and $C_0 = 466$ mg/mL; (c) 250 mL vessel and $C_0 = 566$ mg/mL (d) 250 mL vessel and $C_0 = 633$ mg/mL.....	76
Figure 4.3. (a) Optical microscope image of sodium benzoate re-crystallized from water, (b, c) SEM images of sodium benzoate re-crystallized from water, (d) optical microscope image of raw material (anhydrous) form of sodium benzoate and (e) SEM image of raw material (anhydrous) form of sodium benzoate.....	78
Figure 4.4. Hot stage microscopy (HSM) images of sodium benzoate. Images (a-d) are during the heating phase and (e- l) are during the cooling of the melt	79
Figure 4.5. Birefringent crystal of the anhydrous sodium benzoate crystal re-crystallised from melt.....	79
Figure 4.6. XRPD results for (a) raw material and sodium benzoate (air-dried and TGA applied) and (b) raw material and sodium benzoate re-crystallized from water	80
Figure 4.7. NMR data of ^{13}C , ^{23}Na and ^1H spectra for the anhydrate and hydrate form of sodium benzoate	81

Figure 4.8. IR spectra for the anhydrous form and re-crystallized from water sample of sodium benzoate	82
Figure 4.9. DSC results for (a) raw material form of sodium benzoate and (b) samples of sodium benzoate re-crystallized from water.....	83
Figure 4.10. TGA results for the raw material form of sodium benzoate and sodium benzoate re-crystallized from water at the 1 mL and 250 mL scale	84
Figure 4.11. DVS results for sodium benzoate showing how the sample mass and relative humidity change with time	85
Figure 5.1. Solubility data for sodium benzoate in (a) IPA/water (w) volume ratios and pure IPA, (b) water, (c) different solvent systems at temperatures 32 and 70 °C	90
Figure 5.2. FBRM results for the antisolvent crystallization of sodium benzoate from an IPA/water mixture performed within a 1 L vessel using a (a) 3-blade glass retreat curve and (b) 4-pitched blade turbine (coated with PTFE)	91
Figure 5.3. Visual images of the crystallization vessel using a 4-pitched blade turbine showing (a) a mobile cloudy solution after the first nucleation event and (b) formation of solid clump after the second nucleation event.....	92
Figure 5.4. Optical microscope images of the crystals obtained from the antisolvent crystallization experiments after (a) the first nucleation event and (b) second nucleation event (fluctuation in FBRM counts)	92
Figure 5.5. UV/Vis spectrum for sodium benzoate in water	93
Figure 5.6. FBRM and UV/Vis results for the anti-solvent crystallization experiment with the step additions of IPA.....	93
Figure 5.7. X-ray powder diffraction patterns for (a) anhydrous and hydrated form of sodium benzoate, (b and c) sodium benzoate samples obtained from the Crystal 16 slurry experiment with different water activities (wa). In figures (b) and (c) intensities are shifted for clearer plotting.....	96
Figure 5.8. X-ray powder diffraction patterns for (a) raw material form of sodium benzoate, (b) sodium benzoate re-crystallized from volume ratio of IPA/water of 5:1 and (c and d) sodium benzoate re-crystallized from volume ratio of IPA/water of 3:1 .	98
Figure 5.9. SEM images of (a, c) sample of sodium benzoate re-crystallized from volume ratio of IPA/water 3:1 and (b, d) hydrated form of sodium benzoate.....	99
Figure 5.10. DSC results for (a) raw material form of sodium benzoate, (b) sodium benzoate re-crystallized from a volume ratio of IPA/water of 3:1 and (c, d) sodium benzoate re-crystallized after the second nucleation event at volume ratio of IPA/water of 4.4:1 and 5:1	100

- Figure 5.11. HT-XRPD results of sodium benzoate re-crystallized from volume ratio IPA/water of 3:1 at temperatures within the range 25 to 175 °C. Intensities are shifted for clearer plotting 101
- Figure 5.12. Solid state NMR data of (a) ^{13}C , (b) ^{23}Na , (c) ^1H and (d) solution state ^1H data for anhydrous form of sodium benzoate and sample re-crystallized from volume ratio IPA/water of 3:1 102
- Figure 5.13. IR data for the anhydrous form of sodium benzoate and sample re-crystallized from volume ratio IPA/water of 3:1 showing (a) the full spectrum and (b) the fingerprint region 103
- Figure 5.14. TGA results of (a) anhydrous form of sodium benzoate and crystals obtained from volume ratio IPA/water of 3:1 and (b) anhydrous form of sodium benzoate and crystals obtained from volume ratio of IPA/water of 5:1 104
- Figure 5.15. DSC results for 2 repeated runs of anhydrous form of sodium benzoate showing the re-crystallization and melting of a higher melting polymorphic form 106
- Figure 5.16. Hot stage microscopy (HSM) of hydrated form of sodium benzoate crystals during (a-g) heating phase and (h) re-crystallization from cooling 106
- Figure 6.1. XRPD patterns for the raw material form of PABA and alpha-PABA (simulated) 110
- Figure 6.2. FBRM, turbidity and UV/Vis results for the cooling crystallization of PABA from ethyl acetate using (a) 4-pitched blade turbine and (b) 3-blade glass retreat curve 112
- Figure 6.3. UV/Vis spectrum for PABA in ethyl acetate at 45 °C during 2-6 hours of crusting experiment, showing a peak absorbance of 300 nm 113
- Figure 6.4. Photos of the crystallization vessel during the cooling crystallization of PABA in ethyl acetate showing an increase in crusting on vessel walls as the system is kept at a constant temperature of 45 and 5 °C 113
- Figure 6.5. Optical microscope images of PABA samples obtained during the cooling crystallization experiment at (a) point of first nucleation 2 hours (45 °C), (b) 4 hours from start (45 °C), (c) point of second nucleation 10 hours (5 °C) and (d) 14 hours from start (5 °C)..... 114
- Figure 6.6. DSC plots for PABA samples obtained from the first and second nucleation events during the cooling crystallization experiment in which crusting formed on vessel walls. Heat flows for each plot are shifted by -1 W/g for clearer plotting 115
- Figure 6.7. XRPD patterns for raw material PABA (alpha form) and crystal samples obtained after the first and second nucleation events during the experiment in which crusting formed on vessel walls. Intensities for each pattern are shifted by 3000 for clearer plotting 116

Figure 6.8. FBRM and UV/Vis results for the cooling crystallization of PABA from ethyl acetate in which no crusting formed on vessel walls (full vessel).....	117
Figure 6.9. HSM images of PABA from the cooling crystallization experiments in which no crusting formed on vessel walls. Images 1-5 are during the heating phase and image 6 is cooling from the melt	117
Figure 6.10. DSC plots for PABA re-crystallized from ethyl acetate as the system is kept at 45 °C during the experiment in which no crusting formed on vessel walls. Heat flows for each plot are shifted for clearer plotting.....	118
Figure 6.11. XRPD patterns for raw material PABA (alpha form) and crystal samples obtained after the first nucleation event (45 °C) during the experiment in which no crusting formed on vessel walls. Intensities for each pattern are shifted by 2000 for clearer plotting	119
Figure 7.1. Clear and cloud point curves for PABA in water at the 1 mL and 1 L scale using a ramp rate of 0.3 °C/min.....	124
Figure 7.2. Clear and cloud point curves for PABA in water at the 1 mL and 1 L scale using a ramp rate of 0.5 °C/min.....	124
Figure 7.3. Clear and cloud point curves for MABA in water using different scales of 1 mL and 1 L (3-blade glass retreat curve) at a ramp rate of 0.3 °C/min. Error bars included.....	126
Figure 7.4. Clear and cloud point curves for MABA in water using different agitator types at the 1 L scale and ramp rate of 0.3 °C/min. Error bars included for clear and cloud points for the 3-blade glass retreat curve agitator	128
Figure 7.5. Clear and cloud point curves obtained using different agitator speeds within the 1 L size vessel	130
Figure 7.6. Optical microscope images of crystals obtained during the cooling crystallization of PABA in water using different agitator speeds of (a) 250 rpm, (b) 300 rpm and (c) 400 rpm	133
Figure 7.7. Solubility and nucleation curves for PABA in water at cooling rates 0.5, 0.3, 0.1 °C/min, using a 1 L size vessel.....	134
Figure 7.8. Linear dependence between cooling rate and MSZW according to Nyvlt (1968) for PABA in water at the 1 L scale	135
Figure 7.9. Linearised van't Hoff solubility curve for PABA in water at the 1 L scale	137
Figure 7.10. Clear and cloud point curves for MABA in water at the 1 L scale using a 3-blade glass retreat curve and different ramp rates of 0.5, 0.3 and 0.2 °C/min	138

Figure 7.11. Linear dependence between cooling rate and MSZW according to Nyvlt's (1968) method for the 1 mL scale of MABA in water	139
Figure 7.12. Linear dependence between cooling rate and MSZW according to Nyvlt's (1968) method for the 1 L scale using a 3-blade glass retreat curve for MABA in water	140
Figure 7.13. Linear dependence between cooling rate and MSZW according to Nyvlt's (1968) method for the 1 L scale using a 4-pitched blade turbine for MABA in water.	140
Figure 7.14. van't Hoff solubility curve for MABA in water (a) at the 1 mL scale and 1 L scale using (b) a 3-blade glass retreat curve and (c) 4-pitched blade turbine.....	141
Figure 7.15. Clear and cloud point curves for the three isomers of ABA (<i>ortho</i> , <i>meta</i> and <i>para</i>) using a ramp rate of 0.5 °C/min and 1 L vessel (4-pitched blade turbine)...	143
Figure 7.16. Robust MSZW region for PABA in water at the 1 L scale with variations in clear and cloud point curves for different ramp rates, agitator types and agitator speeds.....	146
Figure 7.17. Robust MSZW region for MABA in water with variations in clear and cloud point curves for different ramp rates, agitator types and scale of vessel	146
Figure 8.1. Four different forms of PABA and the equilibrium between each form....	151
Figure 8.2. Change in pH with (a) solubility and temperature for PABA in ethanol and (b) % ionisation of certain species of PABA	152
Figure 8.3. FBRM results for the cooling crystallization of MABA from ethanol at pH=2.5 using HCl acid	154
Figure 8.4(a) Optical microscope and (b, c) scanning electron microscope images of MABA re-crystallized from ethanol at pH=2.5 using HCl.....	155
Figure 8.5. XRPD pattern for raw material form of MABA and MABA re-crystallized from ethanol at pH=2.5 using HCl acid.....	155
Figure 8.6. Simulated and experimental XRPD patterns for the chloride salt of MABA	156
Figure 8.7. Predicted morphology of the chloride salt of MABA using the BFDH method	156
Figure 8.8. DSC plot of the hydrochloride salt of MABA	157
Figure 8.9. IR spectrum for the hydrochloric (HCl) salt of MABA and the raw material form of MABA	158
Figure 8.10. FBRM results for the cooling crystallization of MABA from ethanol at pH=1.5 using HBr acid	159

Figure 8.11. Optical microscope images of MABA re-crystallized from ethanol at pH=1.5 using HBr acid	159
Figure 8.12. XRPD pattern for the raw material form of MABA and MABA re-crystallized from ethanol at pH=1.5 using HBr acid	160
Figure 8.13. Simulated and experimental XRPD patterns for the bromide salt of MABA	161
Figure 8.14. Predicted morphology of the bromide salt of MABA using the BFDH method	161
Figure 8.15. DSC results for the hydrobromic (HBr) salt of MABA	162
Figure 8.16. IR spectrum for hydrobromic (HBr) salt of MABA and the raw material form of MABA	163
Figure 8.17. DVS results for the hydrobromic salt of MABA showing (a) isothermal plot and (b) change in mass (Dry) plot	163
Figure 8.18. FBRM results for the cooling crystallization of PABA from ethanol at pH=1 using HBr acid	164
Figure 8.19. PABA re-crystallized from ethanol using the (a) optical microscope, (b) PVM image during nucleation, (c and d) SEM images	165
Figure 8.20. XRPD pattern for raw material form of PABA (alpha) and PABA re-crystallized from ethanol at pH=1 using HBr acid	166
Figure 8.21. Simulated and experimental XRPD patterns for the bromide salt of PABA	166
Figure 8.22. Predicted morphology of the bromide salt of PABA using the BFDH method	167
Figure 8.23. DSC results for the hydrobromide (HBr) salt of PABA	167
Figure 8.24. DVS results for hydrobromic (HBr) salt of PABA showing (a) isotherm plot and (b) change in mass (Dry) plot	168
Figure 8.25. IR results for PABA /HBr salt and raw material form of PABA (alpha).	169
Figure 8.26. FBRM results for the cooling crystallization of PABA from ethanol solution at pH=2.5 using HCl acid.....	170
Figure 8.27. Optical microscope image of PABA re-crystallized from ethanol at pH=2.5 using HCl acid	171
Figure 8.28. XRPD pattern for the hydrochloride salt of PABA and the raw material PABA (alpha form).....	172

Figure 8.29. Simulated and experimental XRPD patterns for the chloride salt of PABA	172
Figure 8.30. Predicted morphology of the chloride salt of PABA using the BFDH method	173
Figure 8.31. DSC results for hydrochloride (HCl) salt of PABA.....	173
Figure 8.32. IR results for the HCl salt of PABA and the raw material PABA (alpha)	174
Figure 8.33. Comparison of XRPD patterns for the chloride and bromide salts of PABA	176
Figure 8.34. Comparison of XRPD patterns of the chloride and bromide salts of MABA	176
Figure 8.35. PABA re-crystallized from an ethanol/ H ₂ SO ₄ solution showing (a) optical microscope image from mobile slurry and (b) scanning electron microscope image after filtration	178
Figure 8.36. XRPD patterns for sample re-crystallized from ethanol/H ₂ SO ₄ solution at pH=1.2 and the raw material form of PABA (alpha)	178
Figure 8.37. Simulated and experimental XRPD pattern for the sulphate salt of PABA	179
Figure 8.38. Predicted morphology of the sulphate salt of PABA using the BFDH model	180
Figure 8.39. DSC results for the sulphuric salt of PABA.....	180
Figure 8.40. IR results for the sulphuric salt of PABA and the raw material form of PABA.....	181
Figure 8.41. DVS results for sulphuric salt of PABA showing (a) isothermal plot and (b) change in mass (Dry) plot	182
Figure 8.42. Crystal images of PABA re-crystallized from ethanol/H ₃ PO ₄ solution at pH=3.3 showing (a) optical microscope images and (b) scanning electron microscope	183
Figure 8.43. DSC results for the sample re-crystallized from ethanol solution at pH=3.3 using phosphoric acid	184
Figure 8.44. Optical microscope image of crystals obtained from the beaker precipitation experiment of PABA in an ethanol/H ₃ PO ₄ solution in which all the raw material dissolved	185

Figure 8.45. DSC results for the sample re-crystallized from a clear ethanol/H ₃ PO ₄ solution.....	185
Figure 8.46. XRPD patterns for the crystal samples obtained from the precipitation experiments of PABA in an ethanol/H ₃ PO ₄ solution and the raw material form of PABA (alpha)	186
Figure 8.47. Simulated and experimental XRPD pattern for the phosphate salt of PABA	187
Figure 8.48. Predicted morphology of the anhydrous phosphate salt of PABA using the BFDH model.....	188
Figure 8.49. IR spectrum of the phosphoric salt of PABA and the raw material form of PABA.....	188
Figure 8.50. Optical microscope image of PABA re-crystallized from ethanol at pH=10.7 using NaOH	190
Figure 8.51. XRPD pattern for the sodium salt of PABA and the raw material form of PABA.....	190
Figure 8.52. Simulated and experimental XRPD pattern for the sodium salt of PABA	191
Figure 8.53. DSC results for the sodium salt of PABA	192
Figure 8.54. TGA results for the sodium salt of PABA	193
Figure 8.55. DVS results for sodium salt of PABA showing (a) isothermal plot and (b) change in mass (Dry) plot.....	194
Figure 8.56. Optical microscope image of PABA re-crystallized from ethanol at pH=8.1 using KOH.....	195
Figure 8.57. XRPD patterns for the potassium salt of PABA and the raw material form of PABA	196
Figure 8.58. Simulated and experimental XRPD patterns for the potassium salt of PABA.....	196
Figure 8.59. DSC results for the potassium salt of PABA	197
Figure 8.60. TGA results for the potassium salt of PABA	198
Figure 8.61. DVS results for the potassium salt of PABA	199
Figure 9.1. Results for the cooling crystallization of MABA from water at pH=3	203

Figure 9.2. FBRM results for the cooling crystallization of MABA from ethanol at pH=4.1	203
Figure 9.3. PVM images of (a) MABA crystals during the first dissolution event (see Figure 9.2) showing the formation of agglomerated needles and (b) crystals nucleated from ethanol solution at pH 4.1	204
Figure 9.4. Optical microscope images of (a) raw material form of MABA and (b) MABA re-crystallized from water at pH=3	204
Figure 9.5. XRPD patterns for the raw material form of MABA, sample re-crystallized from water at pH=3 and ethanol at pH=4.1	205
Figure 9.6. IR spectrum for raw material form of MABA, sample re-crystallized from water at pH=3 and sample re-crystallized from ethanol at pH=4.1	206
Figure 9.7. DSC results for the raw material form of MABA	206
Figure 9.8. DSC results for samples of crystals re-crystallized from water at pH=3 for lightly and intense grinding	208
Figure 9.9. DSC results for MABA re-crystallized from ethanol at pH=4.1	208
Figure 9.10. TGA plots for (a) raw material form of MABA and (b) MABA re-crystallized from water at pH=3	209
Figure 9.11. (a) PVM and (b) optical microscope image of MABA re-crystallized from ethanol at pH=1.5 using HBr acid	210
Figure 9.12. PVM images of (a) raw material form of MABA, (b) crystals after HCl acid has been added to solution and (c,d) crystals after nucleation	211
Figure 9.13. FBRM results for the pH swing crystallization experiments using water solution.....	212
Figure 9.14. FBRM results for the cooling crystallization of PABA from water at pH=5.9 using HCl.....	213
Figure 9.15. Optical microscope images of PABA re-crystallized from water at different values (a) pH=2.5, (b) pH=3.6 and (c) pH=5.5 using hydrochloric acid.....	213
Figure 9.16. XRPD patterns for PABA re-crystallized from water within pH range of 2.6 to 5.9 using hydrochloric acid (HCl) and the raw material form of PABA. Intensities are shifted for clearer plotting.....	214
Figure 9.17 FBRM results for the cooling crystallization of PABA from ethanol at pH=5.6	215

Figure 9.18. PVM images of crystals during different stages of the crystallization experiment for PABA in ethanol at set point pH=5 showing (a) raw material form of PABA (needle morphology), (b) dissolution of needles during heating phase, (c) salt formation at temperature 70 °C and (d) nucleation at pH=5.....	216
Figure 9.19. Optical microscope images of crystals nucleated from ethanol solution at pH=5.6	216
Figure 9.20. XRPD patterns for PABA re-crystallized from ethanol at pH=5.6 and the raw material form of PABA (alpha). Intensities are shifted for clearer plotting	217
Figure 9. 21. UV/Vis spectrum for PABA and the HCl salt of PABA.....	218
Figure 9.22. FBRM and UV/Vis results for the cooling crystallization of PABA from ethanol at pH=2.5 in which the moles of PABA is greater than HCl acid	219
Figure 9.23. PVM images of (a) raw material PABA, (b) salt formation during the 1 st dissolution event, (c) salt formation during the 1 st nucleation event and (d) mixture of salt and PABA for the 2 nd nucleation event.....	220
Figure 9.24. Microscope images of (a) hydro-chloride salt of PABA, (b) alpha form of PABA and scanning electron microscope images of (c, d) mixture of hydro-chloride salt of PABA and PABA (alpha form)	221
Figure 9.25 XRPD patterns of (a) sample from 1 st nucleation and HCl salt of PABA and (b) sample from 2 nd nucleation and raw material PABA. Intensities shifted for clearer plotting	222
Figure 9.26 DSC results for the sample nucleated from the second nucleation event during cooling crystallization of PABA from ethanol at pH=2.5.....	222

List of Tables

Table 2.1. 14 Bravais lattices and examples of crystals resembling particular crystal systems (Crystal Structure, 2010; Mineralogy Database, 2010; Minerals by name, 2010)	11
Table 3.1. Summary of experiments performed including method and materials.....	67
Table 3.2. Summary of experiments performed including experimental set-up and parameters.....	68
Table 4.1. Summary of the DVS results for the molecular ratio of sodium benzoate to water.....	86
Table 5.1. Summary of the different conditions and volume ratios of IPA/water for the first and second nucleation events, for all sodium benzoate antisolvent crystallization experiments.....	95
Table 7.1. MSZW values for the cooling crystallization of PABA in water using different ramp rate and vessel sizes	125
Table 7.2. Clear/cloud point temperatures and MSZW values for MABA in water at the 1 L scale using a 3-blade glass retreat curve at different ramp rates	127
Table 7.3. Clear/cloud point temperatures and MSZW values for MABA in water at the 1 mL scale at different ramp rates	127
Table 7.4. Clear/cloud point temperatures and MSZW values for MABA in water at the 1 L scale using a 4-pitched blade turbine at different ramp rates	129
Table 7.5. MSZW values for the cooling crystallization of PABA in water using different agitator speeds.....	131
Table 7.6. Summary of Reynolds number, power number and power input for different agitator speeds.....	132
Table 7.7. MSZW values for the cooling crystallization of PABA in water using a 1 L vessel and different cooling rates.....	134
Table 7.8. Nucleation orders, contact K and R^2 values obtained from the cooling crystallization of PABA in water within the 1 L vessel	136
Table 7.9. Nucleation orders obtained from cooling crystallization of MABA in water within a 1 L vessel using a 3-blade glass retreat curve and 4-pitched blade turbine and within a 1 mL vessel	141
Table 7.10. Enthalpy and entropy of dissolution values for MABA in water at the 1 mL scale and the 1 L scale using a 3-blade glass retreat curve and a 4-pitched blade turbine	142

Table 7.11. MSZW results for the three isomers (<i>ortho</i> , <i>meta</i> , <i>para</i>) of ABA	144
Table 7.12. Summary of results for nucleation order, enthalpy/entropy of dissolution <i>para</i> - and <i>meta</i> -ABA	145
Table 10.1. Summary of results for crystals forms produced during PhD thesis and experimental conditions	229

List of symbols

a_i	Activity of component i
a_{eq}	Activity of component in equilibrium state
a_{ss}	Activity of component in supersaturated state
A	Arrhenius pre-exponential factor
A_b	Absorbance
b	Nucleation order
B	Rate of nucleation
c	Concentration
c_{eq}	Equilibrium concentration
c_i	Solute concentration at the crystal/solution interface
c_{ss}	Supersaturated concentration
d	Distance between planes in the crystal
d_p	Depth of penetration of the evanescent wave
D	Impeller diameter
G	Gibbs free energy
G_o	Gibbs free energy of the solute in a supersaturated solution
I	Intensity of reflective light beam
I_o	Intensity of incident beam
J	Rate of nucleation for spontaneous nucleation
k	Boltzmann constant
k_b	Nucleation rate constant
l	Optical path length
M_T	Concentration of crystals in suspension
n_i	Number of moles of component i
n_o	Order of the diffraction pattern
N	Stirrer speed
N_p	Power number
P	Power input into the system

r	Size of nucleus
r_c	Critical size of nucleus
R	Gas constant
Re	Reynolds number for impeller
S	Supersaturation Ratio
S_{crit}	Critical supersaturation required for spontaneous nucleation
S_L	Solubility
S_o	Intrinsic solubility
T	Temperature
v	Molecular volume
z	Number of reflections

List of Greek letters

γ_i	Activity coefficient of component i
γ_T	Interfacial tension
β	Cooling rate
μ	Chemical potential
μ_{eq}	Chemical potential in the equilibrium state
μ_{ss}	Chemical potential in the supersaturated state
μ_i^0	Standard chemical potential of component i at 1 atmosphere pressure
μ_s	Chemical potential in the solid state
μ_v	Fluid viscosity
σ	Relative supersaturation
ε	Power input into the solution
ε_a	Absorbance coefficient
ρ_L	Fluid density
λ	Wavelength
θ	Angle
θ_c	Critical angle
$\Delta\mu$	Difference in chemical potential
Δc	Concentration driving force (degree of supersaturation)
ΔE	Difference in energy
ΔG	Gibbs free energy change
ΔG_s	Surface excess free energy
ΔG_v	Volume excess free energy
ΔG_{crit}	Gibbs free energy change (formation of critical size nucleus)
ΔH	Enthalpy change
ΔH_d	Enthalpy of dissolution
ΔS	Entropy change
ΔS_d	Entropy of dissolution

Abbreviations

API- Active pharmaceutical ingredient
CLD-Chord length distribution
CSD-Crystal size distribution
DSC-Differential scanning calimetry
DVS-Dynamic vapour sorption
FBRM -Focused beam reflectance measurement
FDA-Food and drug administration
HSM-Hot stage microscopy
IR-Infra-red
MSZW-Metastable zone width
NMR-Nuclear magnetic resonance
PAT-Process analytical technology
PSD-Particle size distribution
PVM-Particle vision monitor
RH-Relative humidity
SEM-Scanning electron microscope
SSA-Solid state analysis
TGA-Thermal gravimetric analysis
XRPD- X-ray powder diffraction

Acknowledgements

I would like to express my appreciation to both my supervisors at Loughborough University, Prof. Zoltan Nagy and Dr. Basu Saha for their continuous support, encouragement and expert guidance throughout my PhD. Their enthusiasm, enlightening suggestions and comments have enabled me to achieve to my full potential and therefore enabling the development of this thesis. I would like to thank them for their time for supportive meetings that were often outside of working hours and for the proof reading of this thesis.

I am very grateful to have had the opportunity to carry out part of my research works at AstraZeneca (Charnwood site), which I thoroughly enjoyed. A special thanks to both my supervisors at AstraZeneca, Dr. Gerald Steele and Dr. Amy Robertson, for the continuous guidance, support and training on the high-tech equipment. I would like to thank Dr. Amy Robertson for her contribution in providing some of the results including the simulated X-ray powder diffraction patterns and structure determination of salts. Also I would like to thank Dr. Gerry Steele for providing some of the scanning electron microscope images. Their expertise knowledge, guidance towards finding the key journal papers and comments in progress meetings has contributed significantly towards the development of this thesis.

I would also like to acknowledge the following people for their help and support during my PhD:

- Dr David O'Sullivan of the department of Early Development of Pharmaceutical and Analytical R&D, AstraZeneca (Charnwood) for performing the dynamic vapour absorption, some thermal gravimetric analysis and differential scanning calorimetry (DSC) analysis.
- Dr Dave Martin of the department of Analytical development, Pharmaceutical and Analytical R&D, AstraZeneca (Charnwood) for performing and producing the nuclear magnetic resonance spectroscopy results.
- Mr Paul Gadd of the department of Process Engineering, Process R&D, AstraZeneca (Charnwood) for the support and help in setting up the equipment for experiments and for training of the DSC.

- Dr Paul Hurved of the department of Process Engineering, Process R&D, AstraZeneca (Charnwood) for the support in using the lab max rig with turbidity probe and for helping with analysing the data.
- Mr Dave Smith, Ms Kim Robertshaw, Mr Graham Moody, Mr Sean Creedon, Ms Monika Pietrzak, Mr Tony Eyre of the Chemical Engineering Department, Loughborough University for their help in finding the right pieces of equipment to use within experiments and ensuring a safe working environment within the lab.
- Mr Paul Izzard of the Chemical Engineering department, Loughborough University for the help with IT problems.
- Ms Tracy Marshall (Academic Librarian) of Loughborough University Library, for her time and effort in helping me find key journal papers.
- Dr David Ross of the Department of Materials, Loughborough University for the training on the optical microscopy and hot-stage microscopy.

I am grateful to both EPSRC and AstraZeneca for their combined financial backing of my PhD, which enabled me to attend conferences both in the UK and abroad.

Thank you to all my colleagues in the Chemical Engineering Department and my other PhD friends whose encouragement and friendship I will always remember. Additionally I would like to thank my badminton friends for making me wake up at 9am on a Saturday morning, and then I had to work. I felt very happy and at home in Loughborough and take this opportunity to thank Chris Taylor and the Newton family who as Christians made me feel very welcome and to remember all my friends at Waterways accommodation. Last but not least I thank my family for their support and helping me move five times within three years.

Chapter 1. Introduction

1.1 Background

Pharmaceutical industries aim for continuous improvement in the manufacturing process of producing medicines (Sistare *et al.*, 2005). The driving force is to produce quality products in a quick and cost effective way (Federsel, 2009). There are many problems and challenges that the pharmaceutical industry faces in the current market. One of the demands is to reduce the time it takes from the discovery of an active pharmaceutical ingredient to marketing the drug. In the past the total time allocated to achieve this was more than 10 years but now demands require this stage to take less putting pressure on the designing and scaling up process (Federsel, 2009). One of the reasons for the increase in speed in developing new medicines is the short patent life of a drug (typical 20 years), giving approximately 11-12 years or less profitable period once launched to market (Sternitzke, 2010). Due to these demands high risk decisions are taken involving the scaling up the chemistry from lab to pilot plant without the full knowledge and understanding of the process, including kinetics, formation of byproducts, isolation and crystallization conditions (Federsel, 2009). This has resulted in late stage failures. Recent examples include a new developed drug for Alzheimer's disease (Dimebon), which showed hopeful signs after passing phase 2 clinical trials but failed phase 3 trials and an antidepressant drug (ealzotan), which was discontinued after phase 1 trials due to the side effects in healthy volunteers (Federsel, 2009; Goldhill, 2010). These late stage failures contribute to a large proportion of the cost of producing drugs, which is estimated at a value of 802 million dollars (Schachter and Ramoni, 2007). Failures can also occur during the crystallization process, which is in effect the final purification stage of the synthesis of the API in the manufacturing process of medicines.

Designing the crystallization process is important so as to produce crystals of desired polymorphic form, shape and crystal size distribution (Chen *et al.*, 2009; Lu and Ching, 2006; Yu *et al.*, 2007; Yu *et al.*, 2004; Abu Bakar *et al.*, 2009a, Abu Bakar *et al.*, 2009b; Aamir *et al.*, 2010). Purity of the compound is also an important parameter to

control (Braatz *et al.*, 2002; Aamir *et al.*, 2010). Different polymorphic forms have the same chemical composition but have different arrangement of molecules resulting in different structures. This leads to variations in morphology and physico-chemical properties between the different forms, including melting point, stability, solubility, dissolution rates and bioavailability, which can have a great effect on the quality of the product and can lead to problems with downstream processing (Davey and Garside, 2000). Compounds are often crystallized as salts to overcome problems with solubility, dissolution rate, stability and hygroscopicity (Forbes *et al.*, 1992, Haynes *et al.*, 2005). Compounds may incorporate solvent molecules within the crystal lattice structure forming a hydrate or solvate. These forms are also known as pseudo-polymorphs. Reddy *et al.* (2009) reported that 50% of 254 active pharmaceutical ingredients (API's) are polymorphic. Another report stated that a new polymorphic form of a pharmaceutical compound used to treat HIV-1 was discovered during late stage development (Desikan *et al.*, 2005), which was fortunately found in this instance to have no significant impact on the development of the drug. However in some cases the discovery of new polymorphs during late stage development or after the drug has been marketed can have a disastrous effect on the supply of an essential drug product as was found to be the case for the drug Ritonavir. Abbott Laboratories discovered a new polymorphic form of the drug Ritonavir after it had been on the market for two years (Chemburkar *et al.*, 2000). Differences in the solubility of the two forms resulted in failed dissolution tests in the originally semisolid capsule, which lead to a market crisis (Chemburkar *et al.*, 2000). Production of the undesired polymorphic form would result in an increase in economic costs (Davey, 2003). It is of very high importance within the pharmaceutical industry that all possible polymorphs, hydrates or solvates of a particular compound are identified and the crystallization process is controlled so that the desired form is produced (Bechtloff *et al.*, 2001).

To produce a quality product and prevent failures during any stage of the development process including crystallization, downstream processing and clinical trials, the demand grows towards process knowledge and understanding (Federsel, 2009). This changes the direction of the pharmaceutical industry towards a quality-by-design (QbD) approach rather than the traditionally method of quality-by-testing (Yu, 2008). Pharmaceutical QbD emphasises processes and product understanding and process control (Yu, 2008). QbD approaches within the crystallization field involve the use of

process analytical technology (PAT), which has been greatly promoted by the Food and Drug Administration (FDA) regulatory body (Yu *et al.*, 2007). PAT tools are probe based methodologies in which various instruments are placed within the process stream for the monitoring of the crystallization process (Birch *et al.*, 2005). These tools provide information about the process and product, which can be used to design a process to produce crystals with the desired properties. The application of these tools has led to the development of novel control approaches for pharmaceutical crystallization, which can lead to significant product quality improvements (Nagy *et al.*, 2008b; Zhou *et al.*, 2006; Abu Bakar *et al.*, 2009a; Woo *et al.*, 2009; Gron *et al.*, 2003; Yu *et al.*, 2007; Fevotte, 2007; Simon *et al.*, 2009). Extensive studies have been carried out which also demonstrate the importance of these tools for the detection or control of polymorphic transformations (Simon *et al.*, 2009; Howard *et al.*, 2009a; Howard *et al.*, 2009b; David *et al.*, 2004; O'Sullivan and Glennon, 2005; Dharmayat *et al.*, 2006; Caillet *et al.*, 2008; Fevotte, 2002; Nagy *et al.*, 2007).

Process analytical tools can be used to indicate a potential polymorphic transformation, however a range of solid state analytical (SSA) techniques usually must also be used to confirm the formation of polymorphs. These techniques provide information that enables the different polymorphic/pseudo-polymorphic forms to be identified. Various combinations of the SSA techniques can be used for the identification of polymorphic forms, including X-ray powder diffraction (XRPD), differential scanning calorimetry (DSC), thermal gravimetric analysis (TGA), dynamic vapour sorption (DVS) and a range of microscopy techniques including hot stage (HSM), optical and scanning electron microscope (SEM) (Brittain, 1999; Giron, 2003; Karpinski, 2006; David *et al.*, 2004; Giron, 1995).

In industry it is often most desirable to crystallize the most stable polymorph to prevent polymorphic conversion during further downstream processing including filtration or drying, transportation and storage. This involves following a set profile within the metastable zone width (MSZW) region of the phase diagram. PAT tools are used for obtaining MSZW values for the crystallization system at laboratory scale (Barrett and Glennon, 2002). There are many factors including rate of supersaturation generation, level of impurities and mixing conditions that affect the MSZW (Lu and Ching, 2006; Trifkovic *et al.*, 2009; Barrett and Glennon, 2002). Obtaining a robust MSZW region,

which takes into consideration variations in process parameters, will provide the operating conditions so scale up of the process from laboratory scale to industrial production can be achieved without affecting the quality of product (Beckmann, 2000; Barrett and Glennon, 2002).

1.2. Aims of current study

The aims of the current study are included within the following points:

- i. To show the benefits of using a QbD approach for the investigation into polymorphism using one of the main model systems, sodium benzoate. PAT tools and SSA techniques are used to detect polymorphic transformations during the crystallization process and discovery of new forms of crystalline compound. Detection of all possible polymorphic forms earlier on in development of a drug can prevent late stage failures
- ii. To highlight the benefits of using a combination of PAT tools and SSA techniques to gain a deeper understanding of the cooling and pH controlled polymorphic crystallization processes using the model system *para*-amino benzoic acid in ethyl acetate and ethanol. These tools prevent the misinterpretation of results obtained during the crystallization process, saving both time and money.
- iii. To identify the common problem of crusting occurring within laboratory scale crystallization vessels, this emphasises the need for improvement within the design of pilot plant and industrial size rigs. Better vessel design would increase the likelihood of producing a quality product when scaling up from lab to manufacturing scale and prevent failed batches.
- iv. To determine whether a robust MSZW can be obtained at the lab scale, which can then be used for designing a crystallization process at pilot plant and then manufacturing scale to ensure a quality product. This will be achieved by studying how various factors including temperature, ramp rate, agitator speed, agitator type and scale (1 mL and 1 L) affect the MSZW using PAT tools. Also

the effect of system set-up (scale of vessel and agitator type) on the nucleation order will be investigated to determine whether crystallization models are system specific.

- v. To gain a deeper understanding of the crystallization of salts and to examine how pH and solvent affects the crystal form which nucleates from solution by obtaining data from PAT tools during the crystallization process and analysing the crystal product using a range of SSA techniques.

1.3. Contributions of the thesis

This thesis discusses the importance of using a QbD approach involving the use of PAT tools and SSA techniques to increase process understanding and knowledge, which can speed up the time of drug discovery to marketing by designing more robust crystallization processes. Information obtained from PAT tools including the FBRM and ATR-UV/Vis provided supporting evidence of polymorphic transformations. SSA techniques confirmed the formation of new undiscovered hydrates/solvates that have not been reported in the literature. Discovery of new polymorphic forms of a compound earlier on in development can prevent late stage failures.

PAT tools have also been used to identify changes occurring during the crystallization process, which were originally thought to be polymorphic transformations but after further analysis using SSA techniques the change was found to be due to crusting (solid forming on vessel walls). A combination of PAT tools and SSA techniques increases process understanding, saving both time and money that would have been spent in researching the possible different polymorphic forms. The increase in process understanding obtained by a QbD approach also highlights the need for improvement in industrial vessel design such as vessels with variable jacket height to eliminate the problems of crusting (solid forming on vessel walls). Better vessel design would reduce the variability in product properties, increasing the likelihood of producing a quality product at manufacturing scale.

By using a QbD approach a robust meta-stable zone width (MSZW) was obtained at lab scale, which takes into consideration variation in ramp rate, vessel size (1 mL to 1 L), agitator speed and type. MSZW is defined as the difference between the solubility (clear) curve and nucleation (cloud) curve at any given concentration value. The robust MSZW was found only to apply for compounds that have a large MSZW. This robust MSZW can be used to design a crystallization process at larger scale (pilot and manufacturing scale) increasing the likelihood of producing a quality product. Nucleation orders were found to vary for different crystallization vessel set-up, which included variation to vessel size and agitator type. This research shows that crystallization models using nucleation orders are system specific and could result in failed batches if used for the design of scale up experiments.

A novel method is presented in the thesis that uses a combination of five PAT tools in a single vessel and a range of SSA techniques to examine the best conditions to produce salts, for the model system *para*- and *meta*-amino benzoic acid in water and ethanol. The best method for crystallizing salts was found to be cooling and evaporation. Precipitation resulted in agglomeration forming poor quality salt crystals. Solid state characterisation of salt crystals showed that crystals which contain the sodium and potassium ions form hydrates and solvent can affect significantly the morphology of the salt. The QbD approach increases process understanding, which enables better design of the crystallization process and identifies the required stages of downstream processing to prevent polymorphic transformations (e.g. involving the formation of hydrates).

1.4. Structure of the thesis

Chapter 1 gives an introduction into the problems pharmaceutical industries face and focuses on the crystallization process, which is one of the final stages in the manufacturing of medicines. The aims of the current study, thesis contribution and structure of the thesis report are discussed.

Chapter 2 reviews the relevant literature on pharmaceutical crystallization. The sub sections within this chapter consist of general concepts including definition of a crystal, phase diagram of a crystallization process, driving force for crystallization and different

methods of nucleation. Polymorphism is discussed together with the thermodynamics and kinetics of polymorphic systems. Various different PAT tools and solid state analytical (SSA) techniques are discussed. The important information that can be obtained about the crystallization process and crystalline product from each technique is mentioned.

Chapter 3 focuses on experimental materials and methods. Experiments performed at the 1 mL scale using the Avantium Crystal 16 equipment include solubility screening, slurry experiments and MSZW measurements. Gravimetric method for solubility determination is described. Cooling crystallization experiments at scales of 250, 750 and 1 L are discussed for model systems sodium benzoate and the isomers of amino benzoic acid (ABA). Other methods of crystallization described are the antisolvent crystallization of sodium benzoate and precipitation and evaporative crystallization experiments of ABA salts. Equipment used for solid state characterisation of the crystals is discussed.

Chapter 4 discusses the experimental results involving the use of PAT tools and SSA techniques for the monitoring of polymorphic transformations during the cooling crystallization of sodium benzoate in water. The PAT tool used for monitoring the solid phase within this study is the FBRM probe. These results highlight the importance of combining PAT tools and SSA techniques for discovering new polymorphic forms.

Chapter 5 discusses the experimental results for the antisolvent crystallization of sodium benzoate from an IPA/water mixture. PAT tools are used for monitoring the crystallization process and for detecting polymorphic transformations. PAT tools within this study include FBRM, ATR-UV/Vis and turbidity probe. A wide range of SSA techniques are used for analysing the crystal product, which provides supporting data on the existence of new undiscovered polymorphic forms.

Chapter 6 highlights the problems of crusting (solid depositing on vessel walls) occurring during a crystallization process which is supported with data obtained from PAT tools and SSA techniques. Data provided from these tools is shown to provide a deeper understanding of the crystallization process preventing the misinterpretation of results, saving both time and money.

Chapter 7 discusses the results obtained from meta-stable zone width (MSZW) experiments using the model systems of amino benzoic acid (ABA) isomers in water. A number of parameters were varied including ramp rate, agitator type, agitator speed and scale (1 mL and 1 L) to examine the effect of these on the MSZW. Combining the effect of all these parameters a robust MSZW region was obtained for the design of larger scale experiments. Calculations are presented on nucleation orders, enthalpy and entropy of dissolution within different crystallization set-ups to examine whether models using nucleation orders are system specific.

Chapter 8 presents the results on solid state characterisation of salts using a range of SSA techniques. The model systems used are *para*- and *meta*-amino benzoic acid (ABA). A range of acids and bases were used to produce the salts including hydrochloric acid (HCl), hydrobromic acid (HBr), sulphuric acid (H₂SO₄), phosphoric acid (H₃PO₄), sodium hydroxide (NaOH) and potassium hydroxide (KOH). Different methods are used to crystallize the salts to examine the best method of producing quality crystals. These methods include cooling, precipitation and evaporation. Structural differences between the HBr and HCl salts of *para* and *meta*-ABA are examined using XRPD to determine whether these are iso-structural.

Chapter 9 presents the experimental results on pH controlled polymorphic crystallization using the zwitterionic model systems *meta*- and *para*-ABA. Combinations of five PAT tools were used to monitor the crystallization process including FBRM, ATR-UV/Vis, PVM, pH and temperature probe. pH of solution and solvent were varied to identify the conditions under which certain forms of the salts form. SSA techniques are used to characterise the crystal products and provide the experimental conditions for which the different polymorphic forms of *meta*-ABA crystallize.

Chapter 10 gives an overall conclusion of all the results discussed within this thesis and a recommendation for future experiments based on the results.

Chapter 2. Literature review

2.1 Definition and detection of a crystal

Crystallization is referred to as a purification technique which involves the formation of a solid from a solution or vapour (Davey and Garside, 2000). A solid is classified by how the constituent molecules, atoms or ions are packed together. There are two solid forms known as crystalline and amorphous. Crystalline solids have an internal structure where the atoms, molecules or ions (growth units) are arranged into a specific order. This order continues throughout the crystal structure over many atomic lengths resulting in long range order. The number of molecules that make up this order can be as much as 10^{20} , which are of specific molecular sizes. No matter how many times the crystallization process is repeated for the same compound, it will result in the same internal structure making this a very unique and powerful technique for obtaining purified products with specific properties (Davey and Garside, 2000). Random distribution of atoms, molecules or ions results in amorphous solids that only have short range order. The arrangement of atoms affects the internal crystal structure and hence the physical properties. These include growth and dissolution rates of particular crystal faces, habit, refractive indices, thermal and electrical conductivity. Crystalline solids are referred to as anisotropic as the properties vary according to the direction in which they are measured. The opposite is true for amorphous solids which are referred to as isotropic (Mullin, 2001). Typical detection of crystalline solids is carried out using differential scanning calorimetry (DSC) for the indication of a sharp and specific melting point and the use of X-ray powder diffraction (XRPD) resulting in a specific powder diffraction pattern (Davey and Garside, 2000).

2.2 Crystal systems and lattices

Crystals are highly ordered crystalline solids with specific arrangement of molecules. A single unit cell is the building block for a crystal (see Figure 2.1). Various lattice parameters including the length of axes and the angles between the axes are used to characterise the crystal.

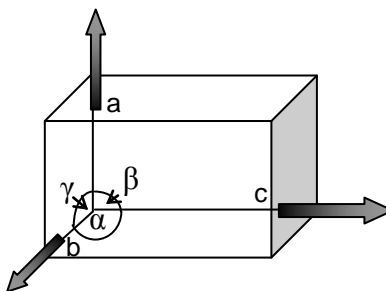


Figure 2.1. A single unit cell. Length of axes: a, b and c. Angles between the axes: α , β and γ (Myerson, 2002)

A single crystal is made up of many unit cells combined together. The internal structure of the crystal affects the lattice parameters, which then affect the degree of symmetry. Crystals are classified into specific crystal systems according to the degree of symmetry. The types of symmetry include symmetry about a point, line or plane (Jones, 2002). There are seven different crystal systems, which are characterized with specific axes lengths and angles between the axes. These are cubic, tetragonal, orthorhombic, monoclinic, triclinic, trigonal, and hexagonal. Within some crystal systems the molecules can be arranged into different positions within the crystal lattice resulting in space lattices. Each molecule within the space lattice is subject to identical environmental conditions resulting in a homogenous structure (Mullin, 2001). Figure 2.2 shows the four different types of space lattices known as primitive (P), end-centred cube (E), body-centred cube (B) and face-centred cube (F).

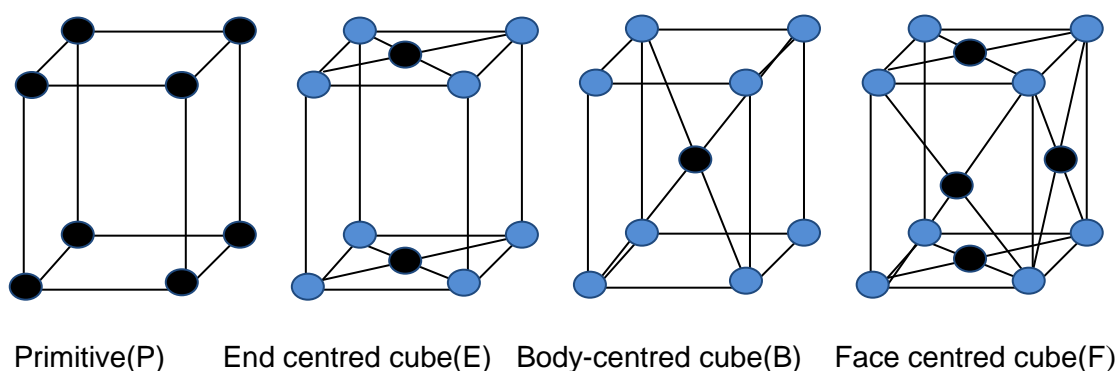
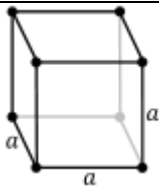
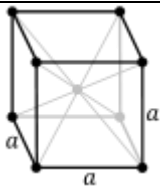
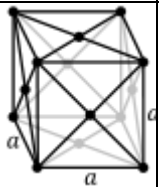

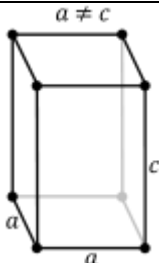
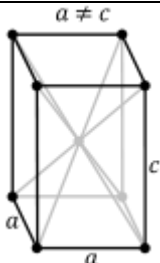


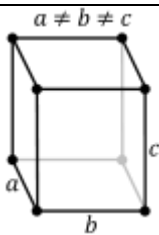
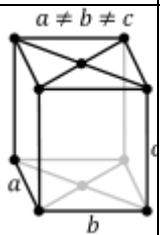
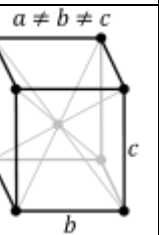
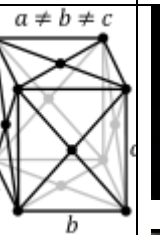

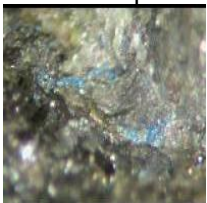
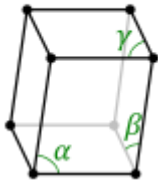
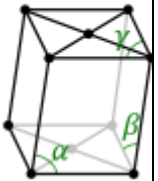

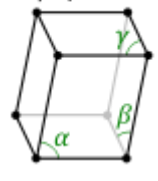

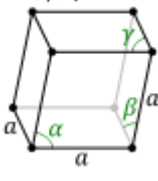
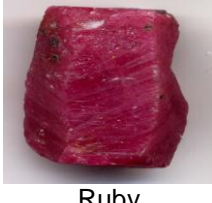

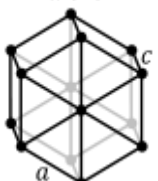



Figure 2.2. Various forms of space lattices

There are 14 possible Bravais lattices, which include the various different forms of space lattices within the 7 different crystal systems (Jones, 2002). These 14 Bravais lattices are shown in Table 2.1 together with crystals that resemble that specific crystal system.

Table 2.1. 14 Bravais lattices and examples of crystals resembling particular crystal systems (Crystal Structure, 2010; Mineralogy Database, 2010; Minerals by name, 2010)

Crystal system (Length of axes and angles between axis: α, β, γ)	Bravais lattice				Crystal example
	(P)	(E)	(B)	(F)	
Cubic (All lengths the same $: a = a = a$) $\alpha = \beta = \gamma = 90^\circ$					 Sodium chloride
Tetragonal Lengths: $a = a \neq c$ Angles: $\alpha = \beta = \gamma = 90^\circ$					 Rutile  Zircon
Orthorhombic Lengths: $a \neq b \neq c$ Angles: $\gamma = \beta = \alpha = 90^\circ$					 Hemimorphite  Empressite

Monoclinic Lengths: $a \neq b \neq c$ Angles: $\alpha = \beta = 90^\circ \neq \gamma$	$\alpha \neq 90^\circ$ $\beta, \gamma = 90^\circ$ 	$\alpha \neq 90^\circ$ $\beta, \gamma = 90^\circ$ 			 Kinoite
Triclinic Lengths: $a \neq b \neq c$ Angles: $\alpha \neq \beta \neq \gamma \neq 90^\circ$	$\alpha, \beta, \gamma \neq 90^\circ$ 				 Copper sulphate
Trigonal (Rhombohedral) Lengths: $a = a = a$ Angles: $\alpha = \beta = \gamma \neq 90^\circ$	$\alpha, \beta, \gamma \neq 90^\circ$ 				 Ruby  Quartz
Hexagonal Lengths: $a \neq c$ Angles:	$a \neq c$ 				 Graphite

2.3 Phase equilibria and crystallization methods

2.3.1 Introduction

A good understanding of the crystallization process is required so it can be controlled to produce a product, which has specific physical properties. This requires knowledge of under what conditions (temperature, pressure and composition) certain phases will be

present. Information obtained from the phase rule and diagram is important for ensuring the manufacturing process runs efficiently leading to the production of quality product.

2.3.2 Phase rule

The phase rule gives an indication of how many variables can be changed for the system to remain in the same phase (Davey and Garside, 2000). This is expressed as the degrees of freedom (F) and is shown in the following equation:

$$P + F = C + 2 \quad (2.1)$$

where P is the number of phases and C is the number of components within a system.

A pure system such as water contains only one component ($C = 1$). There are three possible phases of water, which are ice, liquid water and water vapour giving a value of $P = 3$. Substitution of these values into Equation (2.1) results in zero degrees of freedom. This indicates that in order for all three phases to coexist and be in equilibrium only one set of conditions of temperature and pressure can be applied. This system is referred to as invariant (Mullin, 2001). For a two phase system such as liquid water and water vapour the degrees of freedom is 1. Only one variable, either temperature or pressure, can be varied for the two phases to coexist in a stable state. The system is referred to as a univariant (Mullin, 2001). For a single phase such as liquid water the degrees of freedom is 2. Temperature and pressure are independent, which indicates that the system will remain in the liquid phase if there is a change in both variables. This system is referred to as bivariant (Mullin, 2001).

2.3.3 Phase diagrams

Phase diagrams show under what sets of conditions certain phases will exist and the equilibrium conditions for certain phases to coexist. A system that is in equilibrium is in a state of rest (stable state) and the chemical potential of the phases are the same (Smith, 1990). By changing any of the variables a new equilibrium is established.

An essential requirement for the crystallization process is a supersaturated solution. This is the driving force for crystallization (Collins *et al.*, 1997). The supersaturation can be expressed in a number of ways. In thermodynamics terms the supersaturation is referred to as the difference in chemical potential ($\Delta\mu$) between a molecule in a supersaturated state (μ_{ss}) and a molecule in an equilibrium state (μ_{eq}) (Davey and Garside, 2000):

$$\Delta\mu = \mu_{ss} - \mu_{eq}. \quad (2.2)$$

For a pure substance the chemical potential is expressed as the free energy per mole:

$$\mu = \frac{G}{n_i}, \quad (2.3)$$

where G is the Gibbs free energy and n_i is the number of moles of component i .

For a non-ideal system the interactions between the molecules in solution are taken into account and the concentration of solute in solution is replaced by an effective concentration known as the activity. An equation relating the chemical potential of a component in solution to its activity is shown in the following Equation (Smith, 1990):

$$\mu_i = \mu_i^o + RT \ln a_i, \quad (2.4)$$

where R is the gas constant, T is the temperature and a_i is the activity of component i and μ_i^o is the standard chemical potential of component i at 1atm pressure. For molecules in an equilibrium state and a supersaturated state the following chemical potential expressions are obtained:

$$\mu_{ss} = \mu_i^o + RT \ln a_{ss}, \quad (2.5)$$

$$\mu_{eq} = \mu_i^o + RT \ln a_{eq}. \quad (2.6)$$

Substitution of Equation (2.5) and (2.6) into Equation (2.2) results in the following Equation:

$$\mu_{ss} - \mu_{eq} = \Delta\mu = RT \ln \left(\frac{a_{ss}}{a_{eq}} \right). \quad (2.7)$$

Rearrangement of Equation (2.7) gives:

$$\frac{\Delta\mu}{RT} = \ln \left(\frac{a_{ss}}{a_{eq}} \right). \quad (2.8)$$

Effective concentration known as activity (a) is related to the real concentration (c) by the following Equation (Smith, 1990):

$$a_i = \gamma_i c_i, \quad (2.9)$$

where c_i is the concentration of component i and γ_i is the activity coefficient.

For an ideal system the interactions and hence forces between all molecules are assumed to be the same (Smith, 1990). In this case $\gamma_i = 1$ and therefore $a_i = c_i$.

Substitution of this expression into Equation (2.8) gives:

$$\frac{\Delta\mu}{RT} = \ln \left(\frac{c_{ss}}{c_{eq}} \right), \quad (2.10)$$

where c_{eq} is the equilibrium concentration and c_{ss} is the supersaturated concentration.

Rearrangement of Equation (2.10) gives (Mullin, 2001):

$$\exp \left(\frac{\Delta\mu}{RT} \right) = \frac{c_{ss}}{c_{eq}} = S, \quad (2.11)$$

where S is referred to as the supersaturation ratio.

This equation shows how the chemical potential is related to the supersaturation ratio, which can be used to describe the driving force for crystallization. An alternative expression can be used which is shown in Equation (2.12):

$$\Delta c = c_{ss} - c_{eq}, \quad (2.12)$$

where Δc is the degree of supersaturation. This is known as the concentration driving force (Davey and Garside, 2000).

As the temperature is lowered there is a decrease in the solubility of solute in solution. The equilibrium concentration c_{eq} decreases and the supersaturation concentration c_{ss} increases. This results in an increase in the degree of supersaturation or saturation ratio. The difference in chemical potential ($\Delta\mu$) increases, as can be seen from Equation 2.11. This concludes that the driving force for crystallization increases when the temperature is lowered. This is illustrated in Figure 2.3 when moving from point 1 to 2 and as a result the system enters the metastable zone which is supersaturated.

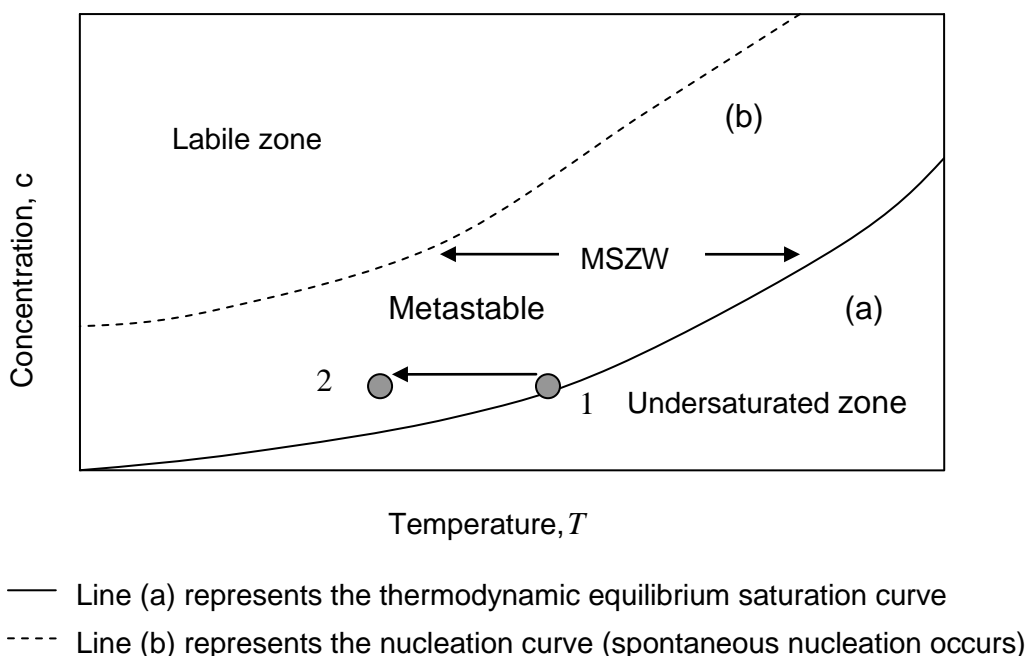


Figure 2.3. Phase diagram of concentration versus temperature showing the various regions within a crystallization process

The phase diagram shown in Figure 2.3 is typical for a crystallization process. There are three key regions, referred to as undersaturated, metastable and labile, which are separated by two curves known as the saturation (solubility) and nucleation curves. The saturation curve is fixed and is based on thermodynamics. It represents the maximum concentration (amount) of solute that can dissolve in the solvent for the system to be in thermodynamic equilibrium at a specific temperature. The region below this curve is referred to as undersaturated. The system is in a stable state and all solute present will dissolve in the solvent. The nucleation curve is kinetically controlled. This curve will vary by alteration to a number of parameters including agitation, cooling rates, impurities, reactor size, which can affect the rate of nucleation. Any point on the nucleation curve represents a system where the degree of supersaturation is high resulting in spontaneous nucleation. The region above the nucleation curve is referred to as the labile zone. Within this region nucleation occurs but too far from the nucleation curve can result in excessive nucleation leading to the production of many small nuclei. The region in between the saturation and nucleation curve is referred to as the metastable region. In this region the system is supersaturated. More solute is dissolved in solution than that at the equilibrium saturation value resulting in a metastable system. The difference between the two curves is known as the metastable zone width (Myerson, 2002; Yu *et al.*, 2007). Within this region crystal growth occurs and nucleation is negligible enabling control over the crystal size distribution (Collins *et al.*, 1997). For seeded systems which contain seeds of the crystals it is desirable to control within these sets of conditions in order to obtain large crystals (Collins *et al.*, 1997). For unseeded systems seeds have to be generated first, which involves passing the metastable zone until the nucleation curve is reached. The determination of the MSZW region of any solute/solvent system is important for the successful scale up of the crystallization process from lab to manufacturing scale. The metastable region can be determined by using the poly-thermal technique which requires heating and cooling a suspended solution at a range of cooling rates to obtain the spontaneous primary nucleation and solubility points (Nyvlt, 1968; Barrett and Glennon, 2002; Kubota, 2008). The nucleation point is obtained by finding the temperature of nucleation at zero cooling rate using an extrapolation method. Solvent is added to solution to lower the concentration and then the heating/cooling cycle procedure is repeated (Barrett and Glennon, 2002).

2.3.4 Crystallization methods

Within the phase diagram of concentration versus temperature the slope of the saturation (solubility) curve is an important indication of what the most suitable crystallization method is for a particular system. Solubility dependence on temperature for a variety number of components is shown in the Figure 2.4.

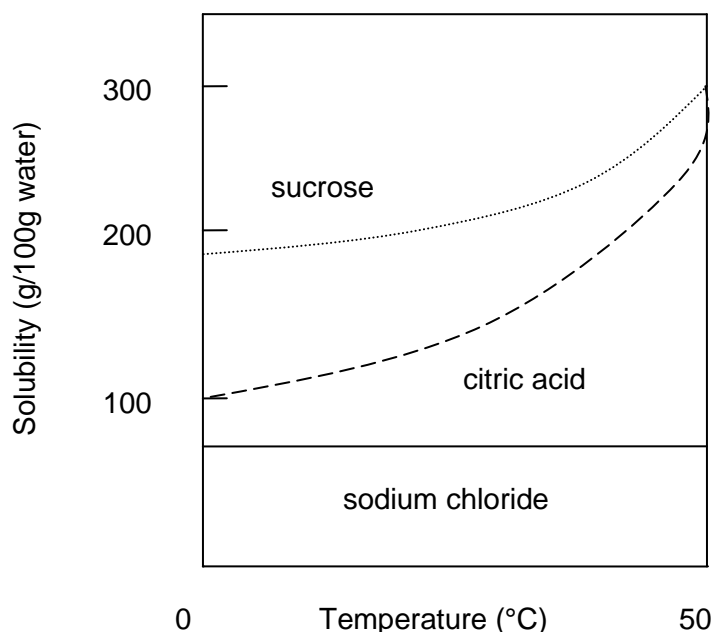


Figure 2.4. Solubility curve for sucrose, citric acid and sodium chloride in water (Davey and Garaside, 2000)

A flat solubility curve as that shown in Figure 2.4 for sodium chloride in water indicates that cooling crystallization is not a suitable method as the solubility does not change much with temperature. An alternative method of crystallization could be evaporative or antisolvent addition.

Antisolvent crystallization involves the addition of a third component to a saturated solution. The third component could be an impurity or a miscible non-solvent, which lowers the solubility of the solute in solution forming a supersaturated solution, which results in the crystallization of the compound (Davey and Garside, 2000; O'Grady *et al.*, 2007; Nagy *et al.*, 2008a). This provides the driving force for crystallization resulting in the formation of crystals. The antisolvent crystallization process must be designed so as to produce the drug with the desired properties. The choice of solvent (or

solvent mixture), dosing rate and initial concentration are factors known to affect the polymorphic form of the compound that crystallizes from solution (Davey, 2003; Davey and Garside, 2000; Kitamura and Sugimoto, 2003).

Both antisolvent and cooling crystallization methods have advantages and disadvantages. One advantage of the antisolvent crystallization method is that high degrees of supersaturation can be created within the solution (Myerson, 2002). This can result in the solute crystallizing out of solution, achieving high yields of the crystalline product that would otherwise not be possible within cooling crystallization. The disadvantage is that the too high supersaturation can lead to the system suddenly nucleating and crystallization occurs rapidly. This is known as precipitation. This can lead to the production of a large number of fine crystals resulting in problems in the downstream processing (Myerson, 2002). Another disadvantage of the antisolvent crystallization method is the cost of separating the two solvents at the end of the process for recovering/recycling and larger capital costs due to higher operating volumes than that required for cooling crystallization. However in some cases where the substances are heat sensitive antisolvent crystallization is preferred as it allows the crystallization process to occur at low ambient temperatures preventing decomposition of the product that would result in failed batches (Myerson, 2002). Recent researchers investigate new methods for cooling and antisolvent crystallization that will improve the quality of the product. Nagy *et al.* (2008a) developed a model-based combined technique for a combined cooling and antisolvent crystallization method, which simultaneously controls the temperature profile and antisolvent additional rate. The combined method improved the quality of the product by providing superior control of the crystal size distribution. Woo *et al.* (2009) investigates the use of concentration control within cooling and antisolvent crystallization experiments, which is proposed to increase the robustness of the process during scale-up. Hermanto *et al.* (2010) developed a modified method for unseeded antisolvent crystallization, which involved the use of the focused beam reflectance measurement to control the size of seed crystals. This method was shown to improve the robustness of product CSD measurements.

2.4 Nucleation

2.4.1 Introduction

Nucleation is the first stage involved in the formation of crystals. This involves the generation of small seed crystals (nuclei) that then grow to form crystals of detectable size. There are different methods involving the generation of the seed crystals including primary and secondary nucleation. The various different forms of nucleation are shown in Figure 2.5. An essential requirement for nucleation is a supersaturated solution (Mullin, 2001). The higher the degree of supersaturation the larger the driving force for nucleation and hence the rate of nucleation is greater. Nuclei exposed to a supersaturated solution are in an unstable state and will either grow or dissolve to reduce the excess Gibbs free energy in order to reach thermodynamic equilibrium.

The time that elapses between forming a supersaturated solution and the appearance of the crystals is referred to as the induction period. This includes the time it takes to form clusters, which grow to the critical size and continue to grow until they are of size detectable by optical probes or by sight (Mullin, 2001).

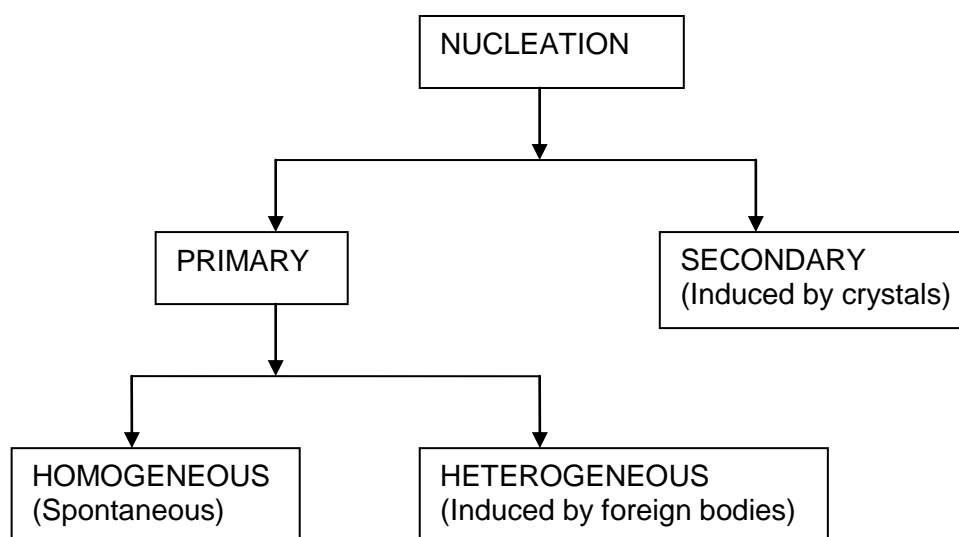


Figure 2.5. A flow chart of the different forms of nucleation

2.4.2 Primary nucleation

Primary nucleation is sub divided into homogeneous and heterogeneous nucleation. Homogeneous (spontaneous) nucleation involves the formation of a new solid phase from a supersaturated solution. This requires energy and is achieved through transfer of energy due to random collisions between molecules. During this process the molecules form clusters, which then grow to a critical size, which is stable in the supersaturated solution. The molecules arrange themselves into a specific order resulting in a specific crystal lattice structure. The process is shown in Figure 2.6.

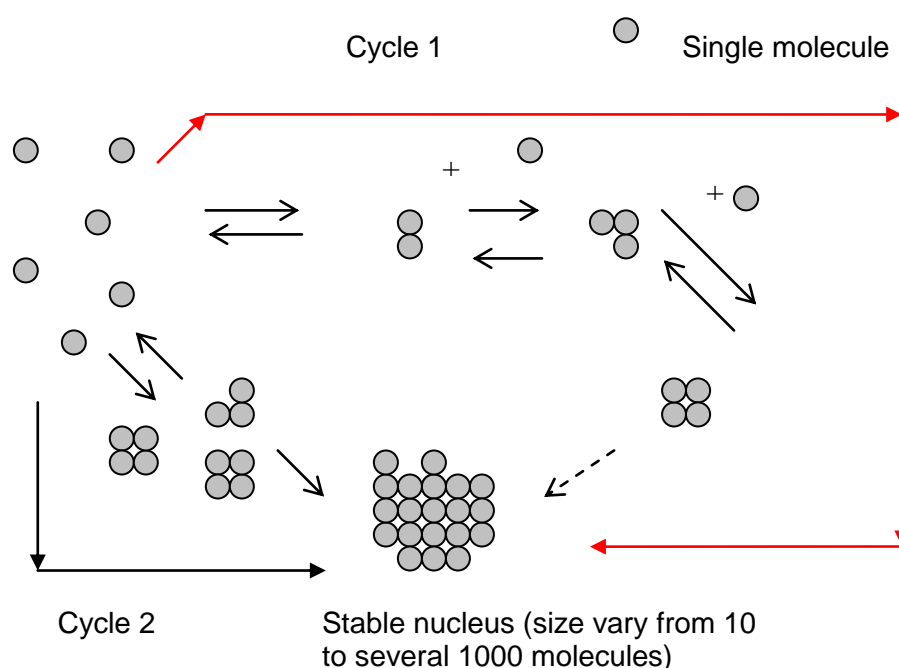


Figure 2.6. Two possible paths for the formation of a critical size (stable) nucleus

In Figure 2.6 cycle 1 represents the formation of a critical size (stable) nucleus through a sequence known as biomolecular addition (Mullin, 2001), whereas cycle 2 represents the formation of critical size (stable) nucleus through the aggregation of clusters. The formation of a critical size nucleus is more likely to occur by cycle 2. Any further molecular additions will result in the formation and growth of the nucleus (crystal growth).

Upon collision in order for the molecules to join together they must have enough energy to overcome the repulsive forces that arise due to the interfacial tension between the different phases-solid and liquid. As the surface area of the molecular clusters increase the interfacial tension increases resulting in more energy required to hold the molecules together. Therefore a critical size nucleus is obtained within local regions of the solution where the degree of supersaturation is high (energy levels are high).

During the formation of the stable nucleus in a homogeneous fluid there is a free energy change (ΔG). The overall excess free energy change is a sum of the change in the surface excess free energy and volume excess free energy (Mullin, 2001):

$$\Delta G = \Delta G_s + \Delta G_v , \quad (2.13)$$

where ΔG_s is the free energy change involved in developing a new surface within a supersaturated solution. This requires energy and is therefore a positive quantity. The term ΔG_v is the free energy change involved in the formation of a solid from a supersaturated solution. Volume change results in a release of free energy, therefore this quantity is negative.

During the formation of a critical size nucleus the Gibbs free energy change (ΔG) passes through a maximum called ΔG_{crit} . This is the amount of energy that must be absorbed by the system in order to form the critical size of the nucleus r_c . If the radius is below the critical value then the newly created crystalline lattice structure will re-dissolve and if it is above then it will grow. Both processes will result in a decrease in free energy of the particle. This is represented in Figure 2.7.

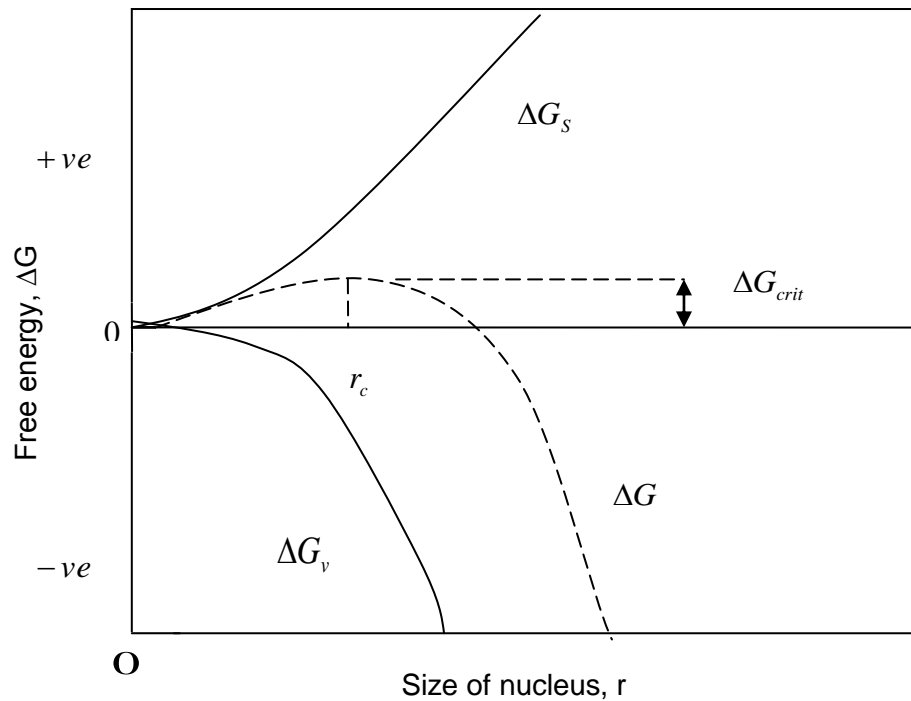


Figure 2.7. Free energy diagram for nucleation explaining the existence of a ‘critical nucleus’ (Mullin, 2001)

Once a nucleus of critical size is reached it will grow to form crystals. The rate at which this occurs is referred to as the rate of nucleation (J). This is defined as the number of nuclei formed per unit time per unit volume:

$$J = A \exp(-\Delta G / kT), \quad (2.14)$$

where A is the Arrhenius pre-exponential factor, k is the Boltzmann constant and T is the temperature. The term ΔG_{crit} is the critical Gibbs free energy and is defined as:

$$\Delta G_{crit} = \frac{16\pi\gamma_T^3 \nu^2}{3(kT \ln S)^2}, \quad (2.15)$$

where γ_T is the interfacial tension, ν is the molecular volume and S is the supersaturation ratio which is defined in Equation (2.11). Substitution of Equation (2.15) into Equation (2.14) gives (Mullin, 2001):

$$J = A \exp \left[\frac{16\pi\gamma_T^3 V^2}{3k^3 T^3 (\ln S)^2} \right]. \quad (2.16)$$

Equation (2.16) expresses the rate of nucleation for spontaneous nucleation. The three major factors that affect the rate of nucleation are temperature (T), degree of supersaturation (S) and interfacial tension (γ_T).

An increase in the degree of supersaturation results in both a decrease in the critical size of the nucleus and the energy required to form it. The rate of nucleation increases. Once some critical value of supersaturation is exceeded this results in a rapid increase in the rate of nucleation as represented in Figure 2.8. From this the nucleation curve on the phase diagram of concentration versus temperature is obtained and hence the MSZW can be determined.

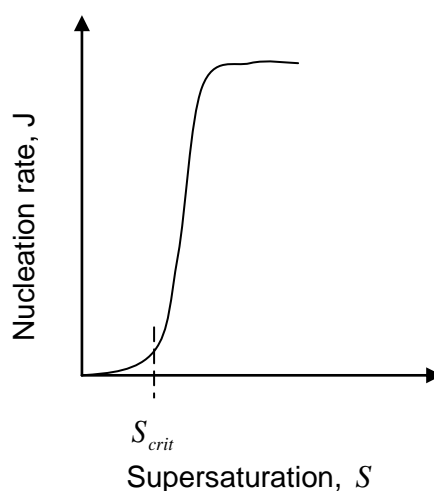


Figure 2.8. Effect of the degree of supersaturation on the nucleation rate

By changing the temperature it alters the degree of supersaturation and is therefore used to control the rate of the nucleation. At lower temperatures both the critical size of the nucleus and the energy required to form this is lower as shown in Figure 2.9. Lower energy processes are favoured resulting in an increase in the rate at nucleation when the system has been cooled down to a lower temperature.

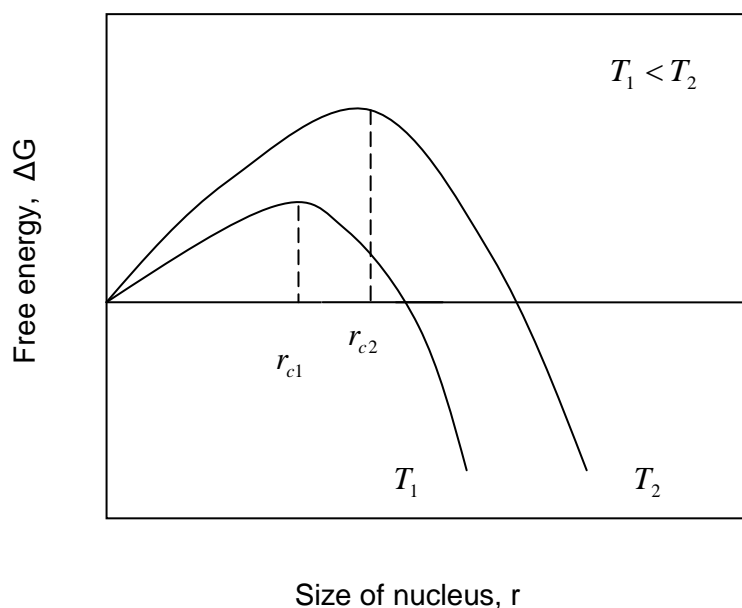


Figure 2.9. Effect of the temperature on the critical size nucleus and the Gibbs free energy change of formation (Mullin, 2001)

Heterogeneous nucleation is the other form of primary nucleation. Nucleation is induced by the presence of impurities. The formation of a solid nucleus from solution takes place on a solid surface. The presence of impurities can either enhance or inhibit the nucleation process. Enhancing the nucleation process results in nucleation occurring at lower degrees of supersaturation and a lower Gibbs free energy change compared with spontaneous nucleation. The nucleation curve is closer to the saturation curve and hence the MSZW is narrower.

2.4.3 Secondary nucleation

Nucleation that occurs within a solution that contains seed crystals that are the same as the crystals that will crystallize out of solution is referred to as secondary nucleation. Nucleation will occur at lower degrees of supersaturation compared to primary nucleation and hence the MSZW will be narrower. Seeded crystallization is widely used in industry at large scale production. It is used to control the crystal size, size distribution and polymorphic form (stable or meta-stable form), which affect the quality of the product (Zencirci *et al.*, 2009; Doki *et al.*, 2004; Beckmann, 2000; Hojjati and Rohani, 2005; Lung-Somarriba *et al.*, 2004). Properties of seeds including seed surface

area, mean size and seed loading are important to consider when designing a crystallization process as optimisation of these parameters can increase the likelihood of producing a quality product (Hojjati and Rohani, 2005; Lung-Somarrriba *et al.*, 2004).

There are many different mechanisms by which secondary nuclei are produced. These include ‘initial’ breeding, ‘polycrystalline’ breeding, ‘needle’ breeding (shear nucleation) and ‘collision’ breeding (contact nucleation). Dry seed crystals may contain dust particles at the surface. Once introduced into a solution, these particles can be swept off from the surface leading to secondary nuclei. Crystals with needle morphology have a weak structure. Agitation can lead to breakage and fragmentation of the needles resulting in polycrystalline breeding. Any weak outgrows from the crystal surface can be removed due to fluid shearing across the crystal surface. This occurs within an agitated vessel and the weak outgrows act as secondary nuclei. This is known as needle breeding. Contact nucleation is one of the most important mechanisms for the production of secondary nuclei (Garside *et al.*, 2002).

For contact nucleation, crystal fragments are produced due to the collisions between crystals, crystal-agitator and crystals and vessel wall. Upon collision there is a transfer of energy resulting in fragments that may contain many dislocations. These fragments tend to grow slower than larger nuclei. Fragments of all different sizes will be produced. The smaller fragments may be unstable in the supersaturated solution and will only become stable if swept into a region where the degree of supersaturation (Δc) is high.

The rate of secondary nucleation (B) is affected by three main factors. These include the degree of supersaturation (Δc), the concentration of seed crystals present in the supersaturated solution (M_T) and the interactions between the crystals and solution expressed as either stirrer speed (N) or power input into the solution (ε) (Davey and Garside, 2000):

$$B = k_b M_T^j N^k \Delta c^b, \quad (2.17)$$

where k_b is the rate constant for secondary nucleation.

Previous researchers involve the use of population balance modelling to developed correlations relating secondary nucleation to a number of different parameters to those expressed in Equation (2.17). Chianese *et al.* (1993) and Matthews *et al.* (1996) expressed secondary nucleation rate as a function of nucleation rate constant, supersaturation ratio, moment of the crystal size distribution, and minimum size of crystals for collisions to produce secondary nuclei. However these expressions did not include stirrer speed or concentration of crystals in suspension. Van Der Heijden *et al.* (1994) includes a new parameter in the expression for secondary nucleation that is not included by the researchers mentioned previously, which is the number of parent crystals per unit volume. The parameters mentioned in these expressions affect the secondary nucleation rate by a number of different ways.

As the stirrer speed increases the thickness of the fluid boundary layer around the blade of the agitator decreases resulting in an increase in the number of agitator and crystal collisions. More fragments are produced leading to higher nucleation rates. As the number of crystals in suspension increases this increases the frequency of collisions leading to more crystal fragments and hence higher nucleation rates. The size of the seed crystals may have an influence on the nucleation rate. Larger seeds have higher contact probabilities and collision energies resulting in higher nucleation rates. Small seeds may circulate in fluid eddies which are created in an agitated system. These act as a stagnant fluid resulting in no collisions (Mullin, 2001).

Contact nucleation is not the only mechanism by which crystal fragments are produced. Adsorption of impurities onto the crystal surface can lead to an increase in internal stress as the crystal grows. This can lead to breakage and the formation of fragments (secondary nuclei) (Mullin, 2001).

2.5 Polymorphism

2.5.1 Introduction

Polymorphism has been a key area of research related to the pharmaceuticals over the last 40 years (Pudipeddi and Serajuddin, 2005). Polymorphs are defined as crystals with

the same chemical composition but have different arrangement of molecules. This affects the structure of the crystal and hence the types of bonds formed between the molecules resulting in different physico-chemical properties. These include melting point, density, electrical and thermal conductivity, stability, solubility, dissolution rates and bioavailability (Cote *et al.*, 2009; Beckmann 2000; Hilfiker 2006; Bernstein 2002, Yu *et al.*, 2004). Compounds are often crystallized as salts to overcome problems with solubility, dissolution rate, stability and hygroscopicity (Forbes *et al.*, 1992, Haynes *et al.*, 2005). Reports state that 50% of pharmaceutical drug products are crystallized as salts (Kumar *et al.*, 2009). Structural differences between the different polymorphic forms affect the morphology of the crystals. This can affect the downstream processing involving filtration and washing (Davey and Garside, 2000). Many compounds are known to have different polymorphic forms that can transform during the crystallization process, downstream processing (filtration, washing and drying) or during storage in the solid state. Polymorphic transformations that occur in solution are referred to as solvent mediated. These types of transformations are more common than solid state transformations. To prevent polymorphic transformations it is essential to know all the possible polymorphic forms of an active pharmaceutical ingredient (API) and under which conditions different polymorphic forms are favoured. This is required so the process can be controlled to produce the desired polymorph with specific physical properties.

A poor understanding of the crystallization process can lead to the production of undesired polymorphs, which would result in an increase in economical costs (Davey, 2003). This is a key area for further research as it is estimated that for the production of about 80% of all pharmaceutical products, a crystallization step will be required (Reutzel-Edens, 2006). Model based approaches have also been proposed, which describe the polymorphic transformation using population balance approaches and introduce innovative control methods for better consistency in polymorphic purity (Ono *et al.*, 2004; Hermanto *et al.*, 2007; Hermanto *et al.*, 2009).

2.5.2 Classification of polymorphs

A large proportion of pharmaceutical products contain the API in the crystalline form. There are three different classes known as anhydrates, hydrates and solvates (Vippagunta *et al.*, 2001). To distinguish hydrates and solvates from the anhydrate forms of a crystalline compound the term pseudo-polymorphs is used (Vippagumta *et al.*, 2001). These contain additional molecules within the crystal structure compared to the anhydrate forms, which are known as polymorphs. If these molecules are water then the crystalline form is referred to as a hydrate and if it contains the solvent molecules other than water it is referred to as a solvate (Khankari and Grant, 1995). The presence of pseudo-polymorphs within organic compounds is of very high importance within the pharmaceutical industry as these have different physical properties which will affect the quality of the product (Bechtloff *et al.*, 2001).

Anhydrate forms are referred to as polymorphs, which can consist of ions, atoms (elements) or molecules. Crystallization of a compound into different forms, which contains only one element, is referred to as allotropy (Mullin, 2001). A common example of this is diamond and graphite where the chemical element is carbon.

Each carbon atom in diamond is covalently bonded to four other carbon atoms resulting in a regular crystal lattice structure. Each carbon atom in graphite is bonded to three other carbon atoms resulting in a hexagonal crystal lattice structure with a free electron that can move between the layers. This affects the physical properties resulting in diamond having a high tensile strength and hard, while graphite is weak and brittle (Fontana, 1987). Structural differences between allotropes/polymorphs affect the morphology and appearance of the crystals. This is clearly seen in the case of diamond and graphite, where diamond has a shiny appearance and in a pure state is transparent while graphite can appear dull and black in colour. Structural differences between polymorphs also affect the stability of the different forms. Graphite is the more thermodynamic stable form at conditions at the earth surface but the rate of transformation from diamond to graphite is very slow (Bernstein *et al.*, 1999).

Hydrates are classified into different groups according to the arrangement of water molecules within the crystal lattice structure and the bonding between the molecules. Due to the presence of water this will result in hydrogen bonds forming and these bonds are maximised within a hydrate (Gillon *et al.*, 2003). Reports state that 33.3% of pharmaceutical compounds are known to form hydrates (Gillon *et al.*, 2003). The types of hydrate formation are classified into three groups including isolate, channel and metal-ion coordinated hydrates (Gillon *et al.*, 2003; Lester *et al.*, 2006; Brittain, 1999). A schematic of the channel and isolate hydrates are shown in Figure (2.10). Isolated hydrates contain water molecules which are isolated from each other within the crystal lattice structure (Gillon *et al.*, 2003). Hydrogen bonds occur between the water and solute molecules within isolate hydrates (Brittain, 1999). Channel hydrates contain channels of water molecules within the crystal lattice structure occupying specific sites (Kennedy *et al.*, 2003; Brittain *et al.*, 1999). These water molecules can be easily lost from the structure resulting in dehydration occurring at low temperature of below 100 °C and the crystal lattice structure can remain intact (Redman-Furey *et al.*, 2005; Lester *et al.*, 2006). These hydrates are also known as non-stoichiometric hydrates in which the ratio of water to drug molecule is not an integer value and generally is less than 1 (Hilfiker, 2006). At high relative humidities expanded hydrates may form if additional water molecules are taken up in the channels within the lattice (Brittain, 1999). Ion-coordinated hydrates contain water molecules, which form bonds with the metal ion. These bonds are very strong resulting in a high temperature required for dehydration (Redman-Furey *et al.*, 2005).

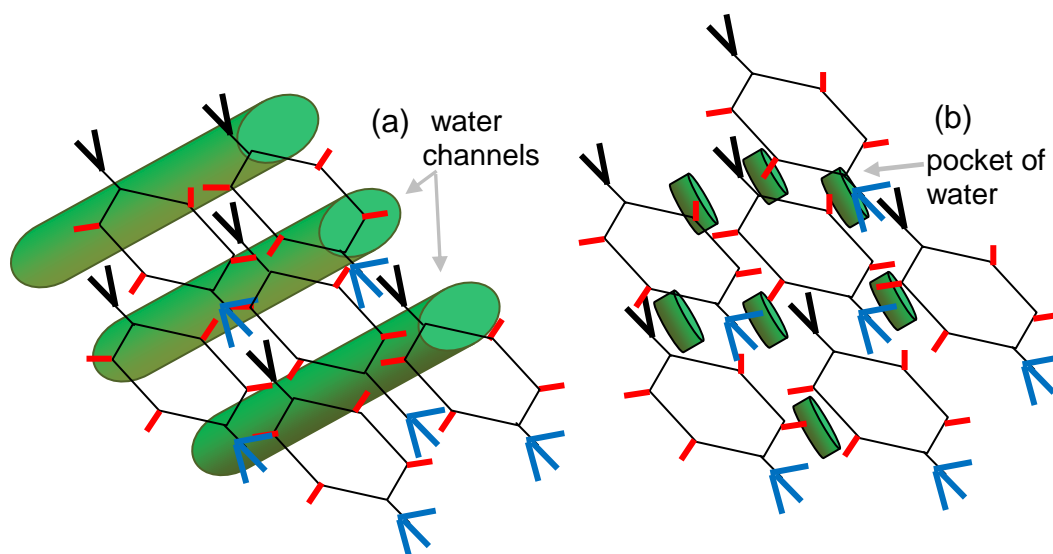


Figure 2.10. Schematic of (a) channel hydrate and (b) isolate hydrate

2.5.3 Thermodynamics of polymorphism

Thermodynamics is an important factor to consider in determining the stability of polymorphs within a given system as this will have an influence on which polymorph crystallizes out of solution. The polymorph that has the lower Gibbs free energy is the more thermodynamically stable form. An expression for the Gibbs free energy at constant pressure is shown in Equation (2.18) (Smith, 1990):

$$\Delta G = \Delta H - T\Delta S, \quad (2.18)$$

where T is the temperature, ΔH is the enthalpy change and ΔS is the entropy change.

Polymorphic transformations will involve enthalpy and entropy changes, which will either be positive or negative quantities. Positive enthalpy changes indicate heat has been absorbed and a negative enthalpy change indicates heat has been released. Entropy measures the change in disorder of the system. A polymorphic transformation that results in an increase in disorder has a positive entropy value. These are known as order-disorder transformations (Davey and Garside, 2000). A useful set of thermodynamic rules, which involve measurements of enthalpy and entropy, can be applied to a polymorphic system that enables the nature (monotropic or enantiotropic) and stability order of the polymorphs to be determined (Burger and Ramberger, 1979). These thermodynamic rules include heat of transition, heat of fusion, density and the infrared rule. Burger and Ramberger (1979) reports that for the heat of transition rule an endothermic transition indicates the two polymorphs are enantiotropic related and an exothermic transition indicates the two forms are monotropic related. The heat of fusion rule states that if the higher melting form has a higher heat of fusion then the two forms are usually monotropic related, otherwise they are enantiotropic. The density rule states that if one polymorphic form has a higher density than the other, it can be assumed to be more stable at absolute zero.

A system containing two polymorphs is referred to as dimorphic. As mentioned previously the nature of the system can be classified as either monotropic or enantiotropic, which depends on how the stability of the polymorphs changes with

temperature (Lin *et al.*, 2007). For a monotropic system the order of stability of the polymorphs does not change with temperature. Polymorphic transformations are irreversible (Bernstein *et al.*, 1999). For an enantiotropic system a change in temperature can result in a change in stability of the polymorphs. Polymorphic transformations are reversible (Reutzel-Edens, 2006). Figure 2.11 illustrates a monotropic and enantiotropic system for a compound containing two polymorphs (A and B).

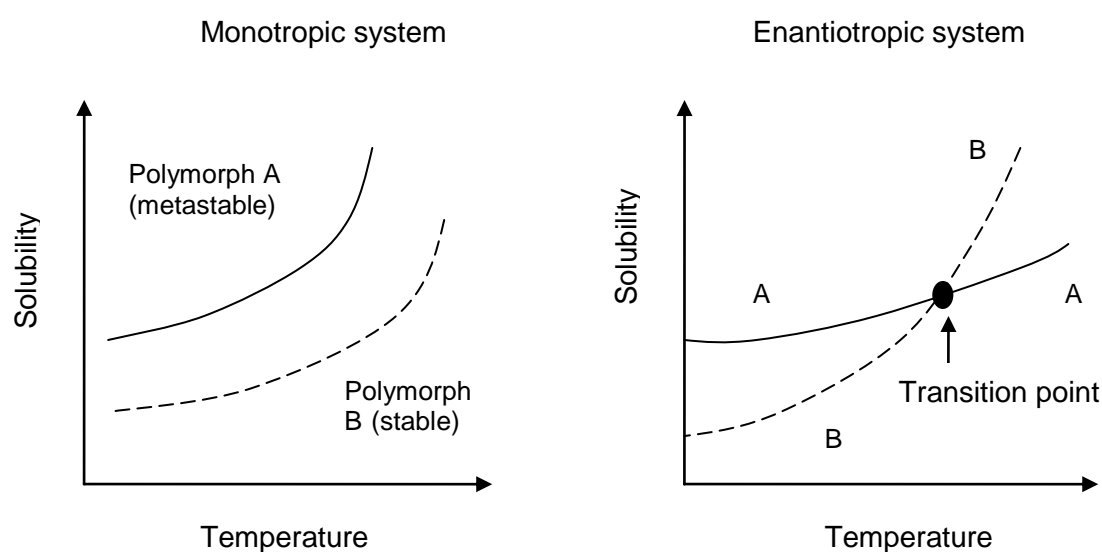


Figure 2.11. Phase diagrams for a compound containing two polymorphic forms (dimorphic) showing a monotropic and enantiotropic system

For the monotropic system polymorph B is the stable polymorph at all temperatures. For the enantiotropic system at low temperatures below the transition point polymorph B is the more thermodynamic stable form. For temperatures above the transition point polymorph A is the more thermodynamic stable form. At the transition point the stability of the two polymorphs is the same and the system is in thermodynamic equilibrium (Bechtloff *et al.*, 2001).

Phase diagrams provide the link between solubility and stability of different polymorphs of a given system. The solubility of the polymorphs is an important parameter to consider as this affects the dissolution rate and bioavailability, which

affects the quality of the product. The polymorph with the lower solubility is the more stable form (Bechtloff *et al.*, 2001).

The polymorph with the lower Gibbs free energy is the more stable form and hence its chemical potential is lower. The relationship between the chemical potential of each polymorph in its solid state is shown in Equation (2.19) (Smith, 1990):

$$\mu_s(B) < \mu_s(A), \quad (2.19)$$

where μ_s refers to the chemical potential of a particular polymorph in its solid state. Equation (2.19) indicates that polymorph (B) is more stable due to its lower chemical potential.

The chemical potential of the solute of a particular polymorph in a saturated solution is shown in Equations (2.20 and 2.21), for ideal systems:

$$\mu_{eq}(B) = \mu^o + RT \ln c_{eq}(B), \quad (2.20)$$

$$\mu_{eq}(A) = \mu^o + RT \ln c_{eq}(A), \quad (2.21)$$

where μ_{eq} is the chemical potential of a polymorph in a saturated equilibrium state within a solution, R is the gas constant, T is the temperature, μ^o is the standard chemical potential at 1 atm pressure and c_{eq} is the equilibrium concentration.

For a solid of polymorph B to coexist and be in equilibrium with a saturated solution of polymorph B, the two phases must have the same chemical potential. This also applies for polymorph A :

$$\mu_{eq}(B) = \mu_s(B), \quad (2.22)$$

$$\mu_{eq}(A) = \mu_s(A). \quad (2.23)$$

Substitution of these expressions into Equations (2.20) and (2.21) gives the following:

$$\mu_s(B) = \mu_{eq}(B) = \mu^o + RT \ln c_{eq}(B), \quad (2.24)$$

$$\mu_s(A) = \mu_{eq}(A) = \mu^o + RT \ln c_{eq}(A). \quad (2.25)$$

Substitution of these expressions into Equation (2.19) gives the following:

$$c_{eq}(B) < c_{eq}(A). \quad (2.26)$$

By comparing Equations (2.19) and (2.26) it shows that the polymorph, which has a lower Gibbs free energy also has a lower saturation concentration. This results in the less soluble polymorph being the more stable form.

The phase diagrams provide important information on the solubility difference between the polymorphs, which is the driving force for phase transformations (Brittain, 1999). These also provide the required operating conditions of the crystallization process in order to produce the desired polymorph. Solubility studies on a range of compounds containing polymorphs were carried out by Pudipeddi and Serajuddin, (2005). The results obtained in most cases showed a solubility ratio between the polymorphs of a value of 2 or lower indicating a small solubility difference between the polymorphs. For these cases it indicates that the presence of different polymorphs will not have any significant effect on the dissolution rate and hence bioavailability. However the importance of control within the crystallization process is essential to ensure a robust manufacturing process that will produce a pure product (Reutzel-Edens, 2006). Within industry the stable polymorph is usually the common choice for the large scale manufacturing of the API as this reduces the likelihood of polymorphic transformation during storage (Gu *et al.*, 2001). A robust crystallization process was designed for the production of the desired stable polymorph within an enantiotropic system by Muller *et al.* (2006). A compound produced from Novartis was used as the model compound. This was achieved through the use of solubility tests in various solvents. Information obtained from the studies included solubility data, possible polymorphic forms and transition temperature between the two polymorphic forms. This provided the information for the conditions required to operate the crystallization process so as to prevent the system from being supersaturated with respect to the undesired polymorph.

A combined method of seeding at low supersaturated solution following by moderate cooling was used to produce the stable desired polymorph (Muller *et al.*, 2006).

There are some cases where the metastable polymorphic form of an API may be desirable as these may have faster dissolution rates and properties resulting in the manufacturing process being more efficient. This was found to be the case for the API of Ritonavir. The metastable form I had faster dissolution rates compared to the stable form II, shorter processing time and a more effective separation of impurities in the crystallization step (Muller *et al.*, 2006).

Within each system, monotropic and enantiotropic, there is a different method that can be used for the formation of the metastable polymorph. Rapid cooling within the monotropic system will lead to the system being supersaturated with respect to both polymorphs and if the energy barrier required for formation of metastable polymorph is lower then this will form. A change in temperature within an enantiotropic system will result in a change in the stability of the polymorph resulting in the formation of a metastable polymorph. Once obtained the metastable polymorph the problem arises of how to prevent conversion into the stable form. Davey *et al.* (1997) used additives to inhibit the nucleation and growth of the stable polymorph (β) of L-glutamic acid. This resulted in the metastable polymorph (α) of L-glutamic acid becoming stabilised.

2.5.4 Polymorphic transformation and kinetics

Transformation between different polymorphs is explained in thermodynamic terms by Ostwald (1897). The polymorph that crystallizes out of solution can be of the metastable form. This will then transfer to the more stable form, which has a lower Gibbs free energy. However this is assumed not to be a direct process but to occur in stages. The transformation that has the lowest energy barrier is favoured leading to a metastable polymorph, which has a lower Gibbs free energy than the previous form. This procedure will continue until the stable polymorph forms, which has the lowest Gibbs free energy. This is known as Ostwald's rule of stages (Bernstein *et al.*, 1999). However there is no theoretical proof of this rule. Investigations were carried out involving the use of kinetics to explain the rule (Bernstein *et al.*, 1999). This involved

investigating the effect of the degree of supersaturation of the rate of nucleation of the different polymorphic forms of a dimorphic system. At certain values of supersaturation the rate of nucleation of the two polymorphs is the same leading to polymorphs crystallizing concomitantly (Bernstein *et al.*, 1999). This indicated that kinetics of nucleation and growth are important factors in determining which polymorph will crystallize out of solution. This concludes that both thermodynamics and kinetics have an effect on which polymorph crystallizes out of solution with kinetics being the more important factor.

The crystallization process involves the formation of solid crystals from solution. This change in phase requires energy. The energy barriers required to overcome for the formation of the metastable and stable polymorph for a dimorphic system is shown in Figure 2.12.

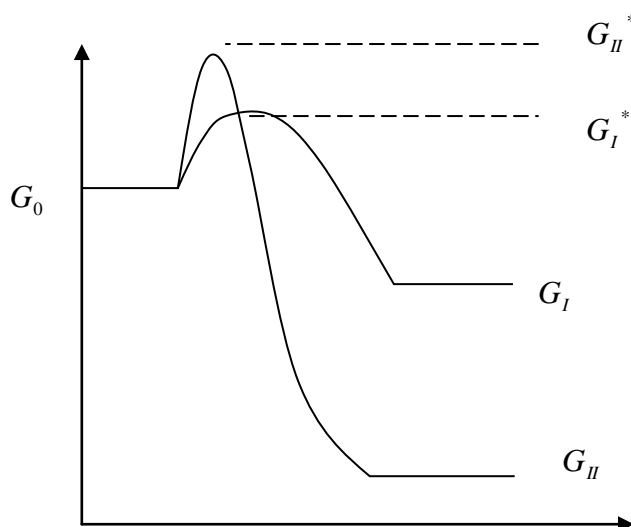


Figure 2.12. Activation energy barriers required to overcome for the formation of the two polymorphs (I and II) within a dimorphic system, where G_0 is the Gibbs free energy of the solute in a supersaturated solution, G_I is the Gibbs free energy of polymorph (I), G_{II} is the Gibbs free energy of polymorph (II), G_I^* is the energy required to form polymorph (I) and G_{II}^* is the energy required to form polymorph (II).

The energy barriers show the energy required in order to form a critical size nucleus for each polymorph. The height of the energy barrier is affected by the size of the critical nucleus. The polymorph that has a smaller critical size nucleus will have a lower energy

barrier and hence this process will be kinetically favoured. Polymorph I is the kinetically favoured form (see Figure 2.12). Thermodynamics predicts that polymorph (II) will crystallize out of solution as it has the lower Gibbs free energy and is therefore the more stable polymorph. Considering the effects of both thermodynamics and kinetics this can lead to the formation of the unstable polymorph (I). Transformation from the unstable (metastable) to stable form will occur over time. The time required for transformation will depend on kinetics.

Transformation between different polymorphic forms can occur by two different processes. These are known as reconstructive (solvent-mediated) or displacive (solid state) transformations (Davey and Garside, 2000). The type of transformation that will take place will depend on the structural change involved. A large structural change will result in reconstructive transformations taking place which involves dissolving the metastable (less stable) polymorph and reconstruction of the stable polymorph involving nucleation and growth. These transformations occur within solution and are referred to as solvent mediated transformations (Gu *et al.*, 2001). There are three factors that affect the rate of polymorphic transformation within solutions; these are the choice of solvent, temperature and rate of agitation. The effect of these parameters on the compound sulfamerazine (SME) was carried out by (Gu *et al.*, 2001). The results showed that the rate of transformation from the metastable to stable form depends largely on the kinetics of nucleation. Slower rates of transformation were found to occur at lower rates of agitation, lower degrees of supersaturation (solubility difference between the two polymorphs is smaller) and a choice of solvent where the solubility of the metastable form was lower. These are empirical findings and there is no theory for example on how the agitation rate is directly related to the polymorph that crystallizes. Solvent choice not only affects the rate of transformation but it can also affect the stability of the polymorphs, which can lead to the production on an undesired polymorph.

The other parameters that affect the stability of the polymorph include relative humidity (RH), temperature and pressure (Bechtloff *et al.*, 2001). A change in conditions will affect the stability and hence which polymorphic form crystallizes out of solution. Relative humidity is referred to as the water vapour pressure within the air. The amount of water present will determine the activity of water, which will affect the stability of

the hydrate. If the compound under investigation forms hydrates then a high RH, where the water activity is high, may lead to the formation of a hydrate as this is the stable form under these conditions. An increase in the RH can lead to the formation of higher hydration states that have lower solubilities (Brittain, 1999). This will affect the dissolution rates, bioavailability and hence dosage form performance (Aaltonen *et al.*, 2006). Temperature is known to affect the stability of the different forms. Hydrates are more stable at lower temperature and anhydrites are more stable at higher temperatures (Bechtloff *et al.*, 2001). This suggests dehydration will take place at high temperatures. It has been reported for some cases that dehydration can lead to the formation of the amorphous solid (Brittain, 1999). The rate of dehydration depends on the hydration form. This process is slow and continuous for channel hydrates and rapid for isolate hydrates once the dehydration temperature is reached (Brittain, 1999). Phase transformations were observed after suspension of a monohydrate (sodium -2-keto-L-gulonate monohydrate) in an organic solvent (methanol) leading to a change in appearance of solution and morphology (Bechtloff *et al.*, 2001). Another possibility where phase transformations can occur in solution is during dissolution testing. This is required to ensure the API is in the correct polymorphic form before scale up from lab to pilot plant. Experiments were performed using *in-situ* probes (Raman and UV/Vis) to monitor phase transformations during dissolution testing (Aaltonen *et al.*, (2006)). The phase transformation of one model system resulted in a clear decrease in dissolution rates. Information obtained by monitoring the solid phase using the Raman probe provided molecular level information resulting in a deeper understanding of the phase transformation during dissolution testing and the consequent effect on dissolution rates (Aaltonen *et al.*, 2006). A deeper understanding of the solvent mediated phase transformations is required in order to prevent undesired phase transformations.

The other type of transformation, known as displacive (solid state) transformation, involves changes in the interactions between neighbouring molecules without affecting the solid state form of the crystal (Davey and Garside, 2000). This occurs when the structural change between the polymorphs is small. Solid state transformations can occur during processing of the drug (tablet compression and milling) and during storage (Gu *et al.*, 2001; Vippagunta *et al.*, 2001). Possible causes for transformations include a change in storage conditions (temperature) affecting the stability of the polymorphs for an enantiotropic system or if the desired state of API is in a metastable form.

Formation of a hydrate due to absorption of water from the air at high RH or from transfer of water from the drug carrier can also result in a solid state transformation. Studies on the dehydration and hydration of solid state aspartame were carried out at 25°C by Leung *et al.* (1998). The results showed that once a RH of 58% is reached it lead to the formation of a higher hydration state forming a 2.5-hydrate from a hemi-hydrate. The rate of these transformations, which depends on kinetics, will determine the shelf life of the drug (Gracin and Rasmuson, 2004). Overall, solution mediated transformations tend to have lower energy barriers than solid state transformations (Davey and Garside, 2000). Lower energy barriers processes are kinetically favoured and the transformation will occur over a shorter period of time.

2.5.6 Conclusion on polymorphism

Crystallization is a major stage involved in the manufacturing of pharmaceutical drugs. For the production of about 80% of all drugs a crystallization step will be required. During this stage the compound can crystallize into different polymorphic forms leading to the production of an undesired polymorph. Transformations can occur during downstream processing involving filtration, washing, drying, wet granulation, tablet compression, milling and also during storage. Production of the undesired polymorph can lead to increases in economical costs. It is therefore essential to control the polymorphic form that crystallizes out of solution and to ensure that it remains in that state.

2.6 Analytical methods for crystallization

2.6.1 Introduction

Process analytical technology (PAT) tools are probe based techniques that can be placed within the process stream providing real-time data resulting in an increase in process understanding, which can be used to design a robust crystallization process during scale up (Wu and Khan, 2010; Nagy, 2009; Kail *et al.*, 2009; Read *et al.*, 2010; David *et al.*, 2004; Birch *et al.*, 2005; Cote *et al.*, 2009). These tools are also used to monitor changes occurring during the crystallization process, which are thought to be

due to polymorphic transformations (David *et al.*, 2004; Birch *et al.*, 2005; Yang *et al.*, 2009; Ferrari *et al.*, 2003; O'Sullivan and Glennon, 2005; Scholl *et al.*, 2006; Gillon *et al.*, 2006; Kobayashi *et al.*, 2006; O'Sullivan *et al.*, 2003). Data obtained from these tools enable the system to be designed ensuring a quality product (quality by design) rather than to achieve a target quality by trial and error (quality by testing). The Food and Drug Administration (FDA) agency encourages pharmaceutical industries to use PAT tools to ensure quality by design (Yu *et al.*, 2004; Abu Bakar *et al.*, 2009a; Wang *et al.*, 2007; David *et al.*, 2004; Yu *et al.*, 2007). This enables the system to be more flexible in terms of changes to the operational procedure so long as the quality of the product is maintained. There are a number of different PAT tools which include turbidity probe, focused beam reflectance measurement (FBRM), particle vision and measurement (PVM), pH probe and a range of spectroscopic techniques. These include nuclear magnetic resonance (NMR), attenuated total reflectance (ATR)-UV/Vis, attenuated total reflection (ATR)-Fourier transform infrared (FTIR) and Raman spectroscopy. These techniques are used to monitor the crystallization processes as it proceeds and are therefore referred to as *in situ* techniques.

Crystal samples are taken during and at the end of the crystallization process for characterising the polymorphic form using a range of solid state analytical techniques. As the samples are removed and analysed far from the process stream this type of analysis is referred to as off-line. Thermal techniques include differential scanning calorimetry (DSC), thermal gravimetric analysis (TGA), and hot stage microscopy (HSM). Other techniques also include optical microscope, dynamic vapour sorption (DVS), X-ray powder diffraction (XRPD), solid state nuclear magnetic resonance (NMR), infra-red (IR) and Raman spectroscopy. Combinations of the above techniques are used for the monitoring, design and control of a particular crystal system ensuring a quality product. Not all of the above techniques are used within this research work. This section discusses each of the techniques used within this research work, giving a description of how they work, the information that can be obtained from the techniques together with the advantages and disadvantages of some techniques.

2.6.2 FBRM and its use with other PAT tools

Focused beam reflectance measurement (FBRM) is an *in situ* probe based technique, which operates by the use of a laser beam that passes through the centre of the probe. The beam is focused on a particular point and is rotated in a circular path at a high speed of 2 m/s to cope with changes in solution velocity (Tadayyon and Rohani, 1998). A schematic representation of the FBRM probe combined with the laser beam is shown in Figure 2.13.

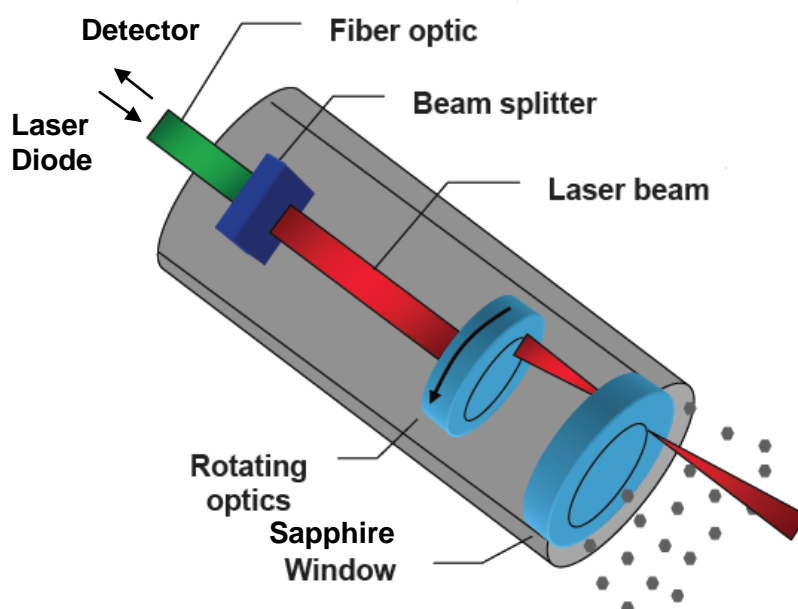


Figure 2.13. FBRM probe tip with laser beam (adapted from Greaves *et al.*, 2008)

The FBRM probe measures the chord length distribution of a crystal population. As the focal beam crosses two edges of a particle it measures the chord length. There is a back scattering of light into the probe. The velocity of this focal beam and the time required for detection of the backscattering of light gives a measure of the chord length. The device is able to measure 1000's of chord lengths per second and can detect many chord lengths for a single particle as shown in Figure 2.14.

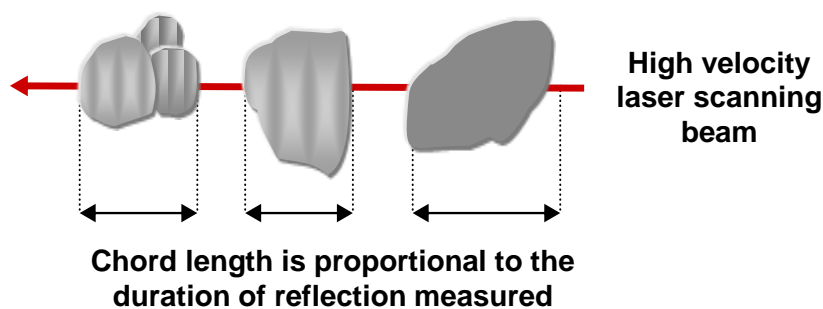


Figure 2.14. Laser beam detection of many chord lengths for a single particle

The size range of the chords that can be detected by this technique is between 0.8/1 - 1000 μm , which is distributed into 38 or 91 channels depending on the model of FBRM probe (Barrett and Glennon, 1999). This enables the detection of nucleation by an increase in the number of fine counts (0-20 μm) and crystal growth or agglomeration by an increase in the number of coarse counts (50-250 μm) (Barrett and Glennon, 2002). Through a change in the number of counts it is able to detect breakage of crystals, and even polymorphic transformations. Selecting certain statistics (e.g. unweighted, square-weighted, cube-weighted mean chord length, etc.) to monitor changes during the crystallization process provides a deeper understanding of the process and minimises the time of process operation resulting in a more efficient process (Yu *et al.*, 2007). Many researchers have used this tool for the detection of polymorphic transformations that can result in a change in crystal size or morphology (O'Sullivan and Glennon, 2005; Scholl *et al.*, 2006; Kobayashi *et al.*, 2006; Gillon *et al.*, 2006; Abu Bakar *et al.*, 2009; Woo *et al.*, 2009; Kail *et al.*, 2009; Howard *et al.*, 2009a; Howard *et al.*, 2009b). Many studies have also used the FBRM for measuring MSZW values for compounds. An alternative *in situ* probe used for measuring MSZW values is the turbidity meter. This technique measures the liquid turbidity (cloudiness). It operates by transmitting near-infrared light into the solution and any particles present will scatter light back into the probe (Parsons *et al.*, 2003). This technique requires a threshold concentration before any particles are detected. Lasentec FBRM has an advantage over the turbidity probe as it is able to detect the presence of a single particle as long as it is within a certain size range.

Chord length distribution (CLD) data obtained from the FBRM can be converted to particle size distribution (PSD). However the conversion of CLD to PSD is relatively complex and requires the assumption of a particular shape for all crystals, which has prevented the use of measurements obtained from the FBRM from being used in a feedback loop for the direct quantitative control of the CSD (Yu *et al.*, 2007). Feedback control provides a more robust process than the traditionally open-loop control (Yu *et al.*, 2007). However recent developments have been made involving the use of FBRM measurements combined with a feedback control loop of temperature, for the control of the PSD within batch crystallization processes (Abu Bakar *et al.*, 2009a; Chew *et al.*, 2007; Doki *et al.*, 2004; Woo *et al.*, 2009).

The position of the probe and the operating conditions can have an effect on the accuracy of the results. In order to ensure the FBRM readings are a good sample representation of the whole system the probe should be positioned so that the probe window faces the direction of flow within the vessel. Barrett and Glennon (1999) investigated the effect of different probe positions relative to the agitator within a crystallization vessel. The results of the studies showed that more accurate results were obtained when the probe is positioned at an angle to the agitator ensuring good flow towards the probe window. The agitator speed has to be chosen properly, to achieve proper suspension of solids but avoid air entrainment since bubbles affect the FBRM readings (Tadayyon and Rohani, 1998).

As mentioned before the PSD is an important parameter to control in the crystallization process to ensure a quality product. There are many techniques that can be used to measure the PSD, as well as the FBRM probe, including sieve analysis, coulter counter and forward light scattering. The FBRM probe is able to operate at high solid concentrations eliminating the need for sample dilution. Another advantage of this technique is that the probe can be placed within the crystallization vessel and can therefore measure changes within the system in real-time, giving more direct information related to CSD than the other methods which require a sample to be removed from the system for analysis (Tadayyon and Rohani, 1998).

FBRM is often used in combination with other PAT tools in order to gain a better understanding of the crystallization process. A combination of FBRM and Raman

spectroscopy was used to determine the kinetics of nucleation, growth and form conversion of a proprietary pharmaceutical compound in a solvent mixture of methyl ethyl ketone (MEK)/water (Birch *et al.*, 2005). The FBRM readings showed a decrease in particle size during dehydration indicating a partial collapse of the crystal structure. This showed that the solvent system was not suitable for the crystallization of the proprietary pharmaceutical compound as the particle size distribution could not be controlled. Gillon *et al.*, (2006) used a combination of FBRM, PVM and ATR-UV/Vis spectroscopy to study crystallization of caffeine. The affect of cooling rate on the MSZW and the effect of agitation and temperature on the kinetics of hydration were studied. FBRM was used in automated MSZW determination, and it was shown that it can detect polymorphic transformation of the anhydrous caffeine into the hydrated form.

2.6.3 Particle vision measurement (PVM) probe

PVM is a probe based tool which is placed within the process stream. This device consists of a high resolution video microscope allowing the images of the crystals morphology to be obtained (Barrett and Glennon, 2002; Braatz *et al.*, 2002). A change in morphology due to a polymorphic transformation can be detected with the use of PVM (Gillon *et al.*, 2006). The *in situ* images which are recorded in real-time can confirm whether an increase in number of coarse counts, as detected by the FBRM probe, is due to crystal growth or agglomeration (Barrett and Glennon, 2002). FBRM can provide such information related to dynamic changes in the crystallization processes however the results must be interpreted carefully since a particular change in an FBRM signal can have various causes. Often FBRM results must be confirmed with other PAT tools or solid state analytical techniques (Howard *et al.*, 2009a; Howard *et al.*, 2009b).

2.6.4 ATR-UV/Vis spectroscopy

Attenuated total reflectance (ATR)-UV/Vis spectroscopy is used to monitor changes in properties of the liquid phase during the crystallization process such as solute

concentration (Thompson *et al.*, 2005; Billot *et al.*, 2010; Doyle and Tran, 1999; Abu Bakar *et al.*, 2009; Aamir *et al.*, 2010). This technique operates by using an electromagnetic radiation beam which interacts with the solute molecules. The radiation beam is directed towards the interface of two surfaces (crystal and solvent) at an angle (θ_1) greater than that of the critical angle (θ_c) resulting in the deep penetration (d_p) of an evanescent wave into solution. The critical angle is the smallest angle for complete reflection of the radiation beam. The solute interacts with the evanescent wave resulting in absorption of a particular wavelength and the radiation beam is reflected as shown in Figure 2.15. Absorption results in the attenuation of the reflected beam.

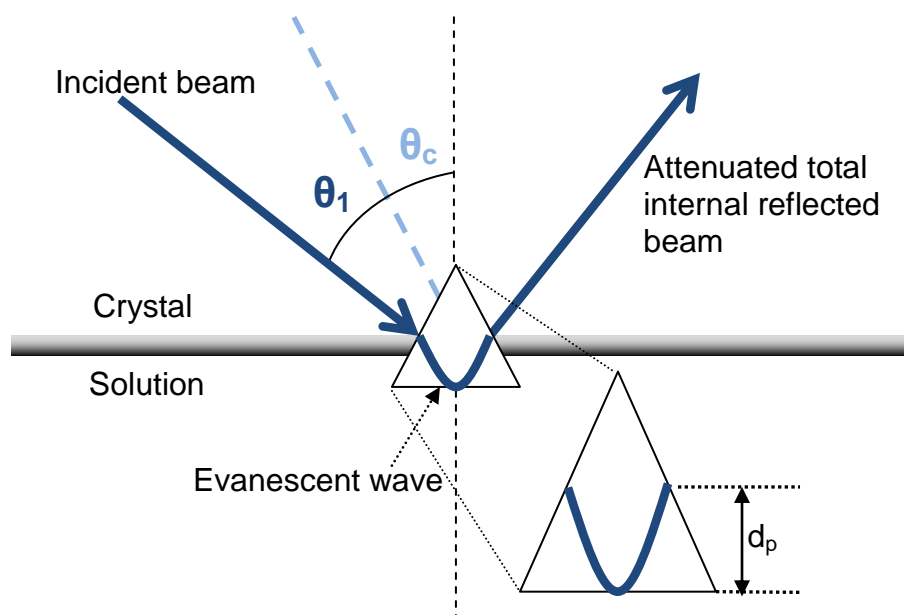


Figure 2.15. Total internal reflection occurring within the ATR-UV/Vis probe (adapted from Billot *et al.*, 2010)

Absorbance of the radiation beam is expressed in terms of the intensities of incident and reflected beam by the following mathematical expression (Billot *et al.*, 2010):

$$A_b = \log\left(\frac{I_0}{I}\right) \quad (2.27)$$

where A_b is the absorbance, I_0 is intensity of incident light beam and I is intensity of reflective light beam.

The concentration of the species is determined from the absorbance using the following Beer-Lambert law (Billot *et al.*, 2010):

$$A_b(\lambda) = \varepsilon_a(\lambda)Cl \quad (2.28)$$

where A_b is the absorbance, λ is wavelength, ε_a is absorption coefficient, C is the concentration of the absorbing species and l is the optical path length, which is equal to the number of reflections (z) multiplied by the depth of penetration of the evanescent wave (d_p).

The UV/Vis wavelength range is between 200-800 nm for which compounds will only absorb if they contain a chromophore (a multiple bond) group (Rao, 1961). Fibre optics used within the probe limit the wavelength range for absorption between 220 and 600 nm (Thompson *et al.*, 2005). A typical UV-Vis spectrum is shown in Figure 2.16. This technique is useful within the pharmaceutical industry as many compounds contain the chromophore group (Billot *et al.*, 2010). For this technique to be successful the crystal and solvent must have significantly different refractive indices with a high refractive index for the crystal (solute) and a low refractive index for the solvent. Also the solvent must not interfere with the absorbance of the solute (Thompson *et al.*, 2005).

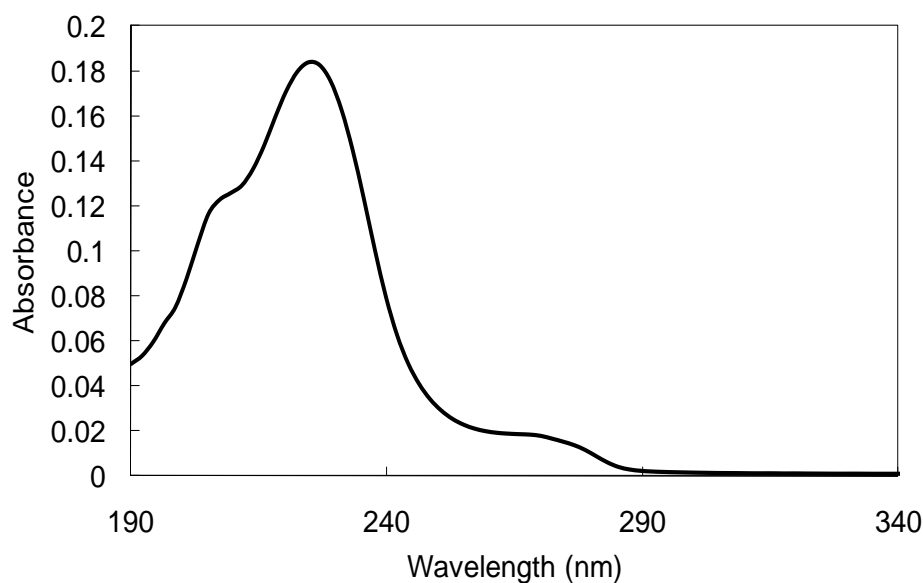


Figure 2.16. UV/Vis spectrum for sodium benzoate in water

One of the advantages of ATR-UV/Vis spectroscopy is that it is able to measure high concentrations and it is not affected by the presence of solid particles or bubbles in solution (Thompson *et al.*, 2005). This technique has also been used for a wide range of other applications including monitoring of polymorphic transformations (Howard *et al.*, 2009b), controlling the crystallization process to produce the desired polymorph and crystal size distribution (Abu Bakar *et al.*, 2009b), solubility curve determination, MSZW and monitoring supersaturation levels (Nagy, 2009; Aamir *et al.*, 2010). ATR-UV/Vis spectroscopy is easy to set up in the laboratory and inexpensive compared to other PAT tools such as ATR-FTIR, which is also used to measure concentration values, giving this technique an additional advantage (Billot *et al.*, 2010).

2.6.5 Introduction to solid state analysis (SSA)

There are many different solid state analytical techniques used to analyse the crystals at any stage during the crystallization process and during formulation. Combinations of SSA techniques are used to characterise the crystal product, for example for identifying the different polymorphic forms of a compound (Braum *et al.*, 2008; Abu Bakar *et al.*, 2010; Howard *et al.*, 2009a; Howard *et al.*, 2009b; Brittain, 1999; Giron, 2003; Giron, 1995; David *et al.*, 2004). These techniques provide additional information to understanding the crystallization process and identify the conditions required to produce the desired form (Yu *et al.*, 2004; Yang *et al.*, 2009; Desikan *et al.*, 2005). The techniques that will be discussed in this section include microscopy (optical, SEM and HSM), DSC, TGA, DVS and XRPD.

2.6.6 Microscopy

There are three types of microscopy that will be mentioned within this report including polarized light, scanning electron and hot stage microscopy. These techniques are used to determine the solid state properties of the drugs, which are useful for the early stages in drug development (Brittain, 1999). The properties that it can measure include refractive index, colour, particle size and particle shape (habit). It can also detect the

presence of inclusions, twinning between crystals and crystallinity within samples. Polymorphic conversions can be detected by the change in habit. SEM can achieve higher magnifications than optical microscopy enabling a more detailed structure analysis of the crystal particles. SEM also gives better 3D information. The difference of hot stage microscopy compared to the other microscopy techniques is that it requires heating and cooling a sample material. This technique requires a small amount of material and provides rapid data (Brittain, 1999) about the thermal behaviour of a solid (e.g. polymorphic transformation, melting point, etc.). This microscopy technique is the most widely used within industry for determining solid state properties and for the detection of polymorphs (Hilfiker, 2006). There are other thermal techniques for the solid state analysis of the crystals including DSC and TGA.

2.6.7 Differential scanning calorimetry (DSC)

Differential scanning calorimetry is a thermal analysis technique used for solid state analysis of the crystalline drug compound. DSC was developed in the 1960's through modifications to an existing technique known as differential thermal analysis (DTA) (Hilfiker, 2006). The DSC technique is simple to operate resulting in it being the most common thermal method used for polymorphic screening within the pharmaceutical industry (Abu Bakar *et al.*, 2010).

DSC measures the melting point and enthalpy of melting of the different polymorphic forms of a given compound. This technique is also used for detecting the presence of hydrates as represented by a broad peak at low temperatures below 100 °C. The operation of this technique involves the heating of two cells, one containing the reference material and the other containing the sample material. The two cells are kept at the same temperature by a constant heating rate. This must be controlled in order to ensure accurate results and a clear understanding of the thermal events. A slow heating rate is required to ensure all the thermal events are detected. The importance of this was clearly indicated by Giron (1995), which showed that once the hydrate form had dissolved, re-crystallization into the anhydrate form was only detected at slow heating rates. Any changes within the system that occur during the heating process, such as a

polymorphic transition from a meta-stable to stable polymorph, will result in a change in the heat flow rate to the sample. The relationship between melting point and enthalpy of melting enables the nature of the polymorphic system to be classified. As discussed by Burger and Ramberger (1979), two polymorphs are monotropic related if the higher melting polymorphic form has a higher enthalpy of melting and the reverse is true for enantiotropic related polymorphs.

The type of polymorphic transformation, solid state or re-crystallization from the melt, can be detected through the use of DSC. The difference in DSC plots for the two types of transformations are shown in Figures 2.17 and 2.18.

As shown in Figure 2.17, the solid-solid transition occurs before the melting point of the high melting point form. A positive enthalpy change (endothermic peak) in the solid state transition indicates the polymorphs are enantiotropic related and a negative enthalpy change (exothermic peak) indicates a monotropic system. DSC can monitor polymorphic transformation by melt crystallization, which is shown in Figure 2.18. This is achieved in three stages, which include melting of the meta-stable polymorph, re-crystallization of the stable polymorph followed by melting of the stable polymorph.

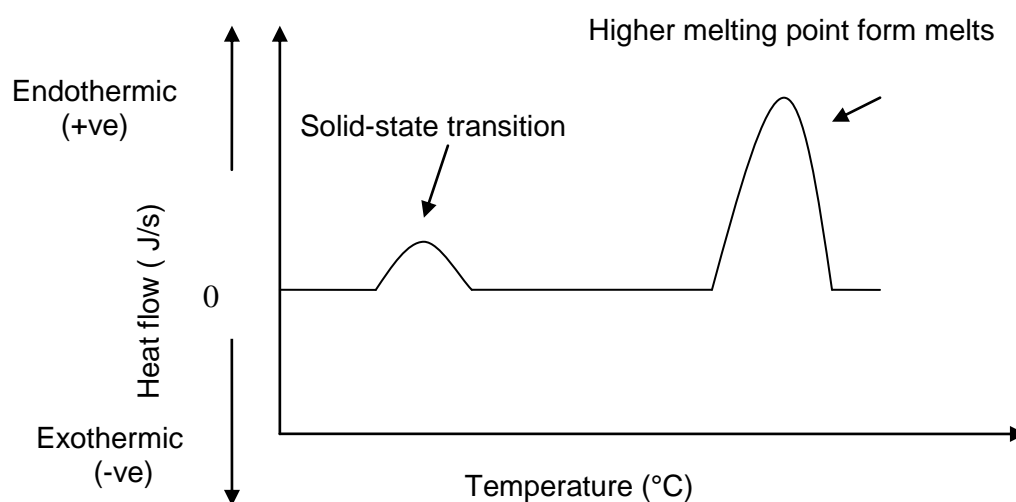


Figure 2.17. Typical DSC plot of a polymorphic transition occurring within the solid state

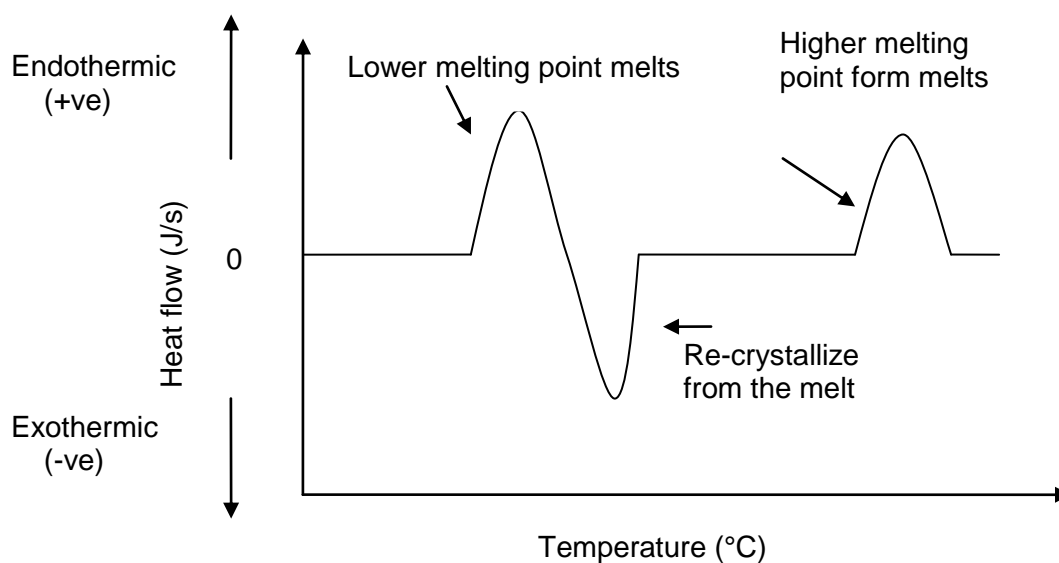


Figure 2.18. Typical DSC plot of a polymorphic transition occurring from re-crystallization of the melt

Preparation of the crystals and the operating conditions of the equipment can have a profound effect on the accuracy of the data obtained from the DSC. During running of the DSC a flow of nitrogen must be on to prevent degradation of the material before the melting point is reached. Gentle grinding of the crystal sample is required to enable even heat flow throughout the crystal sample. This factor, sample mass and the presence of contaminants can broaden the melting peak leading to inaccurate results. A small sample mass gives better resolution of the thermal events as it prevents thermal lags occurring within the sample material, which would lead to a wider temperature range over which the melting point occurs.

An advantage of DSC is that it is simple to use and provides rapid data (Hilfiker, 2006), related to melting points, purity, polymorphic transformation etc. Each experiment requires a small amount of sample material in the range of a few milligrams, which is a major advantage when there is limited amount of drug available in the development stage. It also provides direct quantitative information on the thermodynamic parameters associated with polymorphic transitions that enable the stability relationship between the polymorphs and the temperature of transition to be determined. This data is useful for the design and control of the crystallization process. However this technique does

have disadvantages, which include its inability to detect the presence of different polymorphic forms that have close melting points. Polymorphs with a melting point difference of 10 °C could not be distinguished in a study by Hilfiker (2006). Only one polymorphic form of mannitol was detected through the use of DSC, which is known to have 4 different polymorphic forms (Giron, 1995). The presence of additional peaks can appear in the DSC plot due to a noise factor that can lead to confusion in results (Giron, 1995). Another limitation of this technique is that it does not provide any structural data and therefore cannot be used alone for the quantitative analysis of the polymorphic systems. DSC results are generally supported with XRPD data, which provides the structural information of the different polymorphic forms. David *et al.* (2004) reported the use of DSC combined with optical microscopy to confirm the presence of different polymorphic forms by the appearance of different habits as shown by the microscope images. Giron (1995) mentioned the use of TGA combined with DSC results for the detection of pseudo-polymorphs. Abu Bakar *et al.* (2010) used DSC in combination with HSM and images analysis to study the polymorphic transformation of sulfathiazole crystals.

2.6.8 Thermal gravimetric analysis (TGA)

TGA is a thermal technique used for identification and characterisation of solvent species. TGA is operated by supplying heat to the sample material, which results in a temperature rise. Over the operating temperature range if there is a decrease in mass then this indicates that solvent is present. Solvent can be either on the surface of the crystal or in the internal structure of the crystal. If a solvate or hydrate is present the type of bonds between the molecules can be estimated by the temperature at which solvent is lost from the sample (Hilfiker, 2006). TGA can also determine the stoichiometry of solvates and hydrates. A case study was carried out on a disodium salt by applying different relative humidity's (RH) of values 33, 52, 60 and 75% to a sample, which resulted in the formation of different hydrate states. TGA was then applied to show the different types of hydration states by a different percentage decrease of mass loss over the operating temperature range (Brittain, 1999).

TGA does have the disadvantage that it is unable to determine the nature of the solvent lost (Hilfiker, 2006). The weight loss can be due to either solvent on the surface of the particles indicating the presence of an anhydrate form or from the internal structure of the crystal indicating the presence of a hydrate. An estimation can be made on the nature of the solvent based on the extent of weight loss and the temperature range over which this occurs. A weight loss at high temperatures usually indicates the loss of solvent from the internal structure of the crystal as energy must be supplied to break the bonds. However this is just an estimation, which does not provide any proof and therefore further analysis must be carried out with the use of other techniques such as mass spectroscopy. This technique is used to identify the nature (solvent, hydrate or anhydrate) and chemical structure of the compound (Hilfiker, 2006), to identify potential bonds between the solvent and compound in solid state.

2.6.9 Dynamic vapour sorption (DVS)

Dynamic vapour sorption is used within the pharmaceutical industry to determine the hygroscopicity of solids (Hilfiker, 2006). This is referred to as the extent of moisture taken up by the solid. This method is also used for the detection of different hydrate forms and from the isotherms the kinetic stability of the different hydrates can be determined (Hilfiker, 2006). DVS works by measuring the change in mass as the relative humidity (RH) is increased or decreased while keeping the system at a constant temperature. Different isotherms can be obtained for stoichiometric, non-stoichiometric, amorphous and crystalline solids. The presence of impurities, crystal defects and amorphous compounds can affect are generally combined with other techniques such as XRPD in order to identify the different hydrate forms (Hilfiker, 2006).

2.6.10 X-ray powder diffraction (XRPD)

There are two different types of X-ray diffraction techniques. One is used to determine the structure of single crystals and the other method known as X-ray powder diffraction (XRPD) is used to determine the presence of different polymorphs within a given system. Solid state analysis of crystals will require the use of XRPD, which may be

supported with other techniques to provide back up evidence for the existence of polymorphs (Brittain, 1999).

The determination of the crystal structure through the use of X-rays involves a beam of electromagnetic wavelengths of size less than 1 nm (Breithaupt, 1990). This beam is directed onto a sample material and then diffracted from the sample at certain angles depending on the arrangements of atoms within the crystal lattice. A representation of the set up of the X-ray diffractometer is shown in Figure 2.19.

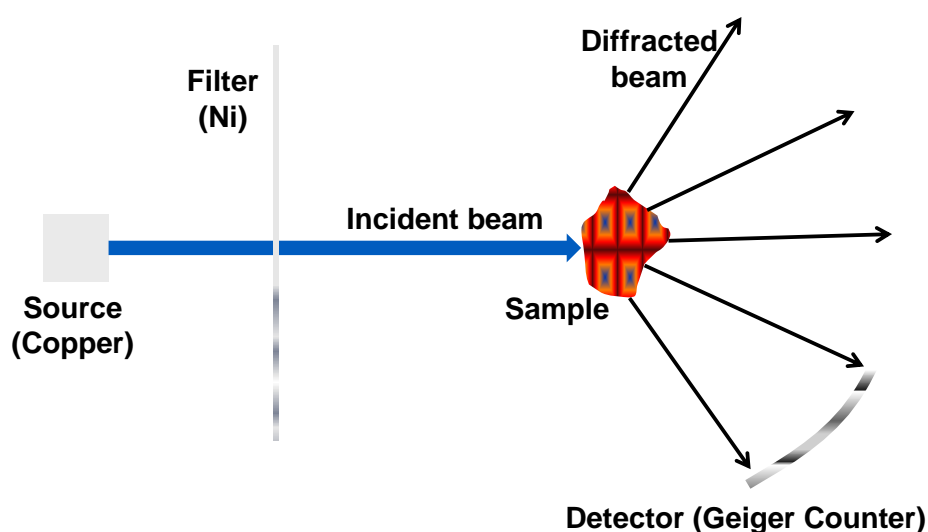


Figure 2.19. Schematic view of an X-ray diffractometer

The measured angles of diffraction are used to determine the arrangement and spacing between the atoms within a crystal lattice by the use of Bragg's law (Brittain, 1999):

$$n_o \lambda = 2d \sin \theta, \quad (2.29)$$

where θ is the angle of beam diffraction from the sample, d is the distance between the planes in the crystal, λ is the wavelength of the incident beam and n_o is the order of the diffraction pattern.

The different angles of diffraction are measured and are presented on an X-ray pattern by the presence of different peaks. A polymorph containing a different structure will result in a different set of diffraction angles and hence a different X-ray pattern. The detection of crystalline or amorphous solids can be detected by the use of X-ray patterns (Stephenson *et al.*, 2001). In order to ensure accurate results the sample material must be prepared so as to reduce the extent of preferred orientation of the crystals. Roberts *et al.*, (2002) studied the effects of preferred orientation of mannitol particles, which contain 3 different polymorphic forms. XRPD showed preferred orientation of the crystals, which lead to difficulties in the quantitative analysis of the different polymorphic forms. The effects of preferred orientation were minimised by reducing the size of the particles and by rotating the samples. This enabled two similar polymorphs to be distinguished. However the grinding of organic samples can lead to polymorphic transformations. An alternative way to prevent preferred orientation is to mix the sample material with an inert amorphous compound (Stephenson *et al.*, 2001).

The identification of the presence of polymorphs within a pharmaceutical tablet is essential as these contain different physicochemical properties. Different techniques involving XRPD, Raman and IR spectroscopy were used in order to identify the presence of a Risperidone polymorph within film coated tablets, which contained other crystal phases and excipients (Karabas *et al.*, 2007). XRPD was the only technique that was able to identify the polymorph showing the importance of XRPD in the detection of different polymorphic forms. XRPD also has the advantage of being able to detect the percentage of different polymorphs within a given sample. Lu *et al.*, (2005) used XRPD for the quantitative analysis of a sample material containing two chlorothalonil polymorphs (A and B). The areas under the peaks of the X-ray patterns were used to determine the percentage of each polymorph present within the sample material. For example for polymorph A has a characteristic peak at $14.5^\circ 2\theta$ and polymorph B has a characteristic peak at $15.5^\circ 2\theta$. For a mixed sample the percentage of form A can be obtained by Equation 2.30.

$$\% \text{ of Form A} = \frac{\text{peak area of the peak at } 14.5^\circ 2\theta}{\text{sum of the peak areas of peaks at } 14.5^\circ \text{ and } 15.5^\circ 2\theta} \times 100\% \quad (2.30)$$

2.6.11 Solid state spectroscopy techniques

Spectroscopy techniques including infra-red (IR) and nuclear magnetic resonance (NMR) are widely used within in the pharmaceutical industry for the characterisation of polymorphs, hydrates and solvates (Bugay, 2001; Threlfall and Chalmers, 2007; Harris, 2006; Harris, 2007).

IR spectroscopy measures the vibrational modes of the molecules in a compound and is therefore referred to vibrational spectroscopy. There are three different types of vibrations, including symmetric stretching, asymmetric stretching and bending vibrations (Atkinson and Hibbert, 2001). As the covalent bonds vibrate within a compound they absorb infra-red radiation. The wavelength range of the IR spectrum is 400 to 4000 cm^{-1} . Each covalent bond within a molecule absorbs infra-red radiation of a particular frequency producing a specific peak in the IR spectrum (Atkinson and Hibbert, 2001). This technique enables the different functional groups within the compound to be detected, which can provide supportive information in the identification of hydrates and solvates. Within each IR spectrum there is a fingerprint region in the wavelength range 400 to 1500 cm^{-1} (Atkinson and Hibbert, 2001). This region is useful for the identification of different polymorphic forms of a compound as each polymorph will have a different pattern in the fingerprint region. The advantages of this technique are that very little sample preparation is required and the spectrophotometers are relatively inexpensive compared to NMR (Bugay, 2001).

NMR spectroscopy is used to determine the structural differences between compounds by studying the different electronic environment of nuclei within the molecule. This technique only applies for atoms with odd numbers of neutrons and protons in the nucleus resulting in an overall charge. Once the nucleus spins it creates a magnetic field and when this is placed within an external magnetic field then the nucleus aligns itself up with the lower energy level. Radio waves of specific frequency will cause the nucleus to resonate between a low and high energy level resulting in a peak in the NMR spectrum. Nuclei of the same atom (e.g. hydrogen) that is within a different chemical environment will resonate between two different energy levels, resulting in a different peak in the NMR spectrum. Chapter 5 of this thesis highlights the importance of proton

NMR for the detecting of a new undiscovered solvate. Hydrogen atoms bonded to a (-CH₃), (-CH₂) and (-OH) group were detected with the latter group indicating the presence of a solvate as this does not appear in the compound studied. One of the strengths of the NMR spectroscopy is that it overcomes problems that arise in diffraction studies and can detect differences in spectrum for different forms of a compound that are not detectable by IR spectroscopy of XRPD (Harris, 2006). Another advantage of this technique is that it can achieve a high degree of spectral resolution compared with the other spectroscopy techniques leading to clear and accurate results (Stephenson *et al.*, 2001).

2.6.12 Conclusions

PAT tools are probe based techniques, which can be placed within the process stream enabling properties of the crystallization process to be measured in real-time. A commonly used tool for monitoring properties of the solid phase is the FBRM probe. This tool measures the chord length distribution of a crystal population, which can be used to detect nucleation, attrition, agglomeration, polymorphic transformations and MSZW values. PVM provides images of the crystals in real time. Changes in morphology of the crystals can be detected indicating possible polymorphic transformations, attrition or agglomeration. ATR-UV/Vis is a useful tool to use in combination with FBRM and PVM as this tool measures properties of the liquid phase. Changes in concentration values of the solute can be used for detecting polymorphic transformations, obtaining MSZW values and monitoring supersaturation levels. Combining all the information obtained from the PAT tools provides a deeper understanding of the crystallization process.

For successful analysis of a drug compound a range of solid state techniques can be carried out to determine the solid state properties of different polymorphic and pseudo-polymorphic forms (hydrates and solvates). Thermal techniques including DSC and HSM determine the melting point of different forms of a substance and can monitor polymorphic or pseudo-polymorphic conversions while TGA and DVS are used for the analysis of different solvate or hydrate forms. However the above techniques do not include information on the crystal structure. Therefore these techniques are used in

combination with XRPD, IR and NMR spectroscopy, which are used to determine the crystal structure of different polymorphic and pseudo-polymorphic forms. The use of these techniques combined with the PAT tools enables the system to be designed and controlled at a certain set of conditions increasing the likelihood of producing a quality product.

2.4 Conclusions on literature survey

The aim of this literature review was to gain a deeper knowledge of the research that has been carried out related to pharmaceutical crystallization within batch systems. Phase rule and diagrams have been briefly mentioned and previous research has shown the importance of operating within the MSZW of the phase diagram in order to obtain crystals of quality standard. The various factors that could affect the MSZW have been mentioned. Following on from this research studies will be carried out using PAT tools within batch crystallization processes to see how various process parameters including temperature, ramp rate, size of vessel, agitator type and speed affect the MSZW. These parameters will be combined to determine whether a robust MSZW region can be obtained, which can then be used in designing crystallization experiments at the larger scale involving feedback loops and the use of PAT tools.

A literature search on polymorphism, salts and PAT has been included, which showed the importance of being able to distinguish the differences between crystal forms of a single compound. The use of PAT tools has been used for monitoring and controlling the crystallization process. The range of SSA techniques available for characterising the crystal product and the information that can be obtained from each technique are mentioned. The work within this thesis aims to progress this field of research in which PAT tools are combined with SSA techniques for monitoring the crystallization process and for the discovery of new polymorphic forms. The literature review highlights the importance of crystallizing salts in order to overcome problems with solubility, dissolution rate, stability and hygroscopicity (Forbes *et al.*, 1992, Haynes *et al.*, 2005). Research within this thesis uses a combination of PAT tools and SSA techniques to investigate the best conditions required to produce salts. Various parameters that will be varied include method of crystallization, strength of acid, solvent and pH of solution.

Chapter 3. Materials, experimental set-up and methodology

3.1 Introduction

This Chapter shall present a detailed description of materials, model systems used and methodology of experiments performed. The process analytical technology (PAT) tools used to monitor the crystallization process and the range of solid state analytical (SSA) techniques used for characterising the crystal products will be discussed. Detailed methodology of small scale (1 mL to 20 mL) solubility and slurry experiments, salt precipitation and evaporation experiments are discussed. The larger scale crystallization experiments of size 250 mL to 1 L were performed in similar jacketed glass vessels with slightly different combinations of PAT tools. Cooling, pH controlled and antisolvent crystallization rig set-ups are shown in separate Figures highlighting the differences in the PAT arrangements.

3.2 Materials

Sodium benzoate was one of the compounds used as the model system for experiments (see Chapters 4 and 5). The raw material (sodium benzoate) is the anhydrous form and was obtained from two different sources. These included Sigma Aldrich and Fisher Scientific, both which had of purity greater than 99.0%. Solubility studies were carried out using a range of solvents including water, methanol, ethanol, propan-2-ol (IPA), butan-2-ol, acetone, acetonitrile, methyl ethyl ketone (MEK) and tetrahydrofuran (see Chapters 4 and 5). Ultra-pure Millipore water generated from a MilliQ reverse osmosis unit was used and all other solvents were of analytical reagent grade, which were obtained from Fisher Scientific. *Para*-amino benzoic (PABA) acid, *meta*-amino benzoic acid (MABA) and *ortho*-amino benzoic (OABA) acid were three other model compounds used in the crystallization studies (described in Chapters 6, 7, 8 and 9). PABA and MABA were obtained from Sigma Aldrich with purity of 99%. OABA was also obtained from Sigma Aldrich with purity of 98%. There are two known polymorphic forms of PABA (Gracin and Rasmuson, 2004), two polymorphic forms of

MABA (Svard et al., 2010) and three polymorphic forms of OABA (Jiang *et al.*, 2008; Rajeshwar and Secco, 1976; Ojala and Etter, 1992). Solvents used include water, ethanol and ethyl acetate. The latter two solvents were of analytical reagent grade and obtained from Fisher Scientific. A range of acids and bases were used in the pH/salt crystallization experiments (described in Chapters 8 and 9) including hydrochloric acid (molarity of 0.5M for pH swing and 5M for cooling crystallization experiments), hydrobromic acid (3M), sulphuric acid (2M), phosphoric (3M), sodium hydroxide (5M) and potassium hydroxide (5M).

3.3 Avantium Crystal 16 experiments and solubility measurements

Solubility screening, slurry and meta-stable zone width (MSZW) measurement experiments were performed at 1 mL scale using the Avantium Crystal 16 equipment. A picture of the Crystal 16 equipment can be found in Appendix A. This contains reactor blocks of 4 by 4 of 1 mL HPLC vials agitated by magnetic fleas which were set at a rotation speed of 700 rpm. Each vial contained a turbidity sensor which was used to detect the clear (all crystals dissolved) and cloud points (apparent nucleation). A turbidity value of zero% represents a cloudy solution and 100% represents a clear solution. The temperature was controlled by a Huber ministat which was connected to a PC.

Solubility screening experiments involved suspending sodium benzoate in a range of solvents and heating using a ramp rate of 0.3 °C/min. Solvents used include water, alcohols (methanol, ethanol, propan-2-ol and butan-2-ol) and 4 other organic solvents (acetone, acetonitrile, MEK and tetrahydrofuran). Results are discussed in Section 4.3 of Chapter 4. Solubility determination for sodium benzoate in water, IPA and volume ratios of IPA/water 2:1, 4:1 and 5:1 were carried out using a gravimetric method. This method involved suspending sodium benzoate in the required solvent using 20 mL vials which were shaken in a water bath at the desired temperature for 22-24 hours to allow the system to reach equilibrium. Three samples of 1-2 mL for each solvent system were placed in petri dishes and left in the oven at 25 °C for 24 hours for solvent evaporation. Results are discussed in Section 4.3 of Chapter 4 and Section 5.3 of Chapter 5.

Slurry experiments were performed in order to determine the stability order of the different crystal forms of sodium benzoate within different solvent mixtures of IPA/water. Vials of 1 mL were used to suspend sodium benzoate in the solvent mixture for 4 days at 25 °C. Results are discussed in Section 5.3 of Chapter 5.

MSZW measurements involved suspending PABA in water using 1 mL vials. The range of concentrations used is 10 to 35 mg/mL. A ramp rate of 0.5, 0.3 and 0.1 °C/min is used for each concentration value to obtain the clear (solubility) points and cloud (nucleation) points. The process is repeated using the isomer MABA using the concentration range of 12 to 28 mg/mL. Results are discussed within Chapter 7.

3.4 Cooling crystallization experiments at scales of 250 mL, 750 mL and 1 L

Cooling crystallization experiments were performed in a range of jacketed glass vessel sizes, including 250 mL, 750 mL and 1 L, using a linear cooling rate of 0.1, 0.2, 0.3 and 0.5 °C/min. Each experiment consisted of a different combination of PAT tools for monitoring the crystallization process. The PAT tools used within these studies include the FBRM, turbidity, PVM, ATR-UV/Vis, pH and temperature probe. The FBRM probe is used for monitoring changes in the solid phase. This PAT tool is used for detecting changes in the number of counts with chord lengths within size range of 1-20 microns (fine counts), 50-250 microns (coarse counts) and 1-1000 microns (total counts). A 90 logarithmic channel mode was used to collect data into specific bins. This PAT tool can be used to detect nucleation, growth, agglomeration, attrition and polymorphic transformations. Turbidity probe is used to detect changes in the cloudiness of the solution. For experiments performed at the 1 L scale a turbidity of zero % indicates a clear solution and a turbidity value of 100% represents a cloudy solution. This PAT tool can be used to detect the point of nucleation and dissolution, which is required for MSZW determination of a crystallization system. An ATR-UV/Vis probe is used for monitoring changes in the liquid phase. Any changes in concentration are detected by a change in absorbance of the peak wavelength at which the compound absorbs. The wavelength range for measuring absorbance is 242 to 614 nm. The ATR-UV/Vis was used for qualitative monitoring of the changes in the crystallization process, hence calibration was not performed. PVM is an in-line video

camera detecting any changes in morphology of the crystals during the crystallization process.

3.4.1 Cooling crystallization of sodium benzoate in water

Cooling crystallization experiments were performed in a 250 mL and 1 L vessel using the model system sodium benzoate in water. Results are discussed within Chapter 4. The 250 mL scale experiments performed at AstraZeneca (AZ) were carried out using a 3-blade glass retreat curve agitator and using a D6001-HC-K FBRM Lasentec probe. The 1 L scale experiments performed at Loughborough University (LU) were conducted using a stainless steel 3-blade marine agitator and an A100 Lasentec FBRM probe. In all experiments a stirrer speed of 300 rpm was used whereas the ramp rates and initial concentrations varied. Ramp rates of 0.1, 0.3 and 0.5 °C/min were used at initial concentrations of 466, 566 and 633 mg/mL solvent. The temperature was controlled using a Huber Ministat unit. For the 250 mL scale this was connected to a computer package known as Labworldsoft, which controlled the temperature at a desired set-point. For the 1 L scale experiments both FBRM and temperature are recorded using a software tool (Crystallization Process Informatics System, Cry PRINS) developed in Labview. Figure 3.1 shows both the schematic of the set-up and picture of the crystallization rig.

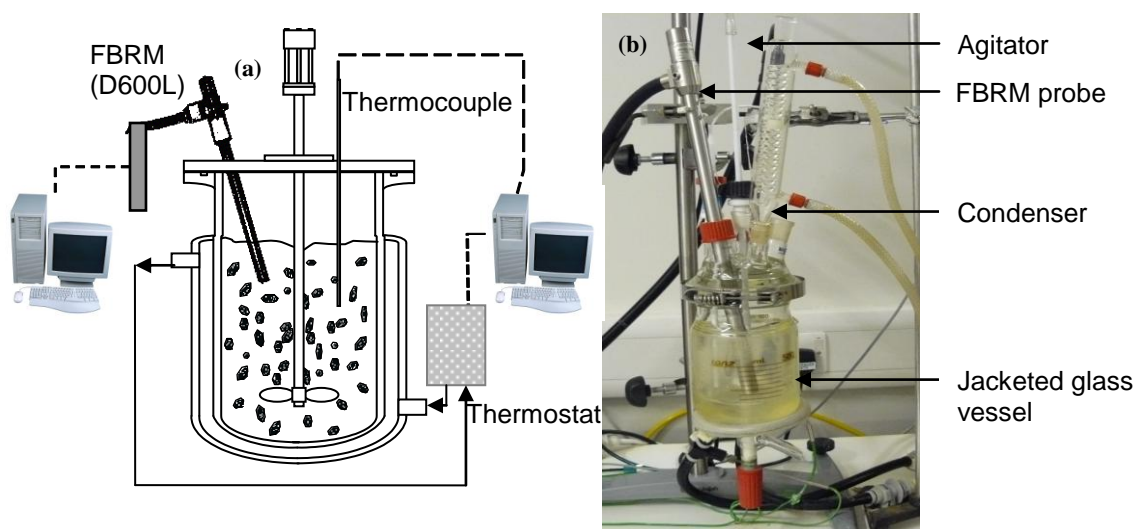


Figure 3.1. (a) Schematic of the set-up and (b) picture of the crystallization rig at LU for the cooling crystallization of sodium benzoate from water experiments

3.4.2 Cooling crystallization of PABA in ethyl acetate

Cooling crystallization experiments using the model system PABA in ethyl acetate were performed within two different setups using a jacketed glass vessel of 1 L. Results are discussed within Chapter 6. A solution of initial concentration 133 mg/mL was heated up from 25 to 70 °C using a ramp rate of 5 °C/min and kept at 70 °C until all the crystals dissolved (clear solution). The method of cooling to crystallize the compound was used by cooling from 70 to 45 °C at a ramp rate of 0.5 °C/min and then the system was kept at 45 °C for durations of 6.8-17.5 hours. The system was further cooled from 45 to 5 °C using a ramp rate of 0.5 °C/min and then kept at 5 °C for durations of 14-22 hours. PAT tools were used to monitor the cooling crystallization experiments. The crystallization rig set-up at AZ consisted of a Mettler Toledo FSC402 turbidity meter and Lasentec (D6001-HC-K) FBRM probe. The type of agitator used is a 3-blade glass retreat curve at a rotation speed of 300 rpm. The crystallization rig set-up at LU consisted of the same model of FBRM probe and a MSC 621 ATR-UV/Vis probe (Carl Zeiss, Inc). A 4-(PTFE coated) pitched blade turbine was used at a rotation speed of 315 rpm. Figure 3.2 shows the schematic representation of the set-ups of both rigs.

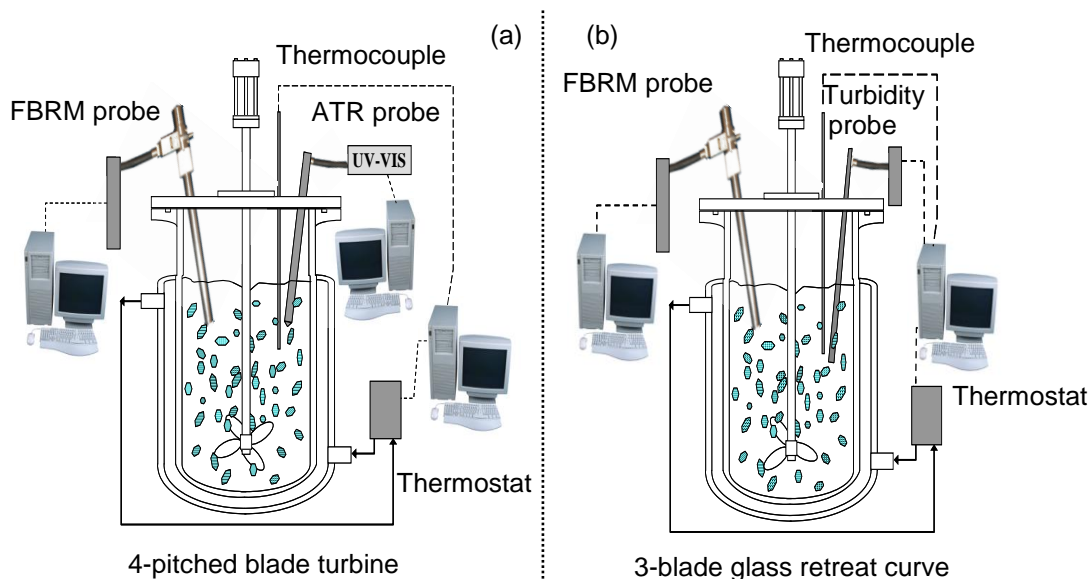


Figure 3.2. Schematic set up of the crystallization rig using (a) 4-pitched blade turbine with FBRM and ATR-UV/Vis (LU rig) and (b) 3-blade glass retreat curve agitator with FBRM and turbidity probes (AZ rig)

3.4.3 Cooling crystallization of PABA/MABA in water for MSZW determination

Cooling crystallization experiments were performed within two different vessels of size 1 L using a Mettler Toledo FSC402 turbidity meter and Lasentec (D6001-HC-K) FBRM probe to obtain MSZW measurements for the model systems PABA, MABA and OABA in water. Results are discussed within Chapter 7. One of the rig set-ups used a 3-blade glass retreat curve agitator and another set-up used a 4-(PTFE coated) pitched blade turbine. Stirrer speeds of 250, 300 and 400 rpm were used to create a well suspended solution. Ramp rates of 0.5, 0.3 and 0.1 °C/min were used to obtain solubility and nucleation points at concentrations in the range 10 to 35 mg/mL. The set-up of the crystallization rig is the same as that shown in Figure 3.1.

3.4.4 pH controlled cooling crystallization experiments of PABA/MABA in ethanol

Crystallization of acidic salts and pH controlled polymorphic crystallization experiments are performed using a linear cooling crystallization method within a 750 mL vessel. Results are discussed within Chapter 8 and 9. The type of agitator used is a 3-blade glass retreat curve agitator at a rotation speed of 300 rpm. Experiments were performed within a crystallization rig at AZ. Model system used in these experiments is PABA and MABA in solvents of pure ethanol and water. PAT tools were used to monitor the crystallization process including a Lasentec (D6001-HC-K) FBRM, MSC 621 ATR-UV/Vis (Carl Zeiss, Inc), Lasentec PVM (supplied by Mettler Toledo) and pH probe. A schematic of the crystallization rig is shown in Figure 3.3.

The method of cooling crystallization involved heating the system to 40 °C to achieve a well suspended solution of raw material in solvent. The next stage involved starting the pH control at the desired set-point and heating to 70 °C using a ramp rate of 0.3 °C. During this stage acid and base is added in steps and at the end of the stage all the crystals dissolve. The system is then cooled to 5 °C using a ramp rate of 0.3 °C/min resulting in nucleation. For the crystallization of PABA in ethanol at pH=2.5 and MABA in ethanol at pH=4.1 the temperature increase from 40 to 70 °C does not start until all the acid is added. A slight modification is made to the method for crystallizing

the hydrobromic (HBr) salts. This involved adding acid to a well suspended solution at 40 °C to achieve the desired pH set-point resulting in complete dissolution. The system was then cooled to 5 °C using a ramp rate of 0.3 °C/min, resulting in nucleation. For the crystallization of MABA in water after cooling the system to 5 °C base (NaOH) is added to achieve the desired pH and the system is left overnight for 13 hours before nucleation occurs.

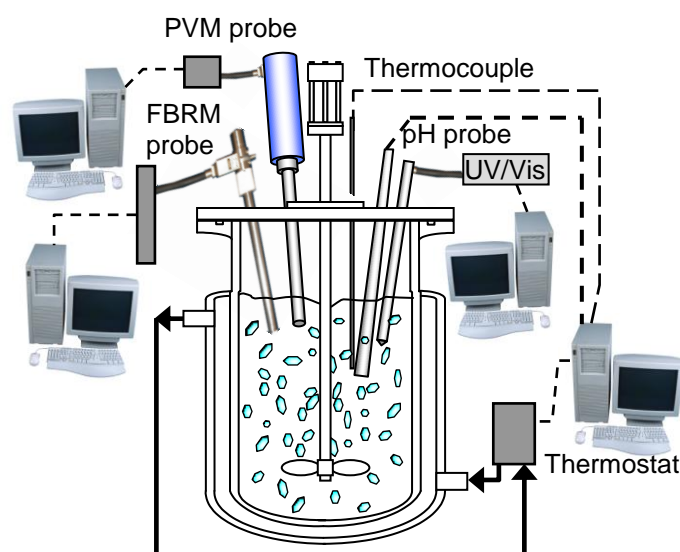


Figure 3.3. Schematic of the crystallization rig for the pH controlled cooling crystallization experiments (AZ rig)

3.5 Antisolvent crystallization experiments

Antisolvent crystallization experiments were performed using sodium benzoate in pure water with an initial concentration of 545 mg/mL. Results are discussed within Chapter 5. The system was heated up from 20 to 25 °C and kept at 25 °C until all the crystals dissolved resulting in a clear solution. IPA (antisolvent) was then added using a dosing rate within the range 0.3-2 g/min, reaching a final volume ratio of IPA/water of 5:1. The temperature of the system was maintained constant at 25 °C using a Huber ministat unit. Experiments were performed using two different rigs within a 1 L jacketed glass vessel. The crystallization rig set-up at AZ consisted of an automated lab reactor

(Mettler-Toledo Lab Max system) using a 3-blade glass retreat curve and a stirrer speed of 300 rpm. PAT tools used to monitor the solid phase include a Lasentec (D6001-HC-K) FBRM probe and Mettler Toledo FSC402 turbidity meter. The crystallization rig set-up at LU consisted of a 1 L crystallization vessel and a peristaltic pump for the addition of the antisolvent to the vessel. The type of agitator used was a 4-pitched blade turbine (coated with PTFE) with a rotation speed in the range of 255-300 rpm. The same model of FBRM probe was used and a MCS 621 ATR-UV/Vis probe (Carl Zeiss, Inc). The wavelength range used for measuring absorbance is 242-614 nm in which sodium benzoate has a peak absorbance at 270 nm. A schematic representation of the set-ups of both antisolvent crystallization systems are shown in Figure 3.4 and a picture of the crystallization rig set-up for experiments performed at LU using the peristaltic pump is shown in Figure 3.5.

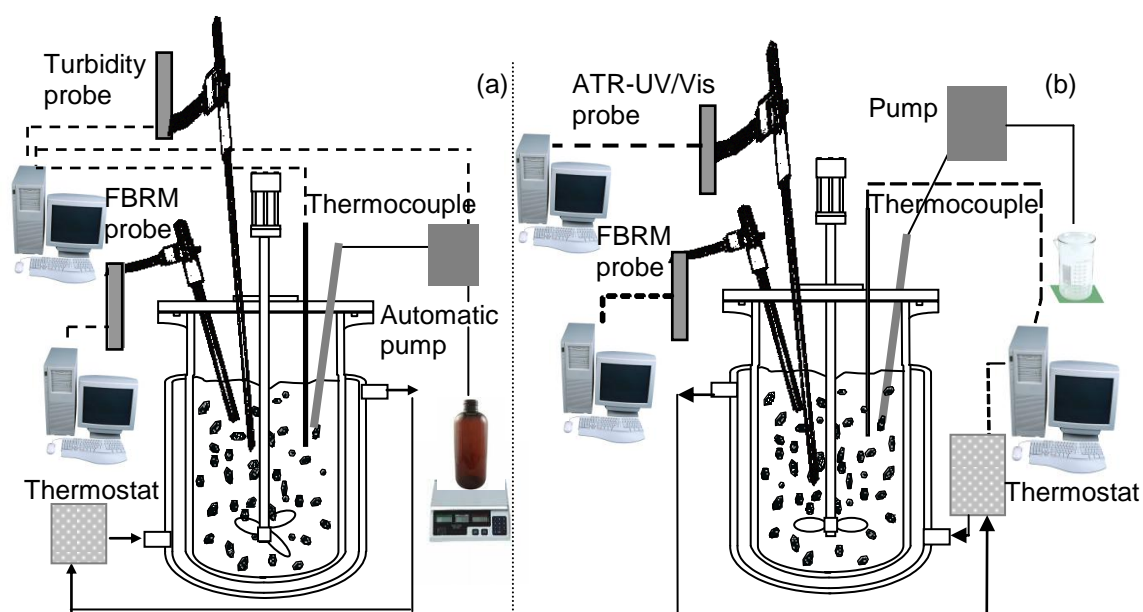


Figure 3.4. Schematic set-up of the crystallization rig for (a) automated LabMax system with a 3-blade glass retreat curve agitator (AZ rig) and (b) laboratory rig with a 4-pitched blade turbine agitator (LU rig)



Figure 3.5. Picture of the antisolvent crystallization rig set-up performed with a peristaltic pump (Loughborough University)

3.6 Salt precipitation and evaporation experiments

Acidic salts including sulphate and phosphate salts of PABA were produced by the method of precipitation. Results are discussed within Section 8.4 of Chapter 8. Vessel size of 750 mL is used with a 3-blade glass retreat curve agitator at a rotation speed of 300 rpm. A well suspended solution is heated to 40 °C and then acid is added with the use of a pump. The moment acid is added to solution crystals precipitate from solution. The experiment is repeated in a 100 mL beaker using a magnetic flea and hot plate to heat the well suspended solution until all the crystals dissolve. Acid is added and crystals precipitate from solution.

Alkali salts of PABA were produced by a method of evaporation using a 100 mL beaker. Results are discussed in Section 8.5 of Chapter 8. The raw material was well suspended in an ethanol solution at room temperature (25 °C) using a magnetic stirrer. Alkali (NaOH) was then added to achieve a high pH of solution. During this stage the crystals dissolved until complete dissolution occurred. The solution was then left in a fume cupboard at room temperature for approximately 48 hours resulting in nucleation. The procedure was repeated using KOH resulting in the crystallization of the potassium salt of PABA.

3.7 Summary of experiments performed within each Chapter

A range of experiments were performed in which process analytical technology (PAT) tools were used to investigate the crystallization of pharmaceutical polymorphs, salts and hydrates. The details of each experiment including crystallization method, model compound, solvent and acids/ bases used are shown in Table 3.1. The details of each experimental set-up and parameters used include vessel size, impeller type, agitator speed, ramp (cooling) rate or dosing rate, PAT tools used and where the vessel is based (AZ or Uni) is shown in Table 3.2.

Table 3.1. Summary of experiments performed including method and materials

Experiment number	Chapter number	Crystallization method	Model (AI) compound	Solvent	Acids/bases
1 and 2	4	Cooling	Sodium benzoate (SB)	water	-
3	4	Cooling (solubility determination)	SB	Organic solvents and water	-
4	4 and 5	Gravimetric method (solubility determination)	SB	Water and water/IPA ratios	-
5 and 6	5	Anti-solvent	SB	Water (solvent) and IPA (anti-solvent)	-
7	5	Slurry experiment at 25 °C	SB	Water/IPA (different ratios)	-
8 and 9	6	Cooling	PABA	Ethyl acetate	-
10 and 11	7	Cooling (MSZW determination)	PABA, MABA	water	-
12	7	Cooling (MSZW determination)	PABA, MABA, OABA	water	-
13	8	Precipitation	PABA	ethanol	H ₂ SO ₄ H ₃ PO ₄
14	8	Evaporation	PABA	ethanol	NaOH, KOH
15	8 and 9	Cooling (pH control)	PABA, MABA	Ethanol and water	HCl, HBr, NaOH
16	9	pH swing	PABA	water	HCl, NaOH

Table 3.2. Summary of experiments performed including experimental set-up and parameters

Exp. no.	Chapter number	Vessel size	Impeller type	Agitator speed (rpm)	Ramp (cooling) rate (°C/min)	Vessel at AZ or Uni	PAT tools
1	4	250 mL	3-blade glass retreat curve (GRC)	300	0.1, 0.3, and 0.5	AZ	FBRM
2	4	1 mL	Stainless steel 3-blade marine	300	0.3	Uni	FBRM
3	4	1 L	Magnetic flea	700	0.3	AZ	Turbidity
4	4 and 5	20 mL	Shaker/ water bath for stirring	-	-	Uni	-
5	5	1 L	3-blade GRC	300	Dosing rate: 0.33g/min	AZ	FBRM, Turbidity
6	5	1 L	4-pitched blade turbine (PBT) (coated with PTFE)	255, 300	Dosing rate: 1 and 2g/min	Uni	FBRM, ATR-UV/Vis
7	5	1 mL	Magnetic flea	700	-	AZ	-
8	6	1 L	3-blade GRC	300	0.5	AZ	FBRM, Turbidity
9	6	1 L	4-PBT	315	0.5	Uni	FBRM, ATR-UV/Vis
10	7	1 mL	Magnetic flea	700	0.1, 0.3, 0.5	AZ	Turbidity
11	7	1 L	3-blade GRC	250, 300, 400	0.1, 0.2, 0.3, 0.5	AZ	Turbidity
12	7	1 L	4-PBT	255, 300	0.3, 0.5	Uni	FBRM
13	8	100 mL beaker and 750 mL	Magnetic flea/ 3-blade GRC	300	-	AZ	pH probe
14	8	100 mL beaker	-	-	-	AZ	pH probe
15	8 and 9	750 mL	3-blade GRC	300	0.3	AZ	FBRM, ATR-UV/vis, PVM, pH probe
16	9	750 mL	3-blade GRC	300	-	AZ	FBRM, pH probe

3.8 Solid state analysis of crystals

Solid samples of the crystals were analysed using a range of SSA techniques. Visual images of the crystals are obtained with the use of two types of optical microscopes including an Olympus BX51 microscope using image Pro Plus software and a Leica DMLM microscope. Crystal samples were placed on a cover slide with a cover slip on top and viewed under the microscope. Crystal samples are viewed using a scanning electron microscope providing 3D images with higher magnification. Samples are gold plated to provide clear images. Two types of hot stage microscopy (HSM) units were used to determine the melting point of polymorphs and for detecting higher melting point polymorphic forms. One of the HSMs consisted of an Olympus BX51 microscope with a Linkam heating stage attachment connected to a 3-CCD colour video camera (JVC model KY-F55B). Another HSM unit consisted of a Leica DMLM microscope with a Mettler Toledo FP90 HS attachment connected to a JVC colour video camera.

Thermal techniques used include differential scanning calorimetry (DSC) and thermal gravimetric analysis (TGA) units which provide data on the melting point of polymorphs, identify polymorphs transitions and the presence of hydrates/solvates. Three types of DSC machines are used to analysis samples including a Perkin Elmer (Pyris 1), Mettler Toledo and TA instrument Q10. The ramp (heating) rate used includes 1 and 10 °C/min. Samples were analysed using a Perkin Elmer TGA unit with a heating rate of 10 °C/min. Dynamic vapour sorption (DVS) is a useful technique for identifying the likelihood of compounds forming hydrates and to determine whether the material is amorphous or highly crystalline. The manufacturer of the DVS unit is Surface Measurements Systems Ltd and the model used is Dynamic Vapour Sorption Analyser, DVS-1. Samples are placed inside a chamber and the relative humidity (RH) is increased from 40 to 90% resulting in a change in mass.

An X-ray powder diffraction unit of model Rigaku Miniflex is used to determine structural differences between the different polymorphic forms of the compound sodium benzoate. All XRPD samples except the samples obtained from the sodium benzoate anti-solvent crystallization experiments at volume ratio IPA/water of 3:1 and 5:1 were gently grinded before being placed onto a shallow aluminium plate. Gently

grinding of the crystals is required to prevent preferred orientation. The aluminium plates are spinning while the XRPD machine is operating, therefore, a thin layer of crystals is placed onto the shallow aluminium plate to prevent the loss of sample from the plate which would contaminate the XRPD chamber and can result in misinterpretation of the results. A scan speed of 1 °/min was used and the start and stop angles were 3 and 35 respectively. Solid state NMR spectra were obtained using a Bruker Avance III NMR spectrometer. Samples were packed into 4 mm OD rotors and spun at 12 kHz. Carbon spectra were recorded at a frequency of 125.64 MHz using the cross polarisation method with a 1 ms contact time and 100 kHz of proton decoupling. Sodium (^{23}Na) spectra were recorded at 132.17 MHz using a one pulse acquire sequence. Proton spectra were recorded at a frequency of 499.66 MHz using a one pulse acquire sequence. IR data were obtained using a Perkin Elmer instrument (FT-IR system) of model spectrum GX. Crystal samples were placed onto a small glass hole in the centre of a plate in which a laser beam is directed towards. The crystals were kept in position with the use of a metal probe and the sample was covered with a lid for containment before analysis.

3.9 Conclusions

A description of the materials used and a detailed methodology of all experiments are discussed within this chapter. The model systems used include sodium benzoate and isomers (*ortho*, *meta* and *para*) of amino benzoic acid (ABA). Small scale experiments were performed at the 1 mL scale using the Avantium Crystal 16. These experiments provide data on solubility measurements, stability determination in various solvents and MSZW values. An alternative method used for solubility determination is the gravimetric method. The methodology of beaker experiments at the 100 mL scale involving salt precipitation and evaporation are mentioned. Larger scale crystallization experiments were performed at the 250 mL to 1 L scale. Methods used include cooling, antisolvent and pH controlled. PAT tools used for monitoring the process include FBRM, turbidity probe, ATR-UV/Vis, PVM and pH probe. A schematic set-up of each experiment is shown in a range of Figures highlighting the differences in PAT arrangements. SSA techniques used in this research work for characterising the crystal

product include optical microscope and SEM, XRPD, DSC, TGA, DVS, NMR and IR spectroscopy. The detailed operating conditions of these techniques are discussed in this Chapter.

Chapter 4. PAT based investigation of the cooling crystallization of sodium benzoate hydrate

4.1 Introduction

Traditionally the cooling crystallization method of an active pharmaceutical ingredient is by trial and error in which an under-saturated solution is cooled down at a constant ramp rate resulting in a supersaturated solution. The process often leads to failed batches due to the crystallization of different polymorphic forms, which may result in an increase in economical costs (Davey, 2003). Recent advances in the pharmaceutical industry have involved the use of process analytical technology (PAT). These tools enable the systematic design and control of the crystallisation systems to produce high quality crystalline products with reduced variability in the properties (Braatz, 2002; Fujiwara *et al.*, 2002; Zhou *et al.*, 2006; Nagy *et al.*, 2008b). Process analytical tools can be used to indicate a potential polymorphic transformation, however a range of solid state analytical (SSA) techniques usually must also be used to confirm the formation of polymorphs.

This chapter presents the advantages of using PAT tools combined with SSA techniques for the monitoring and detection of different polymorphic/pseudo-polymorphic forms of a model system, sodium benzoate. As there is limited literature data on the solubility of sodium benzoate the first stage of experiments involved solubility screening using the Avantium Crystal 16 unit on a 1 mL scale. Scale up experiments were performed from the 1 mL to vessel sizes of 250 mL and 1 L for the cooling crystallization of sodium benzoate from water. The main PAT tool used within these studies was the FBRM probe, which detected the formation of an unknown hydrate. A series of solid state analyses were carried out on the crystals using a range of techniques including DSC, TGA, DVS, XRPD, HSM, optical microscopy, SEM, solid state NMR and IR spectroscopy. The results provide evidence of the existence of a new channel hydrate of sodium benzoate that has not yet been reported in the literature.

4.2 Experiments performed

Solubility experiments were performed using the Avantium Crystal 16 and a gravimetric method. A picture of the Crystal 16 equipment can be found on Appendix A. The materials and solvents used are mentioned in Section 3.2 of Chapter 3. A detailed description of the method can be found in Section 3.3 of Chapter 3. Cooling crystallization experiments were performed in jacketed glass vessels at the 250 mL and 1 L scale using an FBRM probe to monitoring the process. The model of FBRM probe and parameters used in each experiment including type of agitator, stirrer speed, ramp rates and initial concentrations of sodium benzoate in water are discussed in Section 3.4.1 of Chapter 3. A schematic and picture of the crystallization rig is shown in Figure 3.1 of Chapter 3.

4.3 Solubility measurements

The main aims of the experiments were to use PAT tools combined with solid state techniques to identify the different polymorphic forms of sodium benzoate. The first stage of the experiments involved solubility screening in order to find a suitable solvent for which sodium benzoate can be re-crystallized using cooling. For the screening experiments Avantium Crystal 16 equipment was used. This detects the cloud and clear points using turbidity probes. A turbidity of 100 represents a clear solution which indicates that all the crystals have dissolved and a turbidity value of zero indicates a cloudy solution with crystals present. Turbidity values for organic solvents remained at 0% for the concentration range 20-40 mg/mL, indicating that sodium benzoate has a very low solubility in organic solvents. The solubility results for sodium benzoate in organic solvents can be found in Appendix C. Figure 4.1a shows the turbidity results for the cooling crystallization experiments using water as a solvent. A concentration of sodium benzoate in water of 649.8 mg/mL results in a clear point of 85 °C indicating that sodium benzoate has a high solubility in water. The solubility obtained using gravimetric analysis is slightly lower when compared with literature data, as shown in Figure 4.1b, however both these results show a similar solubility curve over the temperature range 30-70 °C. For the gravimetric method a syringe and filter was used to uptake the fluid sample from the slurry mixture. In some cases the uptake of fluid was

slow, which was due to blockage of the filter head. This indicated that crystals from the fluid were crystallizing on the filter head, which would lower the solubility value and would explain why the gravimetric results are slightly lower than literature data. To improve the accuracy of the gravimetric results a fresh filter head would be used for each sample vial. Also the time taken to remove the fluid from the syringe to the crystallizing dish would be kept to a minimum to prevent solid crystallizing inside the syringe due to a drop in temperature (high temperature in water batch to room temperature). Literature solubility data shows that for the operating temperature range of water between 15 and 97 °C the solubility of sodium benzoate is between 628 and 733 mg/mL, indicating a high solubility but small temperature sensitivity of the solubility (flat solubility curve). In the interval 10-50 °C, there is practically no change in solubility and even in the range of 50-90 °C, the change is only about 10%. Due to the high solubility, water was chosen as the solvent for the cooling crystallization experiments, and initial concentrations and operating temperature were carefully selected to be able to crystallize the compound via cooling.

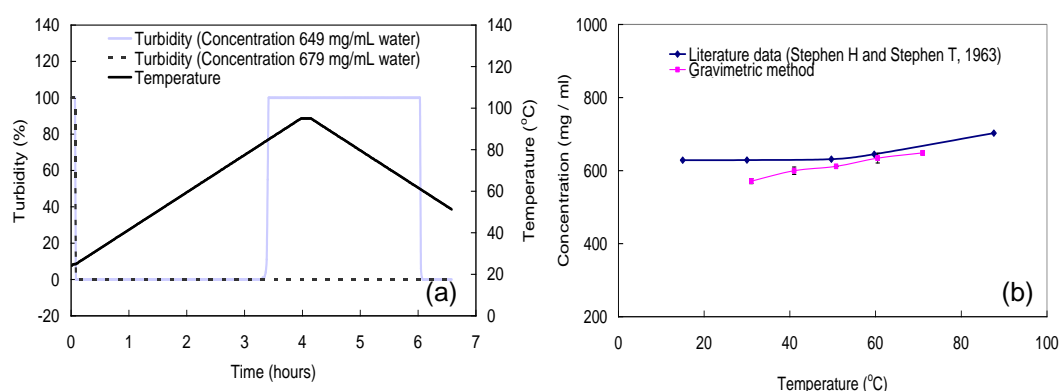


Figure 4.1. Solubility results for sodium benzoate in water obtained from (a) Crystal 16 unit (turbidity points) and (b) literature data (Stephen and Stephen, 1963) and gravimetric method

4.4 Monitoring of sodium benzoate hydrate formation using PAT tools

Experiments were performed at 250 mL and 1 L scales with the use of the FBRM probe to monitor the cooling crystallization of sodium benzoate from water. Figure 4.2 shows

the FBRM results for the 1 L scale and 3 repeated experiments using a 250 mL vessel with variations in the initial concentration of sodium benzoate in water of 466, 566 and 633 mg/mL solvent. The agitator types were varied within the different size vessels to examine the effect of mixing conditions on the behaviour of the system. In all cases as the system was heated the crystals dissolve as indicated by a decrease in the FBRM counts. The larger baseline in the case of the 1 L vessel (Figure 4.2a) is due to the use of an older FBRM probe (model A100) with small defects on the window. At temperatures above 65 °C there is a fluctuation in the number of counts, which is thought to be due to either attrition, agglomeration or a morphology change as the crystals dissolve and grow or a polymorphic transformation. The fluctuation in FBRM counts is repeatable within the same vessel using different concentrations. For a concentration of 566 mg/mL, the fluctuations occurred at all ramp rates of 0.1, 0.3 and 0.5 °C/min. The repeatability of the results using different mixing conditions, within the different vessel sizes, indicates that this factor does not affect the behaviour of the system.

The use of a combination of FBRM statistics including fine (1-20 microns), coarse (50-250 microns) and total (1-1000 microns) counts show that the FBRM signal is not due to attrition or agglomeration as all counts show a similar behaviour during the fluctuation, providing further evidence of a possible morphology change resulting from a polymorphic transformation. Similar results for other model systems were reported in the literature, which involved the use of FBRM statistics to indicate a polymorphic transformation from a meta-stable to a stable form (O'Sullivan and Glennon, 2005; Nagy *et al.*, 2007; O'Sullivan *et al.*, 2003). However, it has to be mentioned that the FBRM signal is very difficult to interpret since various events during the crystallisation may lead to similar changes in the FBRM signal (Yu *et al.*, 2008). Nevertheless FBRM can provide a very useful tool to signal that an event happens in a particular stage of the crystallisation process, which generally requires additional solid-state analytical methods to elucidate.

As hydrates tend to be stable at lower temperatures and anhydrides tend to be stable at higher temperatures (Bechtloff *et al.*, 2001) the hypothesis is that there is a possible polymorphic transformation from a hydrate to the anhydrate form of sodium benzoate at a temperature above 65 °C. This transformation occurs without complete dissolution of

the anhydrous form (FBRM counts do not decrease to zero as shown in Figure 4.2(d)). An additional FBRM statistic including the mean chord length is plotted in Figure 4.2(d). This graph shows that at a temperature of above 65 °C there is an increase in fine counts and a decrease in coarse counts and mean chord length suggesting the formation of fine particles. As the temperature is decreased below 65 °C the coarse counts and mean chord length increase and the fine counts decrease and then increase suggesting the formation of a possible needle like morphology.

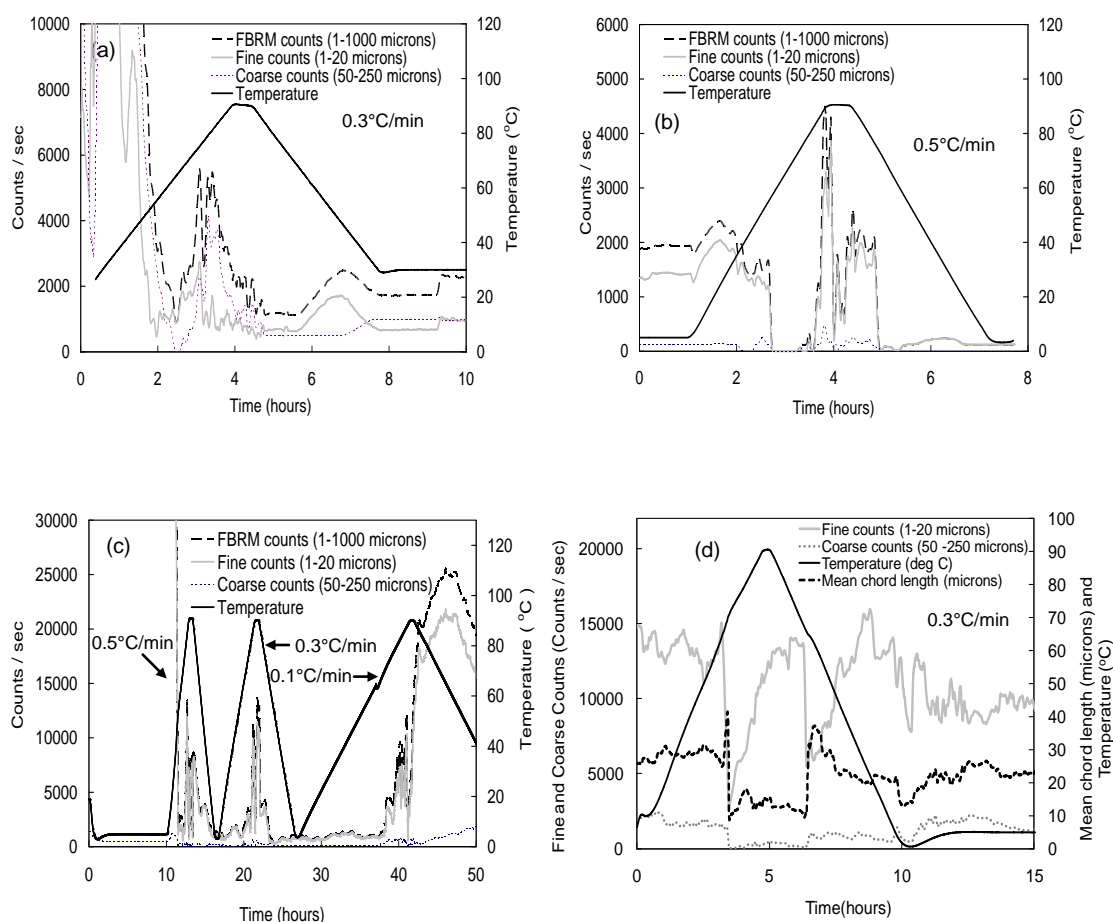


Figure 4.2. FBRM results for the cooling crystallization of sodium benzoate in water at different initial concentrations (C_0): (a) 1 L vessel and $C_0 = 466$ mg/mL; (b) 250 mL vessel and $C_0 = 466$ mg/mL; (c) 250 mL vessel and $C_0 = 566$ mg/mL (d) 250 mL vessel and $C_0 = 633$ mg/mL

4.5 Evaluation of the formation of the new sodium benzoate hydrate using solid state analytical methods

To investigate whether a hydrate forms when sodium benzoate re-crystallizes from water, samples were taken from the cooling crystallization experiments and analysed using a range of SSA techniques, such as optical and SEM, HSM, XRPD, DSC, TGA, DVS, NMR and IR spectroscopy.

Figure 4.3 shows the optical and SEM images of the anhydrous form of sodium benzoate and samples re-crystallized from water. The optical microscope image of the anhydrous form shows large agglomerates made up of many fine particles of size less than 10 μm . The SEM image shows the particles have a rough surface. SEM images of the sample re-crystallized from water show the formation of a solid clump which has a fibrous surface structure. This is in correlation with the optical microscope images, which show long fibrous needles with longest dimension of approximately 200 μm . Any differences in these images is due to the fact that the optical microscope image was obtained from a mobile slurry and the SEM images were obtained after the crystals had been filtered under vacuum resulting in the formation of the solid clump. Comparing the SEM's of the raw material (anhydrous) and sodium benzoate re-crystallized from water, shows a clear difference between the surface characteristics. The change in morphology from fines to needles indicates the possibility of a different form (hydrate). These results fit with the FBRM results shown in Figure 4.2(d) suggesting a polymorphic transformation from anhydrate (fines) to hydrate (needle morphology) form once the temperature is below 65 $^{\circ}\text{C}$. Nagy *et al.*, (2007) reported similar results for the detection of a polymorphic transformation of caffeine from anhydrous form to a channel hydrate that resulted in a change in morphology from fines to needles. During the cooling crystallization of sodium benzoate from water a solid clump formed, which is immobile due to the result that sodium benzoate uses up water during the formation of the hydrate.

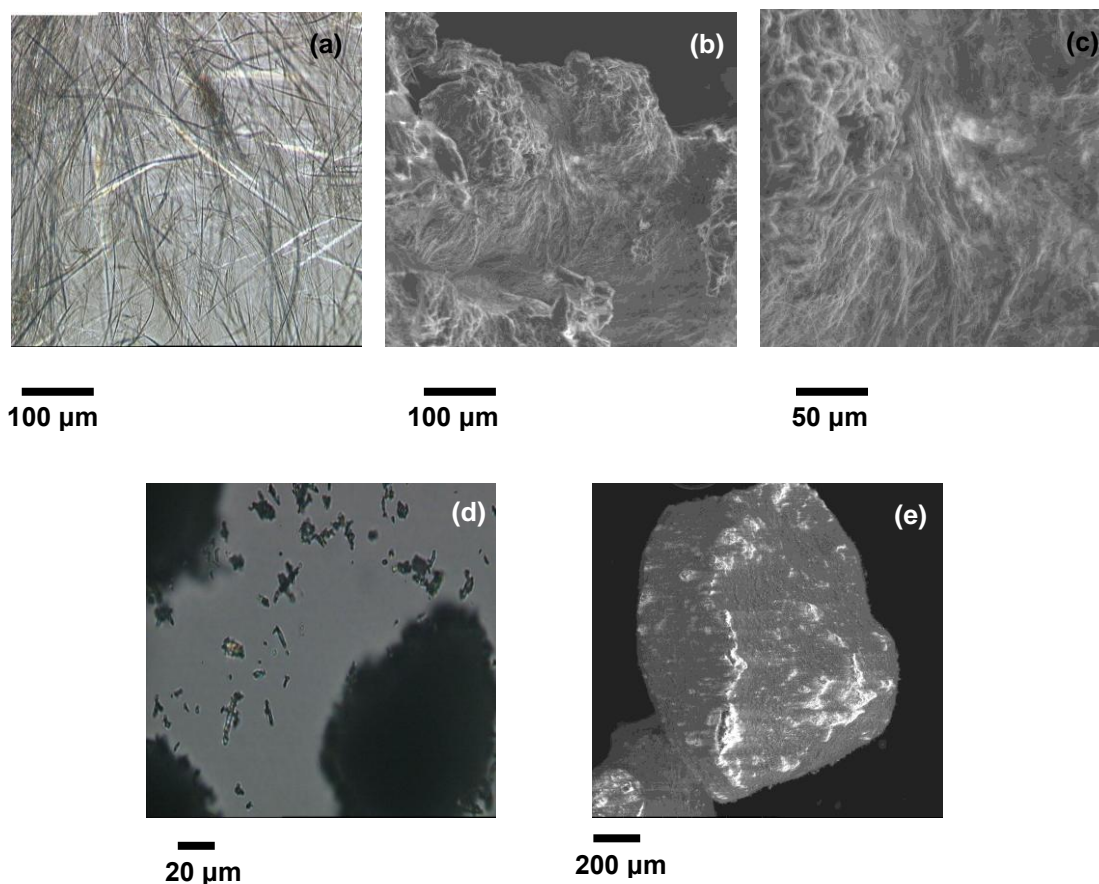


Figure 4.3. (a) Optical microscope image of sodium benzoate re-crystallized from water, (b, c) SEM images of sodium benzoate re-crystallized from water, (d) optical microscope image of raw material (anhydrous) form of sodium benzoate and (e) SEM image of raw material (anhydrous) form of sodium benzoate

Figure 4.4 shows the HSM results for the anhydrous form of sodium benzoate. The HSM images show that the crystals start to melt between 436 and 440 °C which is considered very high for organic compounds even if sodium benzoate is an organic ionic compound (salt). HSM images also show that sodium benzoate re-crystallizes from the melt showing a birefringent crystal behaviour with an anisotropic structure, also illustrated in Figure 4.5. These compounds are known to exhibit a tendency to form polymorphs. HSM was performed on the sample of sodium benzoate re-crystallized from water (hydrate). Brittian, (1999) reported hot stage microscopy as a useful technique in classifying the type of hydrate. For channel hydrates, de-hydration is observed as a progressive darkening of the ends of the crystal towards the centre as the crystals are heated. However, these results showed no change in the appearance of the crystals during the temperature range 25-440 °C (melting point of anhydrous form).

This could be due to the fact that the crystals appeared as dark solid agglomerates made up of very fine fibres as shown by the SEM images in Figure 4.3 (b, c).

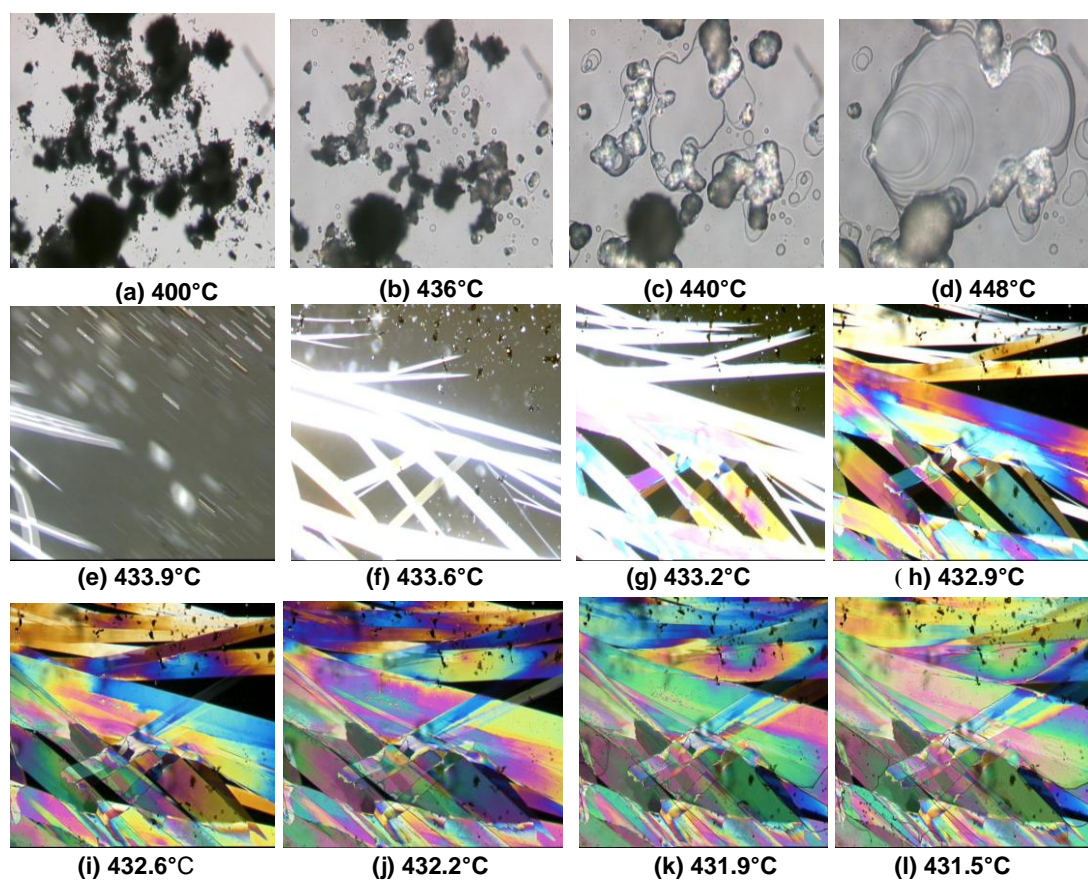


Figure 4.4. Hot stage microscopy (HSM) images of sodium benzoate. Images (a-d) are during the heating phase and (e-l) are during the cooling of the melt

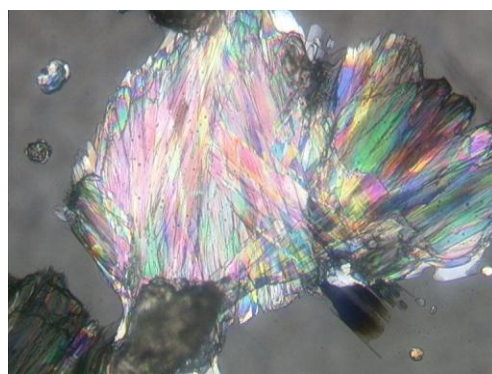


Figure 4.5. Birefringent crystal of the anhydrous sodium benzoate crystal recrystallised from melt

Further analysis was carried out using XRPD. This technique is used for the identification of different polymorphic forms of a given compound as each polymorph is represented by a particular X-ray diffraction pattern (Lu *et al.*, 2005; Yu *et al.*, 2004). Figure 4.6 shows the XRPD patterns for the raw material, anhydrous form of sodium benzoate and the sodium benzoate re-crystallized from water. The anhydrous sodium benzoate for these tests was produced by heating the crystals obtained from the crystallisation in water above the dehydration temperature, using TGA. These XRPD results show similar patterns for the raw material and the anhydrous form, indicating that the raw material is anhydrous however the pattern for sodium benzoate re-crystallized from water shows additional and missing peaks indicating a different internal structure compared to the anhydrate form. This provides evidence that a different polymorphic form exists.

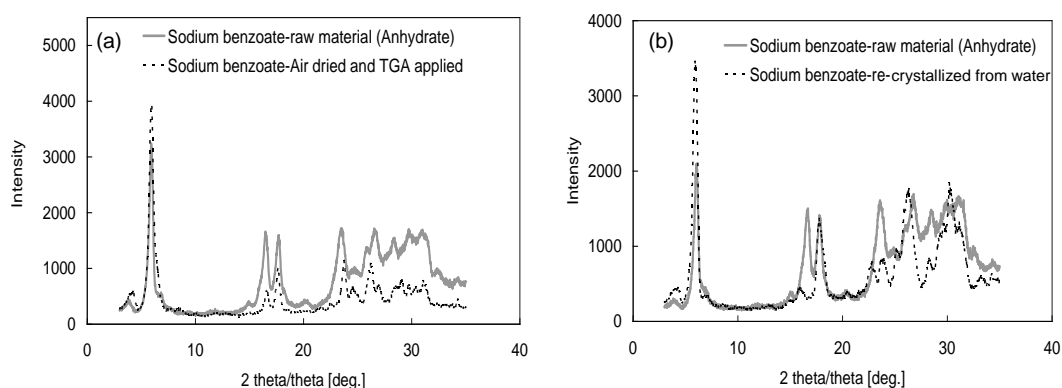


Figure 4.6. XRPD results for (a) raw material and sodium benzoate (air-dried and TGA applied) and (b) raw material and sodium benzoate re-crystallized from water

NMR spectroscopy is a powerful technique for identifying different forms of a compound including (non-stoichiometric and stoichiometric) hydrates and anhydrides (Harris and Jackson, 1987; Harris, 2007). This technique is used with XRPD to provide supporting evidence on the presence of different forms of a compound as related to geometry and compositional differences. The different chemical environments exposed to the carbon and hydrogen atoms within the molecule are represented by specific peaks in the NMR spectrum. Figure 4.7 shows the solid state NMR data of ^{13}C , ^1H and ^{23}Na for the anhydrous form of sodium benzoate and the form re-crystallized from water. ^{13}C data for both forms is very similar showing 4 peaks representing 4 different chemical

environments. The peak at 177 ppm is due to the carboxylate carbon (COO^-) and the 3 peaks within the range 120-140 ppm are due to the carbon atoms in the aromatic ring of sodium benzoate (Harris, 2006). ^{23}Na spectra shows a broad peak for the anhydrous form of sodium benzoate representing immobile sodium ions while the spectra for the sample re-crystallized from water shows an additional sharp peak at 1 ppm. The sharp peak represents mobile sodium ions providing supporting evidence of the presence of water molecules within the internal structure of the crystal. ^1H data for the anhydrous form show a broad peak in the range 0-10 ppm while the spectra for the sample re-crystallized from water shows 2 sharp peaks in the range 4-6 ppm which has been reported due to the $-\text{OH}$ group of a molecule indicating the presence of a hydrate (Atkinson and Hibbert, 2001).

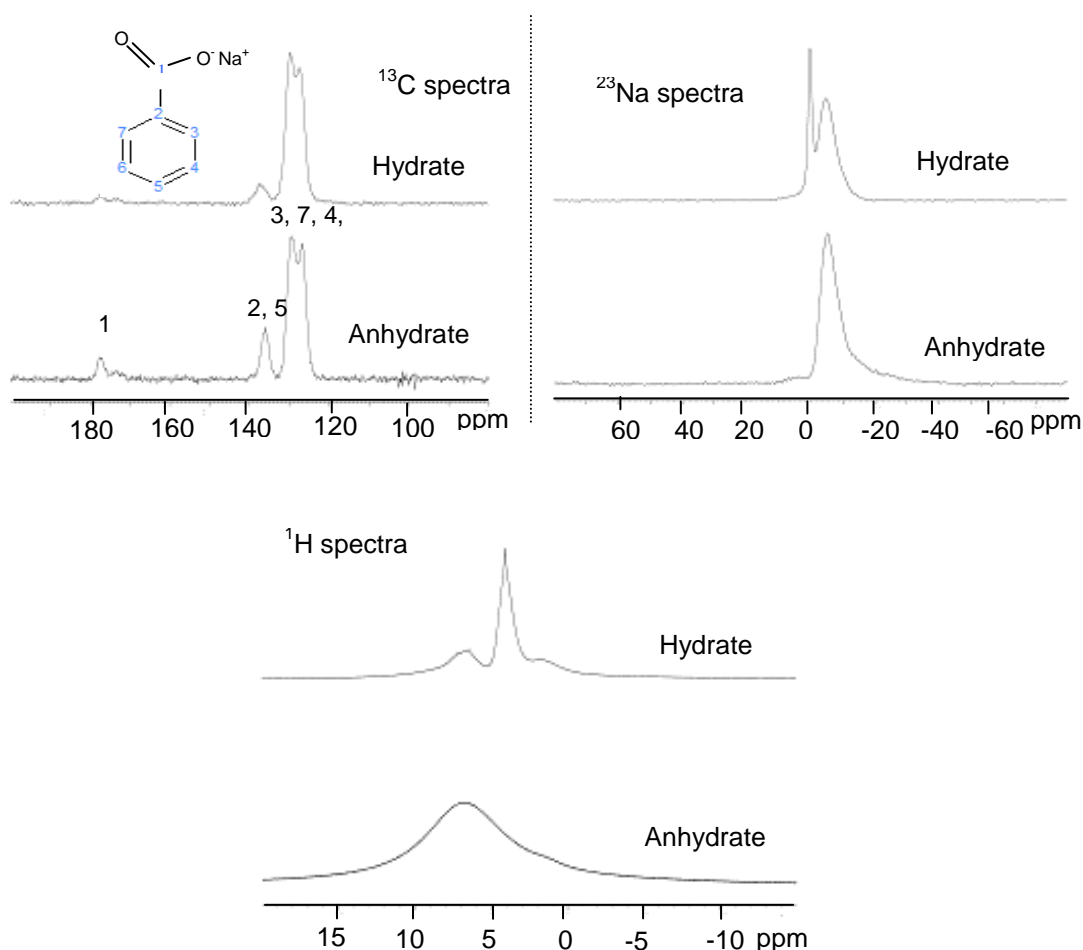


Figure 4.7. NMR data of ^{13}C , ^{23}Na and ^1H spectra for the anhydrate and hydrate form of sodium benzoate

An additional spectroscopy technique involving infra-red (IR) is applied to the anhydrous and a sample of sodium benzoate re-crystallized from water. The IR data is shown in Figure 4.8. There are two additional peaks in the IR spectrum at wavenumbers of 3440 and 3600 cm^{-1} for the sample of sodium benzoate re-crystallized from water. IR data on a hydrated form of a compound showed peaks at wavenumbers within the region of 3400-3700 cm^{-1} and a sharp peak at 3600 cm^{-1} which is due to the hydroxyl group (-OH) of water molecules (Rocco *et al.*, 1995). These data provide supporting evidence that the peaks at wavenumbers 3440 and 3600 cm^{-1} in the IR spectra for sodium benzoate re-crystallized from water are due to the presence of water molecules within the crystal lattice structure signifying the formation of a hydrate.

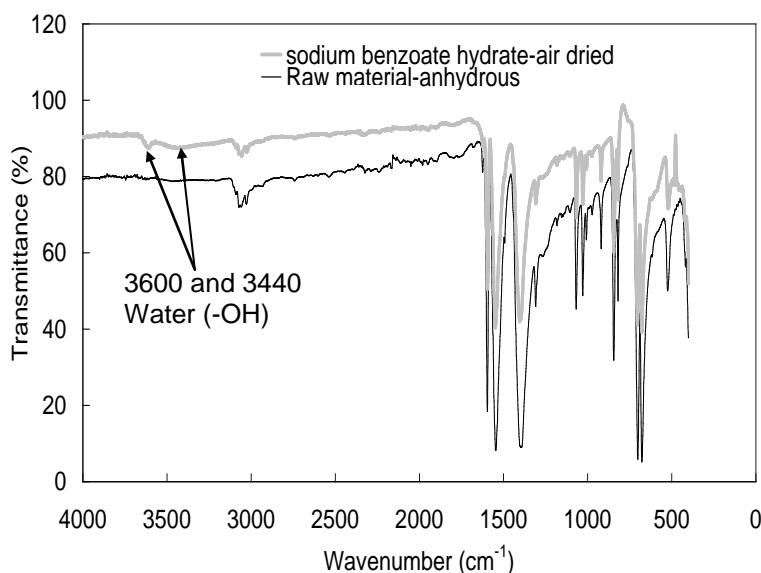


Figure 4.8. IR spectra for the anhydrous form and re-crystallized from water sample of sodium benzoate

Further solid state analysis was performed using DSC. Figure 4.9 shows the DSC results for the raw material (anhydrate) form of sodium benzoate and sodium benzoate re-crystallized from water. The type of pan used is a sealed pan with a pin hole to prevent the build up of pressure. DSC results for the raw material (anhydrous) show a sharp peak at 440 °C which confirms the results obtained from HSM, of a high melting point for the organic compound sodium benzoate. The enthalpy of melting for the raw material is 164 J/g. Figure 4.9(b) shows the DSC results for the sample of sodium benzoate re-crystallized from water, showing two peaks. The first peak occurs at a temperature of 118 °C, which is below the melting point of the anhydrous form. The

sample under analysis has not been completely air dried indicating that this is due to water on the surface of the crystals. The second peak occurs at a temperature of 125 °C, which could be due to the dehydration of a hydrate. Giron (1995) reported DSC results for a hydrated form of a compound which showed the dehydration process as a single endothermic peak occurring within the temperature range 70-130 °C. This also suggests that the second peak at a temperature of 125 °C in the DSC results for sodium benzoate re-crystallized from water is possible due to the dehydration of a hydrate. The enthalpy of dehydration is 10 J/g. The low enthalpy change signifies the formation of a channel hydrate as not much energy is required for removal of water from the crystal lattice structure due to the loosely bonded water molecules throughout the crystal lattice structure. For channel hydrates once dehydration has occurred this forms a crystal structure of low density with empty voids resulting in an unstable structure (Brittain, 1999). The crystal lattice parameters may then alter to obtain a stable structure. From DSC analysis this confirms that the anhydrous form is stable above the dehydration temperature of 125°C.

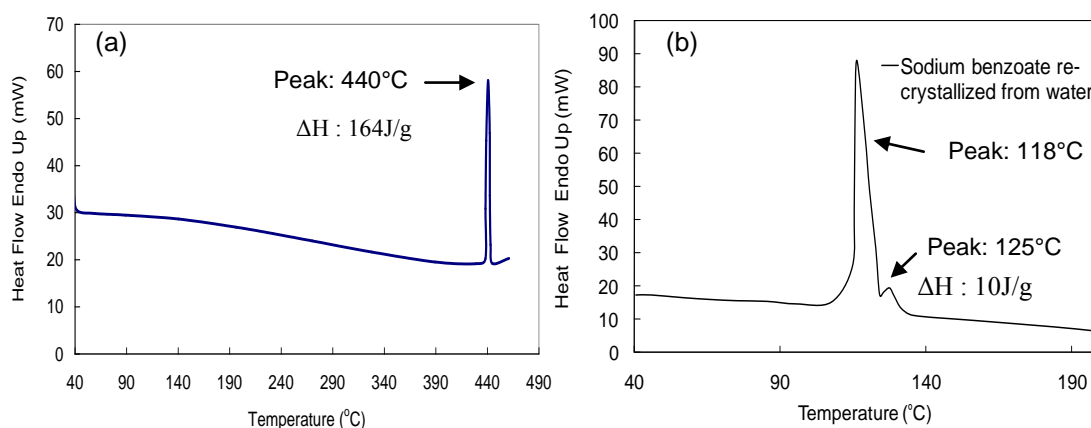


Figure 4.9. DSC results for (a) raw material form of sodium benzoate and (b) sample of sodium benzoate re-crystallized from water

To support the prediction that a channel hydrate forms, TGA analysis is performed on the sodium benzoate crystals. Figure 4.10 shows the TGA results for the air dried sodium benzoate crystals obtained at the 1 mL and 250 mL scales. Similar results are obtained at both scales showing a weight% decrease between 3 and 3.7% over a temperature range of 60-80 °C. The decrease in mass represents a loss in water from the internal structure of the crystals. Based on the weight% decrease the stoichiometry of sodium benzoate to water is calculated. The mean molecular ratio of sodium benzoate to water is 1:0.28 with standard deviation of ± 0.02 . The individual steps for this

calculation is shown in Appendix E. The non-stoichiometric ratio and the relatively low temperature at which the dehydration occurred indicate that the hydrate formed is a channel hydrate.

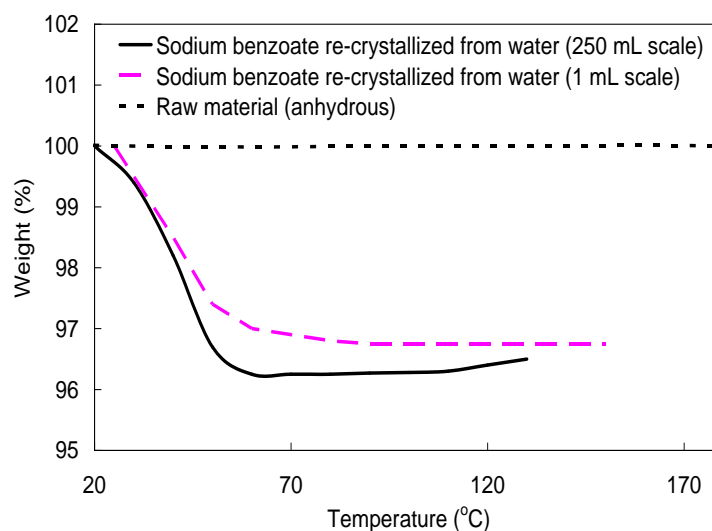


Figure 4.10. TGA results for the raw material form of sodium benzoate and sodium benzoate re-crystallized from water at the 1 mL and 250 mL scale

DVS studies are very useful for classifying hydrates and to determine whether the material is amorphous or highly crystalline. Amorphous or deliquescent material absorb large amount of water at high relative humidity whereas highly ordered crystalline materials can absorb very small amount of water of up to 0.1% weight increase (Hilfiker, 2006). Stoichiometric hydrates show sudden increases in water uptake whereas non-stoichiometric hydrates (channel hydrates) show a small and gradual increase in water uptake as the relative humidity is increased from 0 to 90% (Hilfiker, 2006). DVS was applied to a sample of anhydrous sodium benzoate to see how this behaves when subject to different amounts of water. This is achieved by changing the relative humidity (RH) between 0 and 90% while keeping the temperature constant at a value of 24.7 °C. As the RH increases any uptake in water results in an increase in mass and the reverse is true for when the RH is lowered. The results for two repeated experiments are shown in Figure 4.11.

DVS results show a large increase in the mass% as the RH is increased from 80 to 90% which suggests that during this phase sodium benzoate deliquesces (Hilfiker, 2006). For cycle 2 during the sorption stage as the relative humidity increases from 40% to 60% there is a small and gradual increase in the mass of sodium benzoate. Both desorption cycles also show a small but significant decrease in mass% as the RH is decreased from 30 to 10%. This change is significant enough to suggest the formation of a hydrate. The type of hydrate is assumed to be a non-stoichiometric (channel) hydrate as the weight% change is small and gradual, which is a common behaviour for channel hydrates (Hilfiker, 2006). These observations reinforce the results obtained from TGA which also indicated the formation of a channel hydrate when sodium benzoate re-crystallizes from water. From the small and gradual change in mass during each step in the DVS results the molecular ratio of sodium benzoate to water is calculated and a summary of the results are shown in Table 4.1. A sample calculation can be found in Appendix E. The results show a mean molecular ratio of sodium benzoate to water of 1:0.27 with standard deviation of ± 0.02 . These results are very similar to those obtained from TGA analysis which gave a mean value of 1:0.28 and standard deviation of ± 0.02 . Studies carried out on the hydration of caffeine showed similar findings involving the formation of a non-stoichiometric hydrate with a molecular ratio of caffeine to water of 1:0.8 (Pirttimaki and Laine, 1994). The above results from both TGA and DVS confirm that a hydrate forms from the re-crystallization of sodium benzoate from water, which has a molecular ratio of sodium benzoate to water of 1:0.28, leading to the conclusion that a channel hydrate forms which has not been reported before.

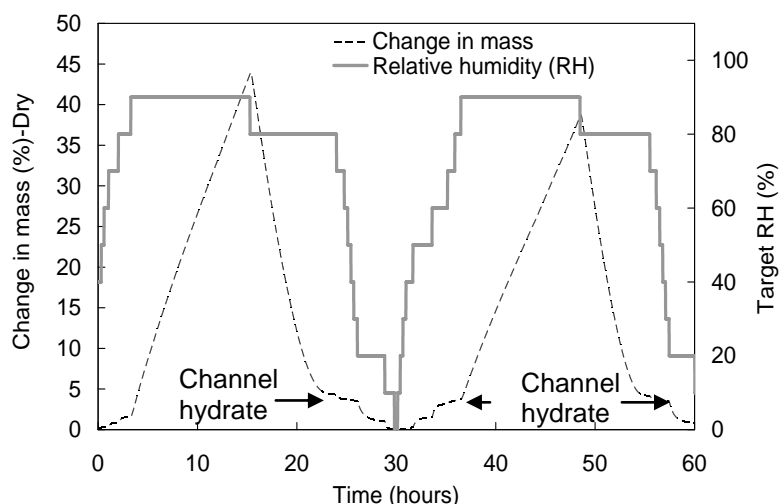


Figure 4.11. DVS results for sodium benzoate showing how the sample mass and relative humidity change with time

Table 4.1. Summary of the DVS results for the molecular ratio of sodium benzoate to water

Step	Change in humidity (%)	Change in mass (%)	Molecular ratio of sodium benzoate to water
Sorption (cycle 2)	40-60	2.89	1 : 0.24
Desorption (cycle 1)	30-10	3.47	1 : 0.29
Desorption (cycle 2)	30-10	3.53	1 : 0.29

4.6 Conclusions

Cooling crystallization experiments were performed with the use of the FBRM probe which detected an unexpected fluctuation in the total number of counts above 65°C. Repeated cooling crystallization experiments under different conditions showed very similar behaviour. The fluctuation indicated that probably a polymorphic transformation occurred during that stage of the crystallisation process. The use of PAT combined with SSA techniques provided evidence of the formation of a new hydrate when sodium benzoate re-crystallizes from water. TGA and DVS confirmed that the molecular ratio of sodium benzoate to water in the new hydrate is 1:0.28 indicating the existence of a previously not reported channel hydrate.

Chapter 5. A PAT based investigation of the polymorphic transformations during the antisolvent crystallization of sodium benzoate from IPA/water mixture

5.1 Introduction

There are many different crystallization methods including cooling, anti-solvent, pH-controlled and evaporation of solvent. The preferred method of crystallization for heat sensitive compounds and for compounds, in which there are insignificant changes in solubility with temperature, is antisolvent crystallization (O'Grady *et al.*, 2007). Extensive studies have been carried out which demonstrate the importance of PAT tools for the detection or control of polymorphic transformations during the crystallization process (Simon *et al.*, 2009; Howard *et al.*, 2009a; David *et al.*, 2004; O'Sullivan and Glennon, 2005; Dharmayat *et al.*, 2006; Caillet *et al.*, 2008; Fevotte, 2002; Nagy *et al.*, 2007).

This chapter presents the importance of using process analytical technology (PAT) tools combined with solid state analytical (SSA) techniques for the monitoring and detection of polymorphic transformations during the antisolvent crystallization process and for the discovery of new forms of the crystalline compound, sodium benzoate. The model system used is sodium benzoate in a propan-2-ol (IPA)/water mixture. Sodium benzoate is extensively used in preservatives of food and medicines. It was used as a model system since it exhibits difficult crystallization behaviour, such as very thin needle like crystal structure, low temperature sensitivity of the solubility (making cooling difficult to use for the control of the crystallization process), features which are often characteristic to pharmaceutical compounds. Additionally, despite the widespread use of sodium benzoate very little has been reported in the literature about its crystallization behaviour. Recent studies by the authors on the cooling crystallization of sodium benzoate in water have lead to the discovery of a new channel hydrate (Howard *et al.*, 2009a). In this research work, the antisolvent crystallization of sodium benzoate is corroborated and the formation of a new

meta-stable IPA solvate and a new polymorphic form (stable at higher temperatures) are reported for the first time.

The use of PAT is demonstrated for monitoring the polymorphic transformation of the channel solvate into the channel hydrate as the amount of IPA increases in the system. The solubility of sodium benzoate in water is very high and in IPA is very low, therefore, water is chosen as the solvent and IPA as the antisolvent. The PAT tools used within this study are the focused beam reflectance measurement (FBRM) probe, turbidity meter and attenuated total reflectance (ATR) ultraviolet/visible (UV/Vis) spectroscopy. Solid samples of filtered and air dried crystals are analysed using a range of SSA techniques including optical microscopy, scanning electron microscopy (SEM), X-ray powder diffraction (XRPD), high temperature X-ray powder diffraction (HT-XRPD) solid and solution state nuclear magnetic resonance (SSNMR), solid state infrared (IR) spectroscopy, thermal gravimetric analysis (TGA), differential scanning calorimetry (DSC) and hot stage microscopy (HSM). A combination of these techniques provides the conditions under which a new unreported channel solvate of sodium benzoate forms, as well as provide evidence of the existence of a new higher melting polymorphic form of the anhydrous form.

5.2 Experiments performed

Solubility experiments involving a gravimetric method were performed to determine the solubility of sodium benzoate in a range of solvents and mixed solvents. A detailed methodology can be found in Section 3.3 of Chapter 3. Antisolvent crystallization experiments were performed for sodium benzoate in an IPA/water mixture. PAT tools were used for monitoring the crystallization process and detecting polymorphic transformations. The methodology and PAT tools are described in Section 3.5 of Chapter 3. Figure 3.4 in Chapter 3 shows the schematic set-up of the crystallization rig. SSA techniques are used to characterise the crystals. The equipment used and the operating conditions are highlighted within Section 3.7 of Chapter 3.

5.3 PAT tools for the monitoring and detection of solvent mediated polymorphic transformation of sodium benzoate in water/IPA mixture

As there is limited literature data on the solubility of sodium benzoate, gravimetric tests were carried out using water and IPA as the solvents. Figure 5.1 shows the solubility results for sodium benzoate in water (including literature data), IPA and solvent mixtures of IPA/water of volume ratio 2:1, 4:1 and 5:1. Solubility curves for all solvent systems are flat indicating that the solubility does not change much with temperature. From the solubility results the method of antisolvent crystallization was chosen to crystallize sodium benzoate using a solvent system of water and IPA. Figure 5.1c shows how the solubility changes with the solvent system at constant temperature. As the extent of IPA present in the solvent mixture increases the solubility decreases. Water is used as the solvent and IPA as the antisolvent, for the antisolvent crystallization experiments, due to the high and low solubilities respectively, as shown in Figure 5.1.

Antisolvent crystallization experiments were performed within two different experimental rigs of vessel sizes of 1 L both, but with different agitator types, to investigate whether the mixing conditions influenced the crystallization behaviour. The temperature was kept constant at 25 °C. Figure 5.2 shows the FBRM and turbidity results for the experiments performed within the different vessels. Experimental results using an automated lab reactor with a 3-blade glass retreat curve at a rotation speed of 300 rpm are shown in Figure 5.2a. The initial concentration of sodium benzoate in water was 545 mg/mL and IPA (antisolvent) was added using a dosing rate of 0.33 g/min. The FBRM results show a peak in the number of counts (1-1000 microns) at the start of the experiment. The high counts are due to the probe not being fully immersed within the solution and the creation of a vortex. The turbidity results show a value of 0% at the start indicating a clear solution. As IPA is added to the solution this reduces the solubility of the solute in solution, forming a supersaturated solution. Spontaneous nucleation occurs once the volume ratio of IPA/water reaches a value between (1.74-1.8):1 which is shown in the FBRM results

by a sudden increase in the total number of counts. As more IPA is added both the FRBM and turbidity probes detected a second nucleation event resulting in a fluctuation in the FBRM counts and an increase in turbidity. The second nucleation event occurred at a volume ratio of IPA/water within the range of (3.9-4.3):1. Similar results, with the use of FBRM statistics, showed that the change in the FBRM readings is due to the different morphologies of the polymorphic forms indicating a polymorphic transformation (Nagy *et al.*, 2007; Hermanto *et al.*, 2009; Scholl *et al.*, 2006).

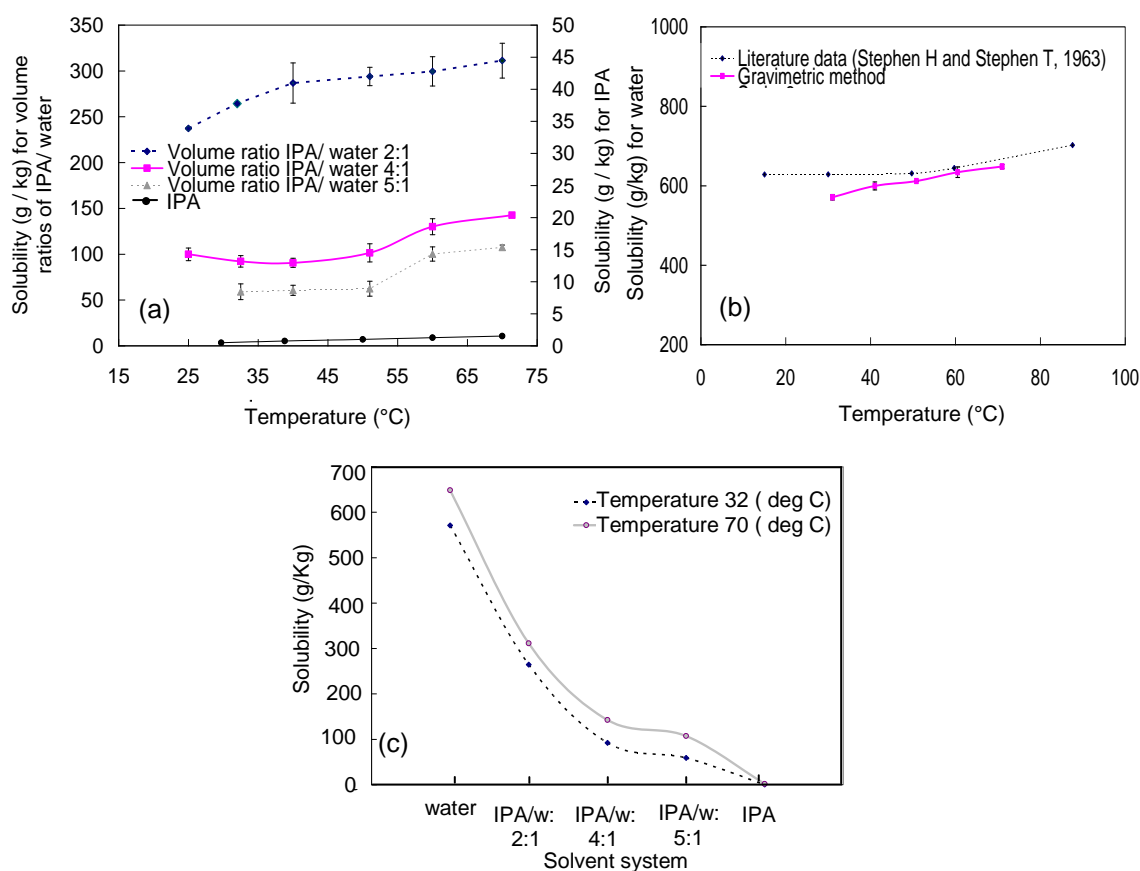


Figure 5.1. Solubility data for sodium benzoate in (a) IPA/water (w) volume ratios and pure IPA, (b) water, (c) different solvent systems at temperatures 32 and 70 °C

Additional antisolvent crystallization experiments were carried out within different mixing conditions using a 4-pitched blade turbine (coated with PTFE) at a rotation speed of 255 rpm. The previous method was slightly altered in which the same amount of sodium benzoate was dissolved in a starting solution of volume ratio IPA/water of 1:1 and IPA was added using a dosing rate of 1 g/min. The FBRM results are shown in Figure 5.2b.

Similar behaviour is observed showing the first nucleation event which occurs at volume ratio of IPA/water of 2.26:1 and a second nucleation event at volume ratio of IPA/water of 4.2:1. At this volume ratio of IPA/water the FBRM statistics show an increase in the coarse counts and mean chord length and an initial decrease in fine counts, which would suggest agglomeration. However there is a fluctuation in fine counts resulting in a final increase in fine counts suggesting a possible morphology change to needles due to a polymorphic transformation.

Figure 5.3 shows images of the crystallization vessel in which a transformation from mobile slurry to the formation of a solid clump occurred after the second nucleation event. These images support the FBRM results as shown in Figure 5.2(b) in which an initial decrease in fine counts (1-20 microns) and increase in coarse counts (50-250 microns) occurs during the second nucleation event, indicating agglomeration of the crystals. The formation of a solid gel clump results in insufficient mixing yielding a ‘spiky’ signal as shown in the FBRM results in Figure 5.2. The crystals may stick to the probe resulting in an increase in the FBRM signal as shown in Figure 5.2(a) or there may be a mobile fluid around the impeller and probe and the rest is a solid clump resulting in a decrease in the FBRM signal as shown in Figure 5.2(b). The sudden change in the FBRM signal indicates a possible polymorphic transformation. A change in morphology of the crystals from fines to needles after the second nucleation event is observed from the optical microscope images in Figure 5.4.

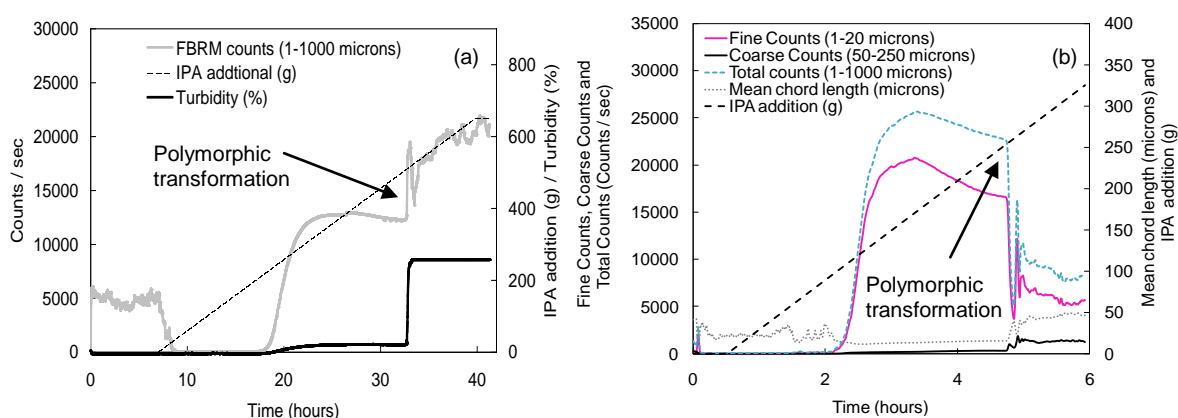


Figure 5.2. FBRM results for the antisolvent crystallization of sodium benzoate from an IPA/water mixture performed within a 1 L vessel using a (a) 3-blade glass retreat curve and (b) 4-pitched blade turbine (coated with PTFE)

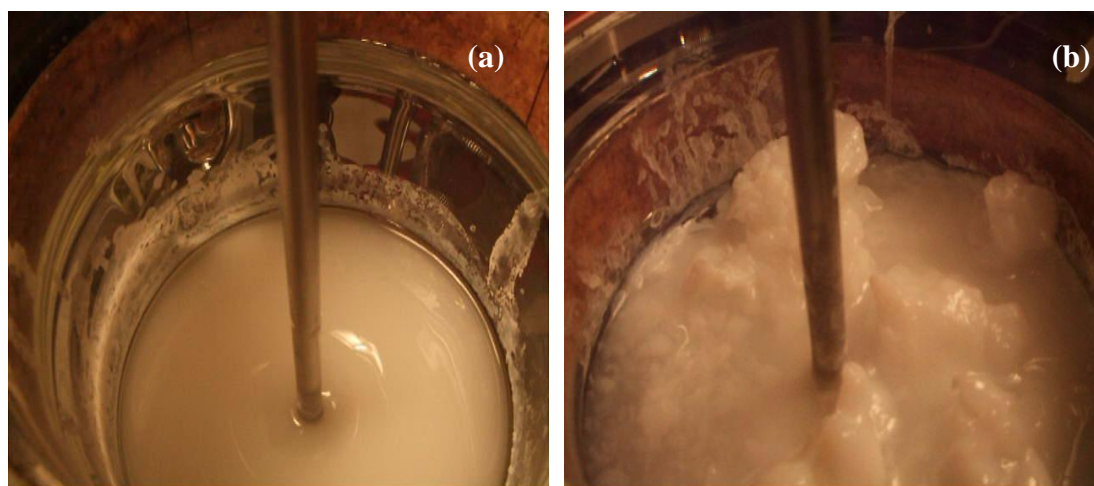


Figure 5.3. Visual images of the crystallization vessel using a 4-pitched blade turbine showing (a) a mobile cloudy solution after the first nucleation event and (b) formation of solid clump after the second nucleation event

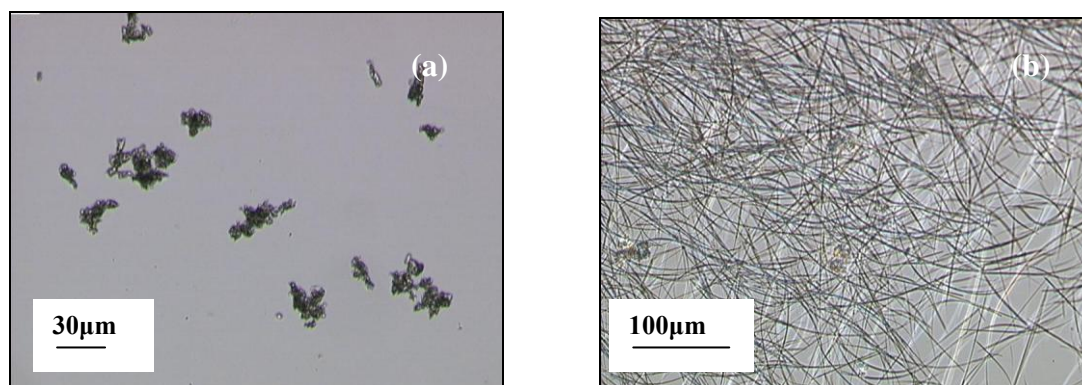


Figure 5.4. Optical microscope images of the crystals obtained from the antisolvent crystallization experiments after (a) the first nucleation event and (b) second nucleation event (fluctuation in FBRM counts)

The change in morphology and appearance of solution combined with repeatability of the results within different crystallization vessels supports the hypothesis that the second nucleation event detected by the FRBM and turbidity probes is due to a polymorphic transformation. Repeats of the experiment were performed with a modified method in order to determine the cause of the transformation. This involved stopping the IPA addition after the first nucleation event reaching a volume ratio of IPA/water of 3:1. The system is kept at this volume ratio and held at 25 °C over night. IPA is then added in small amounts to increase the volume ratio of IPA/water by 0.5:1 and held at 25 °C for 2 hours before the next IPA addition. This is required in order to determine whether kinetics (system exposed to the water/IPA mixture for a longer

period of time) or the extent of IPA present within the solution is the cause of the transformation. A dosing rate of 2 g/min and stirrer speed of 300 rpm were used. ATR-UV/Vis spectrometer is used to measure absorbance in the wavelength range 242-614 nm in which sodium benzoate has peak absorbance at 270 nm. Figure 5.5 shows the UV/Vis spectrum of sodium benzoate in water between 190 and 340 nm. To protect against solarisation the fibre optic connecting the ATR probe to the UV/Vis spectrophotometer, for the monitoring experiments which required longer durations, spectra above 242 nm was only collected, hence the peak value at 270 nm was used to monitor changes in concentration. The FBRM and UV/Vis results are shown in Figure 5.6.

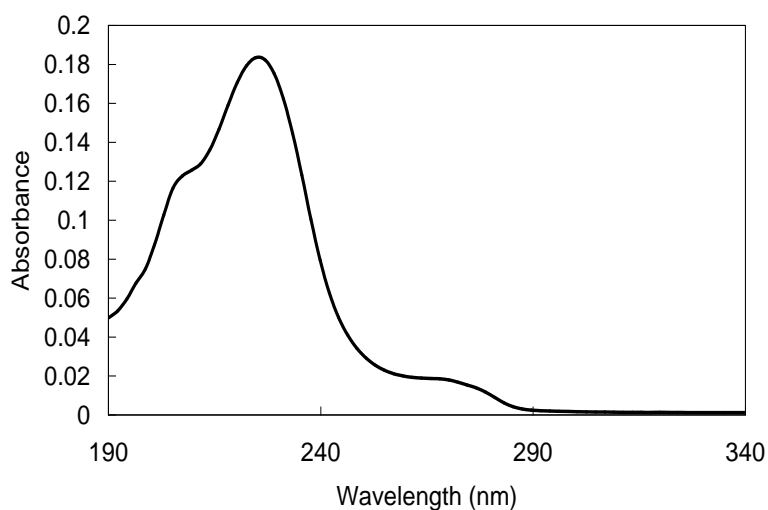


Figure 5.5. UV/Vis spectrum for sodium benzoate in water

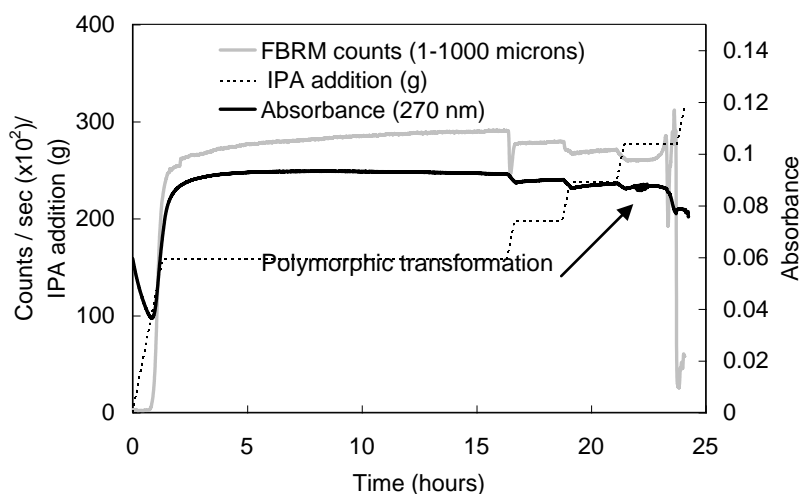


Figure 5.6. FBRM and UV/Vis results for the anti-solvent crystallization experiment with the step additions of IPA

The FBRM results show a second nucleation event as represented by a change in the counts (1-1000 microns), indicating a polymorphic transformation. This event occurs after the system is held at volume ratio of IPA/water of 4.5:1 for approximately 2 hours, showing that both the extent of IPA present within solution and kinetics has an influence on the second nucleation event. The temperature was maintained constant at 25 °C throughout the experiment indicating that this factor has no contribution towards the change occurring within the system which is thought to be due to a polymorphic transformation. The UV/Vis data show a decrease in absorbance at wavelength 270 nm during the second nucleation event. As crystals nucleate from solution this lowers the concentration of solute in solution resulting in a decrease in absorbance. The UV/Vis data correlates with the FBRM results indicating that the second nucleation event is due to a polymorphic transformation and not caused by problems with crystals sticking to the vessel/probe walls or sedimentation of crystals due to insufficient mixing. The increase in the absorbance during the first nucleation event is due to the tendency of sodium benzoate to nucleate from water on the surface of the probe yielding to increase in the absorbance. As the amount of IPA increases in the system the tendency is lower and the second nucleation is already indicated by a decrease in the absorbance as expected.

A summary of the results for all antisolvent crystallization experiments performed within different crystallization vessels using different mixing conditions and dosing rates of IPA is shown in Table 5.1. These results show that the variation in mixing conditions and dosing rate had no effect on the crystallization behaviour but the extent of IPA present in solution has a significant effect, resulting in a polymorphic transformation.

To identify the possible crystal form that nucleates at volume ratio IPA/water 2:1 and 4:1, slurry experiments were performed using the Avantium Crystal 16 equipment. Sodium benzoate was suspended in 1 mL vials using different volume ratios of IPA/water to vary the water content in the solvent mixture which will alter the water activity and hence the stability of the crystal forms (Variankaval *et al.*, 2007; Li *et al.*, 2008; Zhu *et al.*, 1996). Previously performed experiments showed that the hydrate form of a compound or a higher hydrated form is likely to form as the water activity

increases (Variankaval *et al.*, 2007). Figure 5.7 shows the XRPD patterns for each sample obtained from the slurry experiments in which the water activity varies from 0 to 1. XRPD results show that for samples obtained from solutions in which the water activity varies from 0 to 0.66, the anhydrous form of sodium benzoate forms (see Figure 5.7b). For slurry solutions in which the water activity is in the range 0.77 to 1, the hydrate forms (see Figure 5.7c). These results confirm that for water activities above 0.77 the hydrate form of sodium benzoate is more stable. Water activities for solutions of volume ratio IPA/water of 2:1 and 4:1, in which the two nucleation events occur in the anti-solvent crystallization experiment, are calculated from polynomial equations obtained from the literature (Zhu *et al.*, 1996). For volume ratio IPA/water of 2:1 and 4:1 the water activity is 0.86 and 0.83 respectively. For these volume ratios the water activity is above 0.77 in which the hydrate form is stable indicating the likelihood of the formation of the sodium benzoate hydrate. To investigate the type of transformation during the two nucleation events as shown in the FBRM results in Figure 5.2, solid state analyses were carried out on a sample of crystals obtained after the first and second nucleation events.

Table 5.1. Summary of the different conditions and volume ratios of IPA/water for the first and second nucleation events, for all sodium benzoate antisolvent crystallization experiments

Experiment	Type of agitator	Stirrer speed (rpm)	Dosing rate (g/min)	Volume ratio of IPA/water for first nucleation event	Volume ratio of IPA/water for second nucleation event
I	3-blade glass retreat curve (3GRC)	300	0.3	1.8:1	4.3:1
II (Repeat)	(3GRC)	300	0.33	1.74:1	3.9:1
I	4-pitched blade turbine (4PBT)	255	1	2.26:1	4.2:1
II (Modified method)	(4PBT)	300	2	2.26:1	4.5:1 (hold at this ratio for 2 hours)

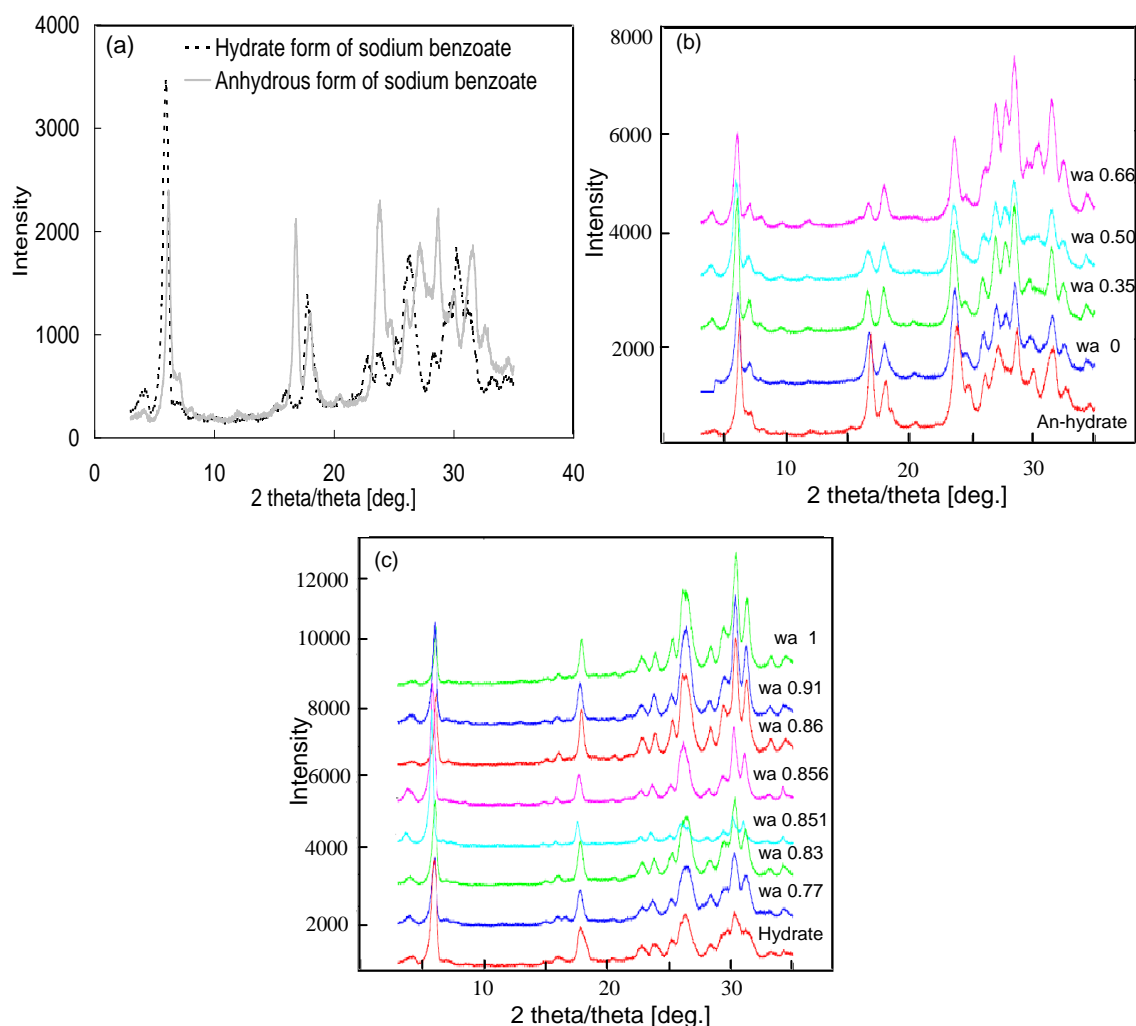


Figure 5.7. X-ray powder diffraction patterns for (a) anhydrous and hydrated form of sodium benzoate, (b and c) sodium benzoate samples obtained from the Crystal 16 slurry experiment with different water activities (wa). In figures (b) and (c) intensities are shifted for clearer plotting

5.4 SSA for the detection of new forms of crystalline compound

The solid state techniques used for analysing the crystal samples include scanning electron microscope (SEM), hot stage microscopy (HSM), X-ray powder diffraction (XRPD), high temperature XRPD, differential scanning calorimetry (DSC), infra-red (IR) spectroscopy, solid and solution state nuclear magnetic resonance (NMR) spectroscopy, and thermal gravimetric analysis (TGA).

5.4.1 Discovery of a new solvate form of sodium benzoate

Figure 5.8 shows the XRPD patterns of the raw material form of sodium benzoate and samples obtained from the antisolvent crystallization experiment after the first nucleation (volume ratio of IPA/water of 3:1) and second nucleation event (volume ratio of IPA/water of 5:1). XRPD results for the hydrated form of the sodium benzoate were obtained from samples re-crystallized from pure water. Wet and air dried samples were analysed using XRPD. Figure 5.8a compares the XRPD patterns for the raw material and anhydrous form of sodium benzoate showing very similar patterns indicating that the raw material is the anhydrous form. Figure 5.8b shows very similar XRPD patterns for the sample of crystals obtained at volume ratio of IPA/water of 5:1 and the hydrated form of sodium benzoate. This indicates that the form that nucleates out at the second nucleation event in the antisolvent crystallization experiment is a hydrate. Figures 5.8 (c) and (d) show that the sample of crystals obtained after the first nucleation event (volume ratio of IPA/water of 3:1) is neither the hydrated form, as there are additional peaks at high angles, nor the anhydrous form similar to the raw material since it has a different XRPD pattern. These XRPD results suggest that either a different polymorphic form or a solvate forms from the first nucleation event in the antisolvent crystallization experiments. XRPD results obtained from the slurry experiments as shown in Figure 5.7 indicated that the hydrate form of sodium benzoate is more stable at volume ratio of IPA/water of 3:1 which suggests that a meta-stable form nucleates from the first nucleation event as shown in the FBRM results of Figure 5.2. Further solid state analysis is performed with the use SEM and DSC, which provides data on the melting point and enthalpy of melting of different forms of a compound.

SEM images of the sample of sodium benzoate crystals obtained after the first nucleation event and a previously reported hydrate form of sodium benzoate are shown in Figure 5.9. Crystal samples have been vacuum filtered resulting in the formation of agglomerates as shown in images (a) and (b) in Figure 5.9. A higher magnification is used to examine the surface characteristics of the two crystal samples, which are shown in images (c) and (d) in Figure 5.9. The surface of the sample at a volume ratio IPA/water of 3:1 is rough, while the hydrate form of sodium

benzoate shows a fibrous surface structure. The clear differences between the two SEMs support the results obtained from XRPD, which suggest that a different polymorphic form or solvate nucleates from the first nucleation event in the antisolvent crystallization experiments.

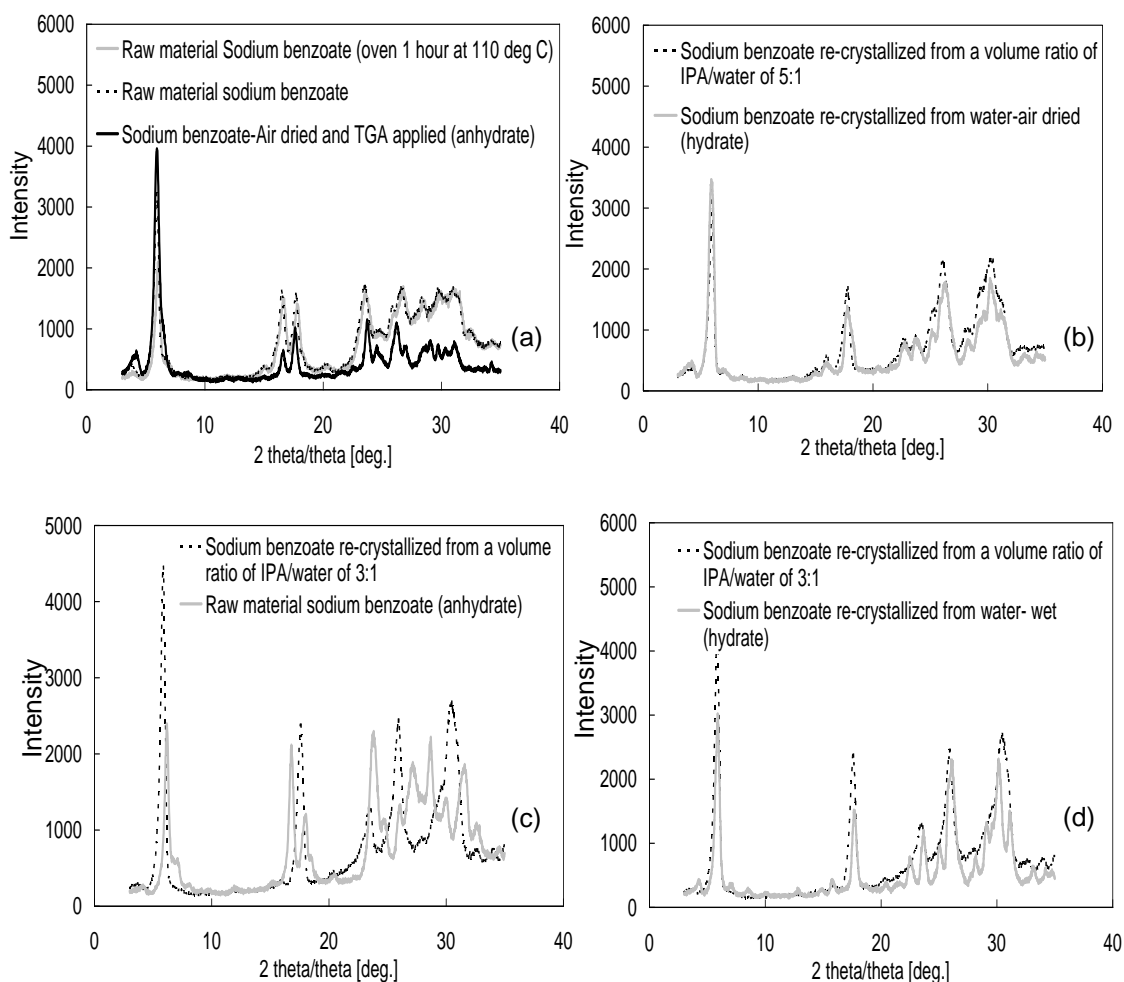


Figure 5.8. X-ray powder diffraction patterns for (a) raw material form of sodium benzoate, (b) sodium benzoate re-crystallized from volume ratio of IPA/water of 5:1 and (c and d) sodium benzoate re-crystallized from volume ratio of IPA/water of 3:1

Figure 5.10 shows the DSC results of the raw material and samples of crystals obtained after the first (volume ratio IPA/water 3:1) and second nucleation event (volume ratio IPA/water of 4.4-5:1) using sealed pans and pans with pin holes. Figure 5.10a shows a peak at temperature of 442 °C which is the melting point of the raw material form of sodium benzoate (anhydrous). The enthalpy of melting is 177 J/g. Figure 5.10b obtained from a sample of crystals after the first nucleation event shows

a peak at temperature of 126 °C with an enthalpy of 7.4 J/g and a second peak at temperature 432 °C. The peak at 126 °C is thought to be due to either a solid state polymorphic transformation or removal of solvent from a solvate. This stable form (raw material) then melts at 432 °C.

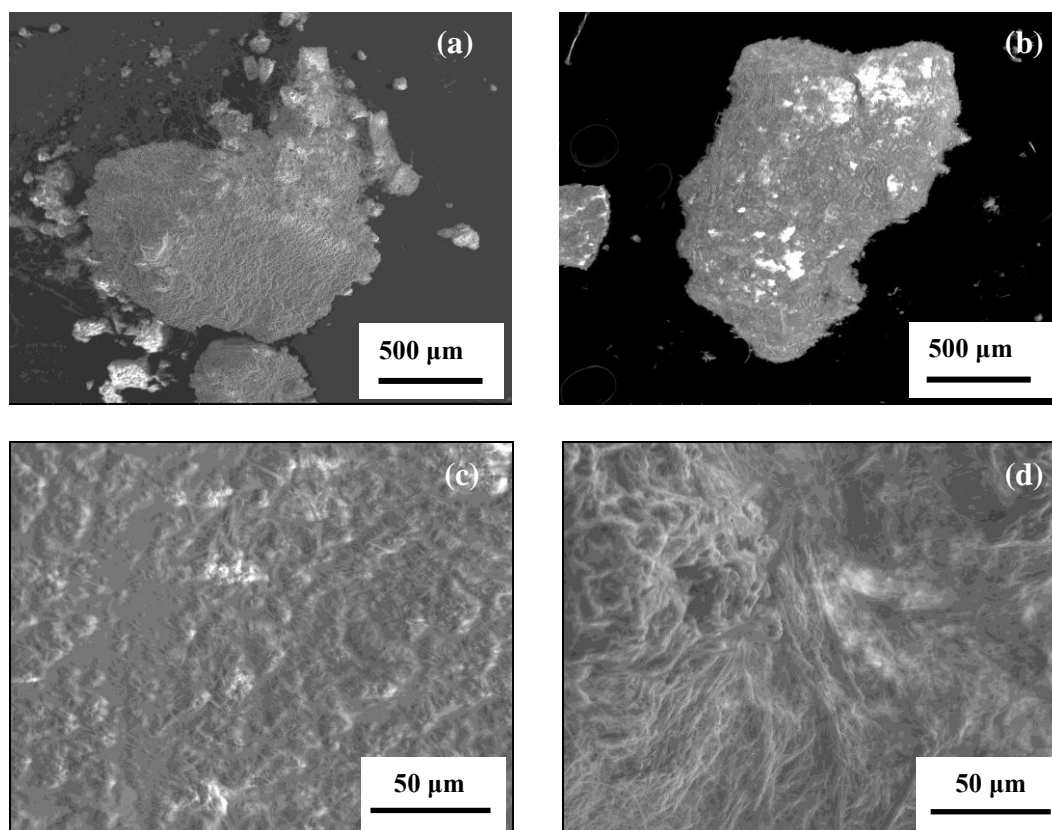


Figure 5.9. SEM images of (a, c) sample of sodium benzoate re-crystallized from volume ratio of IPA/water 3:1 and (b, d) hydrated form of sodium benzoate

Figures 5.10 (c) and (d) show the DSC results for a sample of crystals obtained after the second nucleation event using a sealed pan and a pan with a pin hole. DSC results using a sealed pan show a peak at 132 °C and the melting of the anhydrous form of sodium benzoate at 434 °C. The results obtained using a pan with a pin hole show a peak at temperature of 74.5 °C. Giron (1995) reported DSC results for a dehydrate, which showed dehydration at a peak at approximately 72 °C when using a pan with a pin hole and the melting of the dihydrate at a peak of approximately 125 °C when using a sealed pan. These results suggest that the peaks at 74.5 and 132 °C are due to the dehydration of the hydrate which has an enthalpy of 63.2-64.7 J/g. Dehydration occurs at a higher temperature when using a sealed pan due to the build up of pressure within the pan. DSC and XRPD results provide supporting evidence that a hydrate

forms after the second nucleation event, which is in correlation with results presented in Chapter 4 obtained during cooling crystallisation experiments of sodium benzoate in water (Howard *et al.*, 2009a). However it was uncertain at this stage whether a different polymorphic form or a solvate nucleates from the first nucleation event. Additional solid state analysis involving the use of HT-XRPD is performed on the sample of crystals obtained after the first nucleation event to identify the crystal form.

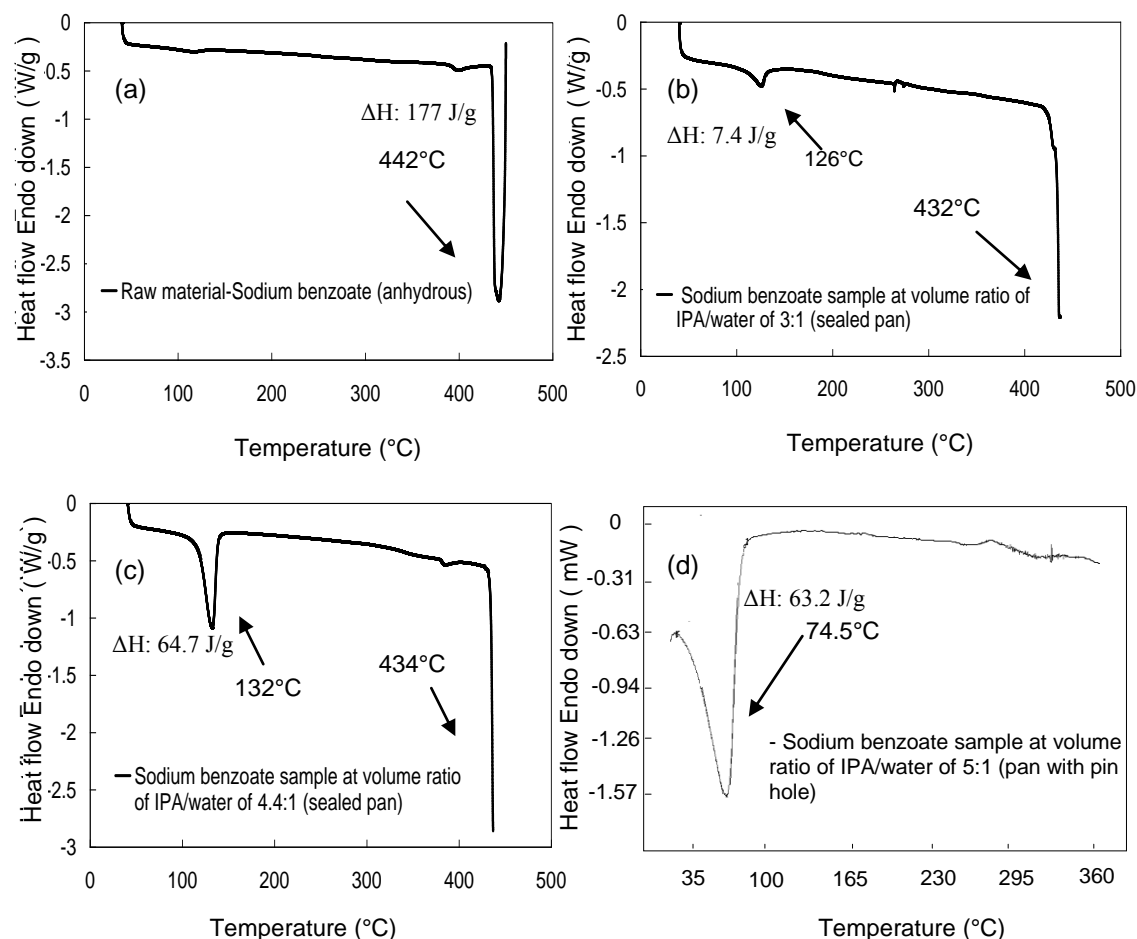


Figure 5.10. DSC results for (a) raw material form of sodium benzoate, (b) sodium benzoate re-crystallized from a volume ratio of IPA/water of 3:1 and (c, d) sodium benzoate re-crystallized after the second nucleation event at volume ratio of IPA/water of 4.4:1 and 5:1

HT-XRPD provides data on how the X-ray powder diffraction pattern of a crystal sample changes with temperature. Figure 5.11 shows the HT-XRPD results for the sample of crystals obtained after the first nucleation event (volume ratio IPA/water of 3:1). XRPD patterns show no change within the temperature range 25-175 °C, which suggests no polymorphic transformation between different forms. However, solvent

molecules can be removed from a channel (non-stoichiometric) solvate crystal without affecting the structure (Hilfiker, 2006), which suggests that possibly a channel solvate forms from the first nucleation event. The XRPD patterns identify geometric changes within a compound. When the cavities within the crystal structure are small due to the elimination of loosely bounded small amount of solvate (which is often the case for channel solvates) the crystal structure will not necessarily rearrange to the form of the anhydrous compound. Since XRPD results may be influenced by sample preparation this technique is useful to be combined with spectroscopy techniques such as NMR and IR, which highlight composition differences between different forms of a compound.

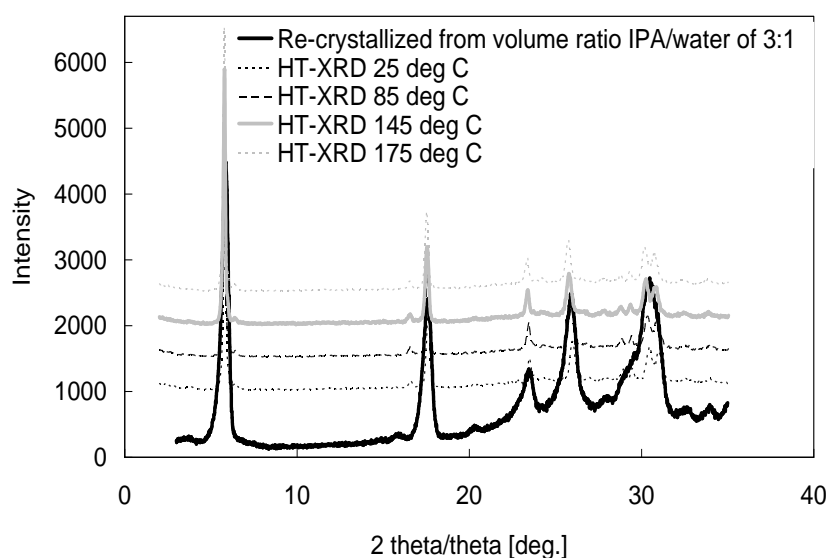


Figure 5.11. HT-XRPD results of sodium benzoate re-crystallized from volume ratio IPA/water of 3:1 at temperatures within the range 25 to 175 °C. Intensities are shifted for clearer plotting

NMR analysis including solid and solution state was performed on the anhydrous form of sodium benzoate and a sample of sodium benzoate re-crystallized from volume ratio IPA/water of 3:1. The NMR results are shown in Figure 5.12. ^{13}C spectra for the two samples are very similar with a slight shift in the peak at 177 ppm, which is due to the carboxylate carbon (COO^-). ^{23}Na spectra for the sample re-crystallized at volume ratio IPA/water of 3:1 shows an additional sharp peak at 1 ppm, which is thought to be due to free mobile sodium ions caused by the presence of solvent molecules in the crystal lattice structure and confirms the existence of channel solvate. ^1H solid and solution state NMR was performed on the re-

crystallized sample at volume ratio IPA/water of 3:1. ^1H solid state spectra shows a peak at 4 ppm, which is due to the (-OH) group and an additional peak compared with the hydrate spectra at 0 ppm which is due to the (-CH₃) group from the IPA, indicating the presence of a solvate (Fox and Whitesell, 1997). Solution state ^1H NMR data shows peaks at 7-8 ppm, which is due to the hydrogen atoms in the benzene ring and the peak at 1 ppm which represents hydrogen atoms in the (-CH₃) and (-CH₂-) groups of the alcohol (IPA), indicating the presence of a solvate (Fox and Whitesell, 1997). NMR results provide supporting evidence that a meta-stable solvate forms from the antisolvent crystallization experiments at volume ratio IPA/water of 3:1, which then transforms into the hydrate at higher IPA/water ratio.

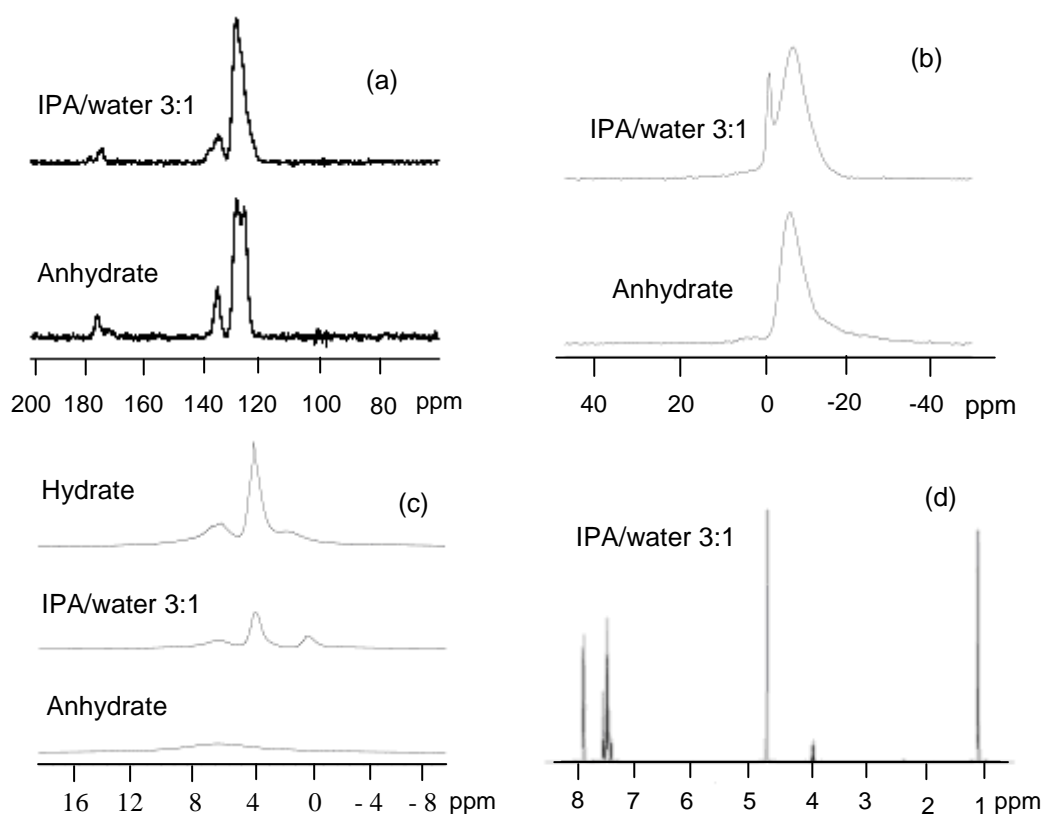


Figure 5.12. Solid state NMR data of (a) ^{13}C , (b) ^{23}Na , (c) ^1H and (d) solution state ^1H data for anhydrous form of sodium benzoate and sample re-crystallized from volume ratio IPA/water of 3:1

IR data on the anhydrous form of sodium benzoate and sample of sodium benzoate re-crystallized from volume ratio of IPA/water of 3:1 is shown in Figure 5.13. The full spectrum for the sample at volume ratio IPA/water of 3:1, as shown in Figure 5.13a, shows an additional broad peak at wavenumber 3403 cm^{-1} , which is due to the

hydroxyl group (-OH) of the alcohol indicating the formation of a solvate (Atkinson and Hibbert, 2001). Figure 5.13b shows that the IR spectra of the fingerprint region (1500-400 cm^{-1}) of the two samples are different, indicating different forms of the compound sodium benzoate. For the sample obtained at volume ratio of IPA/water of 3:1, there are additional peaks at 1165 and 1271 cm^{-1} that are due to the (C-O) bond of an alcohol. The peak at 1484 cm^{-1} is thought to be due to plane blending in the (C-O-H) of an alcohol. Additional peaks are also observed at 1584 and 760 cm^{-1} in which the latter peak is due to (C-H) bending vibrations in aromatic rings (Stuart *et al.*, 1998). These additional peaks in the fingerprint region indicate the presence of a solvate. Both IR and NMR data provide supporting evidence that a solvate forms when sodium benzoate re-crystallizes from volume ratio of IPA/water of 3:1, which has not yet been reported in the literature. Moreover, the apparently paradoxical transformation of the solvate into hydrate with increasing IPA ratio is reported for the first time, but it is strongly supported by the detailed SSA results.

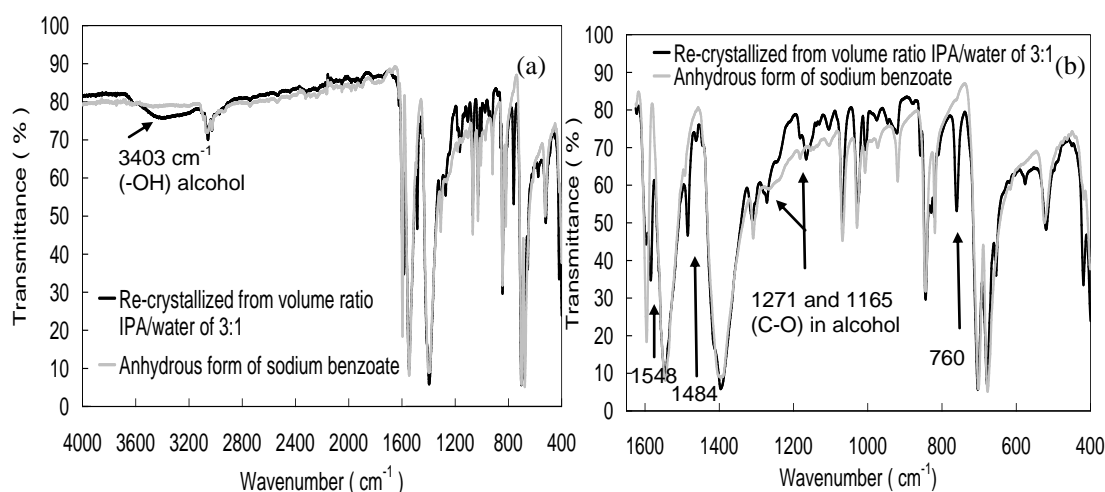


Figure 5.13. IR data for the anhydrous form of sodium benzoate and sample re-crystallized from volume ratio IPA/water of 3:1 showing (a) the full spectrum and (b) the fingerprint region

To identify the formation of hydrates or solvates TGA is also carried out on samples of crystals obtained after the first and second nucleation events from the anti-solvent crystallization experiments and the results are shown in Figure 5.14.

TGA results for the raw material (anhydrous) show a flat line indicating no change in weight%. For the crystals obtained at volume ratio of IPA/water of 3:1 there is a decrease in weight of 0.29%. As the weight% is small and occurs over a low

temperature range this would suggest that a channel solvate forms. This prediction is supported with DSC results shown in Figure 5.10(b), which shows a low enthalpy of 7.4 J/g for solvent removal as not much energy is required to remove the loosely bonded solvent molecules in the crystal lattice structure. HT-XRPD results also support the hypothesis of the formation of a channel solvate.

TGA results for sample of crystals obtained after the second nucleation event (volume ratio of IPA/water of 5:1) for two repeated runs show a small weight decrease of 2.7-3.2%. XRPD results as shown in Figure 5.8(b) and DSC results as shown in Figure 5.10(c) and (d), provide supporting evidence that a hydrate forms. From the weight% decrease the stoichiometry of sodium benzoate to water is shown to be within the range of 1: 0.24-0.27. A sample calculation of the individual steps can be found in Appendix E. These values are very similar to those obtained for the channel hydrate which forms when sodium benzoate is re-crystallized from pure water (Howard *et al.*, 2009a). The non-stoichiometry ratio also indicates the presence of a channel hydrate in which the water molecules form a loosely bonded channel throughout the crystal lattice structure. This supports the TGA results as the weight% decrease occurs over a low temperature range. Previous studies of the cooling crystallisation of sodium benzoate from water also indicated the formation of channel hydrate with very similar stoichiometry (1:0.28) confirmed by TGA and dynamic vapour sorption (DVS) experiments (Howard *et al.*, 2009a).

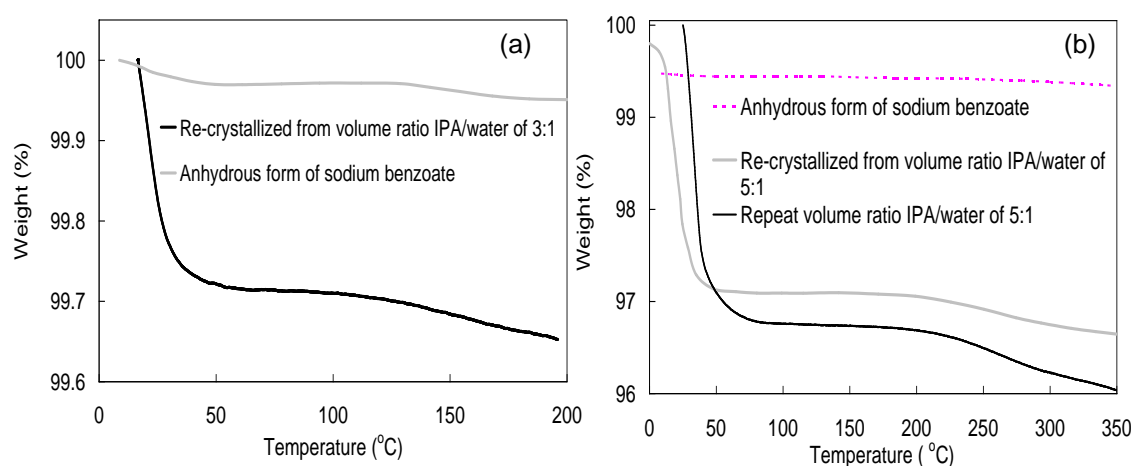


Figure 5.14. TGA results of (a) anhydrous form of sodium benzoate and crystals obtained from volume ratio IPA/water of 3:1 and (b) anhydrous form of sodium benzoate and crystals obtained from volume ratio of IPA/water of 5:1

A combination of SSA techniques provides supporting evidence that a polymorphic transformation occurs from meta-stable solvate to a hydrate during the antisolvent crystallization experiments. SSA techniques provided the evidence for the formation of a new, previously unreported, channel solvate form of sodium benzoate.

5.4.2 Combined DSC and HSM for the detection of higher melting polymorphic forms of sodium benzoate

Combining DSC and HSM for the study of different forms of a compound is useful as both techniques provide supplementary data apart from the melting point, which is an important physical property used to identify the different forms. DSC provides additional data such as enthalpy of melting and re-crystallization allowing the stability of the polymorphs to be identified. HSM is a useful technique for identifying different polymorphic forms of a compound by changes in habit, size and reflectance properties resulting in changes in colour (Hilfiker, 2006; Bernstein, 2002; Abu Bakar, *et al.*, 2009a). DSC results for the anhydrous form of sodium benzoate are shown in Figure 5.15. The first endothermic peak at 437 °C is due to the melting of the anhydrous form of sodium benzoate which then re-crystallizes into a higher melting polymorphic form as shown by the small exothermic peak at temperatures within the range 445-447 °C, with an enthalpy of 4.2-5 J/g. This higher polymorphic form then melts within the temperature range of 452-454 °C, as shown by the second endothermic peak. This form has an enthalpy of melting between 18 and 29 J/g. Similar findings were obtained from DSC results reported from Giron (1995), which supports the above prediction of the formation of a higher melting polymorphic form of sodium benzoate as the system is heated above 437 °C (melting point of anhydrous form).

HSM is applied to the hydrated form of sodium benzoate during the heating stage from 199 to 500 °C and cooling to 402 °C, as shown in Figure 5.16. The hydrate transforms into the anhydrous form at lower temperatures without any noticeable modification in the crystal structure or other properties detectable with HSM. Melting of the anhydrous form occurs at a temperature of 444 °C. A phase transformation is observed by a change in colour of crystals as shown in images c and d in Figure 5.16. This is thought to be due to the crystallization of a higher polymorphic form, which

then melts as shown in Figure 5.16f and completely dissolves at temperature 493 °C. Similar observations were reported from the HSM of sulphathiazole in which two melting stages were observed due to the re-crystallization of a higher polymorphic form which then melts as temperature is increased (Bernstein, 2002). Both DSC and HSM provide supporting evidence of a new higher-melting polymorphic form of sodium benzoate at temperatures above the melting point (437 °C) of the anhydrous form

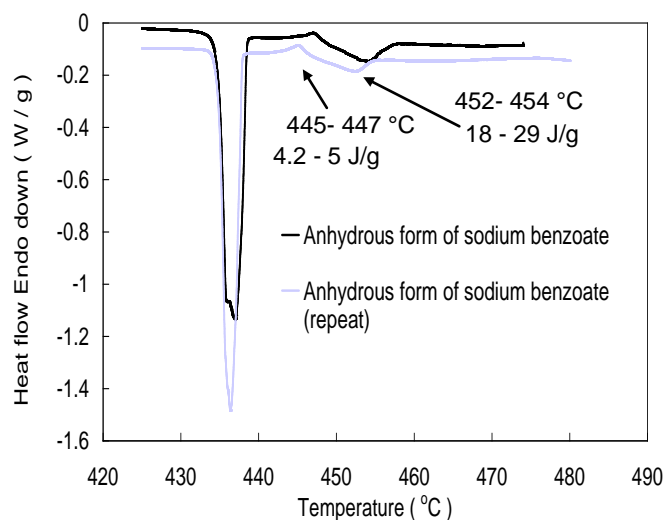


Figure 5.15. DSC results for 2 repeated runs of anhydrous form of sodium benzoate showing the re-crystallization and melting of a higher melting polymorphic form

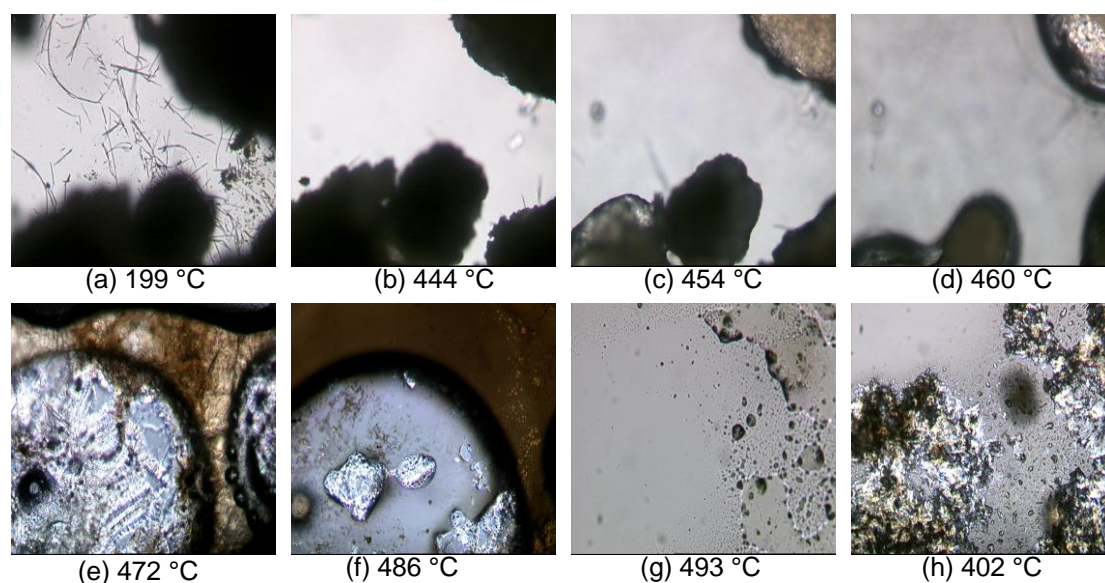


Figure 5.16. Hot stage microscopy (HSM) of hydrated form of sodium benzoate crystals during (a-g) heating phase and (h) re-crystallization from cooling

5.5. Conclusions

The use of PAT tools including the FBRM probe, turbidity meter and ATR-UV/Vis spectrometer showed evidence of a polymorphic transformation during the anti-solvent crystallization of sodium benzoate in propan-2-ol (IPA)/water system. The PAT tools clearly indicate the occurrence of two distinct events during the addition of IPA in a solution of sodium benzoate in water. First a new channel solvate form nucleates at IPA/water volume ratio of approximately 2:1, which transforms into a hydrate as the IPA/water volume ratio increases to a value of about 4:1, evidenced also by change in morphology and mixing properties of the slurry. Solid state analysis including XRPD, solid and solution state NMR, and IR spectroscopy with TGA and DSC provided evidence that the type of transformation is from a meta-stable channel solvate form to a channel hydrate. A combination of these tools identified the conditions under which different forms of the compound sodium benzoate exist and has led to the discovery of a new channel solvate form of sodium benzoate, which has not yet been reported in the literature. Additionally, the combination of DSC and HSM provided supporting evidence of the formation of a higher melting polymorphic form of sodium benzoate at temperatures above 437 °C (melting of anhydrous form) reported for the first time in this contribution.

Chapter 6. Application of PAT tools for the identification of crusting problems within crystallization processes

6.1 Introduction

Understanding of the crystallization process is required to design a robust process with consistence in product quality and purity (desired polymorphic form with no impurities). A narrow crystal size distribution (CSD) and large crystals are often desirable to obtain a quality product (Abu Bakar *et al.*, 2009a), which can be achieved by operating at experimental conditions within the meta-stable zone width (MSZW) region of the phase diagram (Lu and Ching, 2006 and Beckmann, 2000). Monitoring of the crystallization process can be achieved with the use of process analytical technology (PAT). These tools provide real time data, which can be used to gain a better understanding of the crystallization process. Data provided from PAT tools can be used to minimise error during scale up from laboratory to manufacturing scale increasing robustness of the crystallization process and product consistency (Sistare *et al.*, 2009; David *et al.*, 2004; Birch *et al.*, 2005).

The novelty of this research presents the importance of using PAT tools for the identification of common problems such as crusting (solid depositing on vessel walls) occurring during the crystallization process. This would lead to errors in the estimated and actual concentration values resulting in inaccurate MSZW measurements. Scaling up of the crystallization process would then lead to the possibility of product failure and increasing economical costs. This research highlights the need for improvement within vessel design to eliminate the problems of crusting. The model system used is *para*-amino benzoic acid (PABA) in ethyl acetate. PAT tools are used to monitor the cooling crystallization experiments including the focused beam reflectance measurement (FBRM) probe, turbidity meter and ATR-UV/Vis spectrometer. A range of solid state analytical (SSA) techniques were used to characterise the crystal product including the optical microscope, differential scanning calorimetry (DSC), hot stage microscopy (HSM) and X-ray powder diffraction (XRPD) analysis. Combining PAT tools with SSA techniques provides further evidence of changes that occur during the

crystallization process which are initially thought to be due to polymorphic transformations, are due to common problems such as crusting forming on vessel walls. Combining these tools saves both time and money that would be spent in researching the possible different polymorphic forms of the compound.

6.2 Experiments performed

Cooling crystallization experiments were performed in a jacketed glass vessel of size 1 L. The initial volume of solvent used in the experiments was varied to investigate the problem of crusting forming on vessel walls. The initial volume of solvent varied from 0.5 L to 1 L in which all walls of vessel were covered with solvent (ethyl acetate). A detailed methodology and PAT tools used to monitor the crystallization process can be found in Section 3.4.2 of Chapter 3. SSA techniques used to characterise the crystal product and the operating conditions used are mentioned within Section 3.7 of Chapter 3. A schematic of crystallization rig is shown in Figure 3.2 of Chapter 3.

6.3 Monitoring the cooling crystallization process of *para*-amino benzoic acid (PABA) from ethyl acetate using PAT tools

The aims of this research are to identify common problems such as crusting forming on the walls of crystallization vessels, highlighting the need for improvement for vessel design. The model system used in these experiments is *para*-amino benzoic acid in ethyl acetate. PABA contains different polymorphic forms known as the alpha and beta forms with the possibility of new undiscovered polymorphs/solvates due to the hydrogen bond acceptors and donors within the crystal structure (Gracin and Rasmuson, 2004). The alpha form has needle morphology and a melting point of 189 °C. The beta form has a prismatic morphology and a melting point of 145 °C. The two polymorphs are enantiotropic related with a transition temperature of 25 °C. Above this temperature the alpha form is stable and below this temperature the beta form is stable (Gracin and Rasmuson, 2004). XRPD patterns for the raw material PABA and the simulated pattern for the alpha form are very similar as shown in

Figure 6.1, indicating that the raw material is the alpha form (Cambridge Structural Database (Version 5.30; Allen, 2002)).

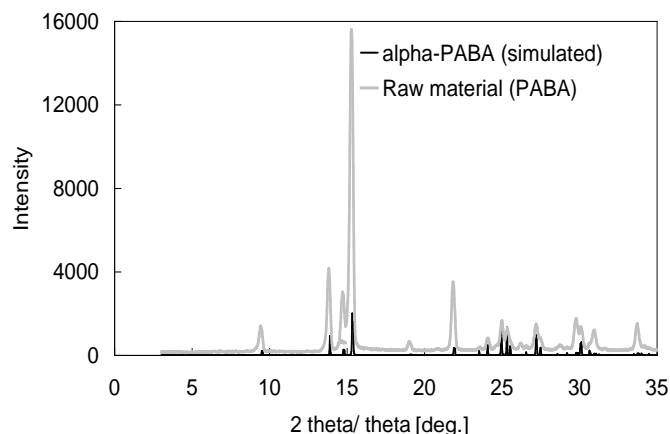


Figure 6.1. XRPD patterns for the raw material form of PABA and alpha-PABA (simulated)

Cooling crystallization experiments were performed within two set-ups using a 1 L jacketed glass vessel with different agitator types to examine if the mixing conditions had any influence on the behaviour of the system. The maximum working volume within the vessels is 0.5 L exposing the top part of the vessel walls to no solution. Figure 6.2 shows the FBRM, turbidity and UV/Vis results for two repeated experiments in which crusting formed on vessel walls. Cooling crystallization experiments using a 3-blade glass retreat curve are shown in Figure 6.2b. As the system is heated up the crystals dissolved, as represented by a decrease in FBRM counts and turbidity. A turbidity value of 0% represents a clear solution. Cooling over the temperature range 70 to 5 °C, results in two nucleation events as shown by an increase in FBRM counts and turbidity. The first nucleation event occurs at a temperature of 51 °C. Complete dissolution of all the crystals (solubility point) occurred at a temperature of 64 °C as indicated by both the FBRM and turbidity probe. A 1 °C temperature difference is detected for the nucleation point during the first nucleation event by both FBRM and turbidity probe. These results show that there is not much difference between the FBRM and turbidity values for solubility or nucleation points.

After cooling the system down to a temperature 45 °C, the system is then kept at a constant temperature of 45 °C in which there is a continuous decrease in FBRM counts and turbidity until the values reach 0 indicating a clear solution. The

continuous decrease in counts could be due to a polymorphic transformation, which would occur due to Ostwald's rule of stages from a meta-stable to a more stable form (Threlfall, 2003). In order for Ostwald's rule to apply the 'meta-stable' form would have a lower solubility than the stable form (alpha) and this stable form then dissolves due to higher dissolution kinetics. An alternative explanation to this continuous decrease could be due to decomposition of the PABA crystals as it is reported that after 4-5 days PABA reacts with ethyl acetate (Gracin and Rasmuson, 2004), or alternatively the effect of crusting could be considered. As solid deposits on the side of the vessel wall the concentration in the liquid reduces, causing additional solid crystals to dissolve. Through this process the solution can reach concentrations below the saturation concentration at the particular temperature. As the temperature is decreased to 5 °C, nucleation corresponding to the lower concentration is observed.

The cooling crystallization experiment was repeated in a different 1 L vessel using a 4-pitched blade turbine. PAT tools used include FBRM probe and ATR-UV/Vis spectrometer and very similar results were observed as shown in Figure 6.2a. Two nucleation events occur at temperatures of 46 °C and 9 °C. As the system is kept constant at 45 and 5°C there is a continuous decrease in FBRM counts. The UV/Vis spectrum for PABA in ethyl acetate shows a peak absorbance at 300 nm, as shown in Figure 6.3, which is monitored throughout the cooling crystallization experiment. During the first nucleation event at 46°C there is a decrease in the absorbance and as the system is kept at 45°C the absorbance remains constant (see Figure 6.2a and 6.3). Once all the crystals have dissolved and the system is kept at 45 °C there is a slight decrease in absorbance. UV/Vis results do not support the prediction that the continuous decrease in FBRM counts is due to decomposition of crystals or polymorphic transformations but favour the prediction of crusting. Decomposition would result in less PABA dissolved in solution and therefore the concentration and absorbance would decrease. The solubility of different polymorphic forms varies in the same solvent system resulting in a change in concentration and absorbance. Solid deposits on the vessel walls during each stage of the crystallization process resulting in an increase in crusting height. As the system is kept at a constant temperature of 45 °C there is a reflux of solvent and solid forms of vessel walls. Solvent evaporates from the slurry and condenses back in the condenser. The solvent falls back into the solution, lowering the concentration and solubility. Any solid crystals present in

solution will then dissolve to reach a saturated equilibrium state and the absorbance would remain constant. Once all the crystals have dissolved the solution becomes undersaturated and crusting continues to form on vessel walls resulting in a decrease in concentration and absorbance. The system is cooled from 45 to 5 °C forming a supersaturated solution resulting in the 2nd nucleation event at temperature of 9 °C and a decrease in absorbance. To reach an equilibrium state once nucleation has occurred crystals will either grow or the system will continue to nucleate. As the system is kept constant at 5 °C the absorbance decreases slightly and then remains constant. The slight decrease in absorbance is due to nucleation. As the system is kept constant at 5 °C crusting continues to form on vessel walls and solid in solution dissolves to maintain an equilibrium saturated state shown by a decrease in FBRM counts and constant absorbance. The decrease in the number of counts/sec at 5 °C is slower than at 40 °C since the evaporation at lower temperatures is significantly slower than at the higher temperatures, yielding slower crust formation.

Figure 6.4 shows photos of the crystallization vessel during the cooling crystallization process. The system starts off as a mobile slurry as shown in Figure 6.4 (a). As the system is heated up crystals dissolve forming a clear solution and crusting forms on vessel walls (see Figure 6.4 (b, c and d)). Figure 6.4 (e, f and g) show that the crusting height increases as the system is cooled down and kept at a constant temperature of 45 °C. Further cooling to 5 °C and holding at this temperature results in the crust height increasing to greater than 8cm as shown in Figure 6.4 (h and i).

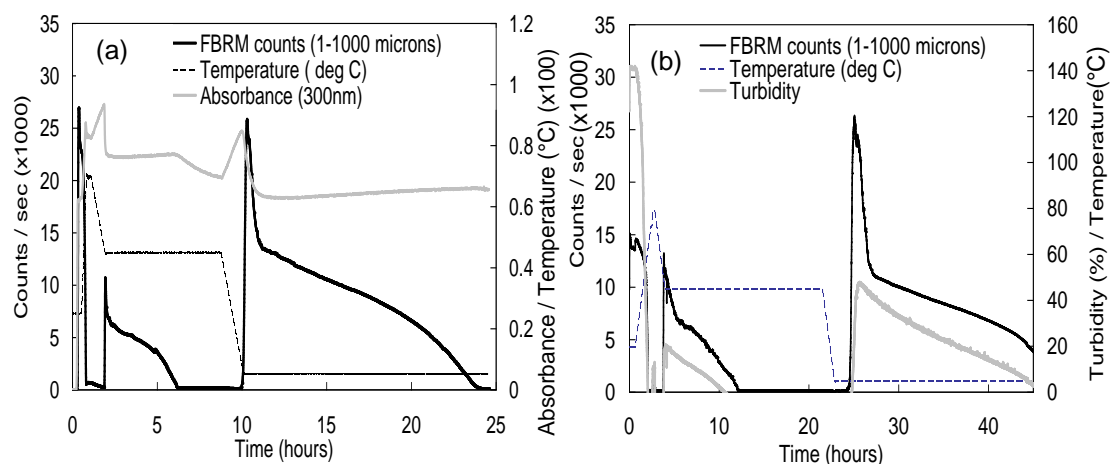


Figure 6.2. FBRM, turbidity and UV/Vis results for the cooling crystallization of PABA from ethyl acetate using (a) 4-pitched blade turbine and (b) 3-blade glass retreat curve

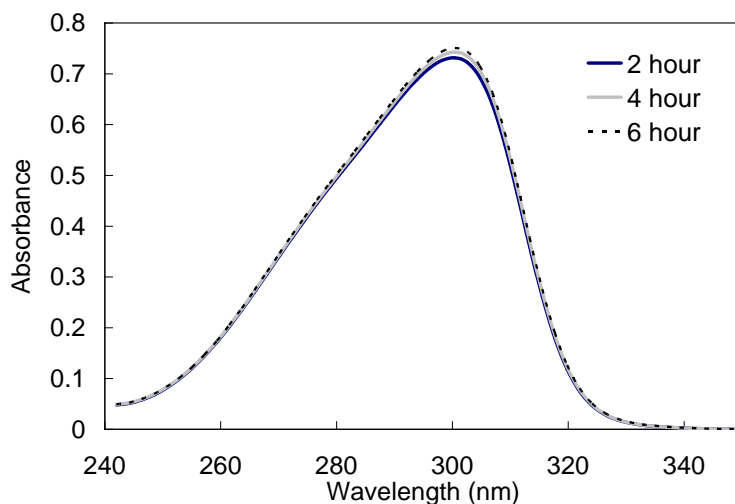


Figure 6.3. UV/Vis spectrum for PABA in ethyl acetate at 45 °C during 2-6 hours of crusting experiment, showing a peak absorbance of 300 nm

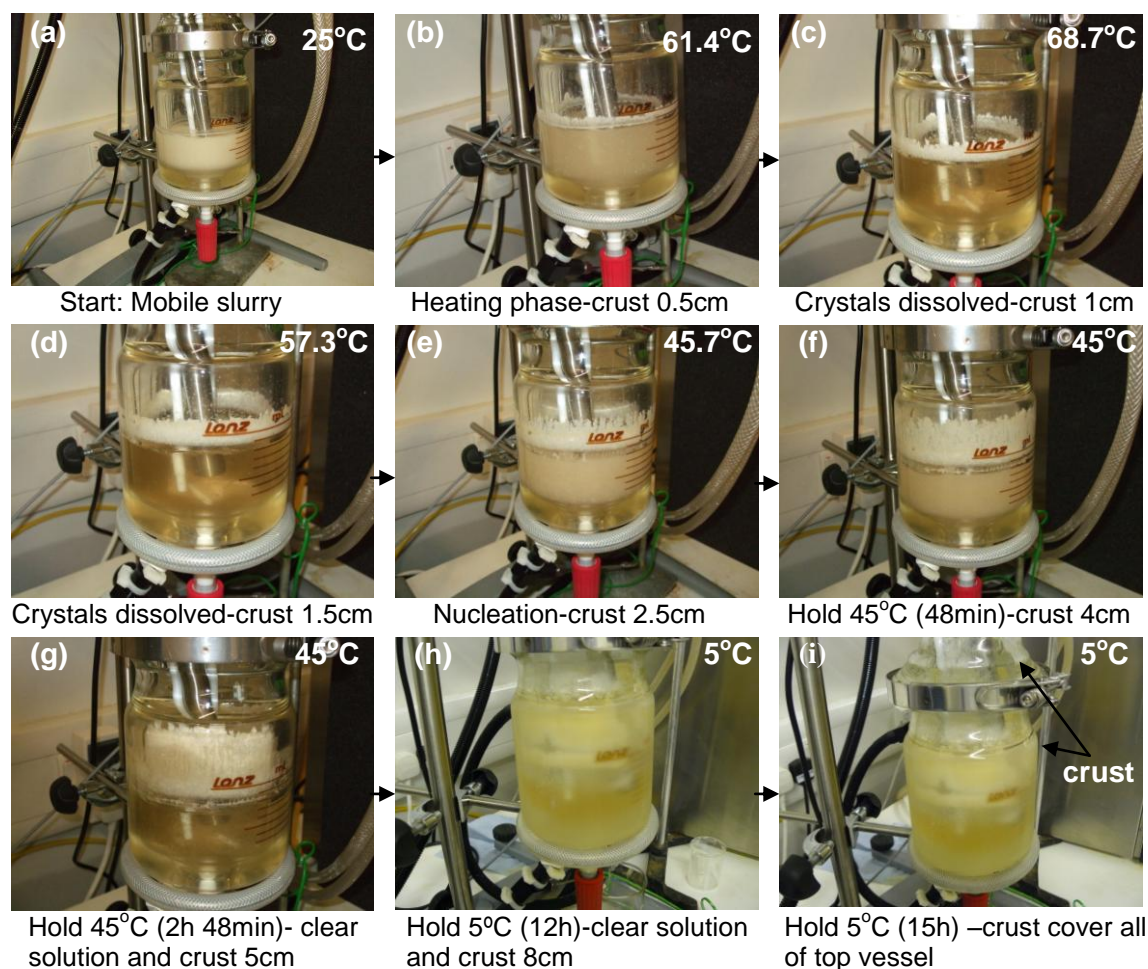


Figure 6.4. Photos of the crystallization vessel during the cooling crystallization of PABA in ethyl acetate showing an increase in crusting on vessel walls as the system is kept at a constant temperature of 45 and 5 °C

6.4 Identifying a common problem of crusting in crystallization vessels through the use of solid state analysis

Crystal samples obtained after the first and second nucleation events were analysed using a range of solid state analytical techniques including optical microscope, differential scanning calorimetry and X-ray powder diffraction. Samples were taken at the point of nucleation and 2-4 hours after nucleation. Figure 6.5 shows the optical microscope images of PABA crystals after both nucleation events showing a needle morphology which is characteristic to the alpha form. However different polymorphic forms of the compound may have the same morphology so further solid state analysis is required to identify the crystal forms.

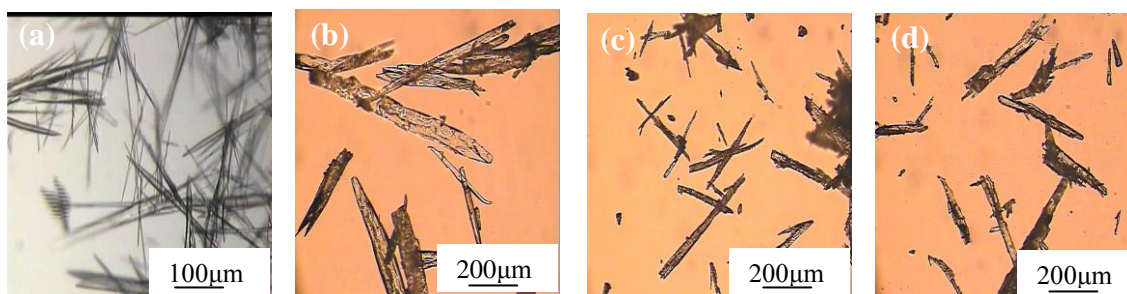


Figure 6.5. Optical microscope images of PABA samples obtained during the cooling crystallization experiment at (a) point of first nucleation 2 hours (45 °C), (b) 4 hours from start (45 °C), (c) point of second nucleation 10 hours (5 °C) and (d) 14 hours from start (5 °C)

DSC is performed on the crystal samples obtained after the first and second nucleation events and the results are shown in Figure 6.6. All samples show a single sharp peak at 191 °C which is the melting point of the alpha form of PABA. The alpha form of PABA nucleates from the first nucleation event at temperatures in the range 46-51 °C as this is the more stable form at temperatures above 25 °C. Kinetics favours the formation of the alpha form of PABA during the second nucleation event. Physical properties of crystals such as melting point vary for the different polymorphic forms. As no additional peaks are observed in the DSC patterns for the samples obtained while the system was kept at a constant temperature of 45 °C (4 hours from start of experiment) and 5 °C (14 hours from start of experiment), this supports the prediction that the decrease in FBRM counts and turbidity as the system

is kept at a constant temperature is not due to a polymorphic transformation but due to crusting. As solid deposits on vessel wall some of the alpha PABA crystals dissolve and the rest remain suspended in solution (i.e. no change occurring within the solution), which corresponds to the constant melting point of 191 °C in the DSC results for all samples.

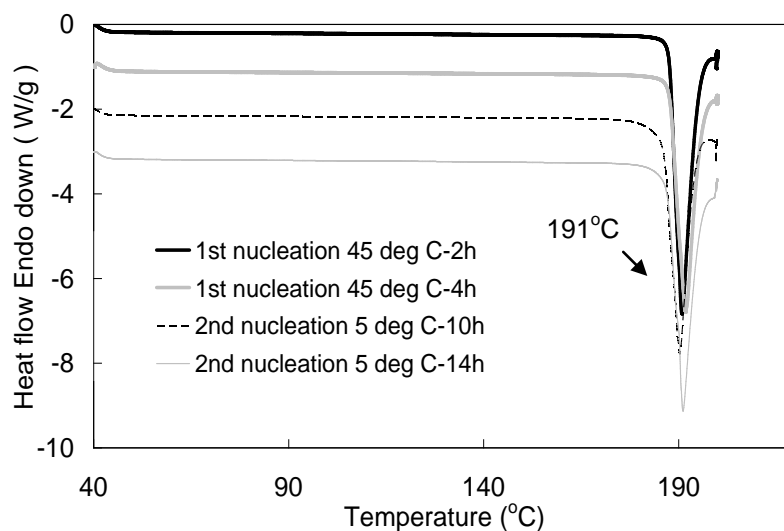


Figure 6.6. DSC plots for PABA samples obtained from the first and second nucleation events during the cooling crystallization experiment in which crusting formed on vessel walls. Heat flows for each plot are shifted by -1 W/g for clearer plotting

Further SSA involving the use of XRPD is applied to the crystal samples. This is a key SSA technique for the identification of different polymorphic forms of a compound as the structural differences between the forms are shown by different XRPD patterns. Figure 6.7 shows the XRPD results for crystal samples obtained after the first and second nucleation events. Patterns are very similar to the alpha form of PABA, which supports the DSC results and the prediction that the continuous decrease in FBRM counts and turbidity as the system is kept at a constant temperature is due to crusting and not a polymorphic transformation or decomposition.

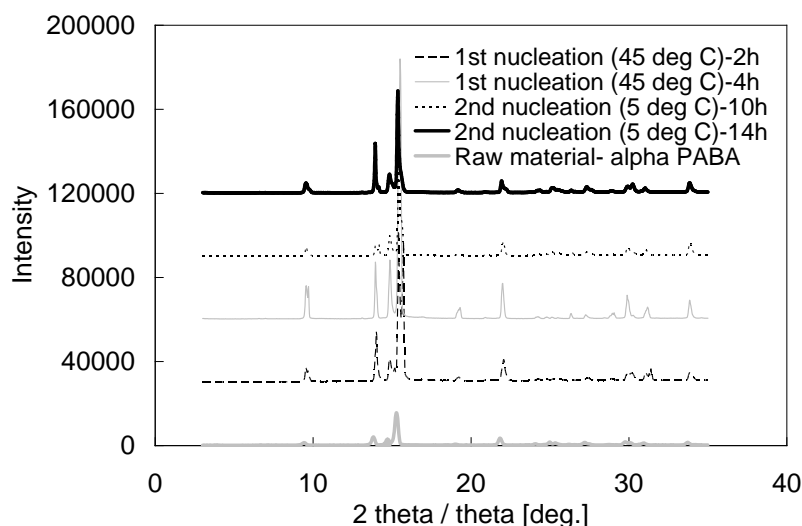


Figure 6.7. XRPD patterns for raw material PABA (alpha form) and crystal samples obtained after the first and second nucleation events during the experiment in which crusting formed on vessel walls. Intensities for each pattern are shifted by 3000 for clearer plotting

Repeats of the cooling crystallization experiment are performed in a 1 L vessel with the solution filled up to the top of the vessel to prevent the formation of crusting on vessel walls. The same 4-pitched blade turbine as in the previous experiment is used for homogeneous mixing. Figure 6.8 shows the FBRM and UV/Vis results for the cooling crystallization experiment. As the system is cooled from 70 to 45 °C both PAT tools detect a single nucleation event at 52 °C shown by an increase in counts and decrease in absorbance. The system is then kept at 45 °C overnight and both the FBRM counts and absorbance remains constant. The vessel walls were covered in solution so no crusting formed, which provides further evidence that the decrease in FBRM counts and turbidity as shown in Figure 6.2, in which crusting formed on vessel walls, is due to crusting increasing with time. SSA including hot-stage microscopy, DSC and XRPD is performed on the crystal samples at the point of nucleation (2 hours and 25min from start of experiment) and at the end (20 hours).

Figure 6.9 shows the HSM images of crystal samples obtained from the single nucleation event as shown in Figure 6.8. The crystal sample was heated from 25 °C to 200 °C. Melting of the crystals is observed at 189 °C, which is the melting point of alpha form of PABA. No other changes are observed in the images during the heating

stage providing evidence that the pure alpha form of PABA nucleates from the experiment in which no crusting formed on vessel walls.

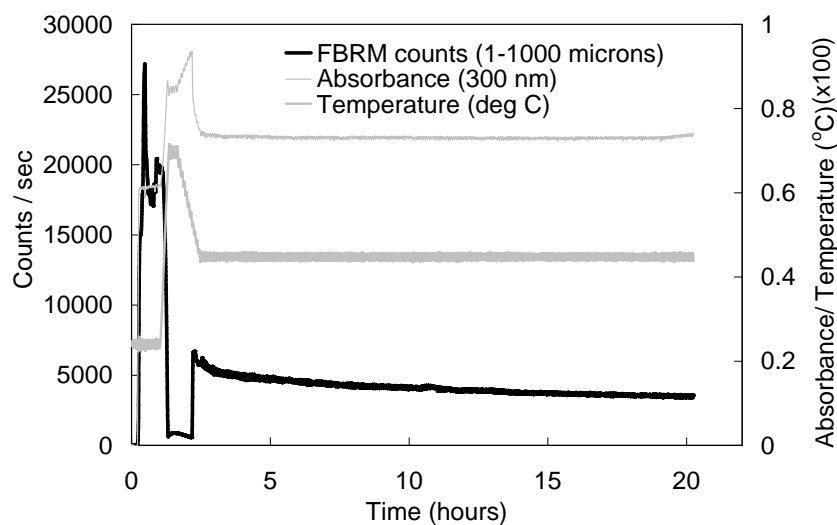


Figure 6.8. FBRM and UV/Vis results for the cooling crystallization of PABA from ethyl acetate in which no crusting formed on vessel walls (full vessel)

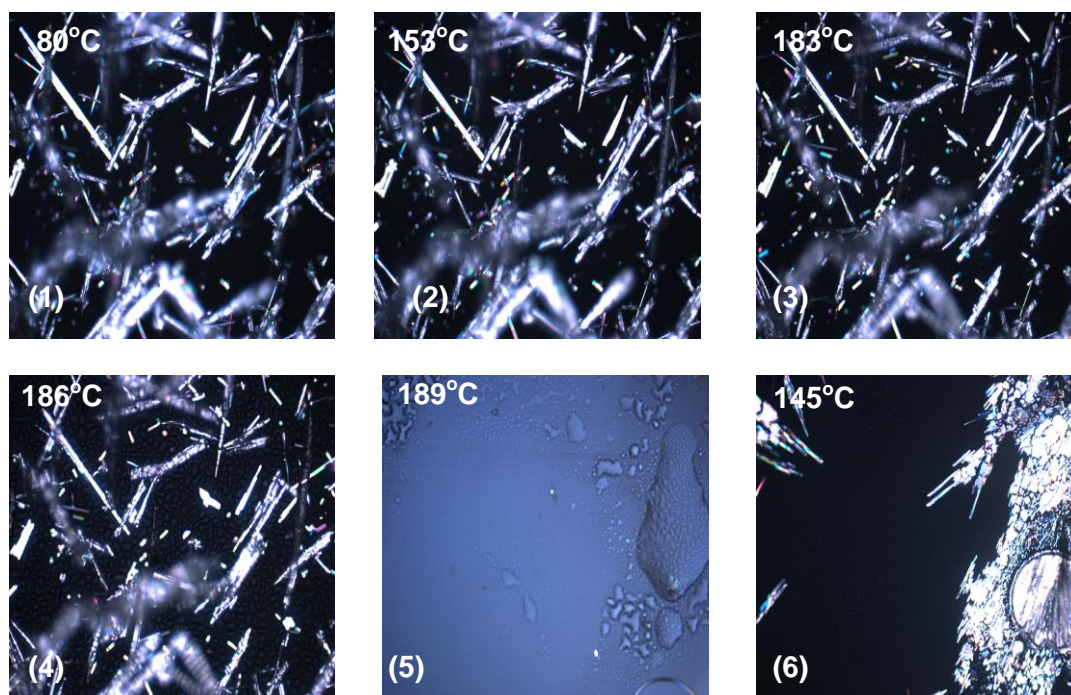


Figure 6.9. HSM images of PABA from the cooling crystallization experiments in which no crusting formed on vessel walls. Images 1-5 are during the heating phase and image 6 is cooling from the melt

Figure 6.10 shows the DSC results for crystal samples obtained at the point of nucleation and after PABA is exposed to ethyl acetate for 18 hours during the experiment in which no crusting formed on vessel walls. A single sharp peak at 191 °C is observed in the DSC results for both samples indicating the formation of the alpha-PABA, which fits with the results obtained from HSM. No additional peaks are observed in the DSC results indicating that PABA does not decompose as the system is exposed to ethyl acetate for 18 hours but remains in the stable state (alpha form).

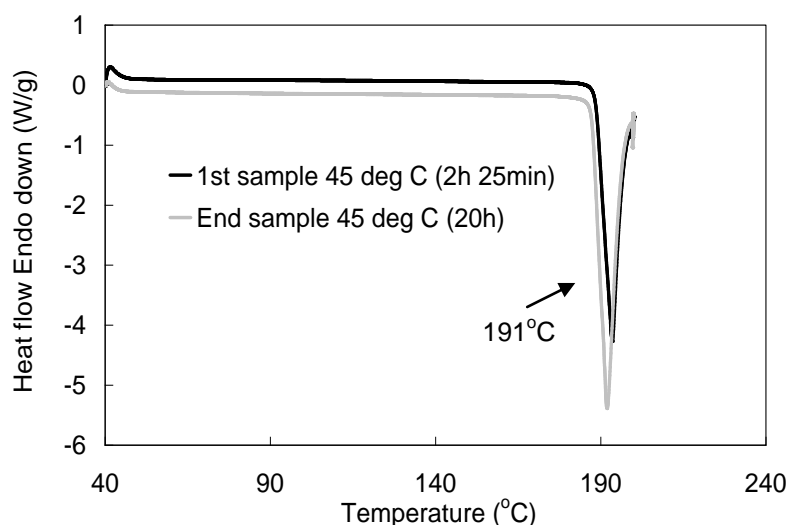


Figure 6.10. DSC plots for PABA re-crystallized from ethyl acetate as the system is kept at 45 °C during the experiment in which no crusting formed on vessel walls. Heat flows for each plot are shifted for clearer plotting

XRPD patterns for the crystal samples obtained from the experiment in which no crusting formed on vessel walls is shown in Figure 6.11. Patterns for samples obtained at the start of nucleation and at the end of experiment (20 hours) are very similar to the alpha form of PABA indicating the presence of this form. All of the SSA techniques provide evidence that the alpha form of PABA nucleates from ethyl acetate at temperatures of 52 °C and below.

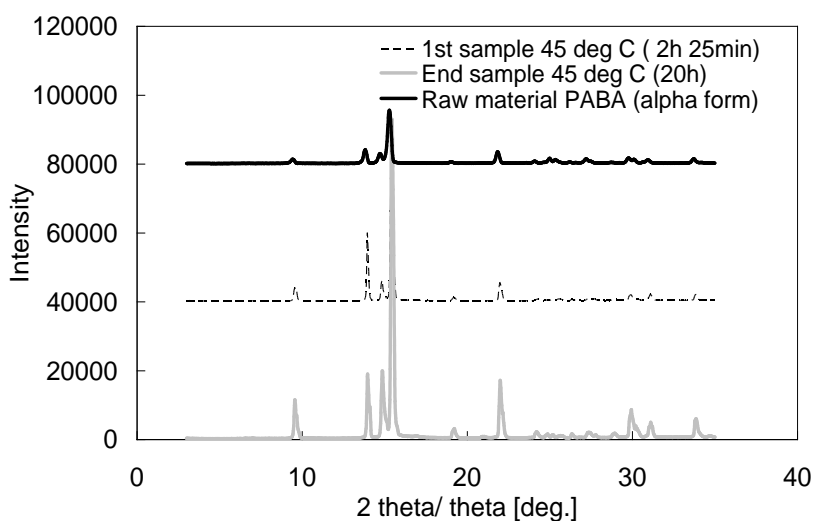


Figure 6.11. XRPD patterns for raw material PABA (alpha form) and crystal samples obtained after the first nucleation event (45 °C) during the experiment in which no crusting formed on vessel walls. Intensities for each pattern are shifted by 2000 for clearer plotting

6.5 Conclusions

The chapter investigates the cooling crystallization of p-amino benzoic acid (PABA), under conditions when crusting can accumulate on the walls of the vessel. PAT tools including the FBRM probe and turbidity meter showed a decrease in counts and turbidity as the system was kept at constant temperatures of 45 and 5 °C. In closed metal industrial vessels the change occurring during the crystallization process could be misinterpreted as a polymorphic transformation or decomposition however the UV/Vis spectrometer provided evidence that the change is due to crusting (solid deposition on vessel walls) increasing with time. SSA techniques including the use of XRPD, DSC, HSM and optical microscopy provided supporting evidence that the alpha form of PABA nucleates from the first and second nucleation events during the cooling crystallization experiments. No additional crystal forms were identified providing supporting evidence that the decrease in FBRM counts and turbidity during the cooling crystallization experiment in which crusting formed on vessel walls is not due to a polymorphic transformation but due to crusting increasing with time. Previous research mentions the important factors, including rate of supersaturation

generation, level of impurities and mixing conditions, which affect measurements of MSZW and can result in product failure. This research highlights the importance of crusting as an additional factor that leads to errors in MSZW measurements and crystallization operation. Combination of PAT tools with SSA techniques identifies common problems such as crusting forming on vessel walls highlighting the need for improvement within vessel design, for example by indicating the need to be able to operate the industrial vessel at partially filled jacket levels. These tools can save both time and money that would have been spent in researching the possibility of the presence of different polymorphic forms of a compound due to misinterpretation of results and can lead to better crystallizer design and optimised operating conditions.

Chapter 7. PAT used to examine the effect of mixing on the crystallization of pharmaceutical products

7.1 Introduction

Batch cooling crystallization is a key unit operation used for producing pharmaceutical drug products (Davey and Garside, 2000). Each crystallization vessel is not designed to produce a particular product but instead small scale laboratory experiments are carried out to find the right conditions that will result in consistent crystal quality upon scale up from laboratory to pilot and then industrial scale (Yi and Myerson, 2006). Nucleation is a key parameter that needs to be controlled for a crystallization processing to ensure a quality product. For successful scale up a robust meta-stable zone width (MSZW) determination is required which takes into consideration variation in process parameters (Gillon *et al.*, 2006; Barrett and Glennon, 2002). Operating within this region can be used to design the trade off between growth and nucleation and achieve good control (Parsons *et al.*, 2003). Developed models containing nucleation kinetic parameters are used to predict growth, attrition, secondary nucleation and are used for controlling the crystallization process to follow a set cooling profile within the robust MSZW region (Nagy *et al.*, 2008c; Mersmann and Bartosch, 1998; Meadhra *et al.*, 1996). Therefore it is of high importance that the nucleation kinetic parameters are accurate (Nagy *et al.*, 2008c). Nucleation kinetics can be determined from accurate MSZW data (O'Grady *et al.*, 2007). The most commonly used method is Nyvlt's correlation which involves plotting $\log(\text{cooling rate})$ against $\log(\text{MSZW})$ (Trifkovic *et al.*, 2009).

Crystallization behaviour is greatly affected by hydrodynamics, which can vary upon scale up. Hydrodynamic effects relate to changes in mixing conditions such as agitator speed and type, which affects the distribution of supersaturation within the crystallization vessel (Liang *et al.*, 2004). This affects the point of nucleation leading to a variation in MSZW. Vessel size and agitator speed affect both the number of sub nuclei sites and the frequency of collisions between these sites required for nucleation (Yi and Myerson, 2006). Agitator type and speed can also have an effect on the size

of the final crystals as high frequency collisions between crystals can lead to breakage affecting the quality of the crystals (Gillon *et al.*, 2006).

A detailed investigation into the effect of mixing conditions within different vessel sizes of 1 mL (Crystal 16) and 1 L is carried out using a Mettler Toledo FSC402 turbidity probe and focused beam reflectance measurement (FBRM) probe. These process analytical technology (PAT) tools are used to detect the point of spontaneous nucleation and hence the MSZW. Variations are made to a range of parameters including ramp (heating/cooling) rate, agitator speed and agitator type to examine the effect of the mixing conditions of the primary nucleation behaviour of the model systems *para*-amino benzoic acid (PABA), *meta*-amino benzoic acid (MABA) and *ortho*-amino benzoic acid (OABA) in water. Combining the effect of these parameters a robust MSZW region is obtained for the isomers of ABA. Nucleation kinetics and enthalpy/entropy of dissolution are obtained from the MSZW results and comparisons are made between the different crystallization vessel set-ups to corroborate the level in which these parameters are system specific.

7.2 Experiments performed

Cooling crystallization experiments were performed at the 1 mL and 1 L scale to investigate the effect of changes in mixing conditions on the MSZW. Other parameters were varied including ramp (heating/cooling) rate, agitator speed and type. A detailed range of experimental parameters used and the PAT tools used to measure the clear and cloud points at a range of concentrations is mentioned in section 3.3 and 3.4.3 of chapter 3. A Figure of the crystallization set-up for the 1 L scale is shown in Figure 3.1 of chapter 3.

7.3 Variation in key parameters on the MSZW and nucleation kinetics for isomers of ABA

There are many parameters such as agitator speed, agitator type, ramp (heating/cooling) rate, dosing rate and point of addition of antisolvent, type of probe

used for measurement, size and shape of vessel and whether the vessel is baffled or not, all which can affect the clear and cloud curves resulting in changes to the MSZW. Significant differences in the MSZW can lead to the production of crystals with undesired properties resulting in failed batches and an increase in economic costs. This sub-section of research focuses on the effect of vessel size, agitator speed, agitator type and ramp (heating/cooling) rate of the MSZW region. The model systems used in this study are PABA and MABA in water. Solubility data for PABA and MABA in water obtained from the literature can be found in Appendix D.

7.3.1 MSZW determination using different size vessels

This section of research investigates the affect of different mixing conditions within a 1 mL and 1 L size vessel on MSZW measurements. Cooling crystallization experiments are performed using the model system PABA and MABA in water. For both scales a turbidity probe is used to detect the clear (solubility) points and cloud (nucleation) points for a range of concentrations using ramp rates of 0.5 and 0.3 °C/min. The types of turbidity probes within each size vessel and measurement method is different, which could have some affect on the clear and cloud points. For the 1 mL scale 0% means no crystals dissolve and 100% means all the crystals dissolve. For the 1L scale the turbidity reading of 0% indicates all crystals dissolve and a positive number indicates crystals have nucleated. A different measurement method is the point at which the reading of clear and cloud points is chosen. Variations in the agitator type and rotational speed of the agitator will affect the mixing conditions within the vessel and hence the point of spontaneous nucleation and rate of dissolution. For the 1 mL scale a magnetic flea is used for suspending the solids and for the 1 L scale a overhead 3 flat blade glass retreat curve is used. The agitator speed used within the 1 mL scale is 700 rpm while the value used in the 1 L scale is 300 rpm. The results for the cooling crystallization experiments for PABA in water are shown in Figures 7.1 and 7.2. The results highlight not only the affect of vessel size on the MSZW but also the affect of different mixing conditions created by different agitator speeds and types, different types of turbidity probes and measurement methods of turbidity.

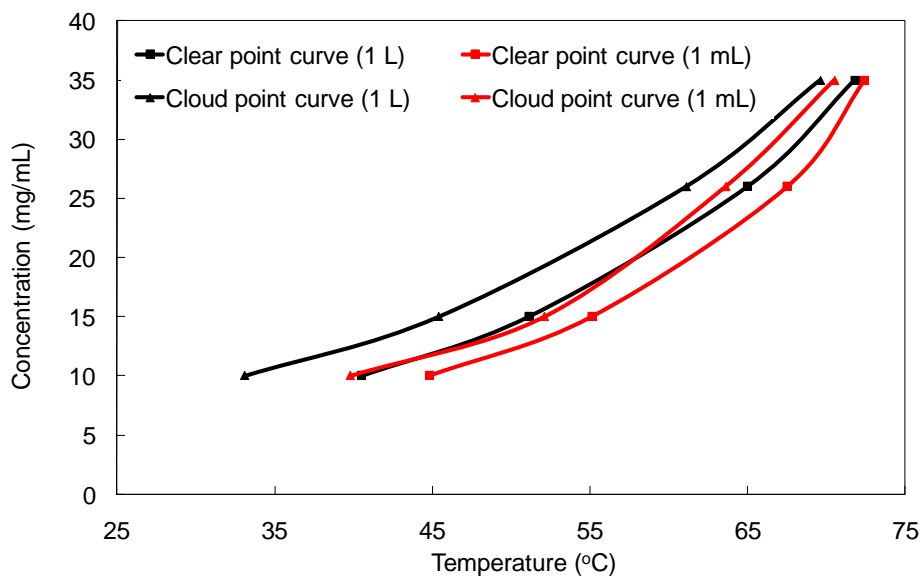


Figure 7.1. Clear and cloud point curves for PABA in water at the 1 mL and 1 L scale using a ramp rate of 0.3 °C/min

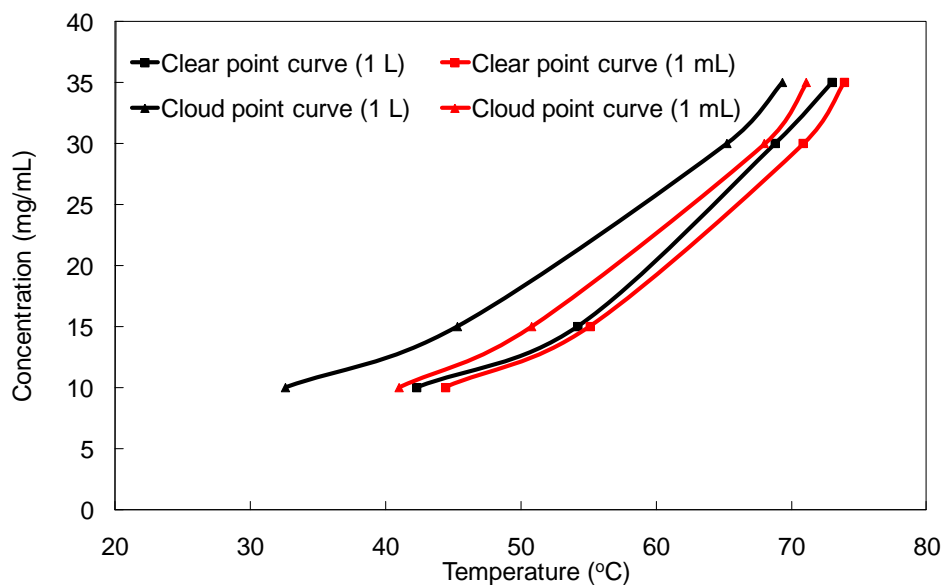


Figure 7.2. Clear and cloud point curves for PABA in water at the 1 mL and 1 L scale using a ramp rate of 0.5 °C/min

The MSZW is determined from the difference between the clear and cloud point curve for all concentrations values and the results for each scale using ramp rates of 0.5 and 0.3 °C/min are shown in Table 7.1.

Table 7.1. MSZW values for the cooling crystallization of PABA in water using different ramp rate and vessel sizes

Concentration (mg/mL)	Ramp rate of 0.3 °C/min		Ramp rate of 0.5 °C/min	
	MSZW (°C) (1 L)	MSZW (°C) (1 mL)	MSZW (°C) (1 L)	MSZW (°C) (1 mL)
10	7.4	5.0	9.7	3.4
15	5.7	3.0	8.9	4.3
26	3.9	3.9	-	-
30	-	-	3.6	2.9
35	2.2	1.9	3.7	2.8

Table 7.1 shows, for a ramp rate of 0.3 °C/min, the MSZW is wider at the larger scale (1 L) for all concentration values. The same behaviour is observed using a ramp rate of 0.5 °C/min. For the 1 mL scale the clear and cloud point temperatures are higher for all concentrations when compared with those obtained for the 1 L scale. The higher cloud (nucleation) temperature indicates enhanced mixing in the 1 mL vial. The poorer mixing in the 1 L scale was visually confirmed by observing solids settling at the bottom of the vessel. Yi and Myerson (2006) performed batch cooling crystallization experiments within vessel sizes of 50 mL and 500 mL. The results showed that for a larger size vessel using a lower agitator speed, nucleation occurred at a higher temperature leading to a narrower MSZW. However this was not found to be the case in the cooling crystallization experiments of PABA in water. The explanation for the different behaviour observed could be due to the different size vessels and types of agitators used to perform the cooling crystallization experiment affecting the mixing conditions within the vessel. Yi and Myerson (2006) used vessel sizes of 50 and 500 mL with stainless steel overhead pitched blade turbines whereas in these studies vessel sizes used include the 1 mL with the use of the magnetic flea and vessel size 1 L using an overhead 3 blade glass retreat curve. The higher nucleation temperature observed in the 1 mL scale could be due to the small vessel size and magnetic flea increasing the frequency of collisions between the solute molecules enhancing the likelihood of forming the critical size nucleus which is required for nucleation (O'Grady *et al.*, 2007). Additionally the MSZW based on

primary nucleation can significantly vary whether heterogeneous or homogeneous nucleation takes place.

Repeats of the MSZW experiments were performed at the 1 mL scale and 1 L scale using the model system MABA in water with ramp rates of 0.1, 0.2, 0.3 and 0.5 °C/min. The results for the clear and cloud point curves using a ramp rate of 0.3 °C/min is shown in Figure 7.3. The clear/cloud point temperatures and MSZW values at both scale (1 mL and 1 L) and at all ramp rates of 0.5, 0.3, 0.2 and 0.1 °C/min is shown in Tables 7.2 and 7.3.

For the 1 mL scale and the 1 L scale using a 3-blade glass retreat curve there is not much difference in the MSZW at high concentration (28-24 mg/ml) but the MSZW increases by 10 °C at low concentration of 15 mg/ml for the 1 L scale. There is a shift in the clear and cloud point curves for the two scales. Clear and cloud point curves occur at higher temperatures for the 1 mL scale. Similar results were observed for the two scales when using a ramp rate of 0.5 °C/min. This behaviour was also observed for the model system PABA in water.

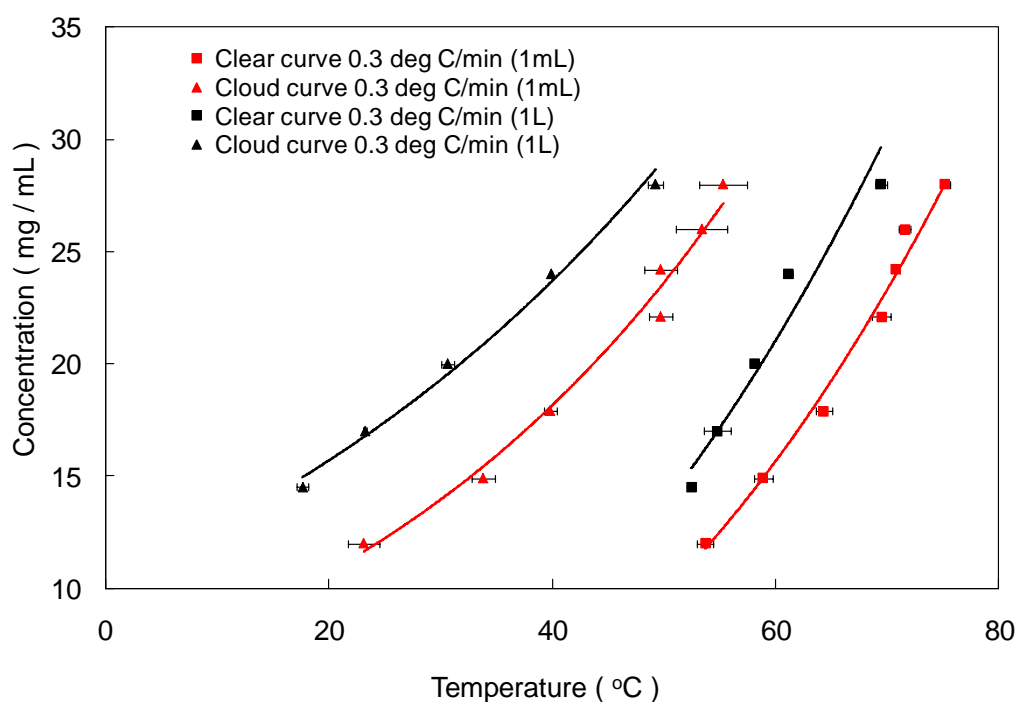


Figure 7.3. Clear and cloud point curves for MABA in water using different scales of 1 mL and 1 L (3-blade glass retreat curve) at a ramp rate of 0.3 °C/min. Error bars included

Table 7.2. Clear/cloud point temperatures and MSZW values for MABA in water at the 1 L scale using a 3-blade glass retreat curve at different ramp rates

Experiment type	Concentration (mg/ml)	Ramp rate (°C/min)	Temperature (clear point)	Temperature (cloud point)	MSZW (°C)
(3-blade glass retreat curve)	28	0.5	73.2	49.7	23.5
		0.3	69.5	49.3	20.2
		0.2	67.4	46.5	20.9
	24	0.5	61.6	39.7	21.9
		0.3	61.2	39.9	21.3
		0.2	60.3	40	20.3
	20	0.5	56	30	26
		0.3	58.1	30.6	27.5
		0.2	58	29.8	28.2
	17	0.5	52.6	22	30.6
		0.3	54.8	23.2	31.6
		0.2	55.6	23.9	31.7
	14.5	0.5	51.7	16.1	35.6
		0.3	52.5	17.6	34.9
		0.2	52.7	17.7	35

Table 7.3. Clear/cloud point temperatures and MSZW values for MABA in water at the 1 mL scale at different ramp rates

Experimental type	Concentration (mg/ml)	Ramp rate (°C/min)	Temperature (clear point)	Temperature (cloud point)	MSZW (°C)
1 mL	12	0.5	53.7	25.6	28.1
		0.3	53.7	23.1	30.6
		0.1	52.3	31.5	20.8
	15	0.5	59.7	33.5	26.2
		0.3	58.9	33.8	25.1
		0.1	58.2	35.8	22.4
	17.9	0.5	63.9	40.8	23.1
		0.3	64.3	39.8	24.5
		0.1	63.4	43.4	20
	20	0.5	65	45.6	19.4
	22.1	0.5	69.4	47.3	22.1
		0.3	69.5	49.7	19.8
		0.1	69.5	52.3	17.2
	24	0.5	72	49	23
		0.3	70.8	49.7	21.2
		0.1	71	54.8	16.2
	26	0.5	73.5	55	18.5
		0.3	71.6	53.4	18.2
		0.1	72.4	55.4	17
	28	0.5	75.3	56.7	18.6
		0.3	75.2	55.3	19.9
		0.1	74.2	58.8	15.4

7.3.2 MSZW determination using different agitator speeds and type

Cooling crystallization experiments were performed at the 1 L scale using different agitator types and agitator speeds to examine the effect of these parameters on the MSZW. The first set of experiments investigated the effect of agitator type on the MSZW using the model system MABA in water. The two types of agitator used in this study are the 3-blade glass retreat curve and a 4-pitched blade turbine. The FBRM was used to detect the clear and cloud points for the vessel with the 4-pitched blade turbine. The turbidity probe was used to detect the clear and cloud points for the vessel with the 3-blade glass retreat curve. The MSZW results using a ramp rate of 0.3 °C/min and an agitation speed of 300 rpm is shown in Figure 7.4. Three previous repeated experiments using a combination of FBRM and turbidity probe for cooling crystallization of PABA in ethyl acetate (Chapter 6) showed that there was no difference in the clear points and only a 1 °C difference in the cloud points detected by the two PAT tools. Taking into account a 1 °C difference in cloud points over the concentration used the MSZW shown in Figure 7.4 still varies by 2-7 °C due to the effect of agitator types. This confirms that the significant differences in clear/cloud points and hence MSZW values shown in Figure 7.4 is mainly due to the effect of different agitator types.

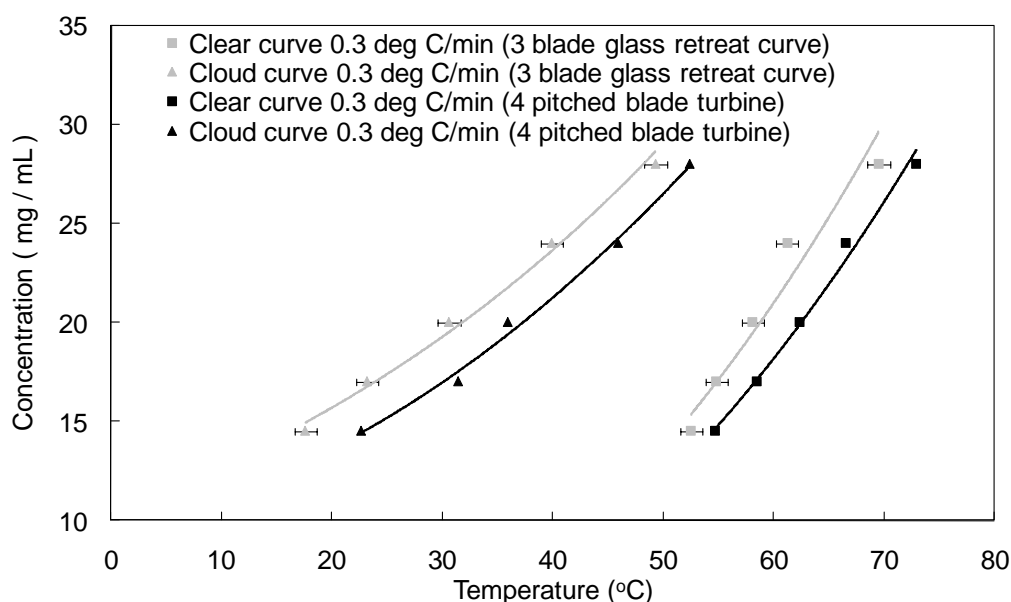


Figure 7.4. Clear and cloud point curves for MABA in water using different agitator types at the 1 L scale and ramp rate of 0.3 °C/min. Error bars included for clear and cloud points for the 3-blade glass retreat curve agitator

Clear/cloud point temperatures and MSZW values for the 3-blade glass retreat curve can be found in Table 7.2 and those for the 4-pitched blade turbine can be seen in Table 7.4.

Table 7.4. Clear/cloud point temperatures and MSZW values for MABA in water at the 1 L scale using a 4-pitched blade turbine at different ramp rates

Experiment type	Concentration (mg/ml)	Ramp rate (°C/min)	Temperature (clear point)	Temperature (cloud point)	MSZW(°C)
1 L (4-pitched blade turbine)	28	0.5	71.2	50.2	21
		0.3	72.9	52.4	20.5
		0.2	74.2	53.9	20.3
	24	0.5	66.9	43.5	23.4
		0.3	66.5	45.9	20.6
		0.2	70.4	49.1	21.3
	20	0.5	61.7	33.8	27.9
		0.3	62.3	35.9	26.4
		0.2	66.4	40.0	26.5
	17	0.5	57.8	28.3	29.5
		0.3	58.5	31.4	27.1
		0.2	61.8	33.3	28.5
	14.5	0.5	54.5	21.7	32.8
		0.3	54.7	22.6	32.1
		0.2	58.1	23.2	34.9

There is no significant difference in the MSZW for the 1 L scale using different agitator types of the 3-blade glass retreat curve and 4-pitched blade turbine. There is a shift in the clear and cloud point curves for the different agitator types indicating a variation in the mixing conditions. Higher clear and cloud points are observed at all concentration ranges (14.5-28 mg/mL) for the 4-pitched blade turbine.

The second set of experiments investigated the effect of agitator speed on the MSZW. Cooling crystallization experiments were performed within a 1 L size vessel using a 3-blade glass retreat curve and a constant ramp rate of 0.3 °C/min. The agitator speeds used were in the range of 250 to 400 rpm. Alterations to the agitator speed will vary the power input into the system. Variations in the power input will affect the mixing

conditions within the vessel and hence the MSZW. The model system used in this study is PABA in water. The turbidity probe was used to detect the clear and cloud points for different concentration values and agitator speeds. The clear and cloud point curves are shown in Figure 7.5. The MSZW is determined for each concentration value at the different agitator speeds and the results are shown in Table 7.5.

Figure 7.5 shows that for all agitator speeds the clear and cloud point curves are very similar. The MSZW values stated in Table 7.5 show that for each concentration value the MSZW does not change significantly by changing the agitator speed from 250 to 400 rpm. For each agitator speed, power number (N_p), power input (P) and Reynolds number for impeller were calculated to provide a crude approximation of the variation in the flow regime by the change in the agitator speed within the range used.

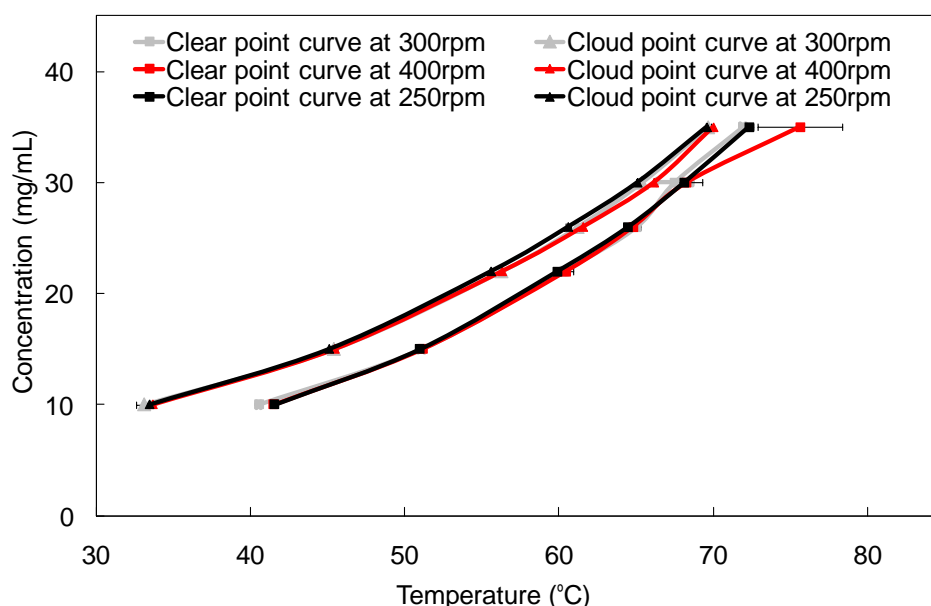


Figure 7.5. Clear and cloud point curves obtained using different agitator speeds within the 1 L size vessel

Table 7.5. MSZW values for the cooling crystallization of PABA in water using different agitator speeds

Concentration (mg/ml)	MSZW (°C) for different agitator speeds		
	250 rpm	300 rpm	400 rpm
10	8.1	7.4	7.9
15	5.9	5.7	5.7
22	4.3	4.0	4.2
26	3.9	3.8	3.3
30	3.1	2.1	2.2
35	2.8	2.15	5.6

The Reynolds number for impeller is defined as

$$\text{Re} = \frac{\rho_L N D^2}{\mu_v} \quad (7.1)$$

where ρ_L is the fluid density, μ_v is the fluid viscosity, D is the impeller diameter and N is the agitator speed (Rielly *et al.*, 2007). The power number is given as follows (Li *et al.*, 2005):

$$N_p = \frac{P}{\rho N^3 D^5} \quad (7.2)$$

where P is the power input into the system. The power number remains constant for $\text{Re} > 10^4$ (Li *et al.*, 2005).

For the calculations of the Reynolds number the properties of the fluid are assumed to remain constant for the temperature range used. The fluid properties are those obtained for water giving a fluid density constant at a value of 1000 kg/m^3 and fluid viscosity is 0.001 Ns/m^2 . The diameter of the retreat curve impeller is 0.05 m .

A summary of the results for Reynolds number, power number and power input into the system for each agitator speed is shown in Table 7.6.

Table 7.6. Summary of Reynolds number, power number and power input for different agitator speeds

Agitator speed (rpm)	Reynolds number	Power number	Power input (J/s)
250	10,417	0.7	0.016
300	12,500	0.7	0.027
400	16,666	0.7	0.06

From the results in Table 7.6 it shows that the Reynolds number is in the region of 10,000-17,000 for the agitator speeds used of 250-400 rpm. Given all values are $Re > 10^4$ the mixing conditions within the vessel is in the turbulent regime, indicating good mixing (Li et al., 2005). Within the range of agitator speeds used the Reynolds number and hence degree of turbulence does not change significantly indicating little change in the mixing conditions within the vessel which could explain why the cloud (nucleation) point curves are very similar as shown in Figure 7.5.

Optical microscopy is used to analyse samples of crystals obtained from the cooling crystallization of PABA in water using different agitator speeds of 250, 300 and 400 rpm. The optical microscope images are shown in Figure 7.6.

The micrographs show long fibrous needles of size greater than 200 μm . The size of the crystals is not affected by the agitator speeds within range 250-400 rpm which indicates that the mixing conditions for these studies, using a 1 L vessel size and a 3-flat blade glass retreat curve, does not affect the quality of the crystals. The increase in turbulence and power input resulting from the increase of the agitator speed from 250 to 400 rpm was not large enough to generate the attrition of the crystals.

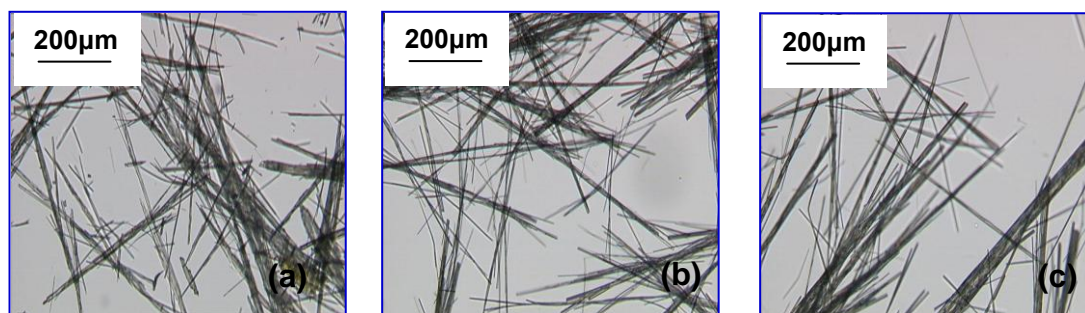


Figure 7.6. Optical microscope images of crystals obtained during the cooling crystallization of PABA in water using different agitator speeds of (a) 250 rpm, (b) 300 rpm and (c) 400 rpm

7.3.3 Evaluation of the effect of cooling rate on the MSZW and investigation of the variability of nucleation kinetics with different crystallization conditions

Cooling crystallization experiments were performed within a 1 L vessel using a 3-blade glass retreat curve and an agitator speed of 300 rpm. The cooling rate is varied using a range of values including 0.5, 0.3, 0.2 and 0.1 °C/min to investigate how this parameter affects the MSZW. The model systems used in this study are PABA and MABA in water. The first set of experiments used the turbidity probe to detect the solubility (clear) point and nucleation (cloud) points for a range of concentrations using the model system PABA in water. From the turbidity results the true thermodynamic solubility curve was obtained by using an extrapolation method in excel to find the temperature corresponding to zero ramp rate and nucleation (cloud) curve for each cooling rate are obtained and the results are shown in Figure 7.7.

For each cooling rate the MSZW is determined by the temperature difference between the solubility and nucleation curves. A summary of the results are shown in Table 7.7.

Figure 7.7 and Table 7.7 show that for a particular concentration the MSZW increases with the cooling rate, which is observed in many generic crystallization processes (Nagy *et al.*, 2007). As the concentration is lowered the MSZW increases, which is true for all cooling rates. From these results nucleation kinetics are determined using the method proposed by Nyvlt (1968) and both the enthalpy and entropy of dissolution are calculated using the Van't Hoff solubility curve for PABA in water.

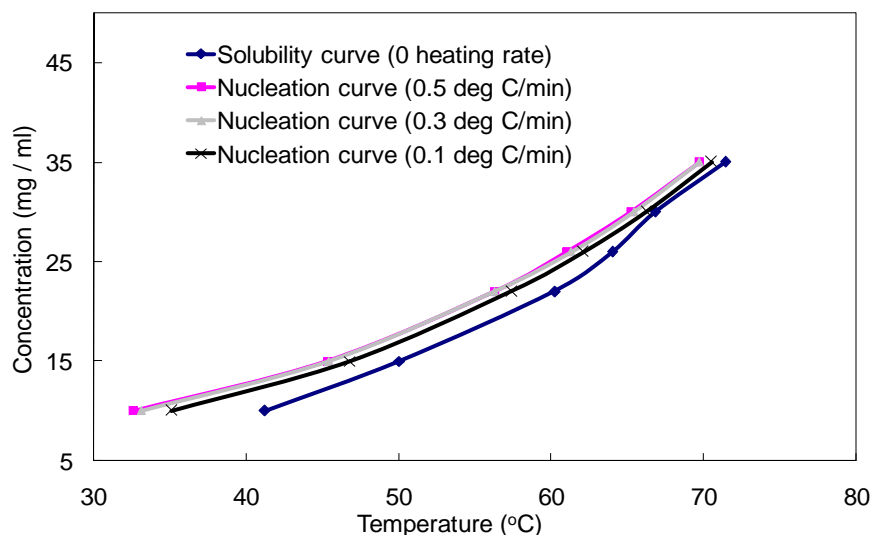


Figure 7.7. Solubility and nucleation curves for PABA in water at cooling rates 0.5, 0.3, 0.1 °C/min, using a 1 L size vessel

Table 7.7. MSZW values for the cooling crystallization of PABA in water using a 1 L vessel and different cooling rates

Concentration (mg/mL)	MSZW (°C) at different cooling rates		
	0.5 °C/min	0.3 °C/min	0.1 °C/min
10	8.6	8.1	6.1
15	4.7	4.6	3.2
22	3.9	3.9	2.8
26	3	2.7	1.9
30	1.6	1.4	0.6
35	1.7	1.7	0.9

Various experiments have been prepared in the literature for nucleation rate (e.g. Mullin, 2001). However for modelling purposes the following power law type semi-empirical expression is often used:

$$B = k_b (C - C^*)^b \quad (7.3)$$

where B is the rate of nucleation, k_b is the nucleation rate constant, b is the nucleation order and $(C - C^*)$ is the degree of supersaturation.

For the experimental determination of B , Nyvlt prepared a method that involves varying the rate of supersaturation generation and measuring the MSZW (Nyvlt, 1968). This method involves cooling a solution down at a constant cooling rate using the same initial concentration. Nyvlt (1968) carried out a large number of experiments involving the cooling crystallization of aqueous solutions and found that a linear relationship by plotting $\ln(\text{cooling rate})$ against $\ln(\text{MSZW})$. The linear relationship is shown in Equation 7.4,

$$\ln(\beta) = b \ln(\text{MSZW}) + K \quad (7.4)$$

where β is the cooling rate, b is the nucleation order, MSZW is the meta stable zone width and K is a constant.

From the results shown in Figure 7.7, for the cooling crystallization experiments of PABA in water within a 1 L vessel, $\ln(\beta)$ is plotted against $\ln(\text{MSZW})$ for each concentration value and the results are shown in Figure 7.8.

Figure 7.8 shows approximately linear relationships between the cooling rate and MSZW at all concentrations for the cooling crystallization of PABA in water at the 1 L scale. From the slope of each line the nucleation order, b , is calculated. The results together with the constant K from equation 7.4 and R^2 values, which represent how close the data points fit the linear line, are shown in Table 7.8.

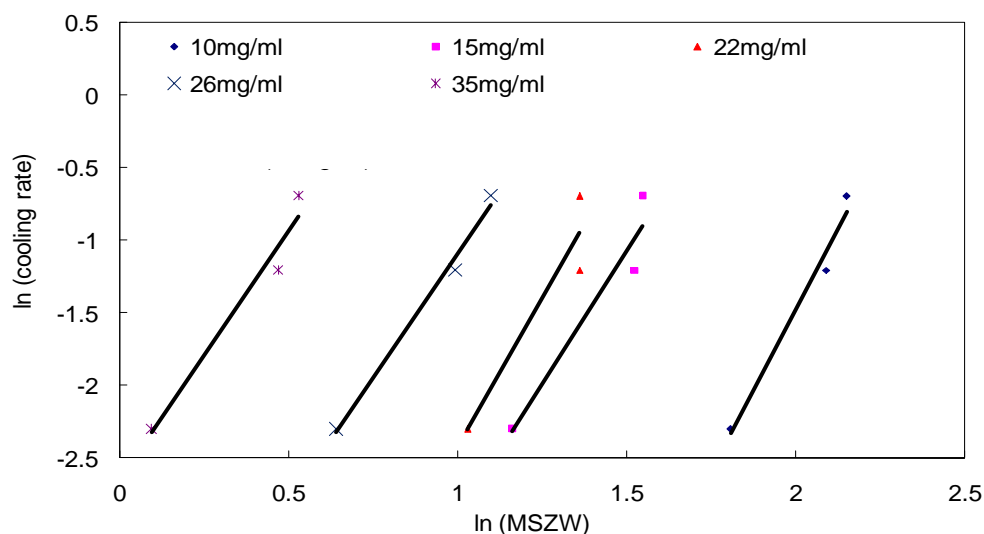


Figure 7.8. Linear dependence between cooling rate and MSZW according to Nyvlt (1968) for PABA in water at the 1 L scale

Table 7.8. Nucleation orders, contact K and R^2 values obtained from the cooling crystallization of PABA in water within the 1 L vessel

Concentration (mg/ml)	Nucleation order (b)	Constant (K)	R^2 values
10	4.4 ± 0.8	-10.34	0.98
15	3.7 ± 0.4	-6.59	0.93
22	4.1 ± 0.3	-6.51	0.90
26	3.4 ± 0.5	-4.52	0.99
35	3.4 ± 0.3	-2.65	0.97

Nucleation order for the cooling crystallization experiments of PABA in water are in the range of 3.4-4.4 with confidence intervals of up to ± 0.8 . Nagy *et al.* (2007) stated that the nucleation order for the cooling crystallization of caffeine in water is 3.18, which is lower than the values obtained within these experiments. Lower nucleation orders indicate a narrower MSZW and hence the system is more difficult to control.

Further calculations involving the determination of the enthalpy and entropy of dissolution were performed using linearised van't Hoff relationship, which is shown in Equation 7.5,

$$\ln(C) = -\frac{\Delta H_d}{R} \frac{1}{T} + \frac{\Delta S_d}{R} \quad (7.5)$$

where C is the concentration, R is the gas constant, T is the temperature, ΔH_d is the enthalpy of dissolution and ΔS_d is the entropy of dissolution. Equation 7.5 represents a linear relationship between $\ln(C)$ and $1/T$ with slope $\Delta H_d/R$ and intercept $\Delta S_d/R$.

Based on the linearised van't Hoff solubility equation, $\ln(C)$ is plotted against $\ln(1/T)$ for the cooling crystallization experiments of PABA in water and the results are shown in Figure 7.9.

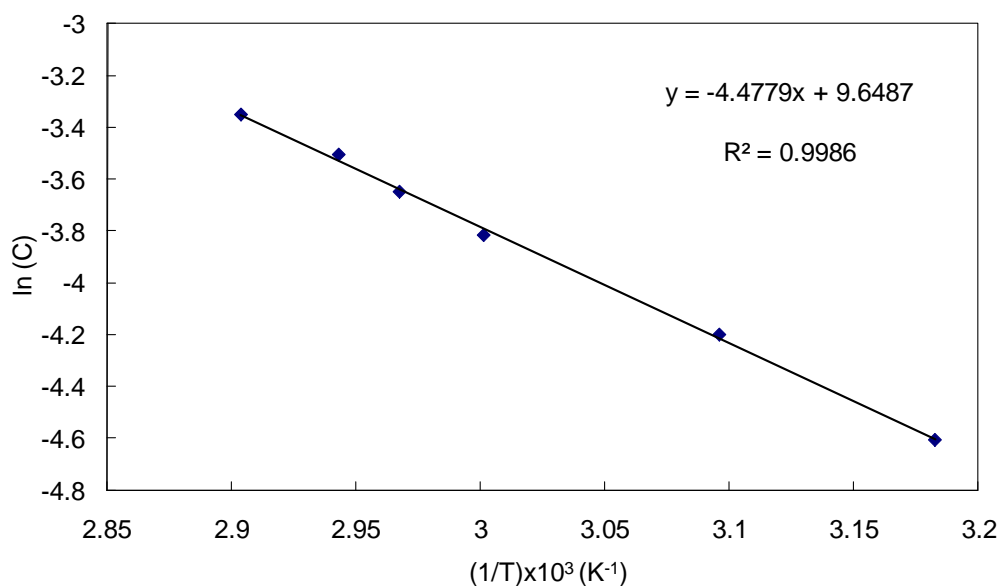


Figure 7.9. Linearised van't Hoff solubility curve for PABA in water at the 1 L scale

The enthalpy of dissolution is obtained from the slope of the line plotted to the data points, giving a value of $\Delta H_d = 37.2$ J/mol. The entropy of dissolution is obtained from the intercept giving a value of $\Delta S_d = 80.2$ J/mol/K. These values are lower than the values obtained from the cooling crystallization of caffeine in water which has an enthalpy of dissolution of 40.8 J/mol and entropy of dissolution of 104.0 J/mol/K (Nagy *et al.*, 2007). Due to the lower melting point of PABA compared to caffeine, it is expected that the enthalpy of dissolution would be lower as less energy is required in order to dissolve the solid. PABA is a less complex molecule in terms of the molecular structure when compared to caffeine and therefore a lower value for the entropy of dissolution is expected for PABA.

The second set of experiments investigated the effect of ramp rate on the MSZW using the model system MABA in water. Cooling crystallization experiments were performed using a 3-blade glass retreat curve with agitator speed of 300 rpm. The ramp rates used includes 0.5, 0.3 and 0.2 °C/min. The results showing the clear and cloud point curves at the different ramp rates are shown in Figure 7.10.

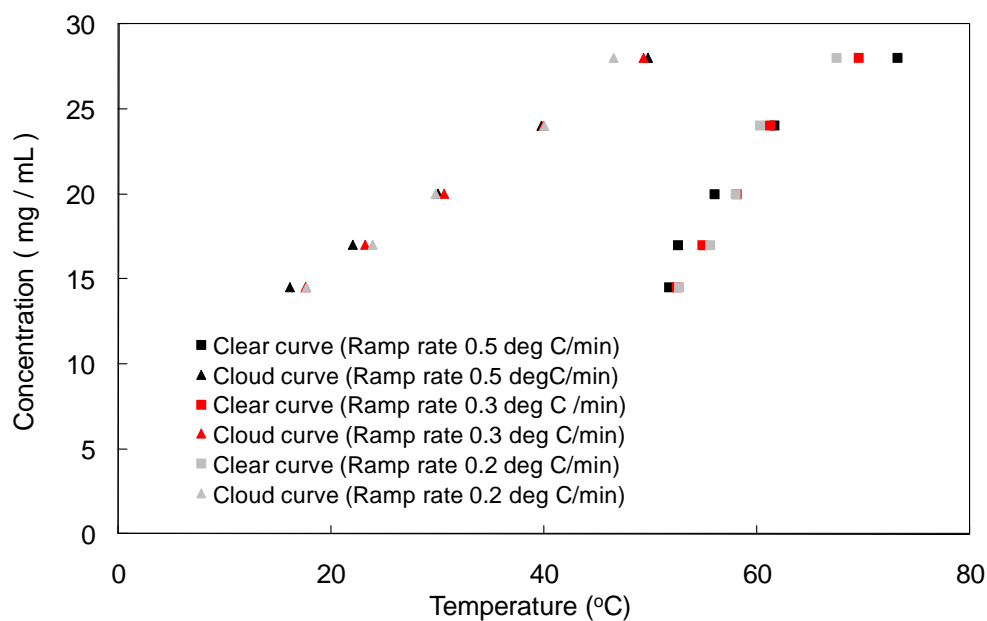


Figure 7.10. Clear and cloud point curves for MABA in water at the 1 L scale using a 3-blade glass retreat curve and different ramp rates of 0.5, 0.3 and 0.2 °C/min

From the results shown in Figure 7.10 there is no significant difference in the clear and cloud point curves at all ramp rates. Similar results were obtained when using a 4-pitched blade turbine within a 1 L size vessel and using a magnetic stirrer at the 1 mL scale. Nucleation kinetics are obtained from the results of clear and cloud point curves at different ramp rates at the 1 L scale using a 3-blade glass retreat curve and 4-pitched blade turbine and at the 1 mL scale. The same method is used to obtain nucleation kinetics as for the previous model system, PABA in water. However the true thermodynamic solubility temperature (zero heating rate) at all concentration values is replaced with the temperature at a ramp rate of 0.2 °C/min for the 1 L scale and 0.1 °C/min for the 1 mL scale. Results showing a linear relationship between $\ln(\beta)$ and $\ln(\text{MSZW})$ for the three different set-ups are shown in Figures 7.11, 7.12 and 7.13.

Nucleation orders were obtained from the slope of the lines in Figure 7.11, 7.12 and 7.13. The results together with the constant K obtained from equation 7.4 and R^2 values, which represent how close the data points fit the linear line, are shown in Table 7.9.

Nucleation orders obtained from the 1 mL and 1 L scale using a 4-pitched blade turbine are within the range 3.9-6.3 with confidence intervals of up to ± 1 . These values are similar to the nucleation order obtained for PABA in water of 3.4-4.4. Although these values are relatively similar the nucleation order for MABA in water at the 1 L scale using a 3-blade glass retreat curve is significantly higher, within the range of 15.6-16.9 with confidence intervals of up to ± 3 . The results provide experimental evidence that the typical model parameters of the semi-empirical nucleation expression (Equation 7.3) often used in crystallization modelling are only valid for a specific crystallization vessel and mixing conditions. Therefore model based design and scale-up of crystallization processes must be used carefully, and considering more detailed mechanistic models and better incorporation of the effect of mixing in these mechanisms can improve the generality and applicability of crystallization models.

Enthalpy and entropy of dissolution values are obtained for MABA within the three different vessel set-ups using the linearised van't Hoff solubility curve. Figure 7.14 shows the van't Hoff solubility curve for each vessel set-up including the 1 L scale with the 3-blade glass retreat curve and the 4-pitched blade turbine and for the 1 mL scale.

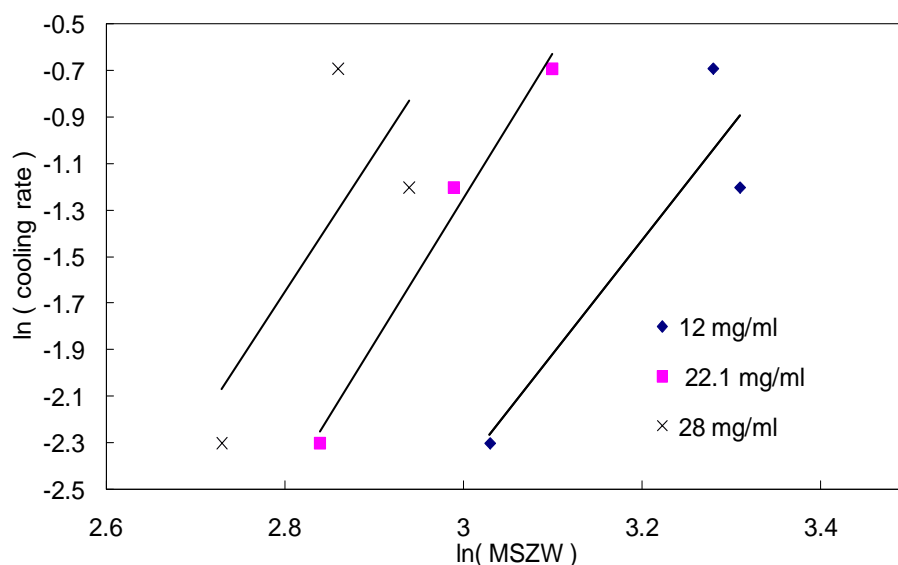


Figure 7.11. Linear dependence between cooling rate and MSZW according to Nyvlt's (1968) method for the 1 mL scale of MABA in water

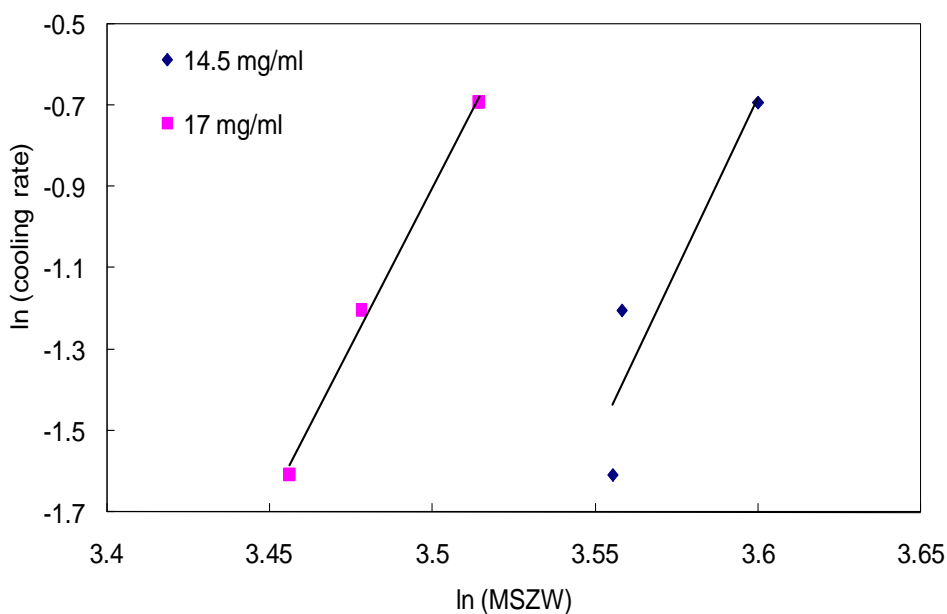


Figure 7.12. Linear dependence between cooling rate and MSZW according to Nyvlt's (1968) method for the 1 L scale using a 3-blade glass retreat curve for MABA in water

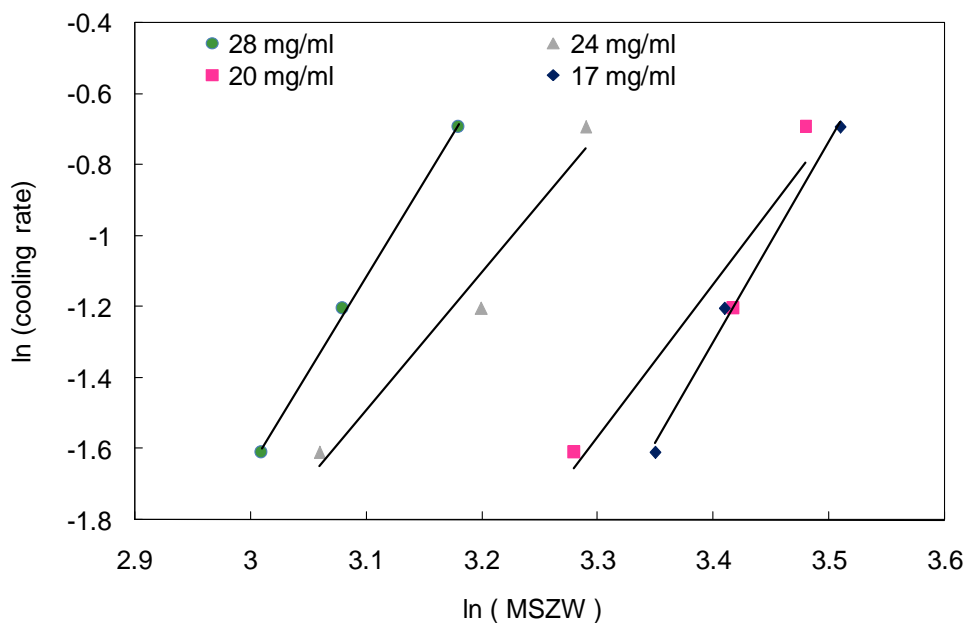


Figure 7.13. Linear dependence between cooling rate and MSZW according to Nyvlt's (1968) method for the 1 L scale using a 4-pitched blade turbine for MABA in water

Table 7.9. Nucleation orders obtained from cooling crystallization of MABA in water within a 1 L vessel using a 3-blade glass retreat curve and 4-pitched blade turbine and within a 1 mL vessel

Vessel type	Concentration (mg/mL)	Nucleation order	Constant (K)	R ² values
1 mL	12	4.9 ± 0.7	-17.11	0.84
	22.1	6.3 ± 1	-20.02	0.99
	28	5.9 ± 0.6	-18.24	0.58
1 L (3-blade glass retreat curve)	14.5	16.9 ± 2.7	-61.51	0.85
	17	15.6 ± 3	-55.40	0.99
1 L (4-pitched blade turbine)	17	5.7 ± 0.5	-20.56	0.99
	20	4.3 ± 0.3	-15.78	0.92
	24	3.9 ± 0.6	-13.55	0.96
	28	5.4 ± 0.9	-17.76	0.99

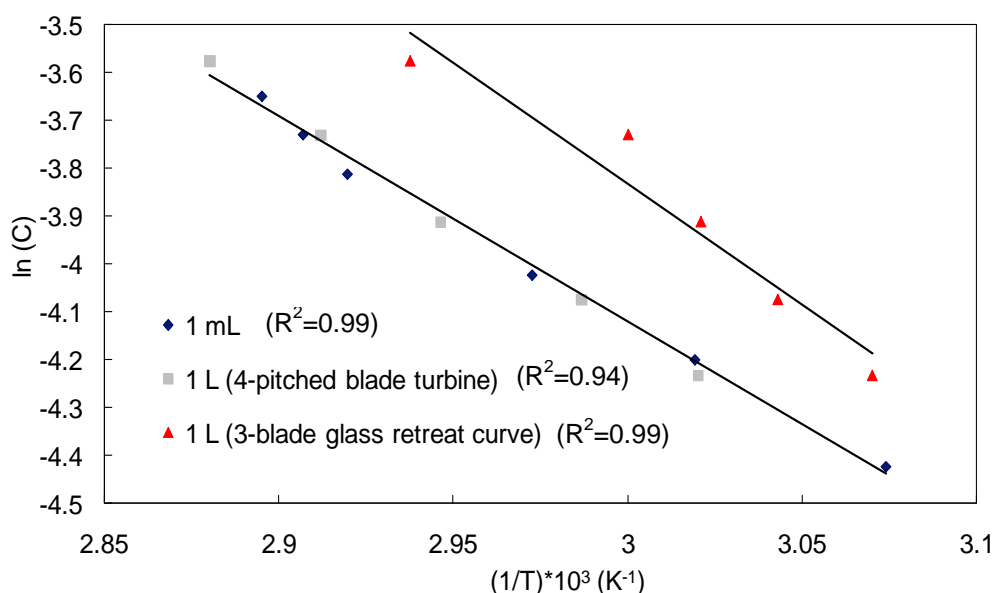


Figure 7.14. van't Hoff solubility curve for MABA in water (a) at the 1 mL scale and 1 L scale using (b) a 3-blade glass retreat curve and (c) 4-pitched blade turbine

From the slope and intercept of the van't Hoff solubility curves the enthalpy of dissolution and entropy of dissolution are obtained for each crystallization set-up, and the results are shown in Table 7.10.

Table 7.10. Enthalpy and entropy of dissolution values for MABA in water at the 1 mL scale and the 1 L scale using a 3-blade glass retreat curve and a 4-pitched blade turbine

Crystallization set up (vessel type)	Enthalpy of dissolution (ΔH) (J/mol)	Entropy of dissolution (ΔS) (J/mol/K)
1 mL	35.7	73
1 L (3-blade glass retreat curve)	37.7	81.8
1 L (4-pitched blade turbine)	38.9	80.2

Enthalpy of dissolution for MABA in water within all crystallization set-ups is very similar giving a value in the range 35.7-38.9 J/mol. As the melting point of PABA (189 °C) is close to that of MABA (177 °C) the enthalpy of dissolution would be predicted to be similar and this is found to be the case as the enthalpy of dissolution for PABA in water is 37.2 J/mol. The entropy of dissolution for MABA is within the range 80.2-81.8 J/mol/K. A slightly lower value of 73 J/mol/K is obtained at the 1 mL scale which could be due to the fact that the temperature values plotted in the van't Hoff solubility curve for the 1 L scales correspond to the clear points obtained at a heating rate of 0.2 °C/min, whereas for the 1 mL scale correspond to the clear points obtained at a heating rate of 0.1 °C/min. The entropy of dissolution for MABA is predicted to be similar to PABA, due to the similar complexity of the molecules since the compounds are isomers. The entropy of dissolution obtained for PABA from this report is 80.2 J/mol/K (see Figure 7.9), which as expected is similar to the values obtained for MABA.

7.4 Robust MSZW region for the isomers of ABA

Controlling the crystallization process to follow a set profile within the MSZW is important to obtain quality crystals with the desired properties. This sub-section investigates the differences in MSZW values for the three isomers of ABA (*ortho*, *meta* and *para*) and uses the results obtained from sub section 7.2 to obtain a robust MSZW region for PABA and MABA. The robust MSZW region can be used to design a crystallization system at larger scale (pilot to manufacturing) increasing the likelihood of producing a quality product.

7.4.1 Variation in the MSZW between the three isomers of ABA

Cooling crystallization experiments were performed in a 1 L vessel using a 4-pitched blade turbine at a rotation speed of 255 rpm and ramp rate of 0.5 °C/min for the three isomers of ABA (*ortho*, *meta*, *para*). The FBRM probe was used to detect clear (all crystal dissolve) and cloud points (first detection of crystals) for a range of concentrations of the three isomers and the results are shown in Figure 7.15. Solubility data for PABA and MABA in water obtained from the literature can be found in Appendix D.

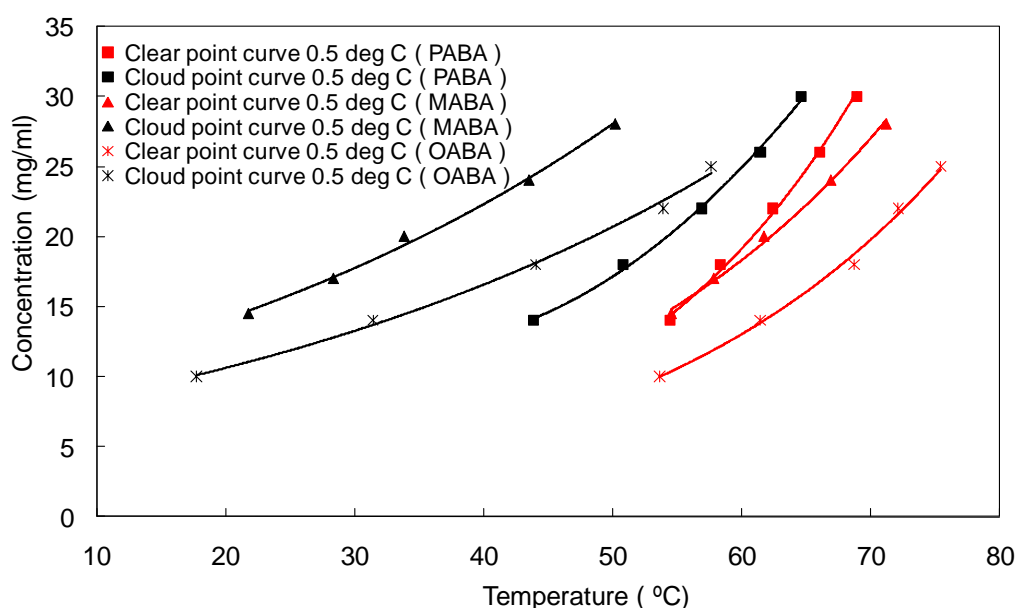


Figure 7.15. Clear and cloud point curves for the three isomers of ABA (*ortho*, *meta* and *para*) using a ramp rate of 0.5 °C/min and 1 L vessel (4-pitched blade turbine)

From the difference in the clear and cloud points in Figure 7.15 the MSZW is determined for each isomer of ABA and the results are given in Table 7.11.

Table 7.11. MSZW results for the three isomers (*ortho*, *meta*, *para*) of ABA

Isomer of ABA	Concentration (mg/mL)	MSZW (°C)
<i>ortho</i>	10	35.9
	14	30
	18	24.7
	22	18.2
	25	17.8
<i>meta</i>	14.5	32.8
	17	29.5
	20	27.9
	24	23.4
	28	21
<i>para</i>	14	10.6
	18	7.5
	22	5.5
	26	4.6
	30	4.3

The MSZW for each isomer of ABA increases in width as the concentration is lowered. The isomer *para*-ABA has a narrower MSZW ranging from 4.3-10.6 °C compared to the other two isomers *ortho* and *meta*-ABA, with MSZW values in the range 17.8-35.9. As the MSZW becomes narrower the crystallization process is more difficult to control. *ortho*- and *meta*-ABA isomers have similar MSZW ranges but *meta*-ABA has a slightly larger MSZW over the concentration range 10-28 mg/mL (see Table 7.11). The three isomers of ABA have significant differences in the clear and cloud point curves. *ortho*-ABA has the highest clear (solubility) points and *para*-ABA has the lowest temperature clear points over the concentration range 10-30 mg/mL. Based on the cloud point data for the three isomers *para*-ABA would be the first to nucleate from a mixed isomer solution and *meta*-ABA would be the final form of isomer to nucleate as the cloud points occur at the lowest temperature values as shown in Figure 7.15. The differences in the clear and cloud point curves of

any molecular compound with isomers would be important information for the design of experiments involving the separation of isomers via crystallization.

In the previous sub-section 7.2 the nucleation order, enthalpy and entropy of dissolution are obtained for the *meta*- and *para*-ABA isomers. A summary of these parameters for the three isomers are highlighted in Table 7.12.

Table 7.12. Summary of results for nucleation order, enthalpy/entropy of dissolution *para*- and *meta*-ABA

Isomer-ABA	Nucleation order	Enthalpy of dissolution (J/mol)	Entropy of dissolution (J/mol/K)
PABA	3.4-4.4	37.2	80.2
MABA (1 mL)	4.9-6.3	35.7	73
MABA (1 L) (3-blade glass retreat curve)	15.6-16.9	37.7	81.8
MABA (1 L) (4-pitched blade turbine)	3.9-5.7	38.9	80.2

7.4.2 Robust MSZW region for PABA and MABA

Determination of the robust MSZW region is important in the design of crystallization processes. The robust MSZW is defined as the distance between the thermodynamic solubility curve and the lower limit curve through the cloud points. Often in industry for new active ingredient (AI) compounds the thermodynamic solubility curve is unknown. So an alternative way that will be used in this research to define the robust MSZW is the distance between the lower limit curve through the cloud points and upper limit curve through the clear points (free point zone). This method is a quick way of obtaining a robust MSZW when the thermodynamic solubility curve is unknown and with the high demands in the pharmaceutical industry this will help them achieve their targets of project timelines. Considering all the parameters mentioned in section 7.2, including ramp rate, scale, agitator speed and type, a robust MSZW region is obtained for PABA and MABA and the results are shown in Figures 7.16 and 7.17.

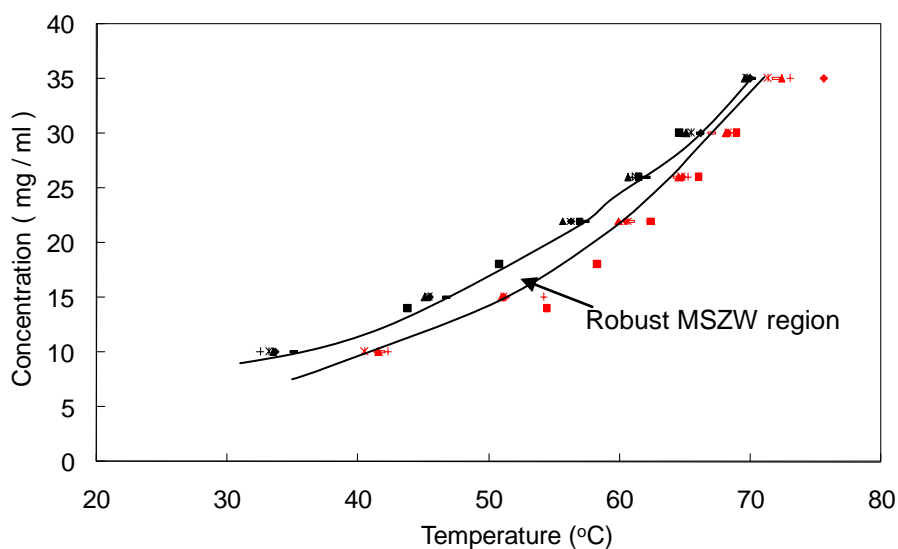


Figure 7.16. Robust MSZW region for PABA in water at the 1 L scale with variations in clear and cloud point curves for different ramp rates, agitator types and agitator speeds

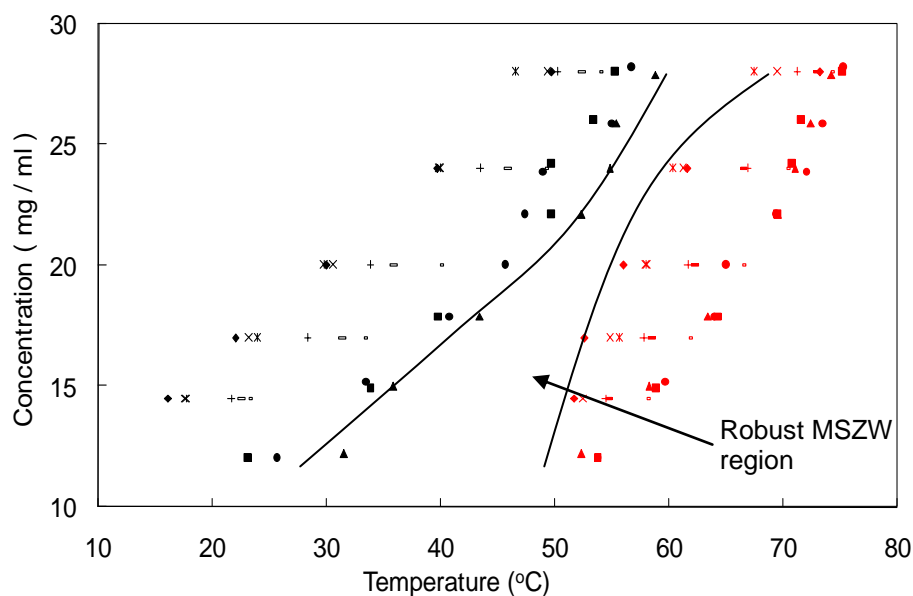


Figure 7.17. Robust MSZW region for MABA in water with variations in clear and cloud point curves for different ramp rates, agitator types and scale of vessel

Figure 7.16 shows a robust MSZW region for the model system PABA in water. This region is obtained by the limits of the clear (all crystals dissolve) and cloud (first appearance of crystals) curves as represented by the red and black points respectively. The robust MSZW region takes into consideration variations in process parameters including cooling rate (0.5, 0.3 and 0.1 °C/min), agitator speed (250, 300 and 400 rpm) and agitator type (3-blade glass treat curve and 4-pitched blade turbine). The general MSZW for PABA in water is narrow resulting in a narrow robust MSZW region ranging from 0.9-5.4 °C. This robust MSZW region provides the experimental conditions for seeding and the degree of supersaturation required to control the crystallization process at large scale so as to produce crystals with the desired properties. However this robust MSZW region does not apply at the 1 mL scale due to overlaps of the clear and cloud point curves as a result of a narrow MSZW.

Figure 7.17 shows the robust MSZW region for MABA in water. This robust MSZW takes into consideration variations in cooling rate (0.5, 0.3, 0.2 and 0.1 °C/min), agitator type (3-blade glass retreat curve and 4-pitched blade turbine) and scale (1 mL and 1 L). The robust MSZW region varies in width from 5.5-20.8 °C which provides a suitable candidate for a model system involving the design of larger scale crystallization experiments in which a supersaturation profile is followed within the robust MSZW region for obtaining quality crystals.

These results indicate that for compounds with broader MSZW, such as MABA, it is possible to determine the robust MSZW by performing automated MSZW experiments under various operating conditions (e.g. heating/cooling rates, agitator speed, agitator type, etc) and at different scales (e.g. 1 mL and 1 L). The robust MSZW identified can then be extrapolated for larger scale operations. However if the compound has a narrow MSZW (such as in the case of PABA) this approach may not be applicable, due to the overlapping boundaries of the MSZW's determined under various conditions.

7.5 Conclusions

Cooling crystallization experiments were performed with the use of the turbidity and FBRM probes to investigate the effect of ramp rate, scale, agitator type and speed on the clear and cloud point curves and hence MSZW for isomers of ABA. Larger MSZW values were observed for the 1 L scale compared to the 1 mL scale for PABA and MABA in water. These results have significant practical relevance as they indicate that at larger scale the MSZW can be broader, hence the laboratory scale design of crystallization condition can be conservative enough to provide consistent product properties at the larger scale. Also these results highlight the careful usage of the Crystal 16 data (1 mL scale) for the design of larger scale (pilot and industrial) experiments as there is a large variation in the MSZW at the 1 mL and 1 L scale. Clear and cloud point curves occur at higher temperatures for the 1 mL scale indicating enhanced mixing, which could be due to the small vessel size and magnetic flea increasing the frequency of collisions between the solute molecules.

Changes in agitator types (including the 3-blade glass retreat curve and 4-pitched blade turbine) did not have significant effect on the MSZW values, but clear and cloud point curves occurred at higher temperatures when using the 4-pitched blade turbine. Agitator speeds within the range 250-400 rpm showed no significant effect on the clear and cloud point curves and hence the MSZW, for the 3-blade glass retreat curve at the 1 L scale. Optical microscope images showed that the quality of crystals is not affected within the studied agitator speed range of 250-400 rpm.

Nucleation orders, MSZW, enthalpy and entropy of dissolution values were obtained from results of cooling crystallization experiments at different ramp (cooling/heating) rates for model system *meta*- and *para*-ABA in water. MSZW values were found to increase with the cooling rate for PABA in water. Enthalpy and entropy of dissolution values are similar for PABA and MABA isomers. Nucleation orders were found to vary for the model system MABA within different crystallization set-ups involving different size vessels and mixing conditions, highlighting that crystallization models containing nucleation parameters are only valid for a specific crystallization set-up. Therefore model based design and scale-up of crystallization processes must be used carefully and more detailed mechanistic models, which take into consideration the

effect of mixing need to be designed to improve the generality and applicability of crystallization models.

MSZW values for the three isomers (*ortho*, *meta* and *para*) of ABA are obtained at the 1 L scale, which showed that PABA has a narrow MSZW while MABA and OABA have wide MSZWs. A robust MSZW region, which takes into consideration variation in operating conditions (ramp rate, agitator speed and impeller type) and different scales (1 mL and 1 L), is obtained for MABA. However this robust MSZW does not apply for PABA at the 1 mL scale due to an overlap of clear and cloud point curves. This research shows that a robust MSZW can be obtained for compounds with broad MSZWs, which can then be extrapolated for the design of larger scale operations increasing the likelihood of producing a quality product.

Chapter 8. Crystallization and characterisation of salts of o, m, p-amino benzoic acid isomers

8.1 Introduction

Crystallization of salts is a method used to change the structure of pharmaceutical products resulting in drugs with enhanced physicochemical properties (Reutzel-Edens *et al.*, 2003, Forbes *et al.*, 1992, Haynes *et al.*, 2005, Jones *et al.*, 2005, Stephenson and Diserod, 2000). Salt formation is used to overcome problems with solubility, dissolution rate, stability and hygroscopicity (Forbes *et al.*, 1992, Haynes *et al.*, 2005). Reports state that 50% of pharmaceutical drug products are crystallized as salts (Kumar *et al.*, 2009). A common morphology of crystals is needles, which results in problems in downstream processing such as long filtration times due to blockage of filter. To overcome this problem often compounds are crystallized as salts producing large crystals with a well defined shape. There are a number of variables that can affect whether a salt nucleates from solution and the type of salt including solvent, pH of solution and acid/base used to achieve the desired pH (Towler *et al.*, 2004, Jones *et al.*, 2005).

Many active pharmaceutical ingredients are organic compounds containing both amino and carboxyl groups (e.g. amino acids) as is the case of the model system PABA and MABA. Due to the presence of these groups within the molecule four forms of the compound are known to exist. These forms consist of the neutral form (no charge), zwitterion which contains both negative charge on the (COO⁻) group and positive charge on the (NH₃⁺) group, single positive charge (-NH₃⁺) and single negative charge (COO⁻). Figure 8.1 shows the four different forms of PABA and the equilibrium between each form.

Variations in pH and temperature will alter the solubility of the compound and the percentage ionisation of the different species in solution. Figure 8.2 (a) shows the solubility curves for pH range 1-11 for the model system of PABA in ethanol solution. These curves were obtained using the equations (8.1) and (8.2). The isoelectric point of PABA is 3.6 and the pKa values are 2.5 and 4.8 (Seok *et al.*, 1995).

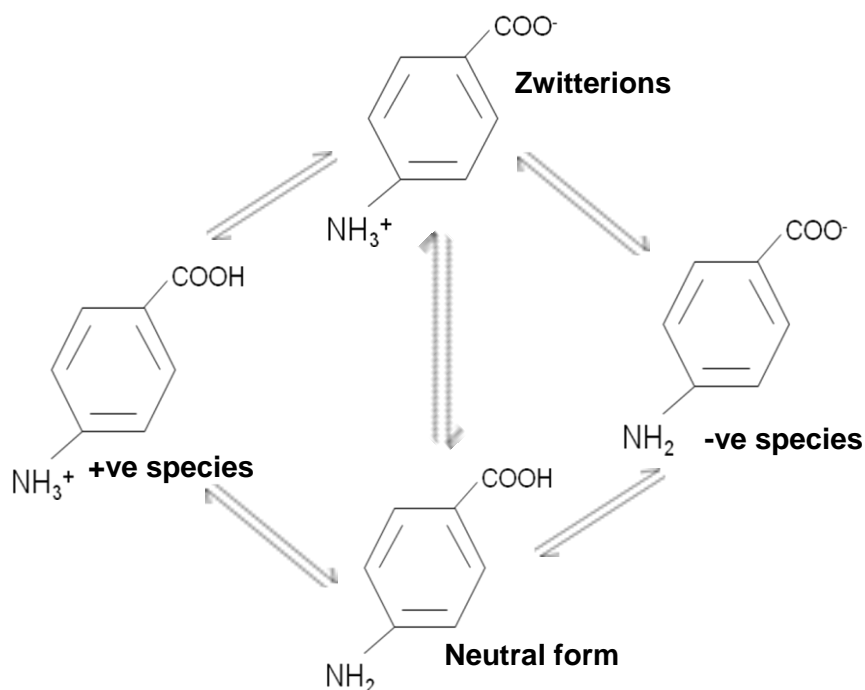


Figure 8.1. Four different forms of PABA and the equilibrium between each form

For the neutral form of the compound the solubility has a minimum at pH within the range 3 to 6. At low pH (acidic conditions) and high pH greater than 8, there is a large increase in solubility. Figure 8.2 (b), shows how changing the pH affects the percentage ionisation of the different species in solution. At pH values below 3 the (NH_3^+) species is 100% ionising, pH in the range 3-6 the neutral form of the compound is most likely to nucleate from solution and at high pH the (COO^-) species has 100% ionisation. This confirms that at low pH the acidic salt is likely to form and at high pH the basic salt is likely to form when an acid or alkali is added to the solution. The relationship between the solubility and pH can be expressed as:

$$pH - pKa = \log\left(\frac{S_o}{S_L - S_o}\right), \quad (8.1)$$

where S_o is the intrinsic solubility at specific temperature and S_L is the calculated solubility at specific pH and temperature (Florence and Attwood, 1981); and

$$pH - pKa = \log\left(\frac{S_L - S_o}{S_o}\right). \quad (8.2)$$

Equation (8.1) applies for pH values below the iso-electric point and equation (8.2) applies for pH values above the iso-electric point (Florence and Attwood, 1981). A derivation of Equations (8.1) and (8.2) can be found in Appendix G.

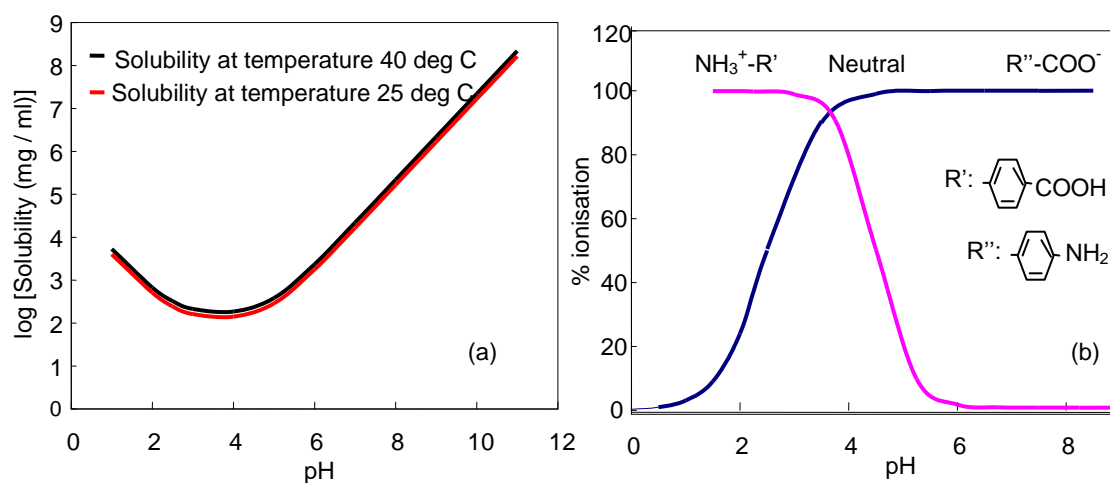


Figure 8.2. Change in pH with (a) solubility and temperature for PABA in ethanol and (b) % ionisation of certain species of PABA

This study focuses on combining PAT tools with SSA techniques to crystallize and characterise a range of acidic and basic salts. The strength of acid used is varied to determine whether this affects salt formation. Crystallization methods include cooling, precipitation and evaporation. An organic solvent (ethanol) is used in all experiments. To crystallize acidic salts a low pH of the solution (below 3.3) is required and to crystallize basic salts the pH of the solution should be above 8. The acids used to achieve a low pH in solution include hydrochloric acid (HCl), hydrobromic acid (HBr), sulphuric acid (H₂SO₄) and phosphoric acid (H₃PO₄). The bases used to achieve a high pH in solution include sodium hydroxide (NaOH) and potassium hydroxide (KOH). The novelty of this research is the use of a combination of four PAT tools, including FBRM, PVM, pH and temperature probe, in a single vessel to monitor the cooling crystallization process and a range of SSA techniques to characterise a combination of acidic and basic salts. Simulated XRPD patterns of salts

are produced using the software package Mercury (version 2.2; Macrae *et al.*, 2008). The predicted morphology of salt crystals is obtained by Bravais, Friedel, Donnay and Harker (BFDH) crystal morphologies method using the software package Mercury (version 2.2; Macrae *et al.*, 2008). This method predicts the crystals morphology assuming crystal growth occurs within a vacuum and therefore it does not take into account any bonding interactions between solvent molecules or impurities with the crystal surfaces. The model system used in this study is *meta*-amino benzoic acid (MABA) and *para*-amino benzoic acid (PABA). Salts of MABA and PABA are characterised using SSA techniques providing information on properties on the crystals that have not yet been reported in the literature.

8.2 Experiments performed

Cooling, precipitation and evaporation experiments were performed using a range of acids and bases as mentioned in section 3.2 of Chapter 3, to produce salts of the model systems. Vessel size used for the cooling crystallization experiment is 750 mL. The PAT tools used to monitor the crystallization process and a detailed methodology of the all experiments is within section 3.4.4 and 3.6 of Chapter 3. A schematic set-up of the crystallization rig for the cooling crystallization experiments is similar to the one shown in Figure 3.3 but does not include the ATR-UV/Vis probe. The range of SSA techniques used and the operating conditions for each technique is described in section 3.7 of Chapter 3.

8.3 Acidic salts of PABA and MABA by cooling crystallization

8.3.1 Introduction

Compounds are often crystallized as salts to overcome problems with solubility and stability. The most common method used to crystallize the salts is cooling crystallization as it is a simple and slow process that allows growth of the crystals resulting in large crystals, which is a desirable characteristic. To produce acidic salts the pH of solution must be below 3. The acids used include hydrochloric acid and

hydrobromic acid. These acids are classified as strong acids resulting in 100% ionisation in solution and are therefore likely to produce the salt when mixed with the compound. These acids are the top two acids in salt formation with compounds (Haynes *et al.*, 2005).

8.3.2 Solid state characterisation of the hydrochloric salt of MABA

Cooling crystallization experiments were performed for MABA in ethanol by using a 3M solution of hydrochloric acid to crystallize the salt under very acidic conditions of pH=2.5. FBRM results for the cooling crystallization experiment are shown in Figure 8.3. A single nucleation event is detected by a sudden increase in FBRM counts followed by a gradual increase in counts indicating additional nucleation.

A range of solid state analytical techniques were used to characterise the crystalline product. Optical and scanning electron microscope images of MABA re-crystallized from ethanol at pH=2.5 using HCl acid are shown in Figure 8.4. Images show rectangular rod shape crystals which are different to the two polymorphic forms of MABA of needle morphology (Svard *et al.*, 2010). Differences in the morphology provide evidence that the hydrochloric salt of MABA forms when re-crystallized from ethanol under very acidic conditions (pH=2.5). The crystals are fine particles, which are yellow in colour with a sparking tint as shown in Figure B1 of appendix B.

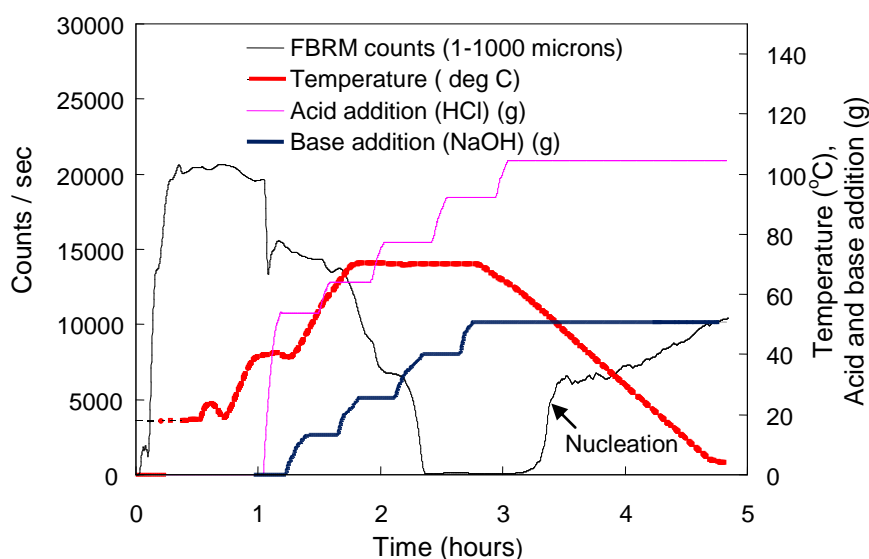


Figure 8.3. FBRM results for the cooling crystallization of MABA from ethanol at pH=2.5 using HCl acid

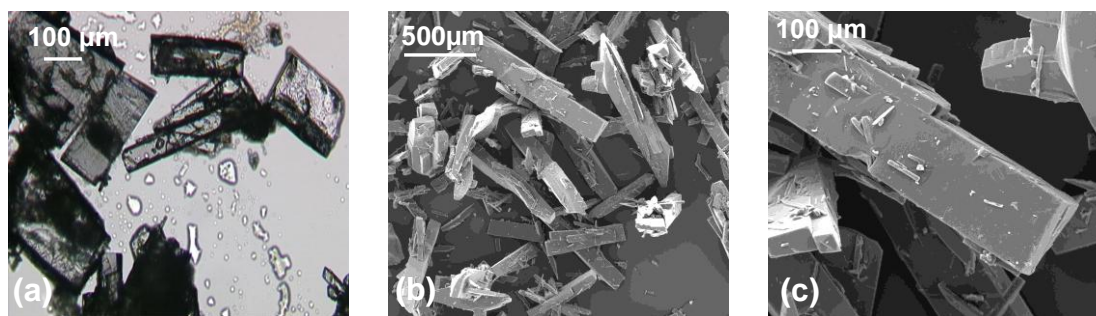


Figure 8.4(a) Optical microscope and (b, c) scanning electron microscope images of MABA re-crystallized from ethanol at pH=2.5 using HCl

Further solid state analysis involving the use of XRPD, DSC and solid state IR spectroscopy are used to characterise the crystals. XRPD patterns for the sample re-crystallized from ethanol at pH=2.5 using HCl acid and the raw material form of MABA are shown in Figure 8.5. XRPD patterns for the two samples are completely different indicating the presence of the hydrochloric (HCl) salt of MABA.

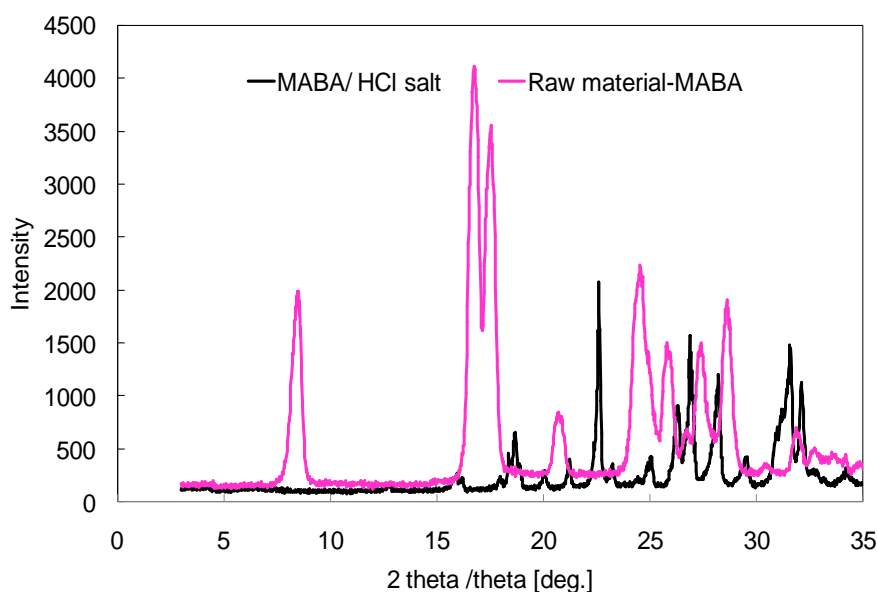


Figure 8.5. XRPD pattern for raw material form of MABA and MABA re-crystallized from ethanol at pH=2.5 using HCl acid

There is only one form of the chloride salt of MABA known to exist which is anhydrous (Cambridge Structural Database (Version 5.30; Allen, 2002) refcode MAMBZA (Arora and Sundaralingam,1973)). The simulated XRPD pattern of the anhydrous chloride salt of MABA and the crystals produced experimentally are

shown in Figure 8.6. These patterns are very similar indicating that the salt crystals produced experimentally are indeed the anhydrous form.

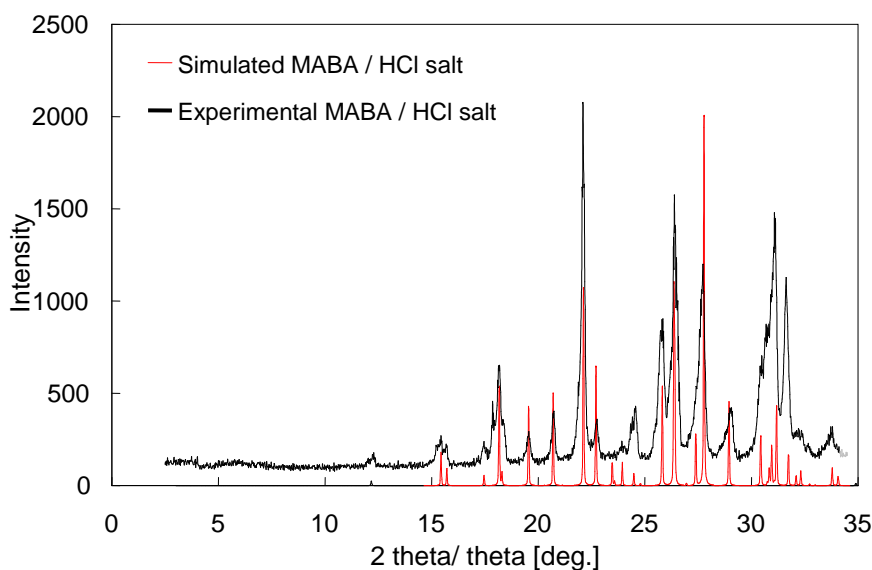


Figure 8.6. Simulated and experimental XRPD patterns for the chloride salt of MABA

The unit cell dimensions of the chloride MABA salt crystals reported by Arora and Sundaralingam (1973) can also be used to predict the morphology of the crystals. The predicted morphology of the chloride salt of MABA is rod shaped as shown in Figure 8.7. The crystals produced experimentally from ethanol as shown in Figure 8.4 are a similar morphology to the prediction but are much longer indicating that solvent interacts with certain crystal faces preventing growth in one direction.

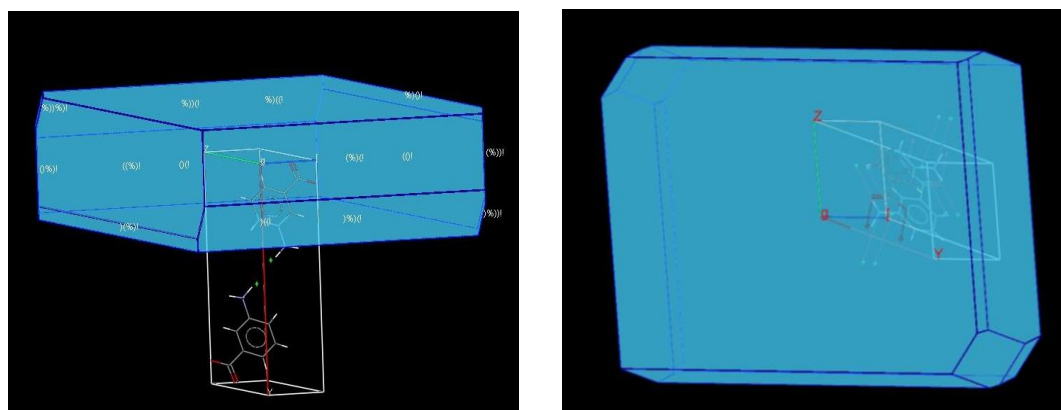


Figure 8.7. Predicted morphology of the chloride salt of MABA using the BFDH method

The DSC result for a sample of MABA re-crystallized from ethanol at pH=2.5 using hydrochloric acid is shown in Figure 8.8. A sharp peak appears at a temperature of 291 °C which is the melting point of hydrochloride salt of MABA. A single peak indicates the formation of the pure salt.

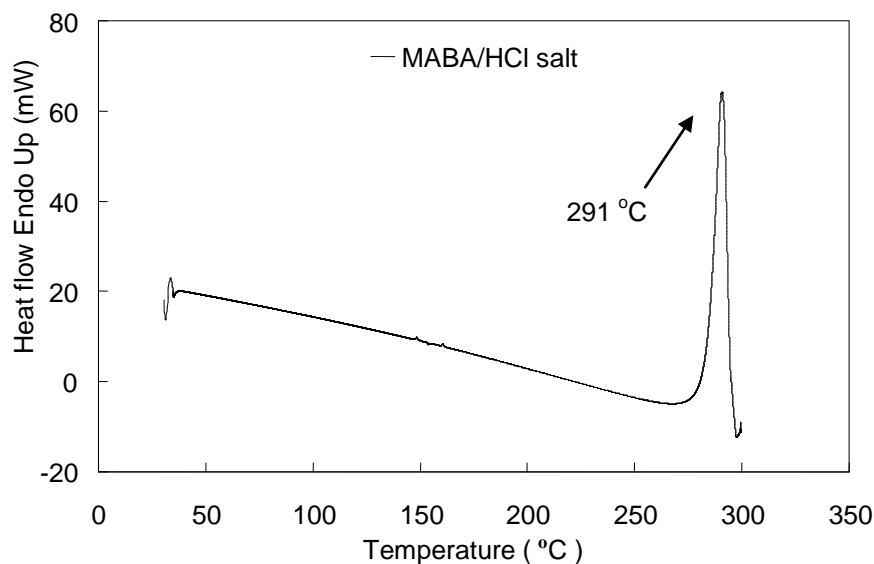


Figure 8.8. DSC plot of the hydrochloride salt of MABA

IR spectrum for a sample of the hydrochloride salt of MABA and the raw material form of MABA are shown in Figure 8.9. There are many differences in the IR spectrums of the two forms. Two significant peaks at wavenumbers of 2548 and 2804 cm^{-1} appear in the IR spectrum for the hydrochloric salt of MABA and a peak at wavenumber 2950 cm^{-1} appears in the spectrum for the raw material form of MABA. These peaks are due to the stretching of (O-H) bonds within the molecules. Wavenumbers in the range 1580-1650 cm^{-1} are due to the bending of the (N-H) bonds. As the HCl salt of MABA forms an ionic compound with a positive charge on the amine (NH_3^+) group this affects the (N-H) bending resulting in variations in the peak pattern of this wavelength range. In-plane bending of the (C-O-H) bond appears at wavenumber 400 cm^{-1} and for out-of-plane bending of the (C-O-H) bond a peak appears at wavenumber 900 cm^{-1} . There is a slight shift in both the in-plane and out-of-plane bending of these bonds for both the HCl salt of MABA and the raw material form as shown in Figure 8.9.

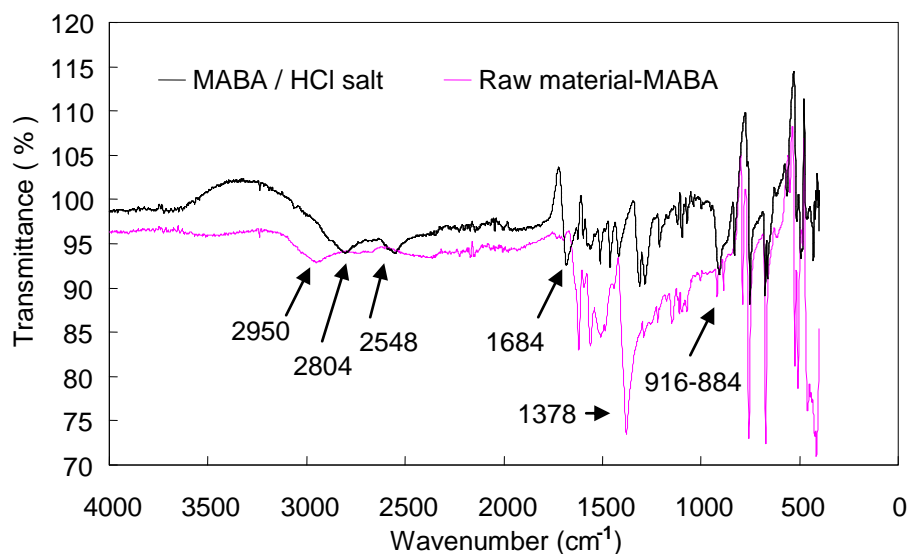


Figure 8.9. IR spectrum for the hydrochloric (HCl) salt of MABA and the raw material form of MABA

Combining PAT tools with SSA techniques provided the experimental conditions required to produce the hydrochloride salt of MABA. This salt forms when using an organic solvent (ethanol) and at very low pH conditions of 2.5 (highly acidic). A combination of solid state analytical techniques were used to characterise the crystal product showing that the hydrochloride salt of MABA forms large rectangular rod shape crystals of size greater than 500 μm with a melting point of 291 $^{\circ}\text{C}$. Simulated and experimental XRPD patterns confirmed that the salts produced experimentally are the same anhydrous form as those reported in the Cambridge Structural Database. BFDH predicted morphologies confirmed that solvent interacts with the surface affecting the final morphology of the salt crystals.

8.3.3 Solid state characterisation of the hydrobromic salt of MABA

The cooling crystallization experiment is performed using hydrobromic acid (HBr) to crystallise the HBr salt of MABA under low pH conditions of 1.5. FBRM results for the cooling crystallization experiments are shown in Figure 8.10. A single nucleation event is detected by a sudden increase in FBRM counts.

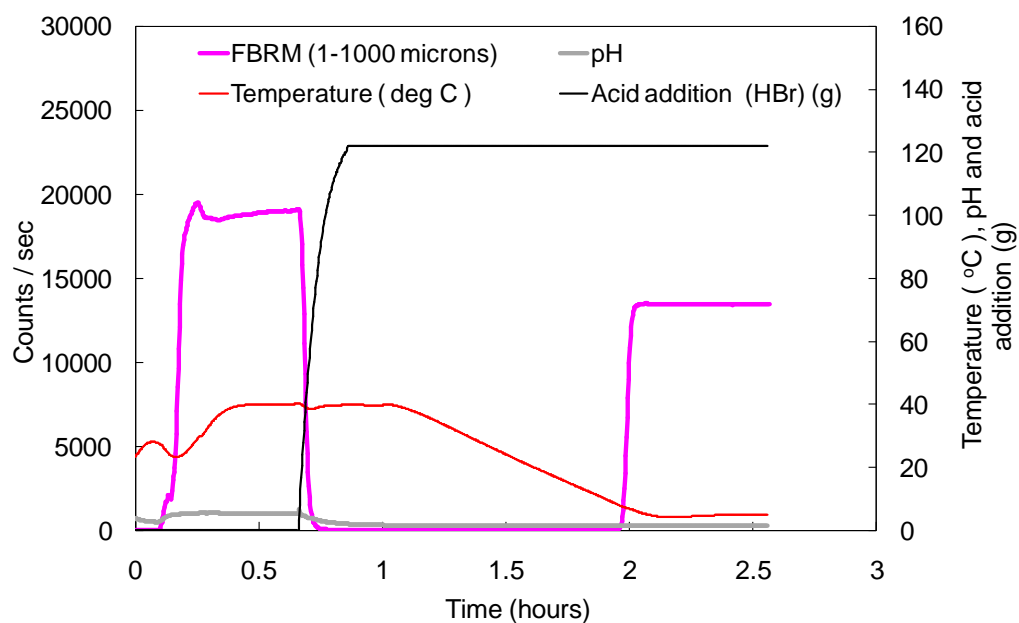


Figure 8.10. FBRM results for the cooling crystallization of MABA from ethanol at pH=1.5 using HBr acid

Once nucleation occurred solid samples were filtered and dried. Solid state analyses of the crystals were carried out using a range of SSA techniques. Optical microscope image of the crystal samples are shown in Figure 8.11. The morphology of the crystals is diamond shaped of size greater than 50 μm . The morphology of the crystals are different to the raw material form of MABA which consists of needles indicating the possible formation of the HBr salt of MABA.

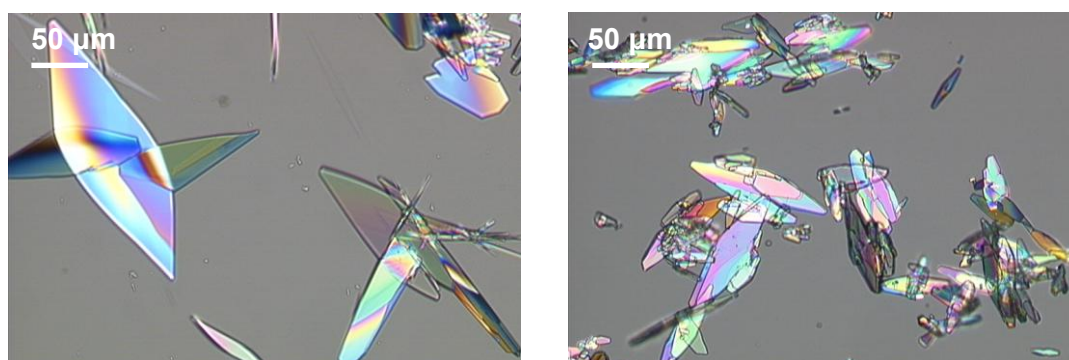


Figure 8.11. Optical microscope images of MABA re-crystallized from ethanol at pH=1.5 using HBr acid

XRPD patterns for the crystal sample of MABA re-crystallized from ethanol at pH=1.5 using HBr acid and the raw material form of MABA are shown in Figure 8.12. The patterns of the two samples are significantly different providing evidence of the formation of the hydrobromic (HBr) salt of MABA from ethanol at pH=1.5 using HBr acid.

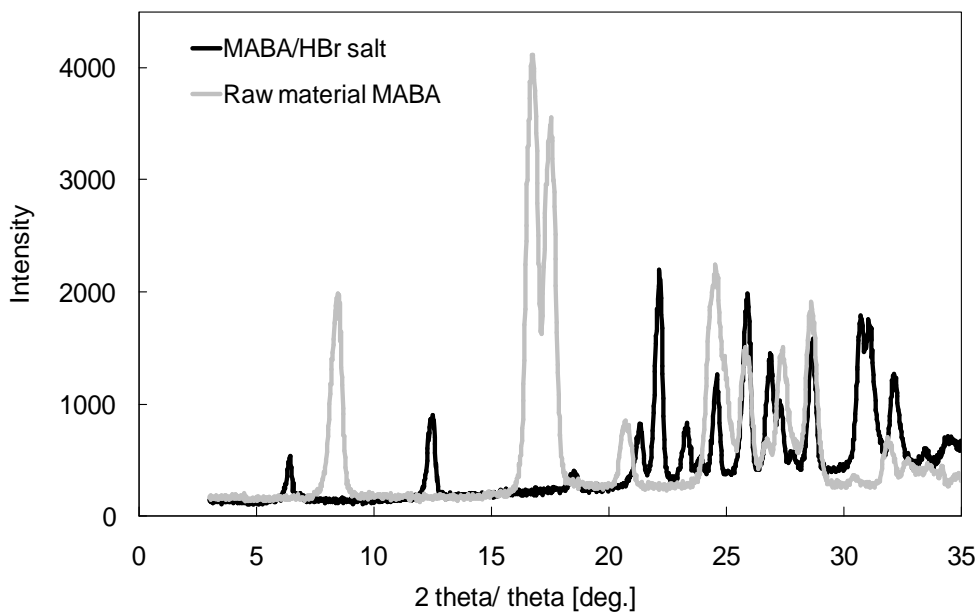


Figure 8.12. XRPD pattern for the raw material form of MABA and MABA re-crystallized from ethanol at pH=1.5 using HBr acid

There is only one form of the bromide salt of MABA known to exist which is anhydrous (Cambridge Structural Database (Version 5.30; Allen, 2002) refcode DIWLIF (Cinci and Kaitner, 2008b)). The simulated XRPD pattern of the anhydrous bromide salt of MABA and the crystals produced experimentally are shown in Figure 8.13. These patterns are very similar indicating that the salt crystals produced experimentally are anhydrous.

The unit cell dimensions of the bromide MABA salt crystals reported by Cinci and Kaitner (2008b) can be used to predict the morphology of the crystals. The predicted morphology of the bromide salt of MABA is rectangular plate like shaped crystals, as shown in Figure 8.14, which is different to the crystals produced experimentally from ethanol, as shown in Figure 8.11, with diamond morphology. The difference in morphology indicates that solvent interacts with certain crystal faces forming bonds and preventing growth.

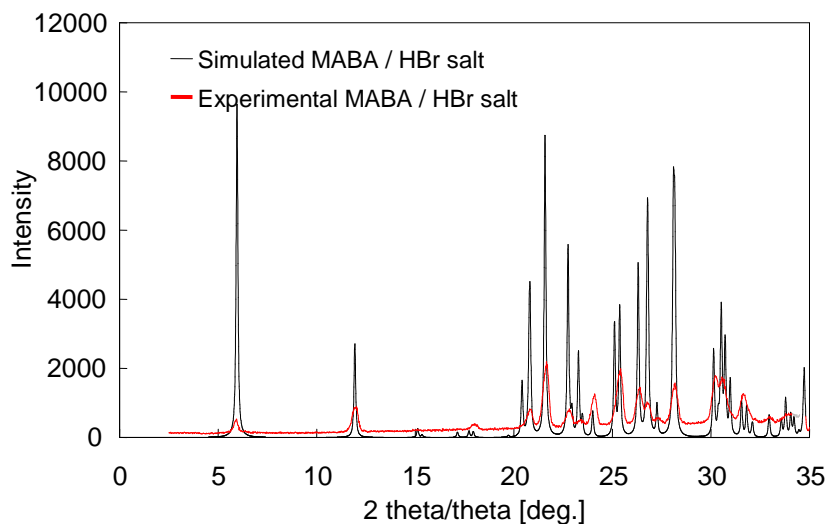


Figure 8.13. Simulated and experimental XRPD patterns for the bromide salt of MABA

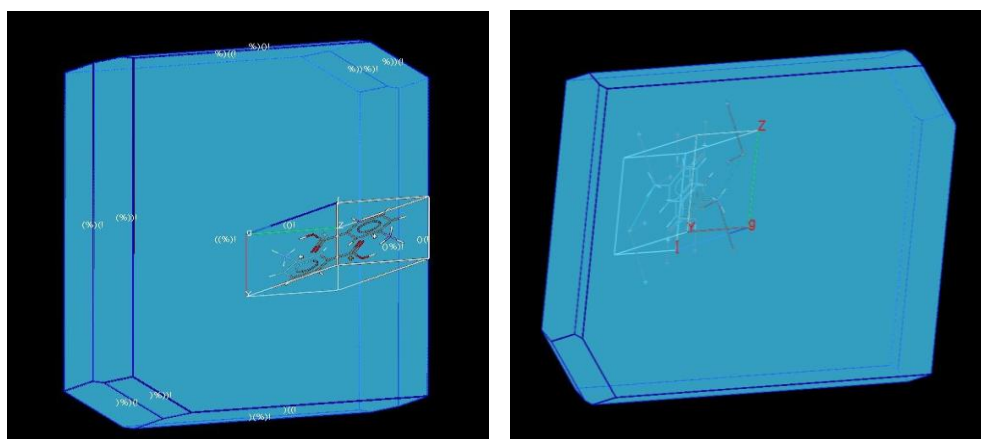


Figure 8.14. Predicted morphology of the bromide salt of MABA using the BFDH method

DSC results for crystals which nucleated from ethanol solution at pH=1.5 using HBr acid are shown in Figure 8.15. A single sharp peak appears at a temperature of 301°C which is the melting point of the HBr salt of MABA. No other peaks appear in the DSC results indicating a pure form of the salt.

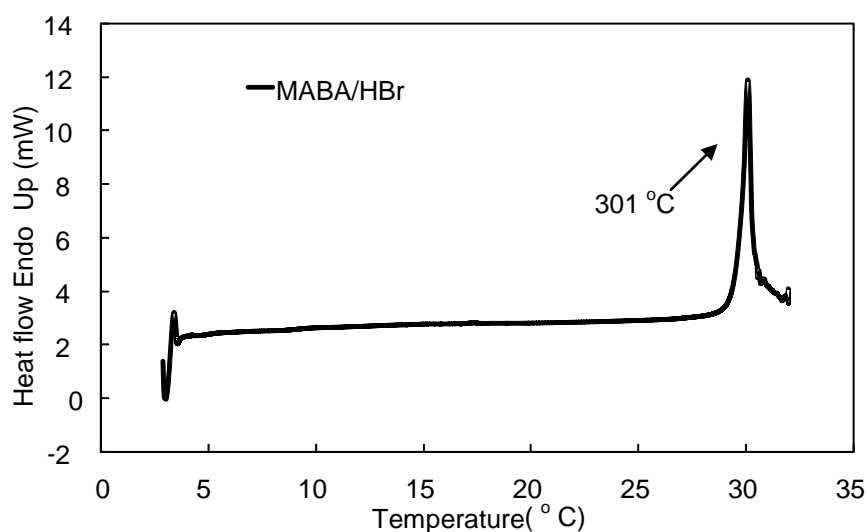


Figure 8.15. DSC results for the hydrobromic (HBr) salt of MABA

IR spectrum for HBr salt of MABA and the raw material form of MABA is shown in Figure 8.16. Two broad peaks at wavenumbers of 2536 and 2824 cm^{-1} appear in the IR pattern of the salt but not for the raw material form of MABA. These peaks are due to the stretching of the (O-H) group in the molecule. The presence of charges on the ionic HBr salt of MABA and the addition of a hydrogen bond attached to the nitrogen atom in the molecule may affect the intermolecular hydrogen bonding between the molecules resulting in variations in the stretching of the (O-H) group. An additional peak appears in the IR pattern for the salt at 1674 cm^{-1} which is due to the stretching of the carbonyl (C=O) group. The fingerprint region for the two forms are different showing three sharp peaks at wavenumbers in the range 1400-1500 cm^{-1} for the salt which does not appear in the IR pattern of the raw material providing evidence of different forms of the compound. A sharp peak at 900 cm^{-1} appears in the IR pattern of the salt, which is due to the out-of-plane bending of the (C-O-H) bond. The bending vibrations of this bond are altered in the raw material form of MABA which shows two peaks at wavenumbers of 885 and 918 cm^{-1} . The clear differences between two the IR patterns provides supporting evidence that the HBr salt of MABA recrystallizes from ethanol at low pH conditions of 1.5.

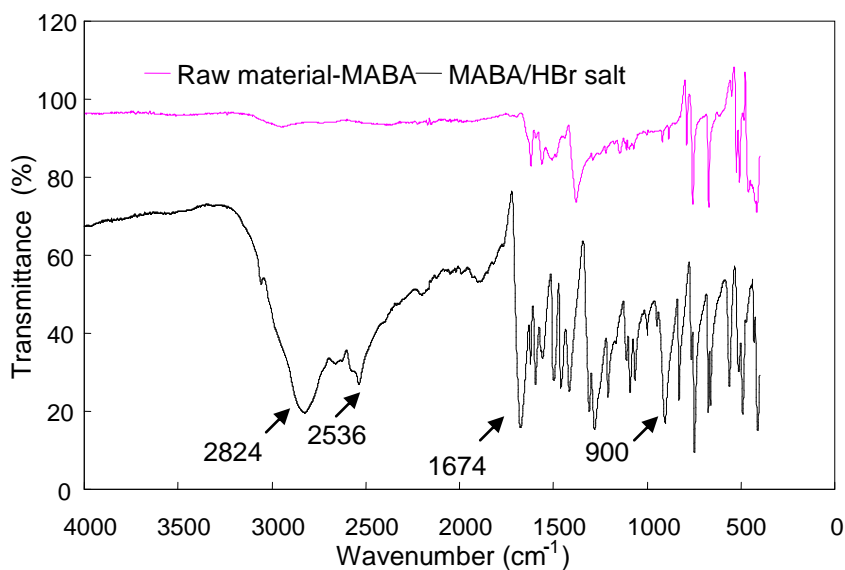


Figure 8.16. IR spectrum for hydrobromic (HBr) salt of MABA and the raw material form of MABA

DVS analysis is a useful technique for studying whether compounds are hygroscopic in nature and the tendency of compounds to form hydrates. DVS results for the hydrobromic salt of MABA are shown in Figure 8.17. As the relative humidity is increased from 40 to 90% there is a small increase in mass of 0.2% which suggests that the salt is not hygroscopic in nature. A similar behaviour occurs during the desorption cycle and the process is repeated during cycle 2, indicating that the salt is a highly crystalline solid (Hilfiker, 2006) There are no large step changes in mass or small and gradual changes in mass indicating that the salt does not have a tendency to form hydrates.

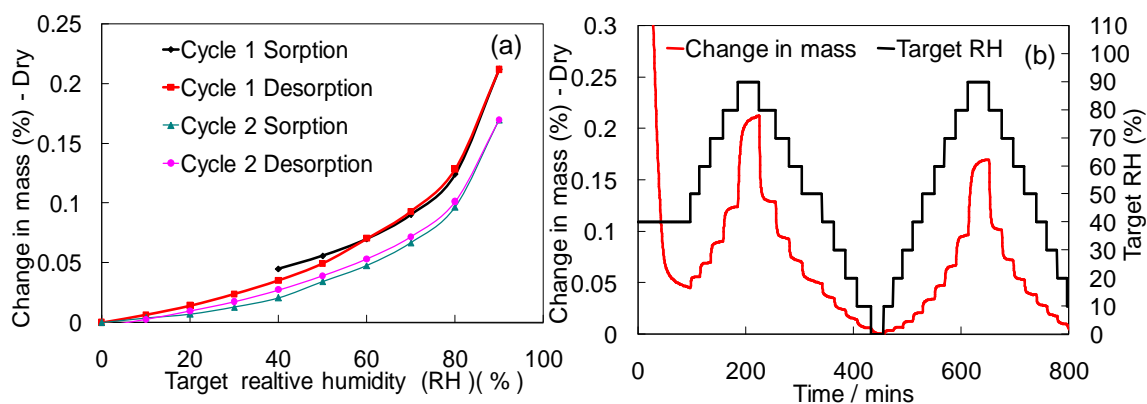


Figure 8.17. DVS results for the hydrobromic salt of MABA showing (a) isothermal plot and (b) change in mass (Dry) plot

Combining PAT tools with SSA techniques provides the experimental conditions required to produce the hydrobromic salt of MABA. This salt forms when using an organic solvent (ethanol) and at very low pH conditions of 1.5 (highly acidic). A combination of solid state analytical techniques were used to characterise the crystal product showing that the hydrobromic salt of MABA forms large diamond shape crystals and the melting point of the salt is 291 °C. Simulated and experimental XRPD patterns confirmed that the crystal produced experimentally are anhydrous. BFDH predicted morphologies confirmed that the solvent (ethanol) interacts with the crystal surface affecting the final morphology. IR analysis showed that the salt affects the stretching and bending vibration of bonds within the molecule. DVS results provided evidence that the hydrobromic salt of MABA is a highly crystalline solid that does not have a tendency to form hydrates.

8.3.4 Solid state characterisation of the hydrobromic salt of PABA

Cooling crystallization of PABA from an ethanol solution is performed using hydrobromic acid to achieve a solution of pH=1. FBRM results for the cooling crystallization experiment are shown in Figure 8.18. A single nucleation event is detected as shown by a sharp increase in FBRM counts.

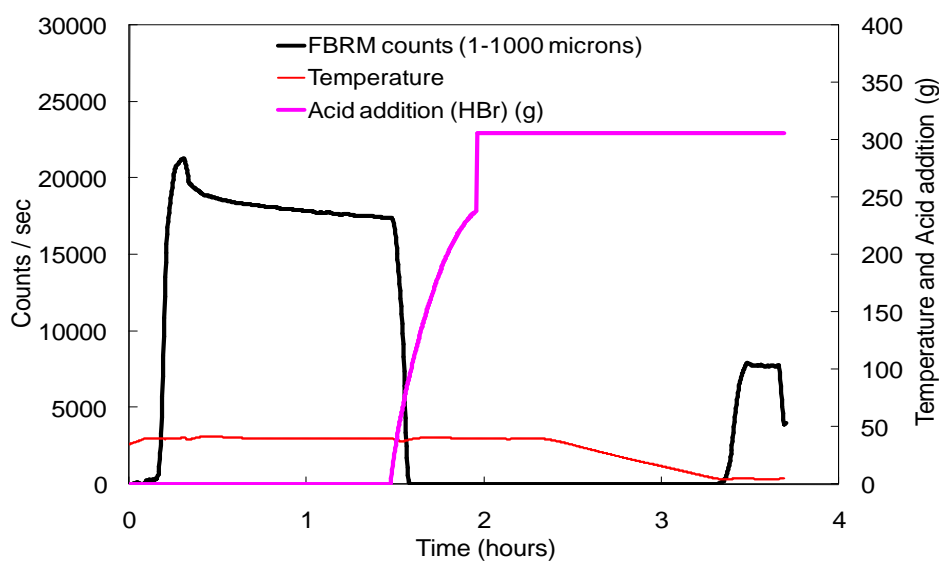


Figure 8.18. FBRM results for the cooling crystallization of PABA from ethanol at pH=1 using HBr acid

Solid samples were removed from the process stream after nucleation and crystals are characterised using a range of solid state analytical techniques. Optical microscope, scanning electron microscope and PVM images of the crystals are shown in Figure 8.19. Crystals appear as rod shape with longest dimension of size greater than 100 μm and a hexagonal face. The crystals are fine particles, which are white in colour with a sparkling tint as shown in Figure B1 of appendix B. Further solid state analysis is required to identify the crystal form.

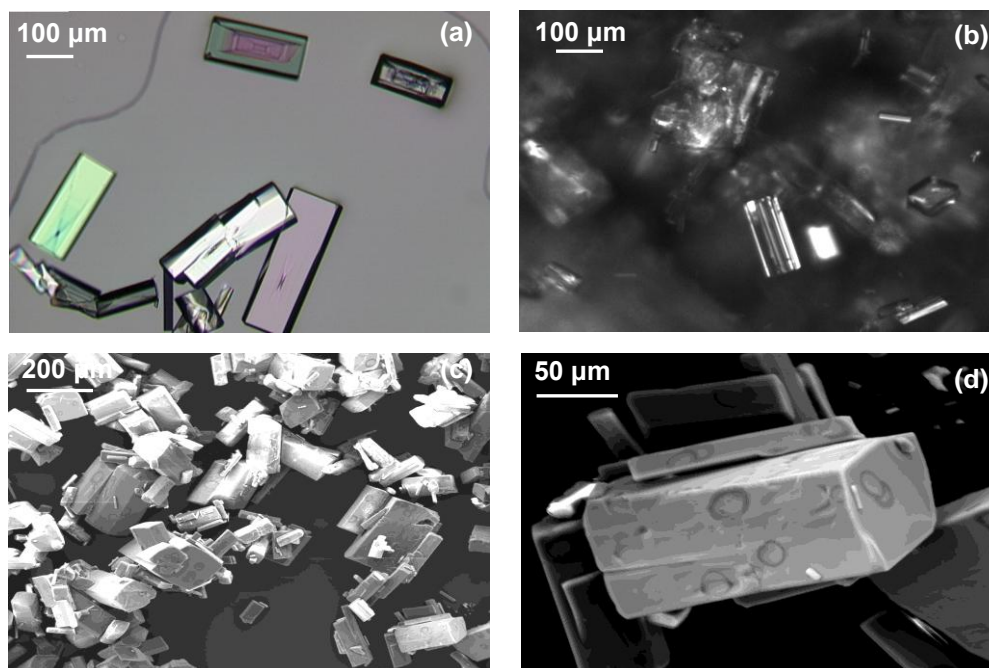


Figure 8.19. PABA re-crystallized from ethanol using the (a) optical microscope, (b) PVM image during nucleation, (c and d) SEM images

XRPD patterns for the sample re-crystallized from ethanol at pH=1 using hydrobromic acid and the raw material form of PABA are shown in Figure 8.20. The XRPD pattern for the raw material shows additional peaks at angles of 9, 14 and 15. The clear differences between the two patterns provide evidence of the formation of the hydrobromic salt of PABA.

There is only one form of the bromide salt of PABA known to exist which is anhydrous (Cambridge Structural Database (Version 5.30; Allen, 2002) refcode WIZLOH (Cincic and Kaitner, 2008a)). The simulated XRPD pattern of the anhydrous bromide salt of MABA and the crystals produced experimental are shown

in Figure 8.21. These patterns are very similar indicating that the salt crystals produced experimentally are the anhydrous form.

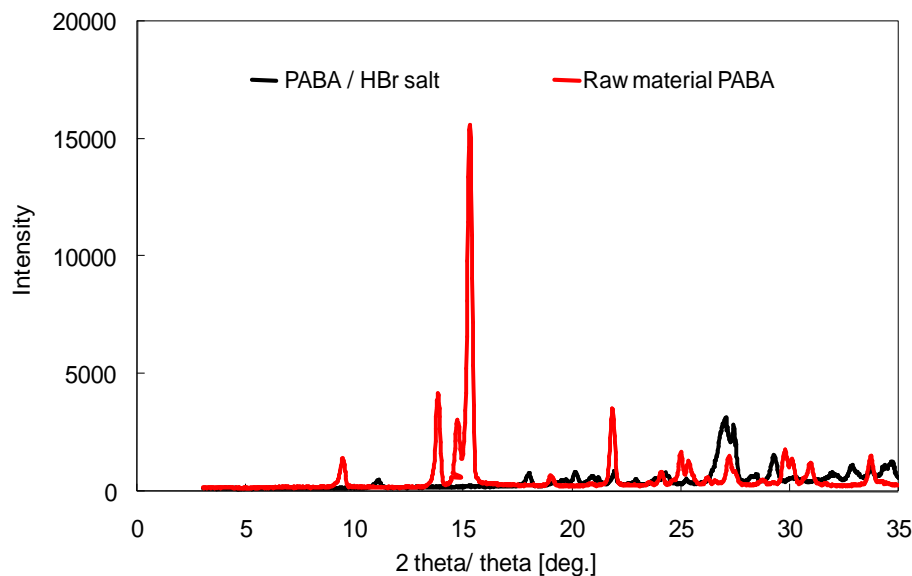


Figure 8.20. XRPD pattern for raw material form of PABA (alpha) and PABA re-crystallized from ethanol at pH=1 using HBr acid

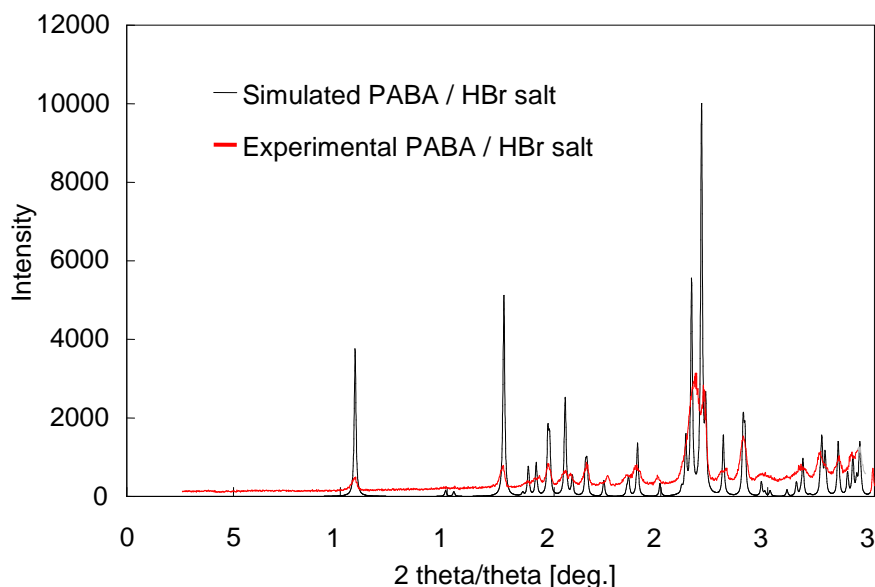


Figure 8.21. Simulated and experimental XRPD patterns for the bromide salt of PABA

The unit cell dimensions of the bromide PABA salt crystals reported by Cinci and Kaitner (2008a) can be used to predict the morphology of the crystals. The predicted morphology of the bromide salt of PABA is rod shape crystals with a hexagonal face as shown in Figure 8.22. The predicted morphology is similar to the salts produced

experimental as shown in Figure 8.19, indicating that the solvent (ethanol) does not interfere with the growth of the individual crystal faces.

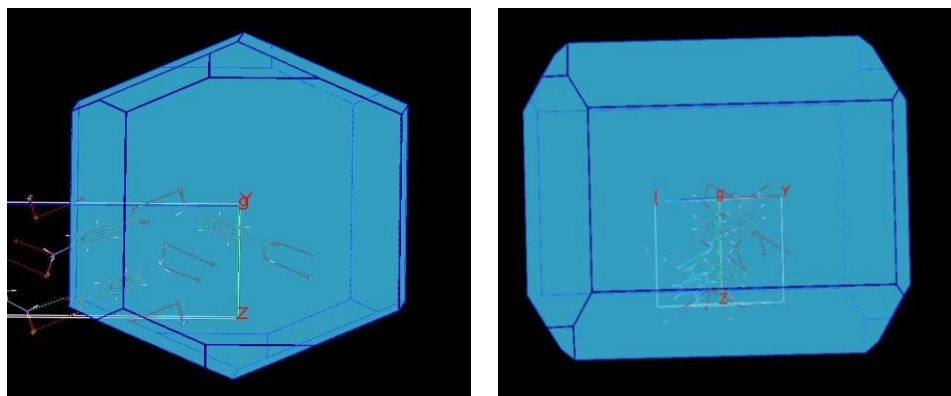


Figure 8.22. Predicted morphology of the bromide salt of PABA using the BFDH method

DSC results for the HBr salt of PABA are shown in Figure 8.23. The single sharp peak at 267 °C is the melting point of the salt. As no other peaks are detected this indicates a pure salt sample.

DVS results for the hydrobromic salt of PABA are shown in Figure 8.24. During the sorption step the relative humidity is increased from zero to 90 % which results in a 0.18 % increase in weight. The process is reversible and repeatable as shown from both cycles 1 and 2. As the weight % change in mass is very low this suggests the salts are highly crystalline solids (Hilfiker, 2006).

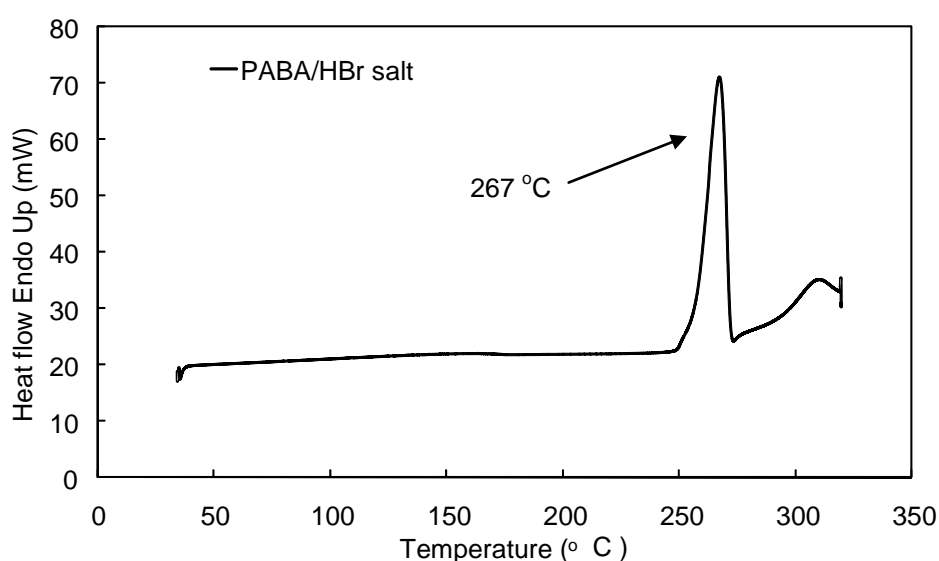


Figure 8.23. DSC results for the hydrobromide (HBr) salt of PABA

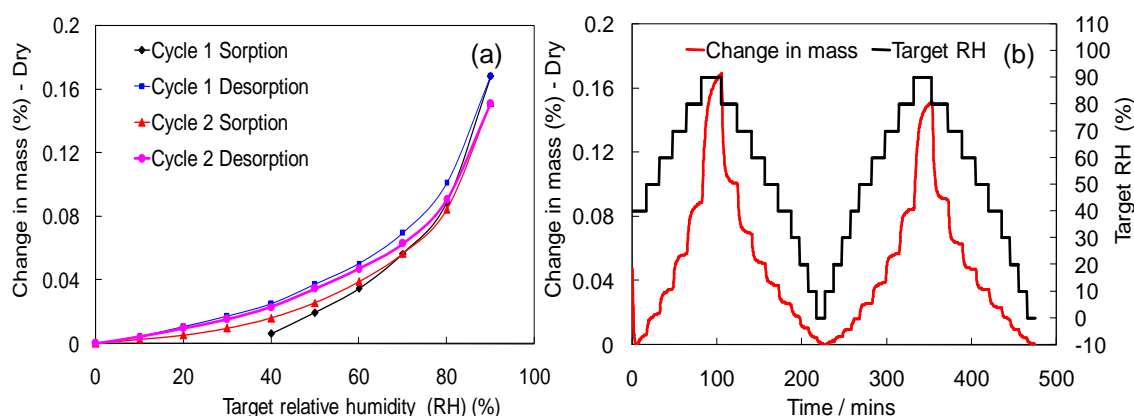


Figure 8.24. DVS results for hydrobromic (HBr) salt of PABA showing (a) isotherm plot and (b) change in mass (Dry) plot

IR patterns of PABA / HBr salt and the raw material form of PABA are shown in Figure 8.25. PABA contains a primary amine (NH_2) and a carboxylic acid (COOH) functional groups. Two sharp peaks appear at wavenumbers of 3360 and 3459 cm^{-1} in the IR pattern for the raw material form of PABA, which is due to the stretching of the N-H bond within the primary amine functional group. Bending of the N-H bond occurs at wavenumbers in the range 1580 to 1650 cm^{-1} . Significant differences appear in the patterns of the two samples within this range indicating that the positive change on the amine group within the HBr salt molecule of PABA affects the N-H bending vibrations. Stretching of the hydrogen bond (O-H) in the carboxyl acid functionally group occurs at wavenumbers in the range 2500 to 3300 cm^{-1} . A much broader peak appears in this wavelength range for the raw material compared to the HBr salt of PABA. There is a slight shift in the peak due to the stretching of the carbonyl group within the two samples. This peak appears at wavenumber 1700 cm^{-1} for the salt and 1658 cm^{-1} for the raw material form of PABA. The differences in the IR patterns for the two samples indicates that the HBr salt of PABA affects the bending and stretching vibrations of the bonds within the amine and carboxylic functional group. The IR pattern of the salt has not yet been reported in the literature providing a novelty aspect to the characterisation of the salt.

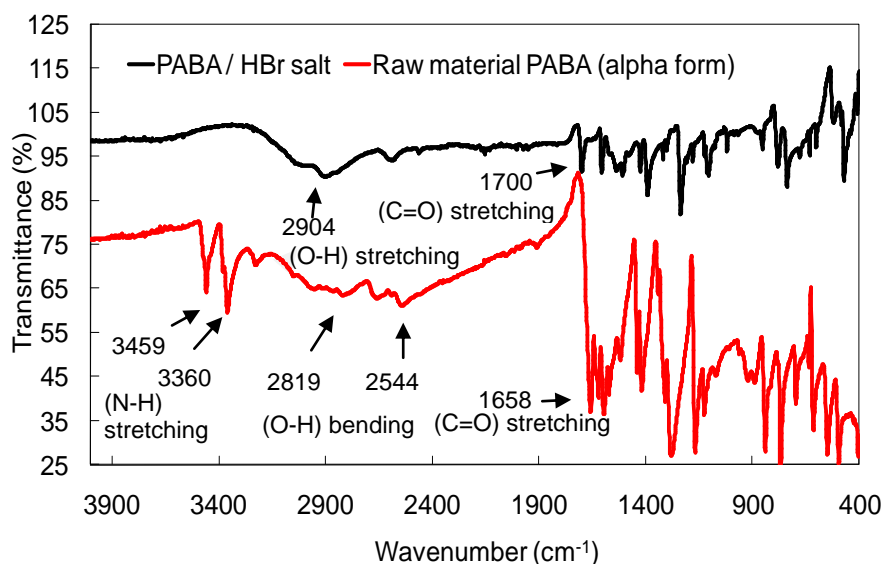


Figure 8.25. IR results for PABA /HBr salt and raw material form of PABA (alpha)

Combining PAT tools with SSA techniques provided the experimental conditions required to produce the hydrobromic salt of PABA. This salt forms when using an organic solvent (ethanol) and at very low pH conditions of 1 (highly acidic). A combination of solid state analytical techniques were used to characterise the crystal product showing that the hydrobromic salt of PABA forms large rod shape crystals with a hexagonal face. Simulated and experimental XRPD patterns are similar indicating that hydrobromic salt crystals produced experimentally are anhydrous. BFDH predicted morphology is the same as those produced experimentally indicating that the solvent (ethanol) does not interfere with the crystal surface during growth. DSC shows that the melting point of the salt is 267 °C. DVS analysis confirmed that the salt is a highly crystalline solid and IR analysis confirmed that the salt affects the bending and stretching vibrations of the amine and carboxyl functional groups within the molecules.

8.3.5 Solid state characterisation on the hydrochloride salt of PABA

PAT tools including the use of the FBRM, PVM, pH and ATR-UV/Vis spectroscopy are used to monitor the cooling crystallization of PABA from an ethanol solution at pH=2.5. Excess hydrochloric acid (HCl) was added to ensure all the PABA reacted to form the hydrochloric salt. UV/Vis data shows a peak absorbance for the HCl salt of PABA at 295 nm and for PABA (alpha form) at 301 nm as shown in Figure 9.21 (Chapter 9).

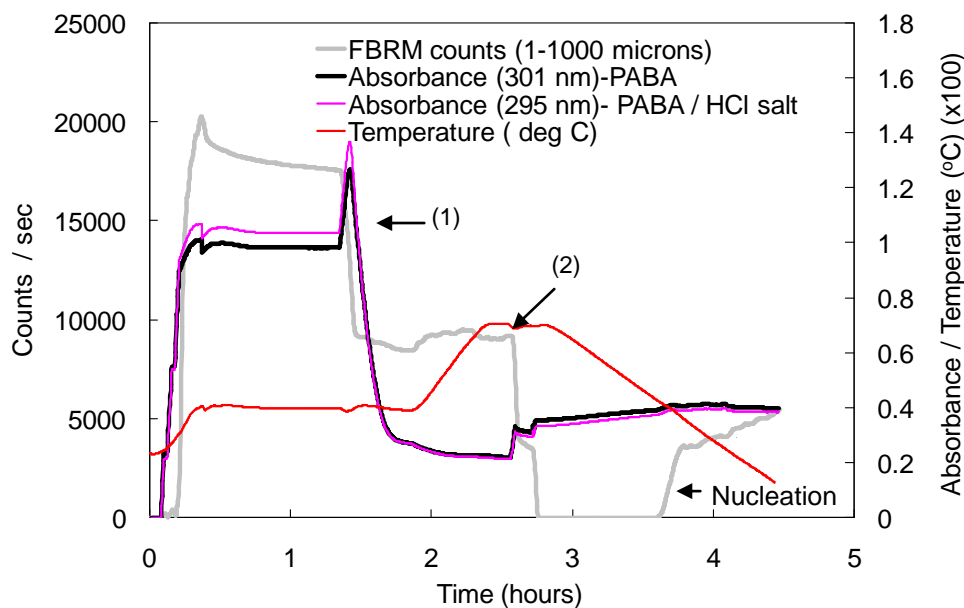


Figure 8.26. FBRM results for the cooling crystallization of PABA from ethanol solution at pH=2.5 using HCl acid

Figure 8.26 shows the FBRM and UV/Vis results for the cooling crystallization experiment of PABA at pH=2.5 in which excess acid (HCl) was added to the solution. The sharp increase in both FBRM signal and absorbance at the start of experiment is due to the addition of solid to solution. FBRM and UV/Vis detects two dissolution events. At the moment acid (HCl) is added the crystals dissolve as shown by a sharp decrease in the FBRM signal and sharp increase followed by a sharp decrease in absorbance at wavelength range 295-301 nm (see point (1) on Figure 8.26). The increase in absorbance is due to the PABA dissolving. As acid is added to solution this reacts with PABA to form the salt which has a lower absorbance within the wavelength range 295-301 nm compared to PABA causing the absorbance to decrease during acid addition. Sodium hydroxide (NaOH) is added at point (2) on Figure 8.26 to dissolve all the crystals forming a clear solution of pH=2.5. The system is then cooled down at a ramp rate of 0.6 °C/min. FBRM detects a single nucleation event shown by a sharp increase in FBRM signal followed by a gradual change indicating additional nucleation. During nucleation the UV/Vis absorbance signal should decrease however there is no significant change in the absorbance within wavelength range 295-301 nm. This is thought to be due to a combined effect of crystals sticking

to the probe window, which occurs when water is present in solution, resulting in an increase in absorbance and as the temperature decreases the absorbance increases.

A range of solid state analytical techniques including optical microscope, XRPD, DSC and IR spectroscopy are used to characterise the crystal product. Optical microscope images of the crystals from the first nucleation event show large rod shape crystals as shown in Figure 8.27. These images are different to the raw material, with needle morphology, indicating the possible formation of the salt. The crystals are fine particles, which are pink in colour with a sparkling tint as shown in Figure B1 of appendix B.

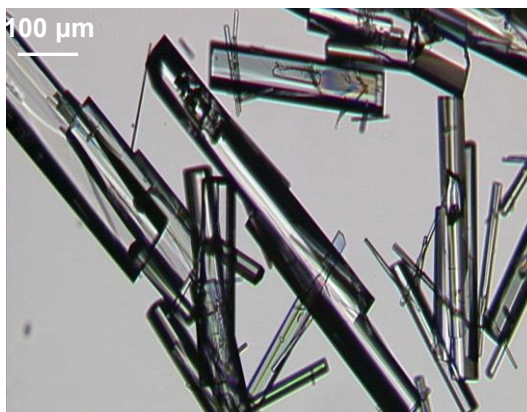


Figure 8.27. Optical microscope image of PABA re-crystallized from ethanol at pH=2.5 using HCl acid

Further solid state analytical techniques including DSC, XRPD and IR spectroscopy were used to analyse the crystals obtained from the experiment in which a single nucleation event occurred during cooling as shown in Figure 8.26.

XRPD patterns for the raw material form of PABA and the sample obtained from the first nucleation event are shown in Figure 8.28. Additional peaks appear in the pattern at angles 9, 14, 15 and 22 degrees for the raw material form of PABA compared to the sample re-crystallized from ethanol at pH=2.5, indicating clear structural differences between the two crystal forms and providing evidence of the formation of the salt.

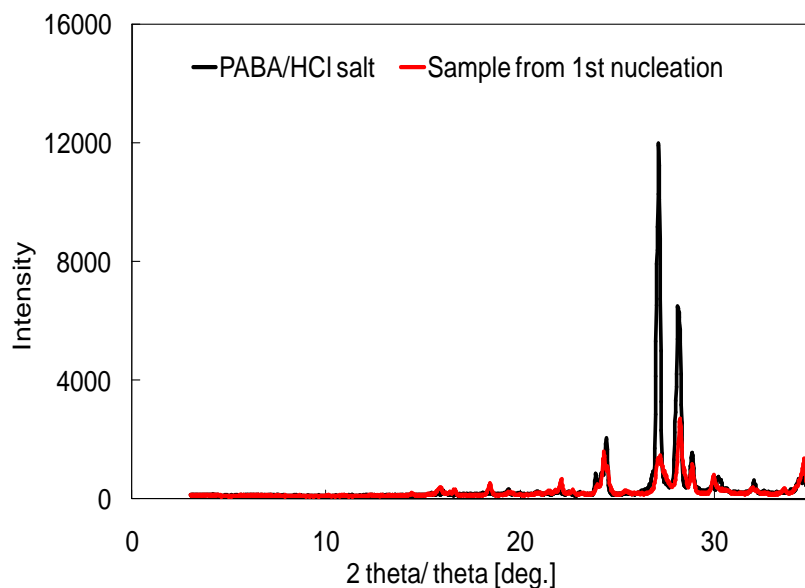


Figure 8.28. XRPD pattern for the hydrochloride salt of PABA and the raw material PABA (alpha form)

There is only one form of the chloride salt of PABA known to exist which is an anhydrous form (Cambridge Structural Database (Version 5.30; Allen, 2002) refcode PAMBZA (Colapietro and Domenicano, 1980)). The simulated XRPD pattern of the anhydrous bromide salt of MABA and the crystals produced in the experiment are shown in Figure 8.29. These patterns are very similar indicating that the salt crystals produced experimentally are the anhydrous forms.

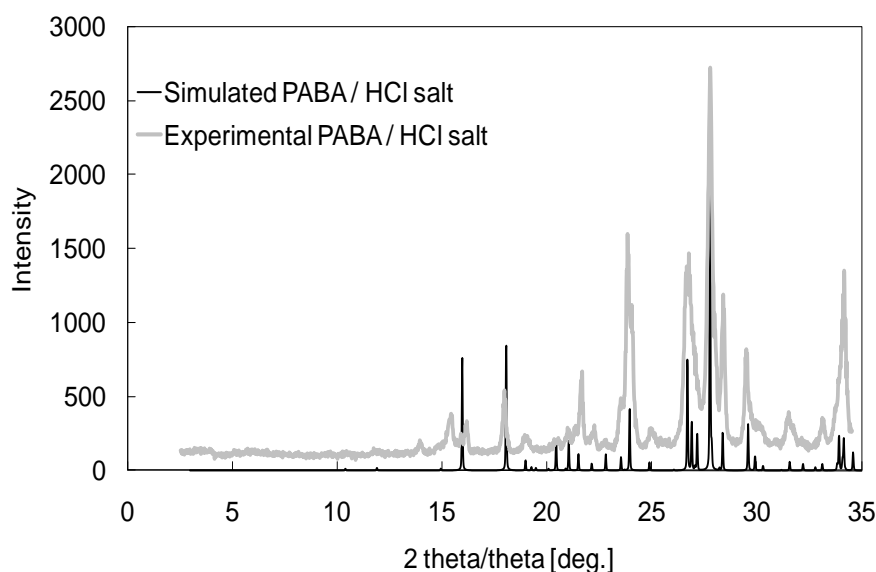


Figure 8.29. Simulated and experimental XRPD patterns for the chloride salt of PABA

The unit cell dimensions of the chloride PABA salt crystals reported by Colapietro and Domenicano (1980) can be used to predict the morphology of the crystals. The predicted morphology of the chloride salt of PABA is rod shape crystals with a hexagonal face as shown in Figure 8.30. The predicted morphology is similar to the salts produced in the experiments as shown in Figure 8.27, indicating that the solvent (ethanol) does not interfere with the growth of the individual crystal faces.

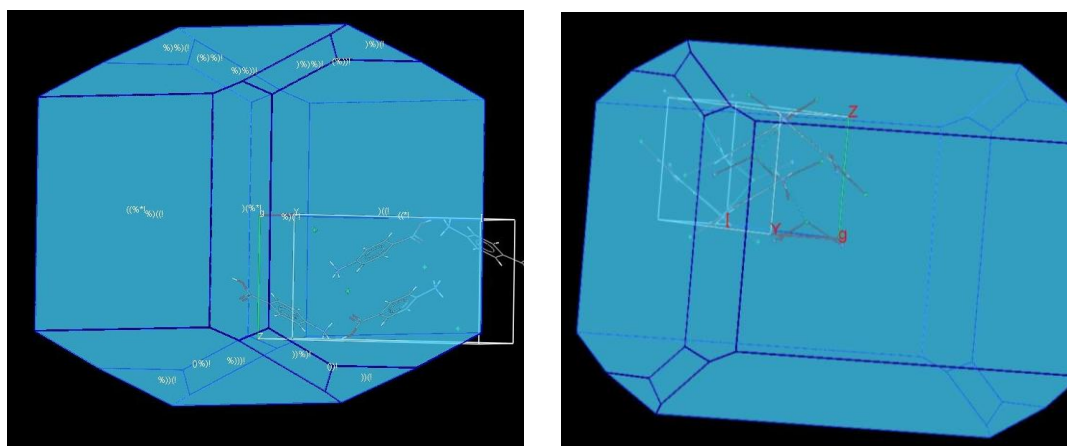


Figure 8.30. Predicted morphology of the chloride salt of PABA using the BFDH method

Figure 8.31 shows the DSC results for the crystal sample obtained from the cooling crystallization experiment of PABA in ethanol at pH=2.5 using HCl acid. A single sharp peak occurs at a temperature of 235 °C, which is thought to be due to the melting point of the hydrochloride salt of PABA. The enthalpy of melting of the salt is 515 J/g.

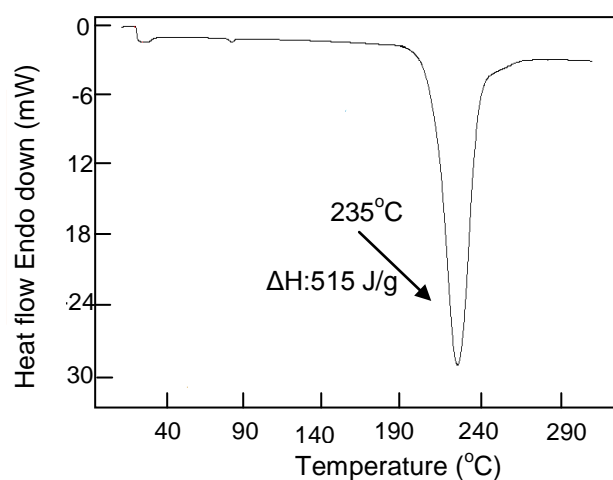


Figure 8.31. DSC results for hydrochloride (HCl) salt of PABA

Figure 8.32 shows the IR data for the hydro-chloride salt of PABA and the raw material PABA (alpha form). Figure 8.31 shows two peaks at wavenumbers 3459 and 3360 cm^{-1} which are observed in both patterns. These peaks are due to the stretching of the amine group ($-\text{NH}_2$). The IR pattern for the raw material shows an additional peak at wavenumber 3220 cm^{-1} which is thought to be due to the stretching on the ($-\text{O}-\text{H}$) group with hydrogen bonds present within the crystal (Stuart *et al.*, 1998). This peak is not observed in the salt as ionic bonds are present between the molecules of the salt due to charges on the molecules. Additional peaks appear in the spectrum of the salt at wavenumbers 2850 and 2599 cm^{-1} indicating a difference in the stretching of the ($-\text{O}-\text{H}$) bond of the carboxylic group of the two samples (Stuart *et al.*, 1998). A sharp peak at wavenumber 1700 cm^{-1} observed in the spectrum for the salt is due to the stretching of the carbonyl group. Figure 8.31 shows the fingerprint region within wavenumber range 1500-600 cm^{-1} which is different for the two samples indicating the presence of different crystal forms. Bending vibration of the ($-\text{N}-\text{H}$) group in the amine occurs at wavenumbers within the range 1630-1500 cm^{-1} (Stuart *et al.*, 1998). Two peaks at 1505 and 1550 cm^{-1} are only observed in the peak pattern of the salt providing evidence that the formation of the salt affects these vibrations. The clear differences between the bending and stretching vibrations within the two samples indicate the formation of the HCl salt of PABA.

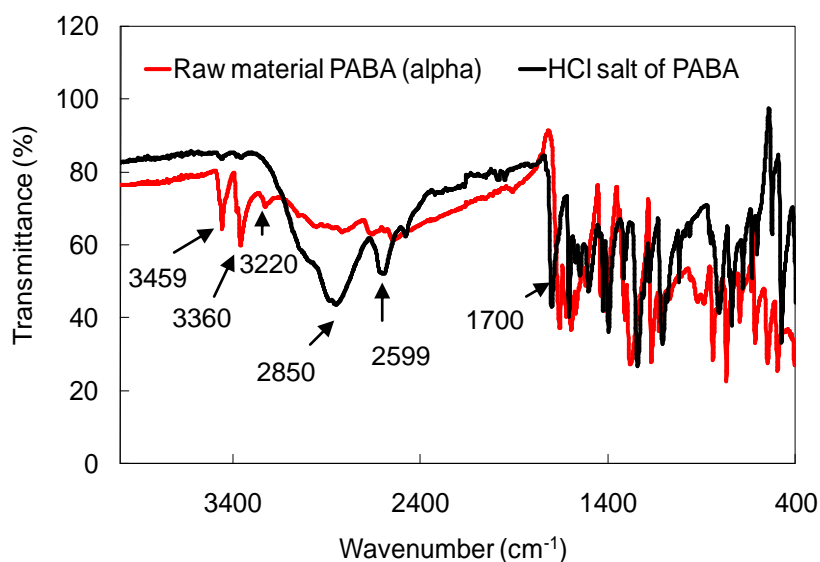


Figure 8.32. IR results for the HCl salt of PABA and the raw material PABA (alpha)

Combining PAT tools with SSA techniques provided the experimental conditions required to produce the hydrochloric salt of PABA. This salt forms when using an organic solvent (ethanol) and at very low pH conditions of 2.5 (highly acidic). A combination of solid state analytical techniques were used to characterise the crystalline product showing that the hydrochloric salt of PABA forms large rod shape crystals. Simulated and experimental XRPD patterns confirm that the hydrochloric salt of PABA produced experimentally is the anhydrous form. BFDH predicted morphology is the same as the experimentally produced crystals indicating that the solvent does not interfere with the crystal surface during crystal growth. The melting point of the salt is 235 °C. IR patterns provided evidence that the salt affects the stretching and bending vibrations of the amine and carboxyl functional groups. Also an addition peak appears in the IR pattern for the raw material which is due to the stretching of the hydrogen (O-H) bond. This peak would not be expected to appear in the IR pattern for the salt as this contains ionic bonds, provided evidence of the formation of the HCl salt of PABA.

8.3.6 Structural comparison of the bromide and chloride salts of PABA

The bonding arrangement between individual atoms within a molecule affects the structure of the crystal form resulting in crystals with specific physico-chemical properties, such as solubility, stability, dissolution rate and bioavailability. Crystallizing the compound with the desired properties is important to obtain a quality product. Previous reported literature (Cincic and Kaitner, 2008a) states that the chloride and bromide salts of PABA are isostructural indicating that the structures are very similar in which the bromide ions replace the chloride ions in the bromide salt. However this statement was based on studies which did not take into account all the hydrogen bonds and more up to date literature reported different values of bond angles resulting in variations in the unit cell dimensions (Cincic and Kaitner, 2008a). This is an important parameter in crystal structure determination (Byrn, 1982). XRDs of the chloride and bromide salts of PABA are shown in Figure 8.33 showing clear differences in the peak positions, indicating that the chloride and bromide salts of PABA are not isostructural.

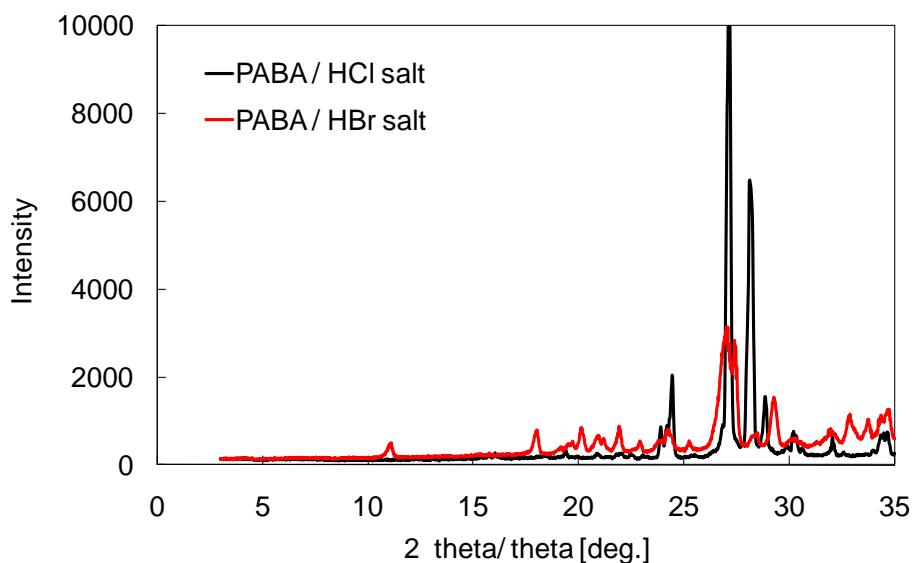


Figure 8.33. Comparison of XRPD patterns for the chloride and bromide salts of PABA

Previous literature (Cincic and Kaitner, 2008b) reported the chloride and bromide salts of MABA are also isostructural but more up to date literature has reported a different sequence in unit cell dimensions (Cincic and Kaitner, 2008b). XRPD results for the chloride and bromide salts of MABA are shown in Figure 8.34. Clear differences in the peak positions indicate again that the two salts are not isostructural.

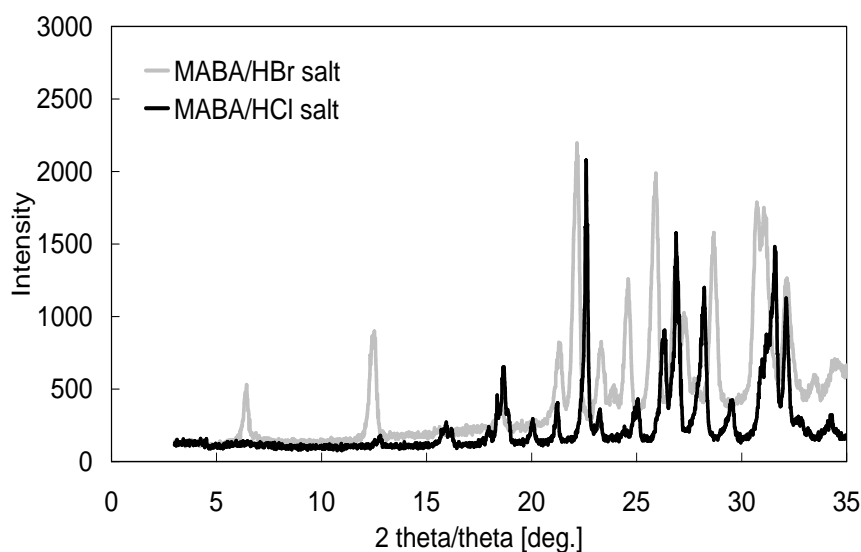


Figure 8.34. Comparison of XRPD patterns of the chloride and bromide salts of MABA

8.4 Acidic salts of PABA formed by precipitation

8.4.1 Introduction

Acids are classified into groups according to the number of hydrogen atoms available for dissociation. Monoprotic acids can dissociate one hydrogen atom, diprotic can dissociate two and triprotic can dissociate three hydrogen atoms resulting in the formation of a number of salts. So far, in chapter 8.2, research has focused on the crystallization of acidic salts of PABA using strong monoprotic acid. This section focuses on the crystallization of salts of PABA using diprotic and triprotic acids. Crystallization experiments are performed using sulphuric acid (H_2SO_4) to crystallize the sulphate salt of PABA and phosphoric acid to crystallize the phosphate salt of PABA. Crystallization in these cases occurs by a process known as precipitation due to the formation of insoluble salts in the organic solvent ethanol. A range of solid state analytical techniques including the optical microscopy, scanning electron microscopy, XRPD, DSC, solid state IR spectrum and DVS are used to characterise the crystal product.

8.4.2 Solid state characterisation of the sulphuric salt of PABA

Crystallization experiments involved adding sulphuric acid to a PABA/ethanol solution. At the moment acid is added to the solution, crystals precipitate from solution. The pH of the solution as crystallization occurs is 1.2. Sulphuric acid is a strong diprotic acid and can dissociate two hydrogen atoms resulting in the possible formation of two salts. Optical and scanning electron microscope images of crystals obtained from the precipitation experiment in which PABA re-crystallized from ethanol/ H_2SO_4 solution are shown in Figure 8.35. Optical microscope images of crystals obtained from mobile slurry show rod shape morphology. Vacuum filtration results in the crystals agglomerating together as shown by the SEM images in Figure 8.35 (b). The morphology of the crystals is different to the needle morphology of the raw material form of PABA indicating the presence of a different form. Further solid state analysis is required to characterise the crystal product.

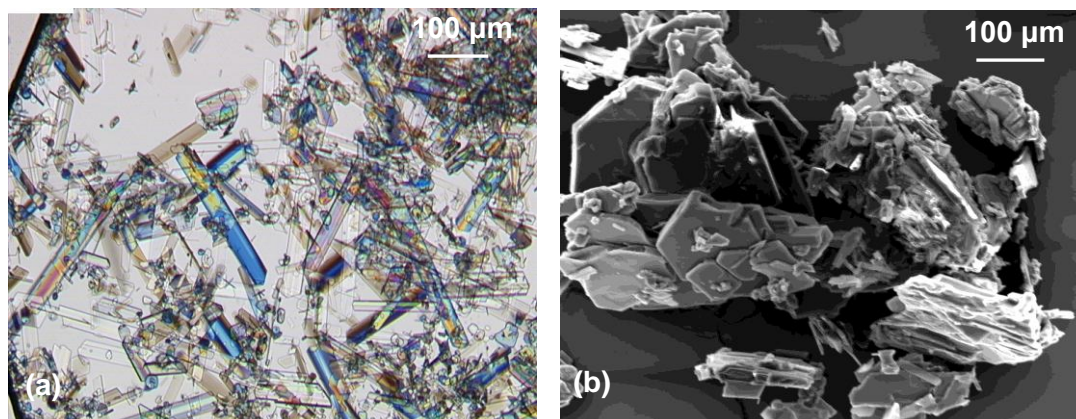


Figure 8.35. PABA re-crystallized from an ethanol/ H₂SO₄ solution showing (a) optical microscope image from mobile slurry and (b) scanning electron microscope image after filtration

XRPD patterns for the sample re-crystallized from an ethanol/H₂SO₄ solution at pH=1.2 and the raw material form of PABA are shown in Figure 8.36. The XRPD pattern for the raw material form of PABA shows additional peaks at angles of 14, 15 and 22. The sample re-crystallized from ethanol/H₂SO₄ solution at pH=1.2 shows an additional peak in the XRPD pattern at an angle of 5. The differences in XRPD patterns of the two samples indicate structural differences providing evidence of the formation of the sulphuric salt of PABA from the precipitation experiment.

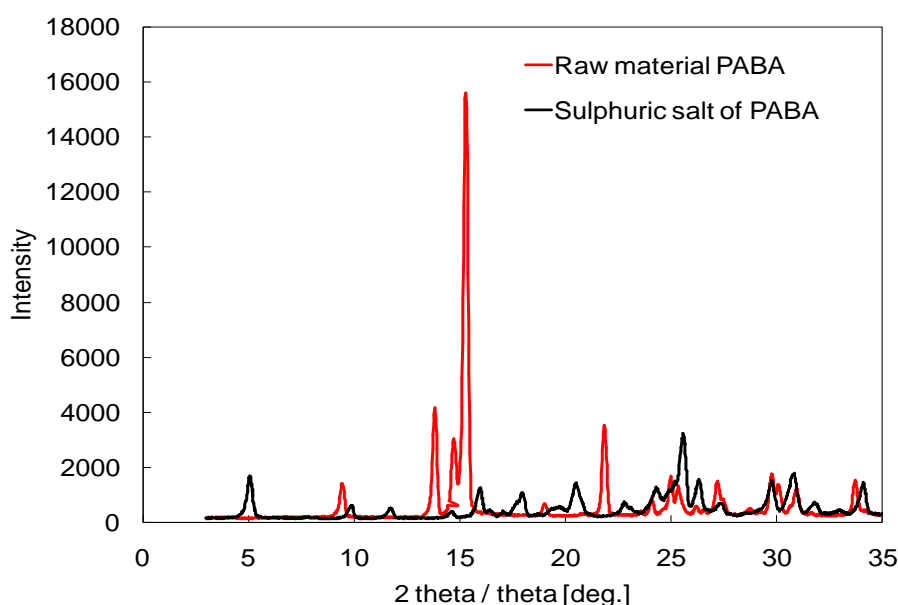


Figure 8.36. XRPD patterns for sample re-crystallized from ethanol/H₂SO₄ solution at pH=1.2 and the raw material form of PABA (alpha)

There are two anhydrous forms of the sulphate salt of PABA known to exist (Cambridge Structural Database (Version 5.30; Allen, 2002) with refcodes RICDOX and WEPVET. The molecular formula of the anhydrous form (RICDOX) is $C_7H_8NO_2+.HO_4S^-$ whereas the molecular formula of the anhydrous form (WEPVET) is $2C_7H_8NO_2+.SO_4^{2-}$. The simulated XRPD pattern of the anhydrous sulphate salt of PABA (refcode: WEPVET (Athimoolam and Natarajan, 2006)) and the crystals produced experimentally are shown in Figure 8.37. These patterns are very similar indicating that the salt crystals produced experimentally are anhydrous form with refcode WEPVET.

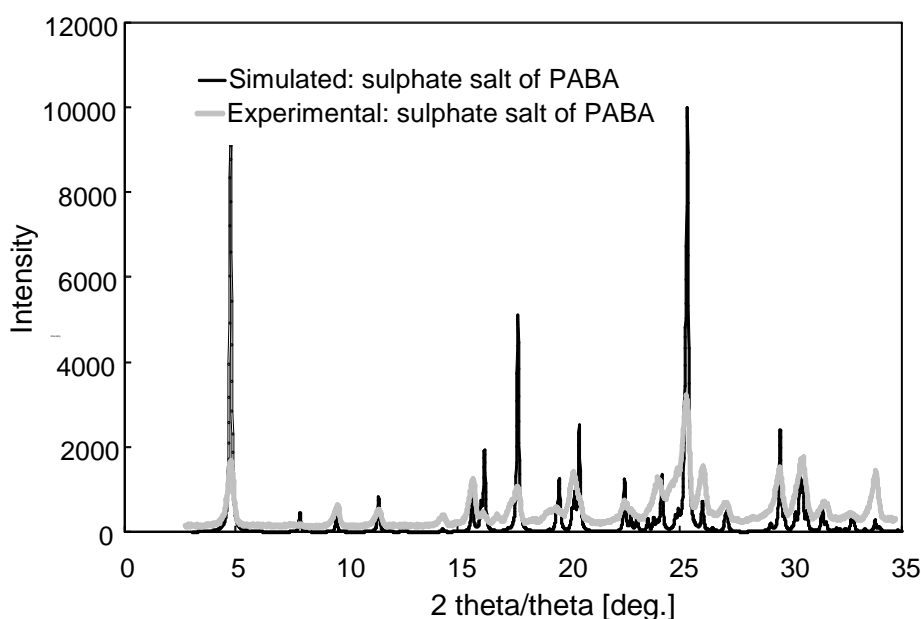


Figure 8.37. Simulated and experimental XRPD pattern for the sulphate salt of PABA

The unit cell dimensions of the sulphate salt of PABA crystals reported by Athimoolam and Natarajan, (2006) can be used to predict the morphology of the crystals. The predicted morphology of the sulphate salt of PABA is rod shape crystals with a diamond shape point at both ends of the crystal as shown in Figure 8.38. The crystals produced experimentally were crystallized from ethanol and those reported by Athimoolam and Natarajan, (2006) were crystallized from water. The predicted morphology is similar to the salts produced experimentally as shown in Figure 8.35 but those produced experimentally are longer and thinner. The slight differences in morphology indicate that the solvent interacts with certain crystal faces affecting the growth.

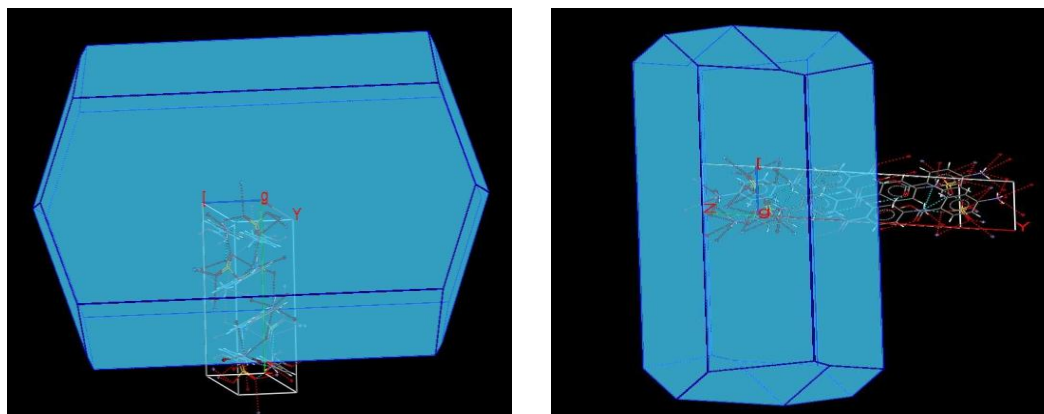


Figure 8.38. Predicted morphology of the sulphate salt of PABA using the BFDH model

DSC results for the sulphuric salt of PABA are shown in Figure 8.39. A single sharp endothermic peak occurs at a temperature of 235 °C which is the melting point of the salt. No other peaks are detected in the DSC pattern indicating the formation of the pure salt.

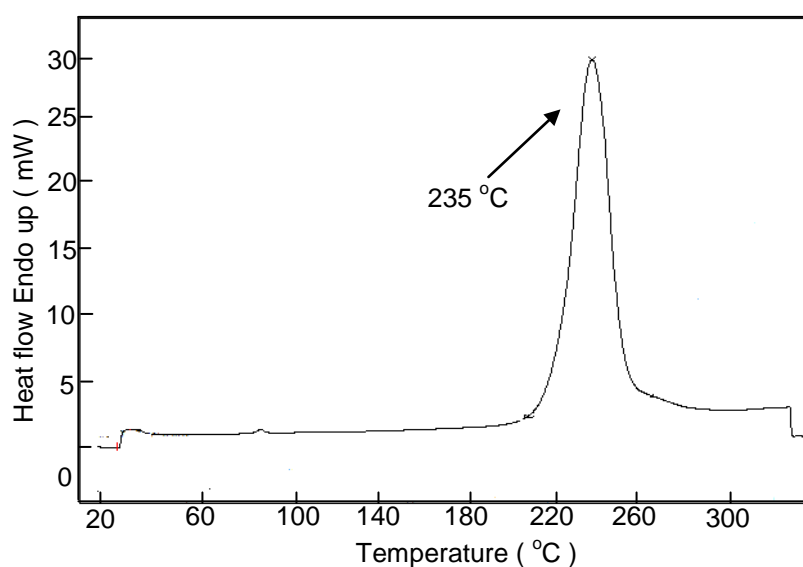


Figure 8.39. DSC results for the sulphuric salt of PABA

IR patterns for the sulphuric salt of PABA and the raw material form of PABA are shown in Figure 8.40. Two additional sharp peaks appear at wavenumbers of 3459 and 3360 cm^{-1} in the pattern for the raw material, which is due to the (N-H) bending in the amine group. Stretching of the carbonyl group (C=O) occurs at wavenumbers in

the range $1650\text{--}1830\text{ cm}^{-1}$ (Stuart *et al.*, 1998). A slight shift in the stretching of the carbonyl group occurs between the two samples. For the salt this peak appears at wavenumber of 1688 cm^{-1} and for the raw material it appears at 1658 cm^{-1} . The fingerprint region of the IR spectrum is in the range of $600\text{ to }1500\text{ cm}^{-1}$. Different forms of a compound can be identified due the differences in the finger region of the IR spectrum. The fingerprint region of the salt shows a large peak at 1020 cm^{-1} which does not appear in the IR pattern of the raw material. This peak is a characteristic peak for the sulphuric salt of PABA.

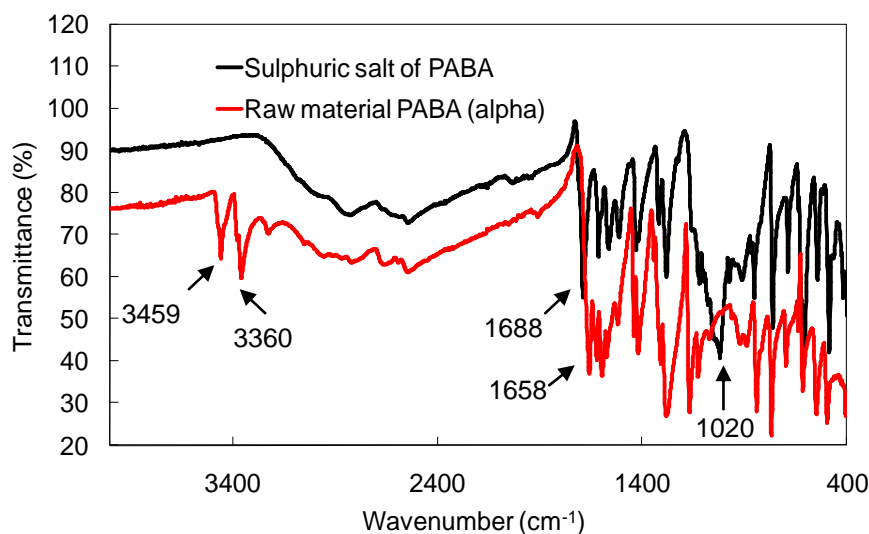


Figure 8.40. IR results for the sulphuric salt of PABA and the raw material form of PABA

Crystal samples from the precipitation experiment are analysed using DVS to determine whether the sulphuric salt of PABA is hygroscopic in nature and to examine the tendency of the salt to form hydrates. DVS results for the sulphuric salt of PABA are shown in Figure 8.41. As the relative humidity is increased from 0 to 90% there is a small increase in mass of 0.45% indicating that the salt is not hygroscopic. The compound's affinity for moisture sorption is repeatable and reversible as shown by the decrease in mass of 0.45% as the RH is decrease from 90 to 0 %. This type of behaviour is typically for highly crystalline solids (Hilfiker, 2006). The sulphuric salt of PABA does not form stoichiometric hydrates as there are no large step changes in the DVS data.

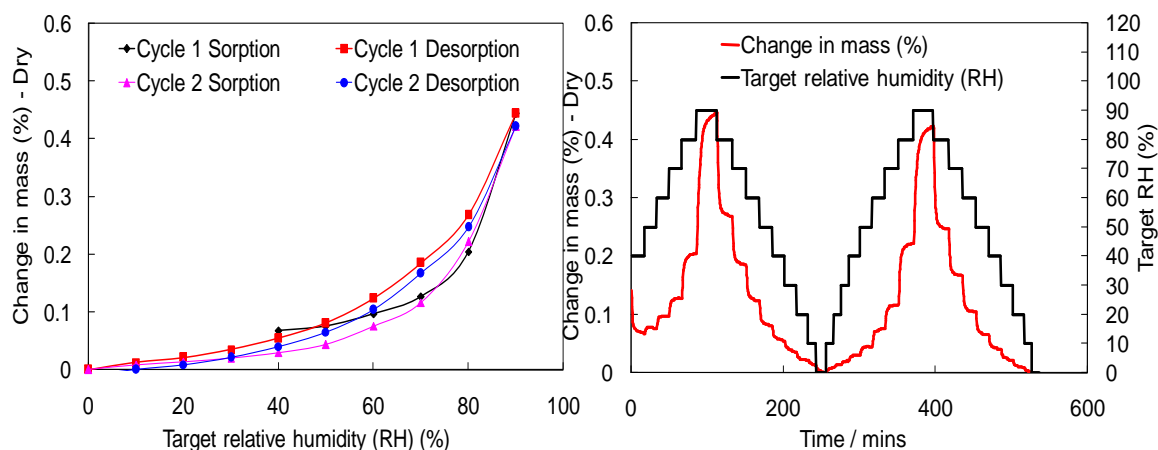


Figure 8.41. DVS results for sulphuric salt of PABA showing (a) isothermal plot and (b) change in mass (Dry) plot

A combination of solid state analytical techniques was used to characterise the sulphuric salt of PABA. XRPD patterns and IR spectrum provided evidence of the formation of the sulphuric salt of PABA. Simulated and experimental XRPD patterns for the sulphuric salt of PABA are similar providing evidence that the crystals produced experimentally are anhydrous. The crystals produced experimentally are similar to those predicted using the BFDH model but are longer in length indicating that the solvent (ethanol) interferes with certain crystal faces affecting growth. The melting point of the salt is 235 °C as shown from the DSC analysis. DVS results showed that the sulphuric salt of PABA does not form a hydrate when exposed to a maximum relative humidity of 90% and that the salt is a highly crystalline solid.

8.4.3 Solid state characterisation of the phosphoric salt of PABA

The choice of acid used to lower the pH of solution and form the acidic salt is important as weak acids do not fully ionise in solution and therefore are less likely to form a salt. However these acids may produce salts that have properties which are more desirable than other forms of salts. Therefore a full investigation and characterisation of salts is important before deciding the most suitable candidate for the next stages of manufacture from laboratory to pilot plant scale production. Literature data (Haynes *et al.*, 2005) reported 2874 known hydrochloric acid salts, 1403 hydrobromic acid salts, 161 sulphuric acid salts and 134 phosphoric acid salts of

pharmaceutical compounds. Crystallization experiments are performed using PABA and phosphoric acid to investigate the likelihood of salt formation using a weak acid. Solid state analytical techniques are used to characterise the phosphoric salt of PABA and to determine whether crystallizing a weak salt gives more suitable characteristics, such as morphology, for drug manufacturing.

Crystallization experiments involved forming a mobile slurry solution of PABA in ethanol and then adding phosphoric acid to achieve a low pH of the solution. The size of the crystallization vessel used is 750 mL and a stirrer speed of 300 rpm was used. Excess moles of phosphoric acid are added to the solution compared to the moles of PABA to increase the likelihood of the formation of the pure salt. At the moment the acid is added to the solution, crystallization occurs by a process known as precipitation. Optical and scanning electron microscope images of the crystal samples are shown in Figure 8.42. Images show rod shape crystals that form agglomerates due to precipitation. These images are different to the raw material form of PABA (α) which has needle morphology. Crystallization occurred before all the raw material dissolved and therefore these crystals act as a seed which is thought to have an influence on the morphology of the crystals produced. Further solid state analysis is performed on the crystal sample to identify the crystal form.

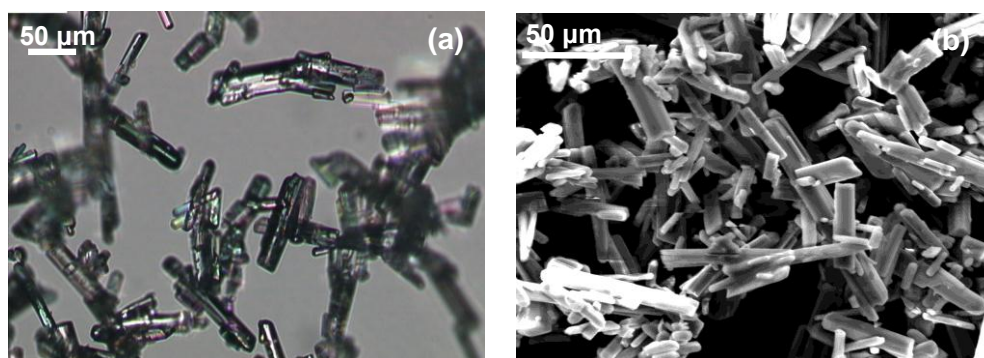


Figure 8.42. Crystal images of PABA re-crystallized from ethanol/ H_3PO_4 solution at pH=3.3 showing (a) optical microscope images and (b) scanning electron microscope

DSC analysis was performed on the crystal sample from the precipitation experiment and the results are shown in Figure 8.43.

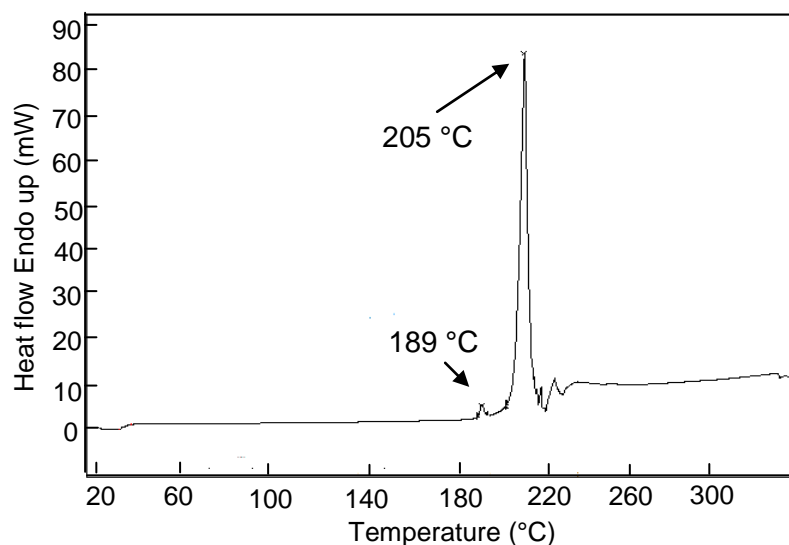


Figure 8.43. DSC results for the sample re-crystallized from ethanol solution at pH=3.3 using phosphoric acid

A sharp peak appears at a temperature of 205 °C which is thought to be the melting point of the phosphoric salt of PABA. Crystals precipitated from a mobile slurry solution in which not all of the raw material (PABA) had dissolved and therefore a small peak at 189 °C appears in the DSC results which is the melting point of the alpha form of PABA.

The crystallization experiment is repeated in a beaker using a magnetic stirrer to achieve mixing. All of the raw material (PABA) dissolved before acid is added to the solution. Optical microscope images of the crystals are shown in Figure 8.44. The morphology of the crystals is plate like, but a few rod shaped crystals also form. Mixing with a magnetic stirrer created a vortex resulting in poor mixing. This affects the mass transfer which can result in crystallization of the same form but with a different morphology due to the high local supersaturation values. An alternative explanation to the different crystal morphologies obtained from the reactor and beaker precipitation experiments could be due to the formation of different phosphoric salts of PABA. Phosphoric acid can dissociate and donate three hydrogen ions to form three different salts. Insufficient mixing in the beaker experiment can result in localised regions of high concentration of acid forming the higher form of the salt (one hydrogen ion dissociates to form (H_2PO_4^-)). Further solid state analysis involving the use of DSC and XRPD is required to characterise the crystals produced.

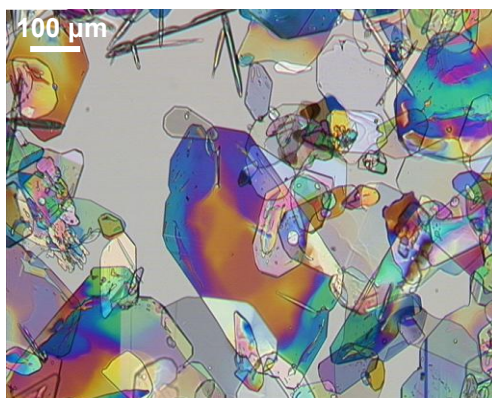


Figure 8.44. Optical microscope image of crystals obtained from the beaker precipitation experiment of PABA in an ethanol/H₃PO₄ solution in which all the raw material dissolved

DSC results for the sample of crystals re-crystallized from a clear ethanol/H₃PO₄ solution (beaker experiment) are shown in Figure 8.45. Fluctuations in peaks occur within the temperature range of the melting point of the raw material (189 °C) and the melting point of the phosphoric salt of PABA (205 °C). The fluctuation in peaks signifies decomposition. The sharp peak at 257 °C is thought to be due to the melting point of the decomposition products.

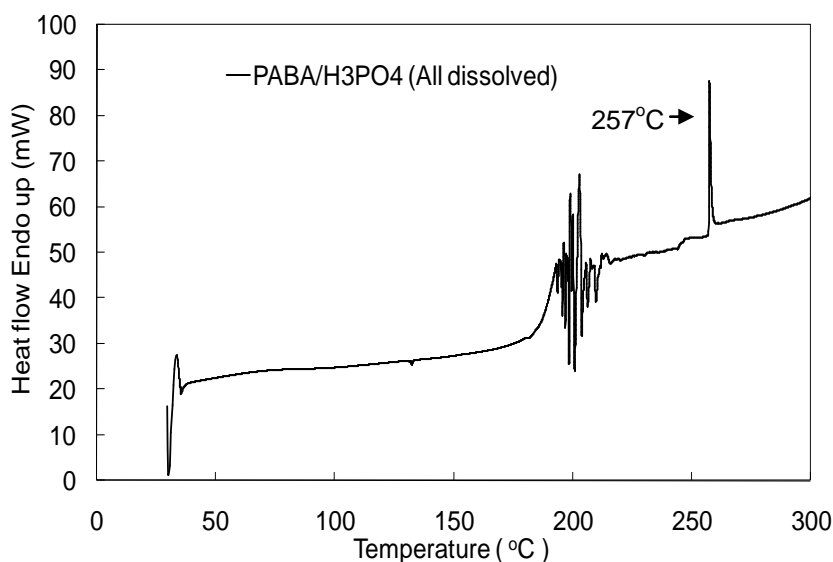


Figure 8.45. DSC results for the sample re-crystallized from a clear ethanol/H₃PO₄ solution

XRPD patterns for the raw material form of PABA and the compound re-crystallized from the beaker experiment (all of the raw material dissolved) and reactor experiment (raw material present in the slurry) are shown in Figure 8.46. The XRPD pattern of the raw material is significantly different to the patterns obtained from the beaker and reactor precipitation experiments. Additional peaks in the raw material pattern appear at angles of 9, 14 and 15. The two XRPD patterns of samples from the precipitation experiments with phosphoric acid are very similar, suggesting the same crystal salt form. This provides evidence that the difference in morphology from the beaker and reactor experiment is due to the difference in mixing conditions and not the formation of different salts.

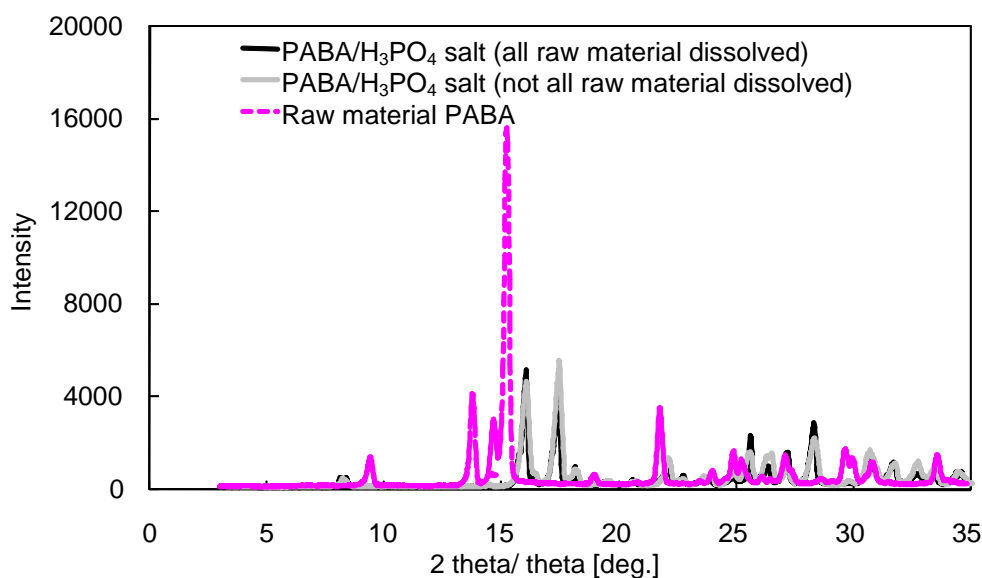


Figure 8.46. XRPD patterns for the crystal samples obtained from the precipitation experiments of PABA in an ethanol/H₃PO₄ solution and the raw material form of PABA (alpha)

There are two forms of the phosphate salt of PABA known to exist including a monohydrate and an anhydrous form (Cambridge Structural Database (Version 5.30; Allen, 2002). The simulated XRPD pattern of the anhydrous phosphate salt of PABA (refcode: RIBWAB (Benali-Cherif *et al.*, 2007)) and the crystals produced experimentally are shown in Figure 8.47. These patterns are very similar indicating that the salt crystals produced experimentally are anhydrous.

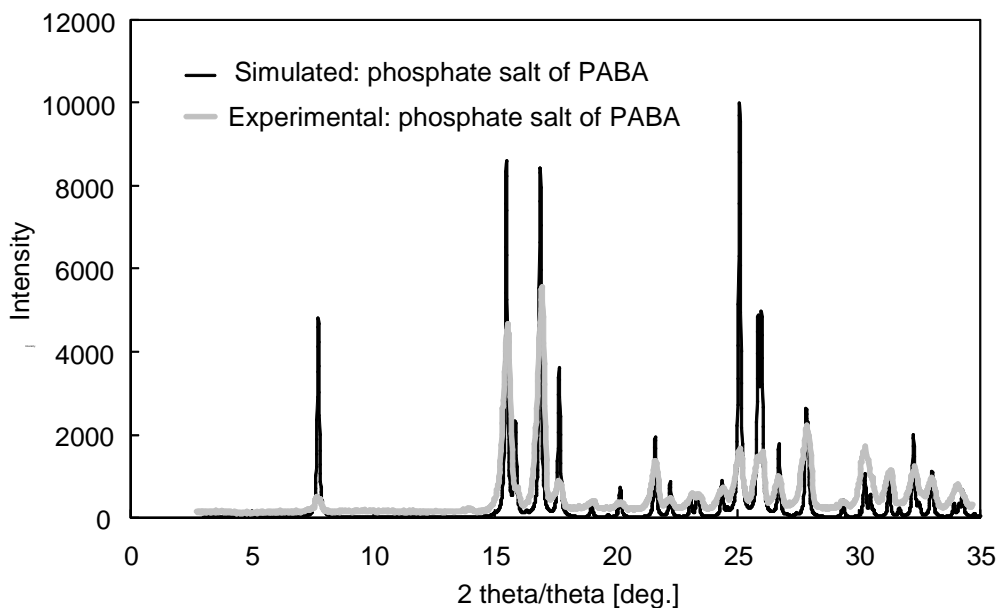


Figure 8.47. Simulated and experimental XRPD pattern for the phosphate salt of PABA

The unit cell dimensions of the anhydrous phosphate salt of PABA crystals reported by Benali-Cherif *et al.*, (2007) can be used to predict the morphology of the crystals. The predicted morphology of the anhydrous phosphate salt of PABA is plate like shaped crystals with a hexagonal face as shown in Figure 8.48. The crystals produced experimentally were crystallized from ethanol and those reported by Benali-Cherif *et al.*, (2007) were crystallized from water. The predicted morphology is similar to the salts produced from the precipitation beaker experiment as shown in Figure 8.44 but those produced experimentally form thinner plates and are irregular. The slight differences in morphology indicate that the solvent interacts with certain crystal faces affecting the growth.

Solid state IR analysis is performed on the phosphoric salt of PABA and the raw material form of PABA. IR results are shown in Figure 8.49. Two additional peaks appear at wavenumbers of 3360 and 3459 cm^{-1} in the IR pattern of the raw material form of PABA, which is due to the stretching of the (N-H) bond in the amine group. The bending vibrations of the (N-H) bond occur at wavenumbers within the range 1580 to 1650 cm^{-1} . The peak pattern at this wavenumber varies for the two samples indicating that the formation of the salt affects the bending vibrations of the (N-H) bond. The fingerprint regions of the two samples are completely different indicating the presence of two different forms. The salt shows additional peaks at wavenumbers

around 1000 cm^{-1} and a sharp peak at wavenumber 1214 cm^{-1} which is characteristic for the phosphoric salt of PABA.

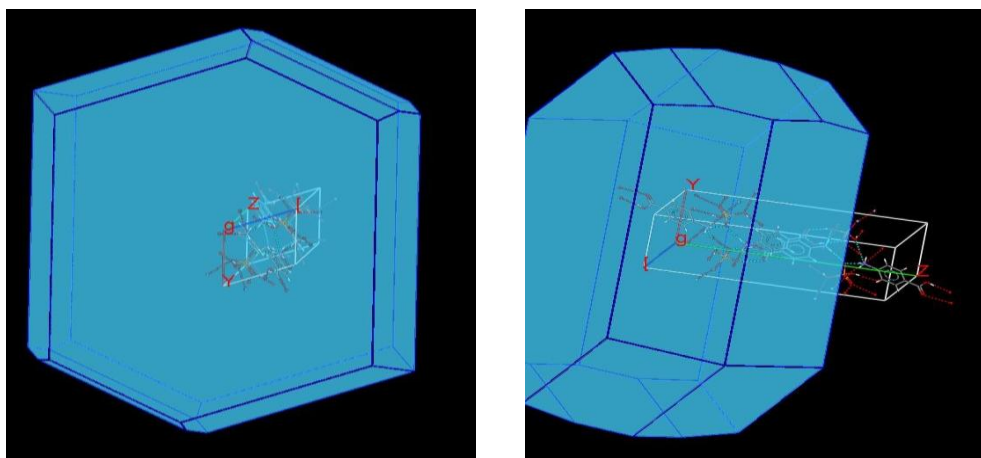


Figure 8.48. Predicted morphology of the anhydrous phosphate salt of PABA using the BFDH model

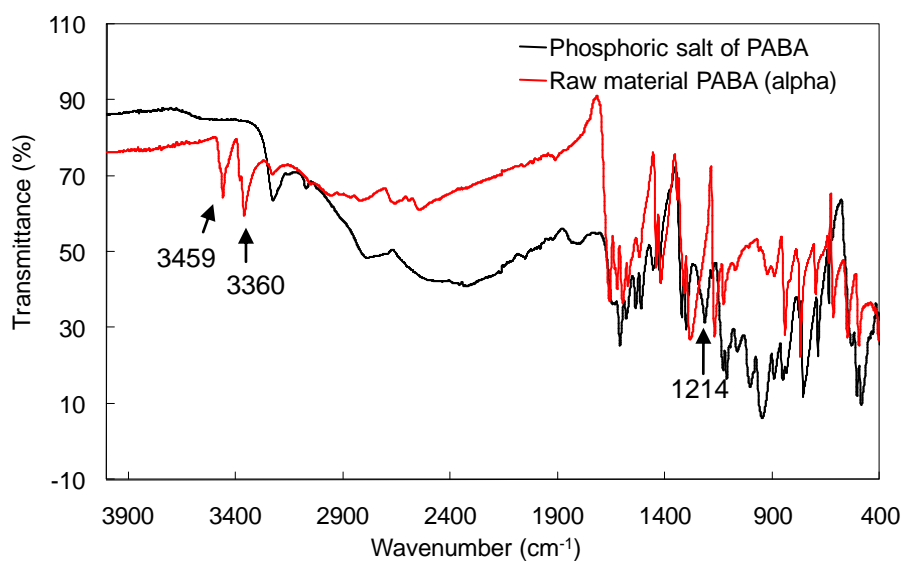


Figure 8.49. IR spectrum of the phosphoric salt of PABA and the raw material form of PABA

A combination of solid state analytical techniques is used to characterise the phosphoric salt of PABA. DSC results showed that the melting point of the salt is $205\text{ }^{\circ}\text{C}$. XRPD patterns confirmed that the same form of phosphoric salt of PABA can crystallize with different morphologies due to differences in mixing conditions.

Simulated and experimental XRPD patterns for the phosphoric salt are very similar indicating the crystals produced experimentally are anhydrous. The predicted morphology of the crystals, using the BFDH model, is similar to those produced experimentally but thinner and more irregular crystals are produced from the beaker experiment, indicating that solvent (ethanol) interferes with the crystal surface during growth. IR analysis showed that the phosphoric salt of PABA affects the bending vibrations on the (N-H) bond in the amine group and a characteristic peak appears around 1000 cm^{-1} and 1214 cm^{-1} for the salt. A combination of SSA techniques confirmed a weak acid such as phosphoric acid can be used to form salts of PABA.

8.5 Basic salts of PABA formed by evaporation

8.5.1 Introduction

The production of alkali salts requires crystallizing under high pH conditions above a value of 8 in which the $-\text{COO}^-$ group is 100% ionised. The presence of the $-\text{COO}^-$ group increases the likelihood of hydrate salt formation by 35% (Infants *et al.*, 2007). The size of vessel that is used in these studies to carry out cooling crystallization experiments is 750 mL which can hold a total of four PAT tools including the FBRM, pH, ATR-UV/Vis and PVM probe. As the solubility of the compound is very high at pH values above 8, operating at the 750 mL scale would require very large amounts of materials for a cooling crystallization experiment to be successful. Due to this reason an alternative method of evaporative crystallization in a beaker is used to crystallize the hydrated sodium and potassium salts of PABA. This required forming an undersaturated solution of PABA in ethanol at high pH values of 8.1 to 10.7 by adding the desired alkali and then the beaker was left in a fume cupboard for solvent evaporation. Crystal samples were analysed using a range of solid state analytical techniques to characterise the alkali salts.

8.5.2 Hydrated forms of the sodium salt of PABA

Optical microscope images of the sodium salt of PABA are shown in Figure 8.50. The morphology of the crystals is rod shape with a diamond shape end which is very

different to the raw material form of PABA of needle morphology. The difference in morphology provides evidence of the formation of a salt.

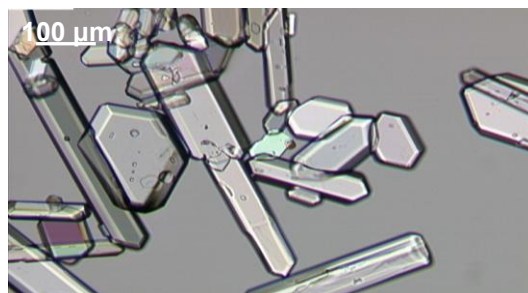


Figure 8.50. Optical microscope image of PABA re-crystallized from ethanol at pH=10.7 using NaOH

XRPD patterns for the sample re-crystallized from ethanol solution at pH=10.7 and the raw material form of PABA (alpha) are shown in Figure 8.51. The raw material shows an additional sharp peak at an angle of 15 and the sample re-crystallized from ethanol at pH=10.7 shows additional peaks at angles 16-18, 27 and 33. The clear difference between the two XRPD patterns indicates the formation of the sodium salt of PABA from the evaporation crystallization experiment.

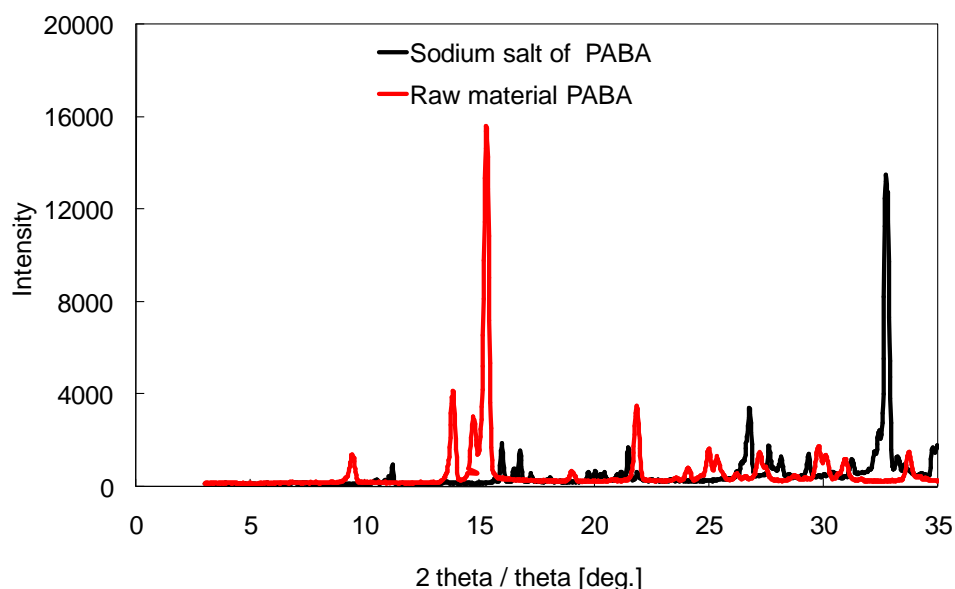


Figure 8.51. XRPD pattern for the sodium salt of PABA and the raw material form of PABA

There is only one form of the sodium salt of PABA known to exist which is a pentahydrate (Cambridge Structural Database (Version 5.30; Allen, 2002) refcode

NAABZH (Salas-Cimingo, 1968a)). The simulated XRPD pattern of the pentahydrate sodium salt of PABA and the crystals produced experimentally are shown in Figure 8.52. These patterns are different indicating that the salt crystals produced experimentally are a different hydrate form to the pentahydrate.

DSC results for the sodium salt of PABA are shown in Figure 8.53. Four endothermic peaks occur at temperature of 67 °C, 118 °C, 328 °C and 396 °C. The first peak at 67 °C is thought to be due to moisture of the surface of the crystals. The peak at 118 °C is due to dehydration of a hydrate. As this peak is wide it is thought that this may consist of two separate peaks indicating the formation of two hydrates. Repeats of the DSC showed two peaks occurring within this temperature range at 120 °C and 136 °C. The peak at 328 °C is the melting point of the anhydrous sodium salt of PABA which has not yet been reported in the literature. Previous studies on sodium benzoate, which contains the sodium ion showed a very high melting point of 440 °C. A higher melting point of 328 °C is observed for the sodium salt of PABA compared to other salts, which is thought to be due to the presence of the sodium ions. Heating the crystal sample up to a very high temperature resulted in decomposition as shown by a peak at 396 °C. Black solid deposits form on the outside of the DSC pan providing further evidence of decomposition.

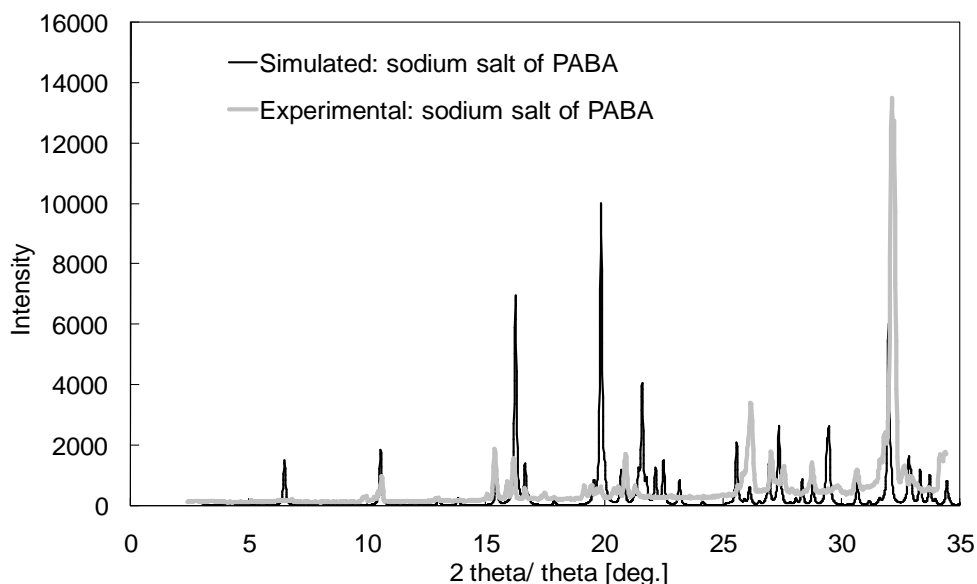


Figure 8.52. Simulated and experimental XRPD pattern for the sodium salt of PABA

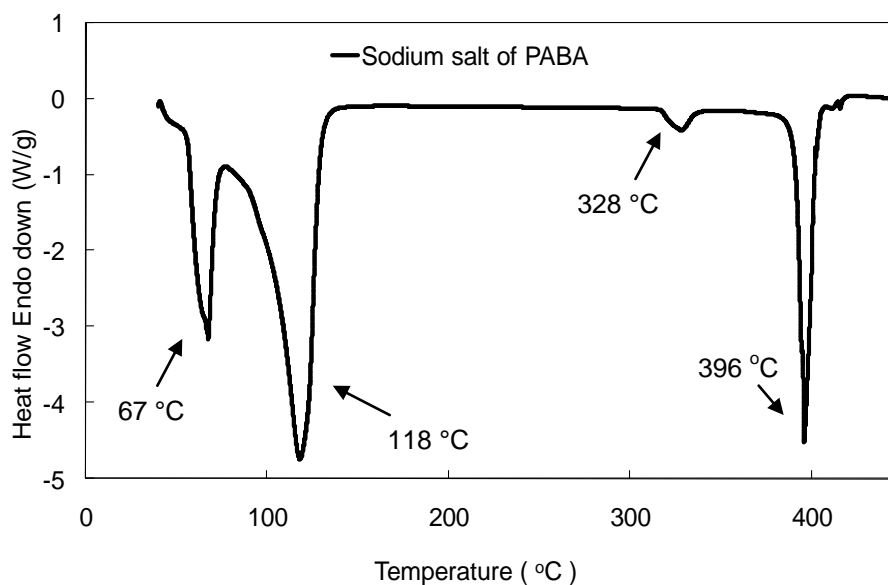


Figure 8.53. DSC results for the sodium salt of PABA

TGA is used to determine the formation of hydrate or solvates of a compound from the weight decrease in mass as the crystals are heated. TGA results for the sodium salt of PABA are shown in Figure 8.54. A large weight decrease of 33.5 % occurs as the system is heated to 110 °C which is due to water removal from the internal structure of the crystal. DSC and DVS results confirmed that there are two hydrate forms of the sodium salt of PABA, which have close stability. Due to this reason it is thought that the loss in water as shown by a single step in the TGA results represents the loss of water from both hydrates so the final form is anhydrous. The molecular ratio of sodium salt to water is calculated from the weight loss which gives a molecular ratio of salt to water of 1:4.4 for the highest hydrated form of the salt. A sample calculation can be found in Appendix E. These results support the prediction from the simulated XRPD results shown in Figure 8.52, which states that a different hydrate form other than the pentahydrate sodium salt of PABA crystallizes from ethanol solution.

DVS is a useful tool in determining whether the material under investigation is amorphous, highly crystalline or the type of hydrate formation (channel or stoichiometric hydrate) by the extent of water uptake and how significant the mass changes with respect to RH. A large step change in mass indicates the formation of a stoichiometry hydrate whereas a small and gradual increase in mass indicates the formation of a channel hydrate (Hilfiker, 2006). DVS results for the sodium salt of PABA re-crystallized from ethanol solution are shown in Figure 8.55. These results

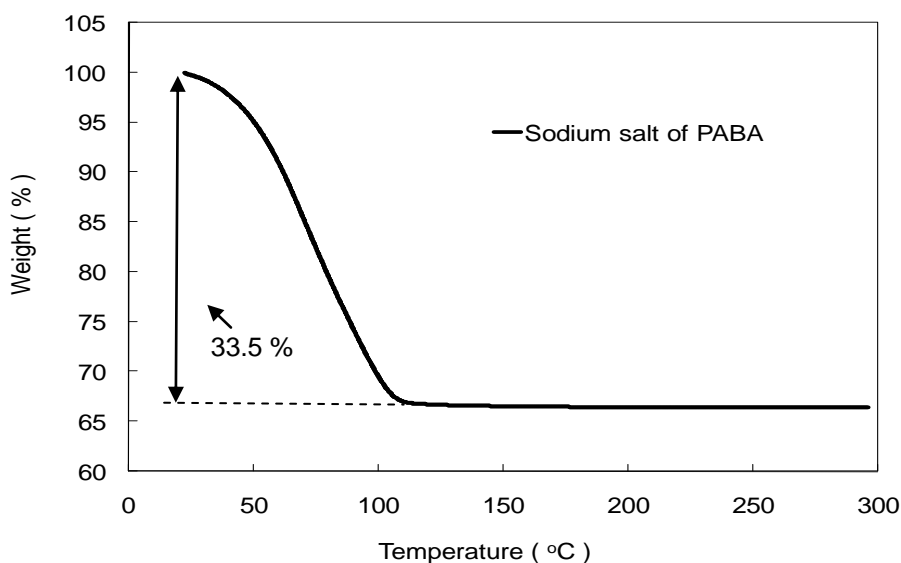


Figure 8.54. TGA results for the sodium salt of PABA

show two step changes in mass as the RH is increased above 30-50% and 80%. The first step change as represented by point (1) on Figure 8.55 (a and b) is due to the formation of a stoichiometric metal co-ordinated hydrate. This type of behaviour is observed in other sodium salt compounds (Stephenson and Diseroad, 2000). The second step change at 80% relative humidity (see point (2) on Figure 8.55 (a and b)) is thought to be due to layers of water building on the surface of the crystal. At high relative humidity of 80% it is assumed that the crystals deliquesce. During both sorption and desorption cycles there is a small and gradual increase in mass between the two step changes as shown by point (3) in Figure 8.55 (b) which is due to sharp changes in relative humidity.

For the first step change the molecular ratio of sodium salt of PABA to water is calculated from the change in mass assuming that zero mass % indicates the anhydrous form of the compound. A sample calculation is shown within Appendix E. At point 1 on Figure 8.55 (b) the molecular ratio of sodium salt of PABA to water is calculated as 1:11 indicating the formation of a stoichiometric metal co-ordinated hydrate.

As the RH is decreased below 40% during the desorption cycle there is a step change in mass as shown by point 4 to 5 on Figure 8.55 (b). This step change is thought to be

due to the formation of a hydrate. The molecular ratio of sodium salt of PABA to water is 1:2.4 indicating the formation of a channel hydrate. As the molecular ratio of salt to water is lower than values obtained from TGA analysis this hydrated salt is thought to be the formation of the lower hydrate state as represented with a dehydration temperature of 118 °C from the DSC analysis.

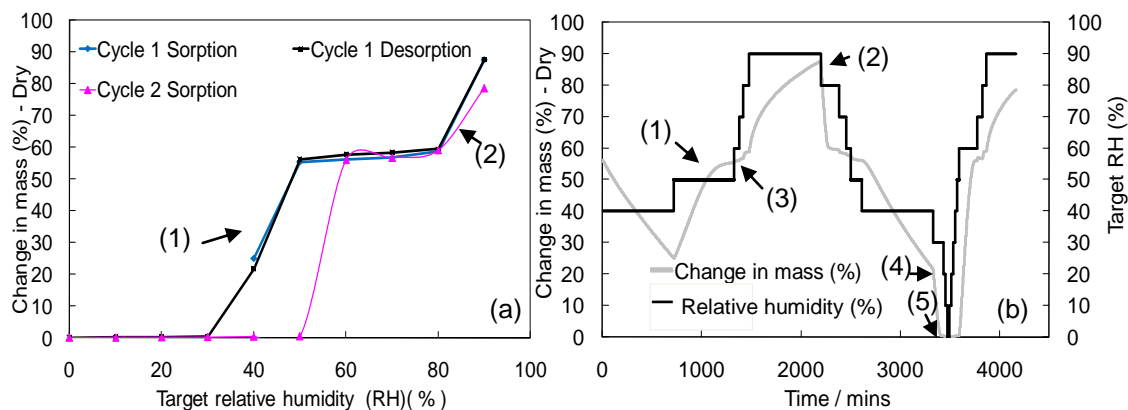


Figure 8.55. DVS results for sodium salt of PABA showing (a) isothermal plot and (b) change in mass (Dry) plot

A combination of SSA techniques including the use of the optical microscope, XRPD, DSC, DVS and TGA were used to characterise the crystalline product obtained from the evaporation experiment of PABA in an ethanol/NaOH solution of pH=10.7. XRPD patterns provided evidence of the formation of the sodium salt of PABA. The melting point of the anhydrous sodium salt of PABA is provided from DSC data giving a value of 328 °C. DSC, DVS and TGA confirmed the formation of two channel hydrate forms of the sodium salt of PABA from the evaporation experiment. The highest hydrate state has a molecular ratio of salt to water of 1:4.4 and lower hydrate state of 1:2.4. The sodium salt reported from the Cambridge Structural Database is a pentahydrate indicating that the lower hydrate states crystallized from ethanol by evaporation are new reported forms. DVS confirmed the formation of a higher stoichiometric hydrate state (molecular ratio salt to water of 1:11) when exposed to high RH showing the high tendency of the sodium salt of PABA to form hydrates.

8.5.3 Hydrated forms of potassium salt of PABA

Optical microscope image of PABA re-crystallized from ethanol/KOH solution of pH=8.1 is shown in Figure 8.56. The image show crystals of rod shape morphology with a diamond shaped end. The sizes of the crystals are greater than 300 μm in length. Crystals of this shape and size are suitable candidates for minimising the problems in further downstream processing. The morphology of the crystals is different to the raw material form of PABA which consists of long needles. Further solid state analysis is required to identify the crystal form.

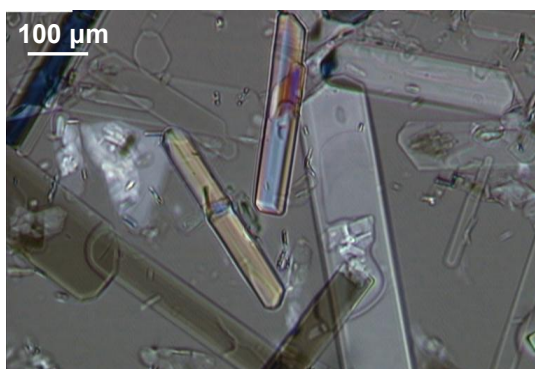


Figure 8.56. Optical microscope image of PABA re-crystallized from ethanol at pH=8.1 using KOH

XRPD patterns of the sample re-crystallized from ethanol/KOH solution at pH=8.1 and the raw material form of PABA (alpha) are shown in Figure 8.57. The raw material form of PABA shows additional angles in the XRPD patterns at values of 9, 14-15, 22 and 30. The clear difference between the two patterns provides evidence of the formation of the potassium salt of PABA. This compound is used in fibrotic skin disorders (Swislocka *et al.*, 2006). The XRPD for the potassium salt of PABA has not yet been reported in the literature.

There is only one form of the potassium salt of PABA known to exist, which is a tri-hydrate (Cambridge Structural Database (Version 5.30; Allen, 2002) refcode KAMBZH (Salas-Cimingo, 1968b)). The simulated XRPD pattern of the tri-hydrate potassium salt of PABA and the crystals produced experimentally are shown in Figure 5.58. These patterns are different indicating that the salt crystals produced experimentally are a different hydrate form to the tri-hydrate.

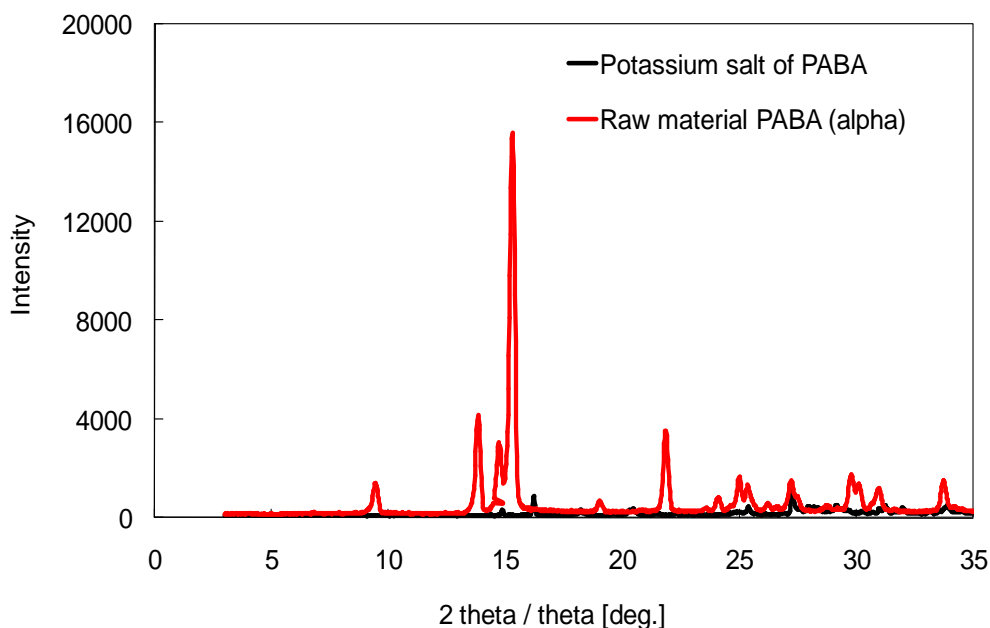


Figure 8.57. XRPD patterns for the potassium salt of PABA and the raw material form of PABA

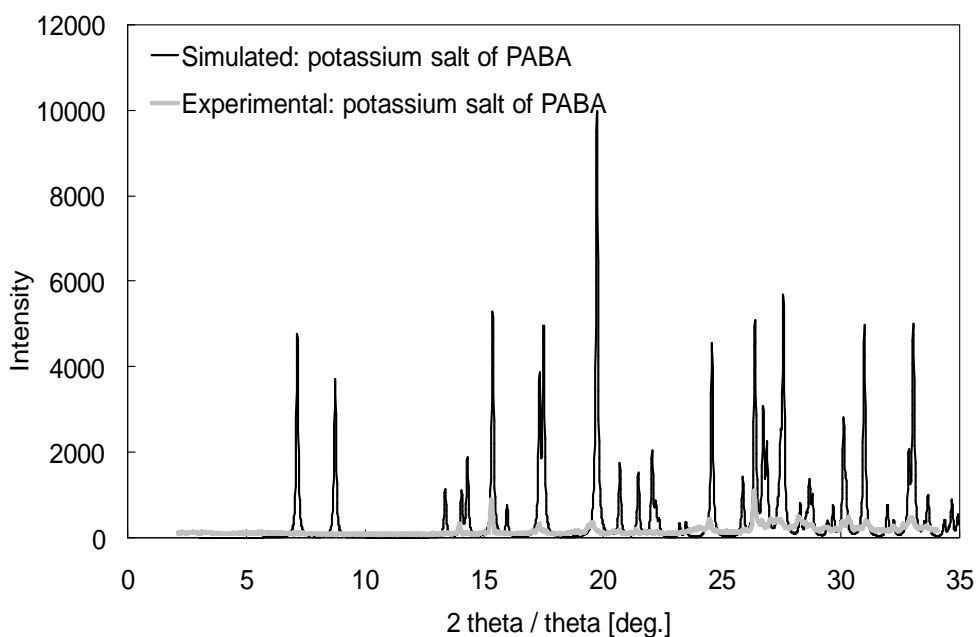


Figure 8.58. Simulated and experimental XRPD patterns for the potassium salt of PABA

DSC results for the potassium salt of PABA are shown in Figure 8.59. Three endothermic peaks appear at temperatures of 44 °C, 105 °C and 205 °C. The peak at 44 °C is thought to be due to moisture on the surface of the crystals. Repeats of DSC analyses showed that the broad peak at 105 °C consisted of two peaks indicating the dehydration of two hydrate forms. The peak at 205 °C could be the dehydration of a

third hydrate state or the melting of anhydrous potassium salt of PABA. As the temperature is low compared to the melting point of other salts the peak at 205 °C is thought to be due to dehydration of a third hydrated form of the potassium salt of PABA.

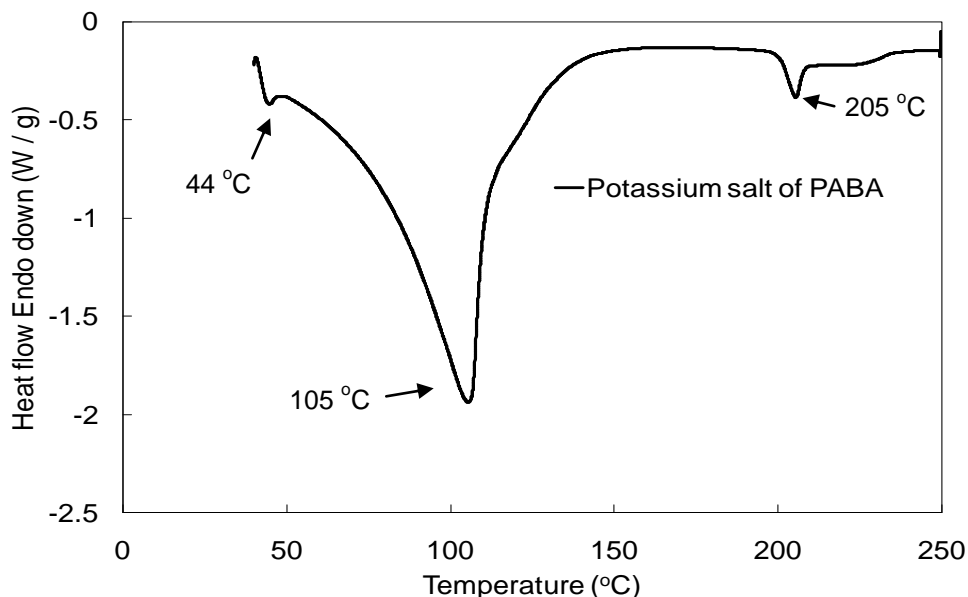


Figure 8.59. DSC results for the potassium salt of PABA

Solid state analyses including DVS and TGA were performed on the crystal samples re-crystallized from an ethanol/KOH solution to study the number and type of hydrate formation of the potassium salt of PABA.

TGA analysis is a useful tool in identifying the formation of hydrates and the type of hydrate by the extent of weight loss and the temperature range over which this occurs. Step changes in weight loss indicate the presence of more than one form of hydrate. TGA results for the potassium salt of PABA are shown in Figure 8.60. Two step changes in weight loss occur over the temperature range 20 to 210 °C. A 20.26 % weight loss occurs for the first step change until a temperature of 110 °C is reached. This weight loss is thought to represent the loss in weight of the two highest hydrated forms of the potassium salt of PABA. This prediction correlates with the results obtained from DSC analysis, which provided evidence of the dehydration of two hydrates at this temperature range. A second step change occurs over the temperature range of 160 to 210 °C showing a weight loss of 2.6%. The loss in weight is thought

to be due to the third hydrate state of the potassium salt of PABA. These results support the results obtained from DSC analysis, which showed a peak at 205 °C representing dehydration of a hydrate. From the % loss in weight the molecular ratio of salt to water is calculated for the lowest and highest hydrated forms of the salt. A sample calculation can be found in Appendix E. The lowest hydrated form of the potassium salt of PABA has a molecular ratio of salt to water of 1:0.26 indicating the formation of a channel hydrate and the highest hydrated form has a molecular ratio of salt to water of 1:3 (tri-hydrate). The hydrated form of the crystals reported by Salas-Cimingo (1968b) is a tri-hydrate. However, the simulated and experimental XRPD patterns as shown in Figure 8.58 are different, indicating that a different polymorphic form of the tri-hydrate crystallizes from ethanol solution (Tian *et al.*, 2010).

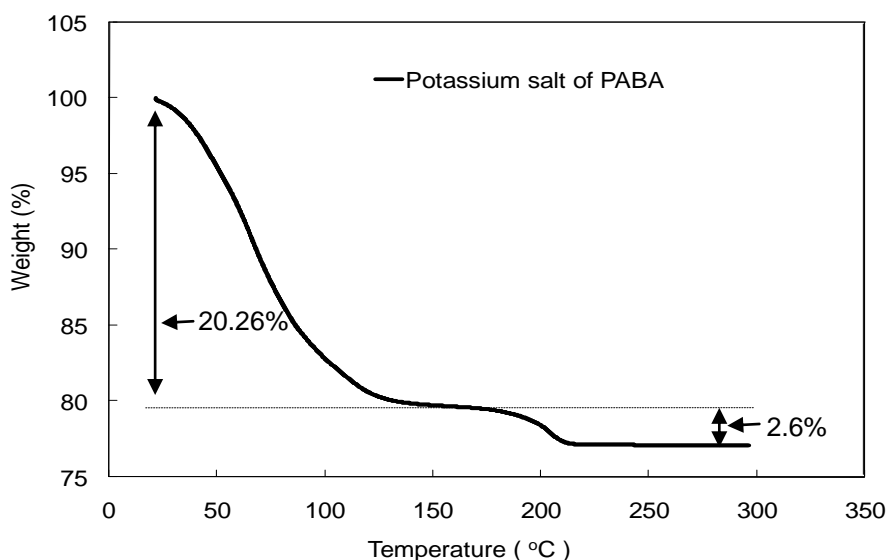


Figure 8.60. TGA results for the potassium salt of PABA

DVS results for the potassium salt of PABA are shown in Figure 8.61. At point 1 on Figure 8.61 there is a step change in mass indicating the formation of a hydrate. The molecular ratio of the potassium salt of PABA to water is calculated from the weight increase during the step change assuming that zero % in mass indicates the anhydrous form of the salt. A sample calculation can be found in Appendix E. The molecular ratio of the potassium salt to water is 1:1.2. This value is in between the lowest and highest hydrated form calculated from TGA analysis confirming that this hydrate is the intermediate meta-stable hydrate form of the salt. At point 2 on Figure 8.61 there is a step change during the desorption cycle indicating the formation of a

stoichiometric hydrate which forms at 60% relative humidity. The molecular ratio of potassium salt of PABA to water is 1:7. The step changes at points 3 and 4 on Figure 8.60 are thought to be due to water molecules building up on the surface of the crystal and not due to the formation of higher hydrates, as the system's mass does not reach a steady state before the relative humidity increases further. DVS analysis confirms that the potassium salt of PABA has a high tendency to form hydrates.

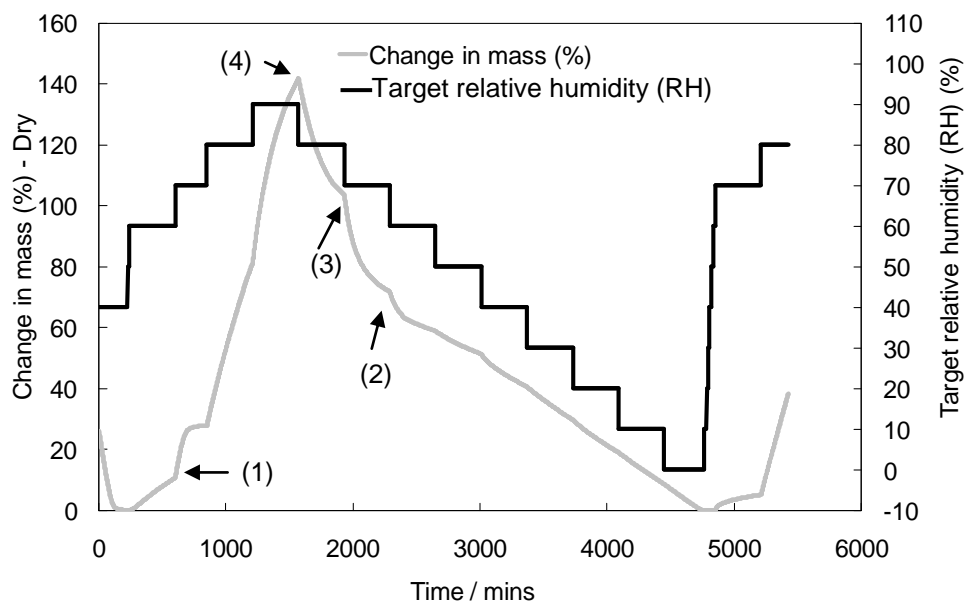


Figure 8.61. DVS results for the potassium salt of PABA

A wide range of solid state analytical techniques including the use of the optical microscope, XRPD, DSC, TGA and DVS were used to characterise the crystal samples re-crystallized from an ethanol/KOH solution by evaporation. XRPD confirmed the formation of the potassium salt of PABA. Microscopic images showed large salt crystals that would minimise the problems in downstream processing. DSC and TGA provided evidence of the formation of three hydrate forms of the potassium salt of PABA. The molecular ratio of the potassium salt to water for the three hydrates starting from lowest to highest hydrate is 1:0.26, 1:1.2 and 1:3 (tri-hydrate) respectively. The tri-hydrate produced experimentally from evaporation in ethanol is a different polymorphic form to the tri-hydrate reported in the Cambridge Structural Database, as shown from the differences in XRPD patterns, providing evidence of a new undiscovered tri-hydrate. The DVS confirmed that the potassium salt of PABA has a tendency to form higher hydrates.

8.6 Conclusions

A range of acidic and basic salts of PABA and MABA were produced using the method of evaporation, precipitation and cooling crystallization. The most suitable method for producing the salts is cooling crystallization which is a slow controlled process resulting in large crystals and prevents the formation of agglomerates, which was observed in the case of the precipitation experiments. PAT tools used to monitor the cooling crystallization experiments include the FBRM, ATR-UV/Vis, PVM and pH probes. Combining these tools enables the crystallization process to be designed to produce the desired form of the compound. Strong monoprotic acids including HCl and HBr were used to crystallize salts by cooling crystallization whereas the strong diprotic acid (H_2SO_4) and the weak triprotic acid (H_3PO_4) resulted in the salt crystals precipitating from solution. Acidic salts were found to crystallize at pH values below 3 and when using an organic solvent (ethanol). Strong and weak acids were used in each experiment to see whether the strength of the acid has any affect of the formation of salts. Hydrobromic salts of PABA and MABA form highly crystalline solids that are not hygroscopic in nature and do not have a tendency to form hydrates. Phosphoric acid which is the weakest of acids used in these experiments resulted in the crystallization of salts. Variation in mixing conditions using a 3-blade glass retreat curve in a 750 mL vessel and a magnetic stirrer in a beaker resulted in the crystals of the phosphoric salt of PABA with different morphologies. Comparison between predicted and experimental morphologies of salt crystals showed that the solvent (ethanol) affected the morphology of 4 out of a total of 6 salt crystals, indicating that solvent is an important parameter for designing a crystallization experiment. Alkali salts produced by evaporation at pH values above 8, including the sodium and potassium salts of PABA, were found to have a high tendency to form hydrates.

Chapter 9. pH controlled polymorphic crystallization

9.1 Introduction

Crystallization is a critical unit operation in the late stage of development of an API which is used for the separation and purification of the desired crystal form (Thompson *et al.*, 2005). Purity of the compound is an important property to control (Braatz *et al.*, 2002). pH and solvent are parameters that can affect the crystal form which nucleates from solution (Varshney *et al.*, 2007; Braun *et al.*, 2008; Reddy *et al.*, 2009).

The research presented in this chapter focuses on using PAT tools and SSA techniques to examine the effect of solvent and pH on the crystal form, which nucleates from solution. The model system used in this study is PABA and MABA. PABA is known to contain two polymorphic forms (alpha and beta) (Gracin and Rasmuson, 2004; Gracin *et al.*, 2005). Very limited data exists on the crystallization of MABA. It has been reported that MABA has a tendency to form hydrates (He *et al.*, 2005). From this thesis research work solid state analytical techniques including the use of the optical microscope, XRPD and solid state IR spectroscopy provided evidence that salts of PABA and MABA do not form when using water as a solvent or when using an ethanol solution at pH value above 3. DSC provided data on the melting point of crystal forms and detected a new undiscovered meta-stable form of MABA. PAT tools used to monitor the crystallization process include FBRM, ATR-UV/Vis, PVM and pH probe. PVM provided in-situ images of the crystals in real-time, indicating the formation of different forms of the crystalline compound. FBRM and ATR-UV/Vis detected changes occurring during the crystallization process which were originally thought to be due to a polymorphic transformation. Further analysis using a range of solid state analytical techniques confirmed that two different forms of the compound PABA crystallized resulting in an impure product. Combined PAT tools and SSA techniques have been used to increase process understanding that can prevent misinterpretation of results and provide the experimental conditions to produce the desired pure form of the compound.

9.2 Experiments performed

Cooling crystallization experiments were performed within a 750 mL vessel using the model systems PABA and MABA. Variations were made to both pH and solvent to examine the effect of these parameters on the formation of salts. Section 3.2 of Chapter 3 lists the material used including acids/bases, solvents and the molarities of each acid/base used. The experimental conditions including all PAT tools used and a detailed experimental methodology are discussed in Section 3.4.4 of Chapter 3. A schematic of the crystallization rig is shown in Figure 3.3 of Chapter 3. Only experiments discussed in Section 9.6 use the ATR-UV/Vis probe.

9.3 Evaluation of pH sensitivity and effect of solvent on the crystallization of MABA and the discovery of a new polymorphic form of MABA

Cooling crystallization experiments were performed for MABA in water at pH=3 and in ethanol at pH=4.1. The acid used to achieve the desired pH of solution is hydrochloric acid. PAT tools used to monitor the crystallization experiment include the FBRM, pH and PVM probe. A single nucleation event is observed during both experiments by an increase in the FBRM counts. When using water as a solvent nucleation occurs after the system was cooled to 5 °C and kept at this temperature overnight. Nucleation is a slow process as represented by a gradual increase in FBRM counts as shown in Figure 9.1. Nucleation occurs very rapidly when using ethanol as a solvent, which is represented as a sharp increase in FBRM counts as shown in Figure 9.2.

PVM images of crystals during the cooling crystallization of MABA from ethanol at pH=4.1 are shown in Figure 9.3. The raw material form of MABA consists of small fine needles and once HCl acid is added to solution this forms star shape agglomerates as shown by Figure 9.3 (a). Nucleation at conditions of pH=4.1 results in the form of long fibrous needles as shown in Figure 9.3 (b). These images are similar to the raw material which suggests possible the formation of the same polymorphic form.

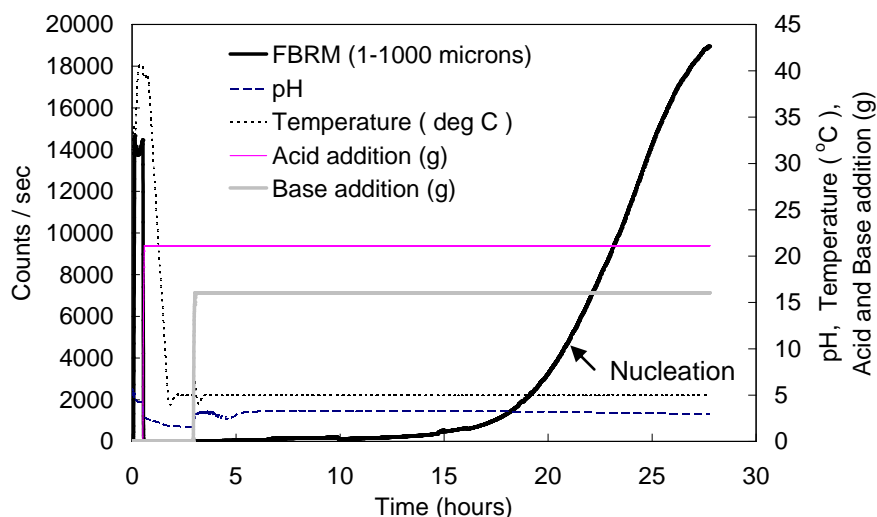


Figure 9.1. Results for the cooling crystallization of MABA from water at pH=3

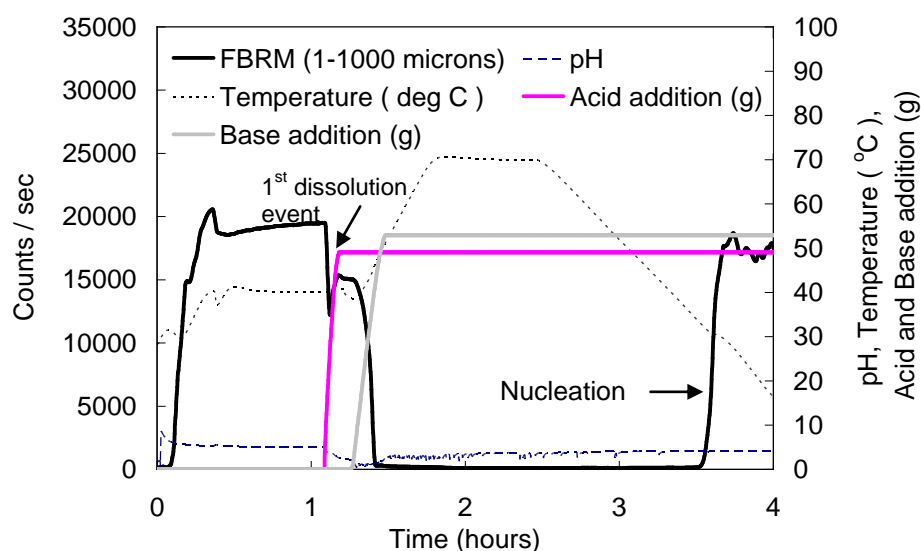


Figure 9.2. FBRM results for the cooling crystallization of MABA from ethanol at pH=4.1

After filtration the crystals form agglomerates, which appear grey in colour after re-crystallizing from water and white when re-crystallized from ethanol. These crystals appear different to the raw material form of MABA, which is in a white powder form. A range of solid state analytical techniques were performed on crystal samples to identify the crystal form which nucleated from solution.

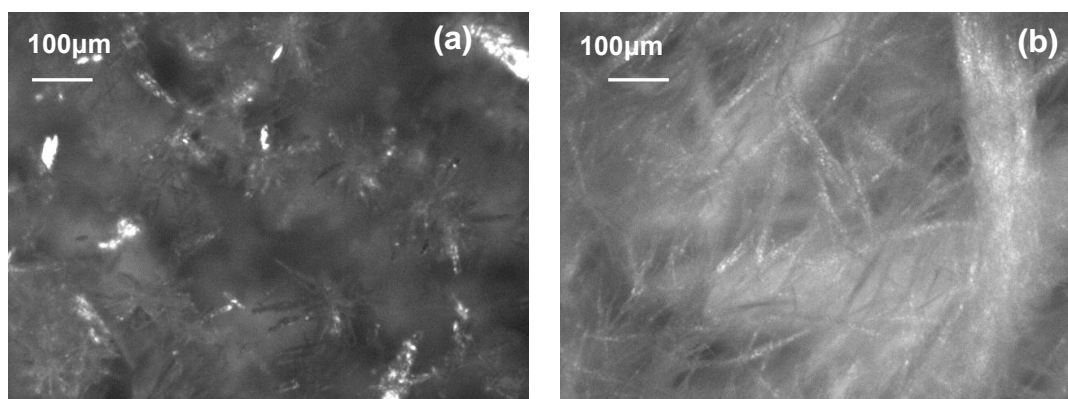


Figure 9.3. PVM images of (a) MABA crystals during the first dissolution event (see Figure 9.2) showing the formation of agglomerated needles and (b) crystals nucleated from ethanol solution at pH 4.1

The morphology of the crystals is an important parameter, which can affect the downstream processing including filtration and drying. The morphology of the raw material form of MABA and sample re-crystallized from water at pH=3 are in the form of fine needles as shown in Figure 9.4. Images of crystals re-crystallized from ethanol at pH=4.1 are similar to those shown in Figure 9.4 (b).

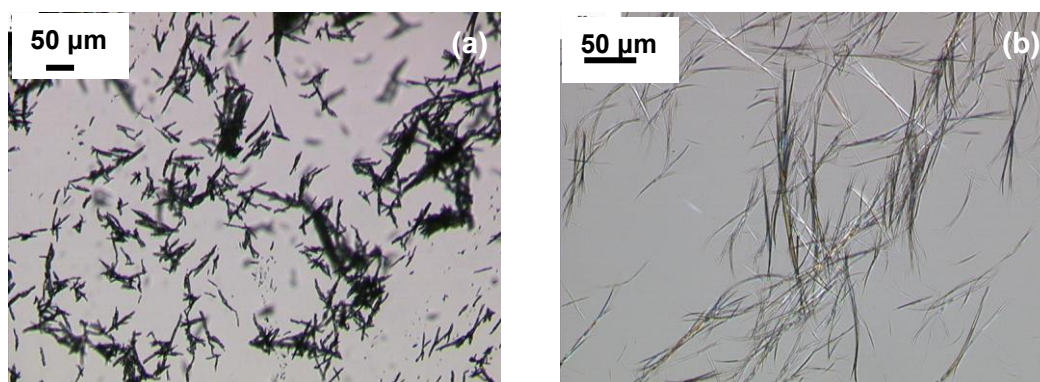


Figure 9.4. Optical microscope images of (a) raw material form of MABA and (b) MABA re-crystallized from water at pH=3

XRPD patterns for the raw material form of MABA, sample re-crystallized from water at pH=3 and sample re-crystallized from ethanol at pH=4.1 are shown in Figure 9.5. Patterns for the three samples are very similar indicating that the samples re-crystallized from water and ethanol are of the same form as the raw material.

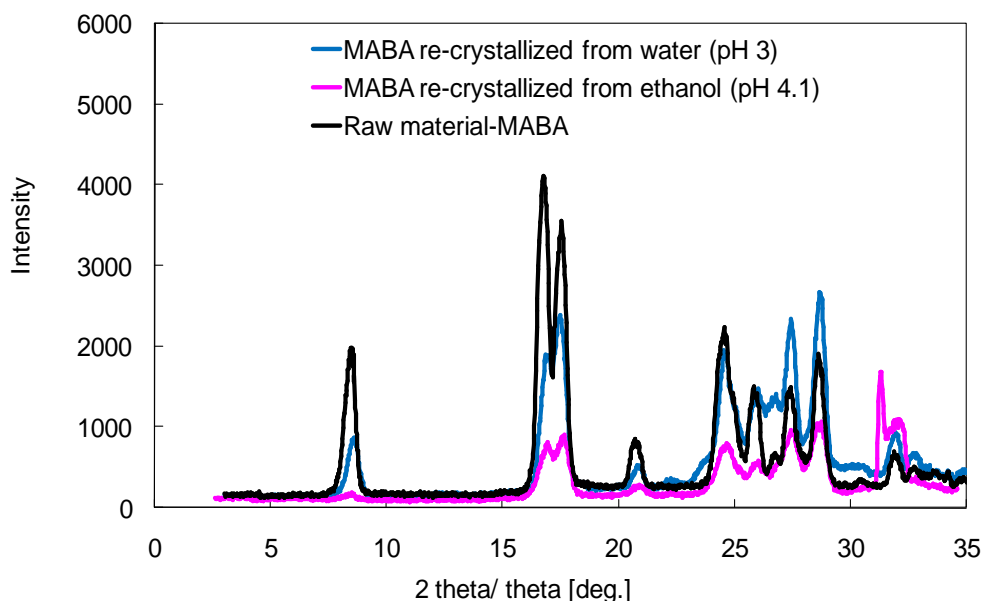


Figure 9.5. XRPD patterns for the raw material form of MABA, sample re-crystallized from water at pH=3 and ethanol at pH=4.1

IR spectra for the raw material form of MABA, samples re-crystallized from water at pH=3 and ethanol at pH=4.1 are shown in Figure 9.6. The broad peak at 2950 and 2962 cm^{-1} is due to the vibrations of the (O-H) bond of the carboxylic acid within the molecule. The sample of MABA re-crystallized from water forms agglomerates resulting in water molecules trapped on the surface of the crystals. The broader peak observed at 2962 cm^{-1} for MABA re-crystallized from water is thought to be due to the presence of hydrogen bonds formed between water and MABA molecules, which absorb in the range of 2500 and 3500 cm^{-1} (Stuart *et al.*, 1998). The fingerprint region of wavelength range 400-1500 cm^{-1} is very similar for all samples indicating that the samples are of the same form. A recent report on MABA states the IR spectra for two different polymorphic forms including Form I which is stable and Form II which is meta-stable at ambient temperature (Svard *et al.*, 2010). The IR spectra of all samples from these experiments are similar to Form I indicating the nucleation of the stable form (Svard *et al.*, 2010).

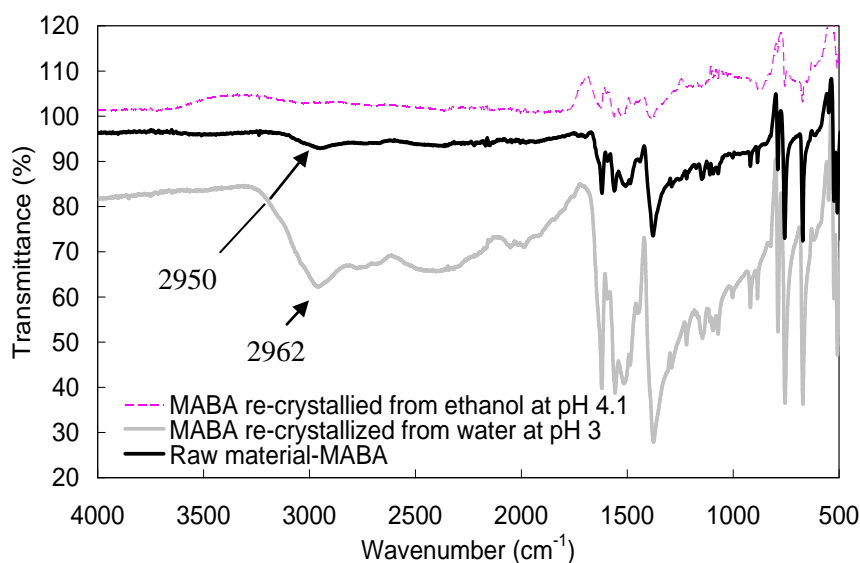


Figure 9.6. IR spectrum for raw material form of MABA, sample re-crystallized from water at pH=3 and sample re-crystallized from ethanol at pH=4.1

DSC analysis is performed on the raw material for of MABA and the samples re-crystallized from water at pH=3 and ethanol at pH=4.1 to provide data on the melting point of the crystals. DSC results for two different batches of raw material form of MABA were performed using different ramp rates and the results are shown in Figure 9.7

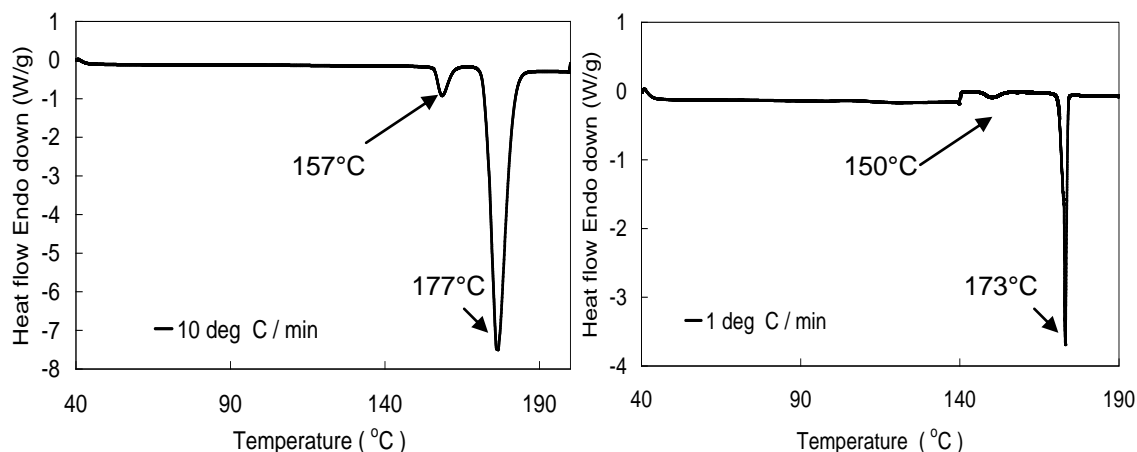


Figure 9.7. DSC results for the raw material form of MABA

For both repeats two peaks are observed at temperatures in the range of 150-157 °C and 173-177 °C. The first small peak at 150-157 °C is thought to be due to a

polymorphic transformation from stable to meta-stable form, which then melts at a temperature in the range 173-177 °C. The two polymorphic forms of MABA are enantiotropic with a transition temperature of approximately 156 °C. The raw material form of MABA at room temperature is the stable form and is in the form of a very fine powder, which results in complete conversion from stable to meta-stable form at a transition temperature 150-157 °C.

Differential scanning calorimetry results for repeated samples of MABA re-crystallized from water are shown in Figure 9.8. Sample preparation required grinding the crystals from light grinding to intense grinding, in which the consistence was similar to the raw material (powder form). Both DSC plots show a small peak at 157 °C which is due to the polymorphic transformation from stable to meta-stable form. As the filtered and grinded crystals are in the form of small agglomerates only a proportion of the sample transforms at the transition temperature (157 °C) resulting in a mixture of stable and meta-stable form. This stable form then melts at 170 °C. An exothermic peak at 172 °C appears in the DSC results for the sample that was lightly grinded, which is due to the re-crystallization of the meta-stable form. This form then melts at a peak of 177 °C. Similar results are reported in previous literature (Bernstein 2002). Grinding the sample from lightly to intense (powder form) resulted in a larger percentage of conversion from stable to meta-stable form, which is shown in the DSC results by a decrease in melting enthalpy from 75 to 43 J/g at the melting of the stable form (170 °C) and an increase in melting enthalpy from 149 to 186 J/g at the melting of the meta-stable form (177 °C). The melting points of the two forms are very close and therefore due to kinetics an exothermic peak (re-crystallization of meta-stable form) does not appear in the DSC results for the intense grinded sample or the presence of the stable form is very low and therefore there is not enough supersaturation available for the meta-stable form to re-crystallize from the melt.

DSC analysis is performed on crystal samples re-crystallized from ethanol at pH=4.1 and very similar results are observed as for the case when water was used as the solvent. Three endothermic peaks occur at temperatures of 148, 171 and 178 °C as shown in Figure 9.9. The peak at 148 °C is thought to be due to a polymorphic transformation from stable to meta-stable form, which does not undergo complete conversion due to the formation of agglomerates, resulting in a mixture of two forms.

The stable form melts at 171 °C and the meta-stable form melts at 178 °C. A recent report on MABA (Svard *et al.*, 2010) showed similar findings to these results, supporting the predictions and confirming the existence of two polymorphic forms of MABA.

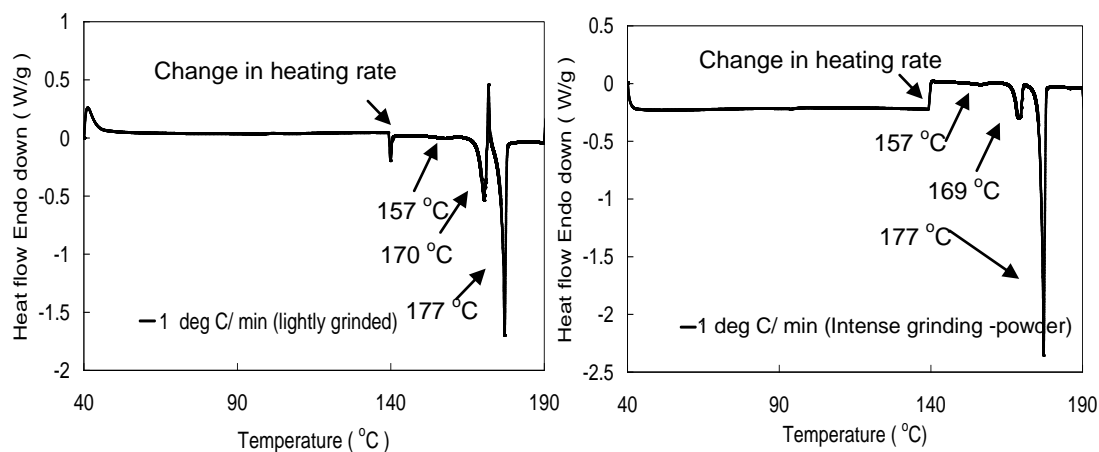


Figure 9.8. DSC results for samples of crystals re-crystallized from water at pH=3 for lightly and intense grinding

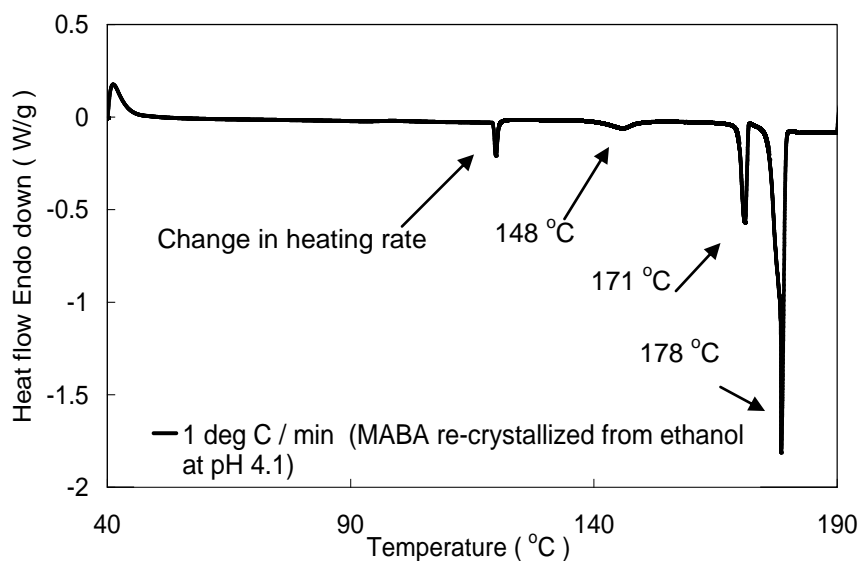


Figure 9.9. DSC results for MABA re-crystallized from ethanol at pH=4.1

TGA results for the raw material form of MABA, sample re-crystallized from water at pH=3 and ethanol at pH=4.1 are shown in Figure 9.10. As the samples are heated from room temperature to 150 °C there is no change in weight loss indicating the presence of the anhydrous form. There is a significant decrease in weight percentage at the transition temperature of the two polymorphs of MABA at 155 °C, which is

below the melting point of the two polymorphic forms. At this point the stable form transforms to the meta-stable form and a process of sublimation occurs resulting in a large decrease in weight. This is in correlation with results in the literature stating that MABA sublimates before melting (Rotich *et al.*, 2001).

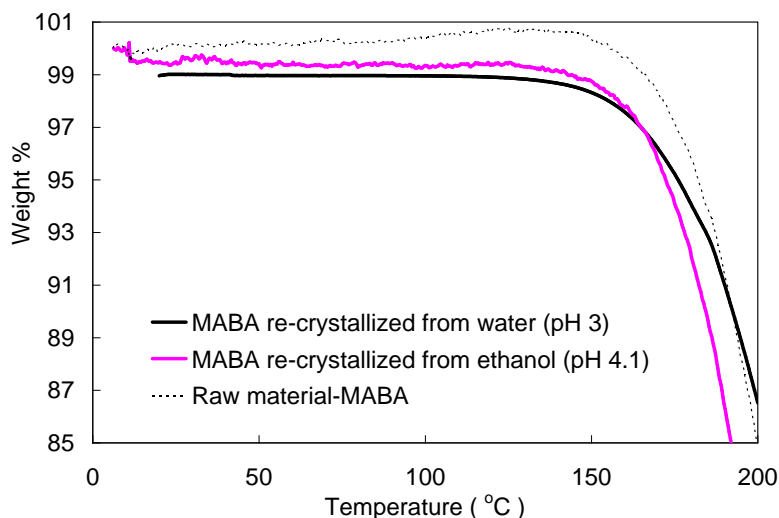


Figure 9.10. TGA plots for (a) raw material form of MABA and (b) MABA re-crystallized from water at pH=3

Process analytical technology tools were used to monitor the crystallization process. FBRM detected the experimental conditions for which each system nucleated. A pH probe was used to monitor and control the pH of the system, so that nucleation occurred at a low pH (acidic conditions). Solid state characterisation of the crystals provided evidence that a salt does not form when using water as a solvent or when an organic solvent (ethanol) is used at pH=4.1. DSC analysis provided evidence that there are two different polymorphic forms of MABA which are enantiotropic related with a transition temperature of 157 °C. TGA confirmed that at the transition temperature sublimation occurs. XRPD and solid state IR analysis provided evidence that the stable form of MABA nucleated from solution when using water at pH=3 and ethanol at pH=4.1. These results are in correlation with results obtained from Svard (2010) who also confirmed the nucleation of the stable form from solvents of water and methanol.

9.4 Application of PVM for identifying the crystallization conditions of different forms of compounds of MABA

PVM probe captures images of the crystals during the crystallization process while the optical microscope is an off-line solid state technique requiring sample removing from process stream. Changes in conditions of temperature and relative humidity can affect the stability order of different polymorphic forms of a compound which may have a different morphology. Transformations between the different forms after removal of samples from process stream can lead to misinterpretation of results obtained from the optical microscope images. PVM and optical microscope images of MABA re-crystallized from ethanol solution at pH=1.5 using hydrobromic acid (HBr) are shown in Figure 9.11. PVM shows a diamond shape crystal forms upon nucleation which is similar to the optical microscope images as shown in Figure 9.11b. The morphology of the crystals are different to the raw material, which has a needle shape (see Figure 9.4a), providing supporting evidence that possibly a salt forms under very acidic conditions ($\text{pH} < 2.5$). FBRM data which support these results is shown in Figure 8.10 of Chapter 8.

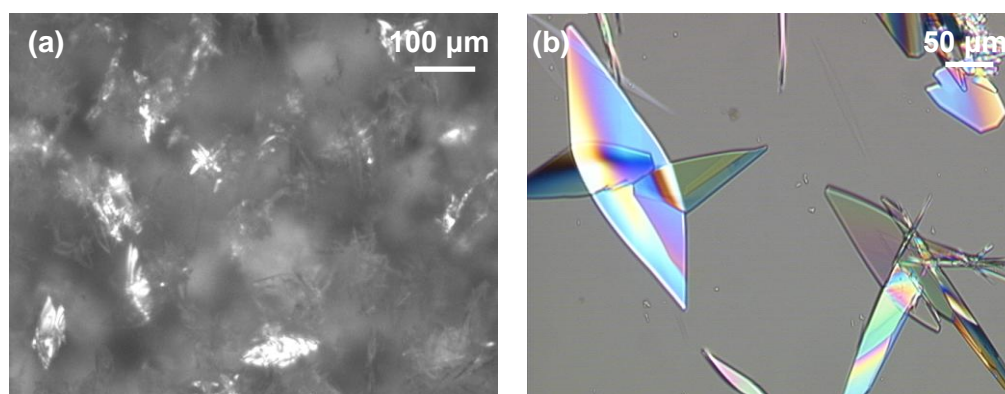


Figure 9.11. (a) PVM and (b) optical microscope image of MABA re-crystallized from ethanol at pH=1.5 using HBr acid

PVM images of MABA re-crystallized from ethanol at pH=2.5 using HCl acid are shown in Figure 9.12. PVM images show a change in morphology from fine needles to small rod shape crystals forming agglomerates once acid is added to solution. Images 9.12c and d show long rod shape crystals during nucleation. These images are

similar to the optical and scanning electron microscope images as shown in Figure 8.4 of Chapter 8. PVM images provide supporting evidence of the formation of the HCl salt of MABA under acidic conditions of low pH of 2.5 when using an organic solvent (ethanol). FBRM data which supports these results is shown in Figure 8.3 of Chapter 8.

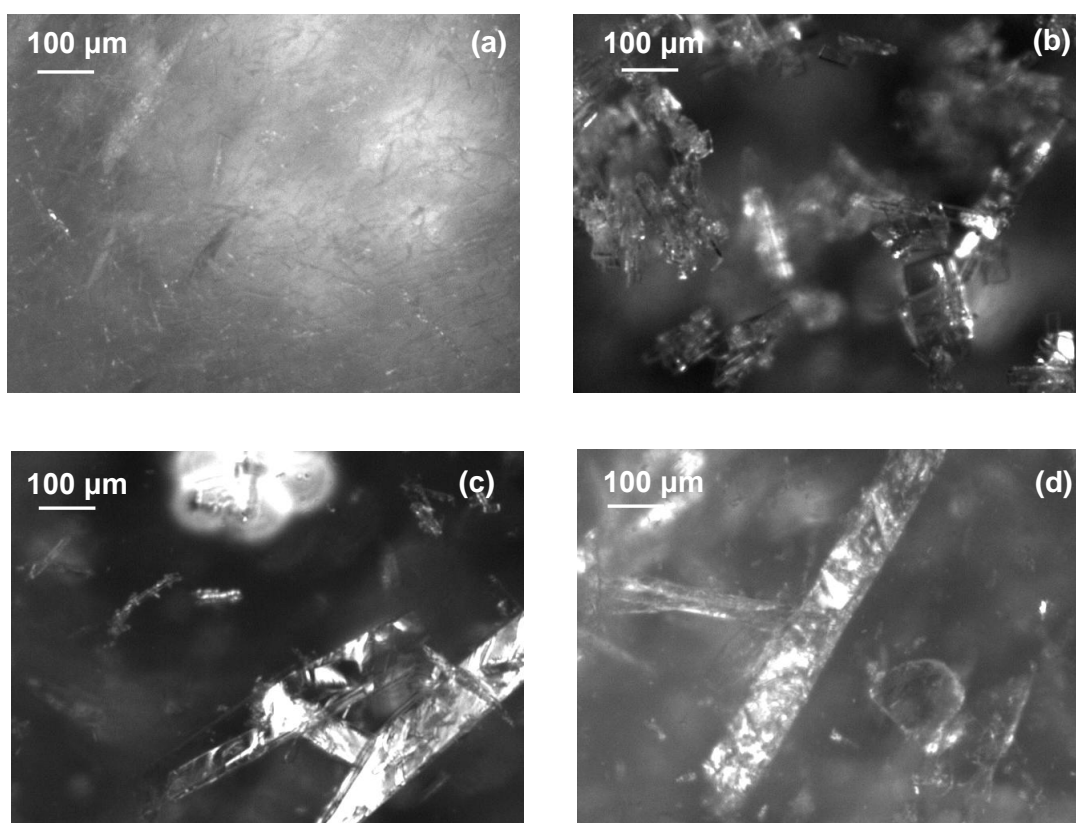


Figure 9.12. PVM images of (a) raw material form of MABA, (b) crystals after HCl acid has been added to solution and (c,d) crystals after nucleation

PVM images provide supportive information on the experimental conditions required to produce different salts forms of MABA. Differences in morphology from the starting material, indicates the presence of the salt. HCl salt of MABA shows long rod shape crystals while HBr salt of MABA is a diamond shape. Both these morphologies are desirable for further scale up, eliminating the problems in downstream process such as blockage of filter due to very fine crystals or needles.

9.5 Evaluation of pH sensitivity and effect of solvent on the crystallization of PABA

Crystallization experiments were performed using the pH swing method and cooling. Crystallization of PABA using the pH swing method involved the addition of a base (NaOH) to dissolve the crystals and then acid (HCl) was added to the solution resulting in re-crystallization of the compound. Water was used as the solvent. The temperature was kept constant at 20 °C. Nucleation occurred at pH=4.7 and the pH of the final solution in which crystals were suspended in solution was 3.6. FBRM results of the pH swing crystallization experiment are shown in Figure 9.13. A single nucleation event is detected by the FBRM probe as shown by a sudden change in the FBRM counts followed by a gradual increase in counts indicating additional nucleation.

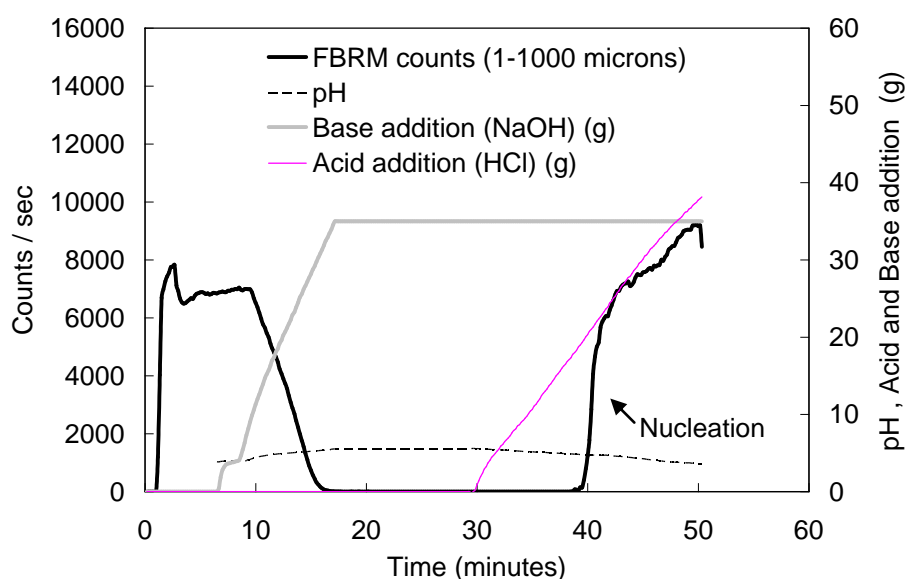


Figure 9.13. FBRM results for the pH swing crystallization experiments using water solution

Cooling crystallization experiments were performed using water as the solvent. HCl and NaOH were added to solution to control the pH at a value of 2.6 in which nucleation occurred. The process was repeated at a higher pH value of 5.9. FBRM results show a single nucleation event during crystallization, at the desired pH values of 2.6 and 5.9, indicated as a sudden increase in FBRM counts as shown in Figure 9.14.

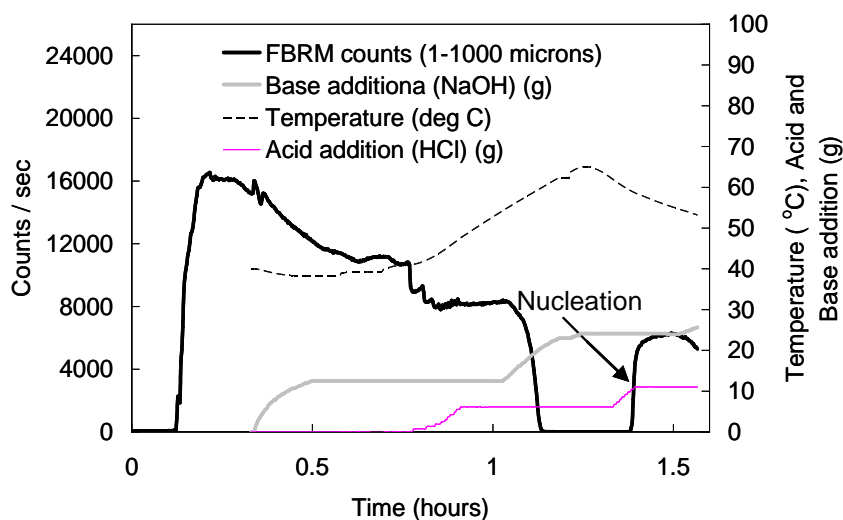


Figure 9.14. FBRM results for the cooling crystallization of PABA from water at pH=5.9 using HCl

Samples from both pH swing and cooling crystallization experiments were removed from the process stream after nucleation and analysed using a range of solid state techniques to identify the crystal form. Optical microscope images of the crystals are shown in Figure 9.15. Images show long needles which are similar to the raw material form of PABA (alpha form).

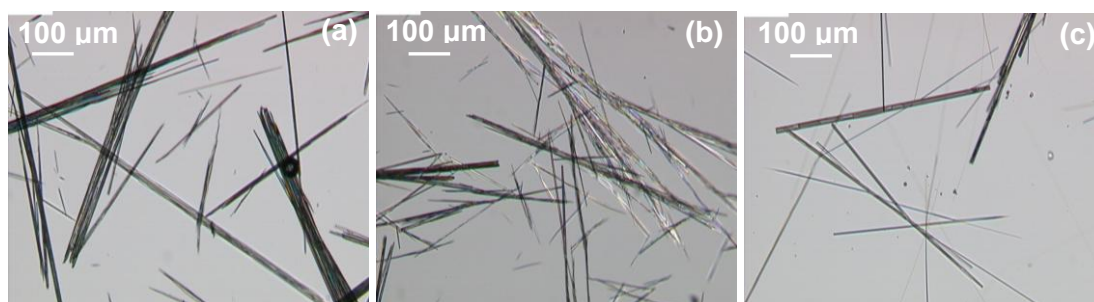


Figure 9.15. Optical microscope images of PABA re-crystallized from water at different values (a) pH=2.5, (b) pH=3.6 and (c) pH=5.5 using hydrochloric acid

XRPD patterns of the sample re-crystallized from water at pH=2.6, 3.6, 5.9 and the raw material form of PABA (alpha) are shown in Figure 9.16. The XRPD patterns are very similar indicating the formation of the alpha form of PABA from water within the pH range 2.6-5.9.

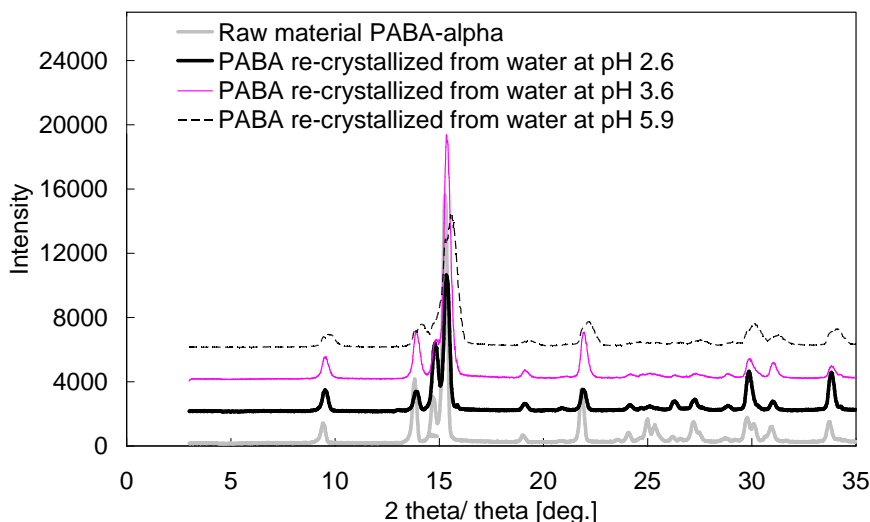


Figure 9.16. XRPD patterns for PABA re-crystallized from water within pH range of 2.6 to 5.9 using hydrochloric acid (HCl) and the raw material form of PABA. Intensities are shifted for clearer plotting

Solid state characterisation of the crystals which nucleated from water at pH ranges 2.6-5.9 provided evidence of the formation of the alpha form of PABA. At pH values below 3 the (NH_3^+) species within the molecule are 100% ionising indicating the likelihood of acidic salt formation (see Chapter 8). However for the cooling crystallization experiment of PABA from water using a pH value of 2.6 the salt does not form indicating that water is not a suitable solvent to crystallize salts. Cooling crystallization experiments were repeated using an organic solvent such as ethanol at pH value of 5.5. The acid and base used to achieve the desired pH of solution were HCl and NaOH. FBRM results for the cooling crystallization of PABA from ethanol solution at pH=5.5 are shown in Figure 9.17. FBRM results show a large decrease in counts at the start of the experiment which is due to a combination of heating and diluting the system with the addition of acid and base to maintain the pH of solution at a set point value of 5. Once a maximum temperature of 70 °C is reached the FBRM counts decrease to 1300 indicating the presence of crystals in solution. Fluctuations in pH around the set point value of 5 results in the continuous addition of acid and base to the solution, which causes a fluctuation in FBRM counts as the system is kept at a constant temperature of 70 °C. The increase in counts occurs as acid is added to the solution, which is thought to be due to the formation of the NaCl salt or HCl salt of PABA. As base (NaOH) is added to solution this results in a decrease in counts, which is due to diluting the system and increasing the solubility. The cycle was

repeated, resulting in the fluctuation in FBRM counts, until the system becomes undersaturated and all the crystals dissolve as shown by the zero counts in the FBRM reading. A single nucleation event is detected by a sudden increase in FBRM counts after 4 hours from the start of the experiment followed by a gradual increase in counts indicating additional nucleation. PVM probe is used to monitor the crystallization process providing images of the crystals in real time. These images are shown in Figure 9.18.

The raw material form of PABA is in the form of small needles, which forms agglomerates due to the high density of solution as shown in Figure 9.18 (a). During heating the crystals start to dissolve and the solution becomes less dense. Figure 9.18 (c) shows images of very fine particles which form agglomerates. These images are obtained as the system is kept constant at 70 °C and there is a continuous addition of acid/base causing a fluctuation in FBRM counts. At this point it is thought that either the NaCl salt or HCl salt of PABA forms. The solubility of sodium chloride in water at 70 °C is 378 g/L (Perry and Green, 1998). Calculations were made on the concentration of NaCl in water at an approximate time of 1.5 hours from start of experiment in which the fluctuation in FBRM counts occurred (see Figure 9.17). The calculation showing the individual steps can be found in Appendix F. As this point the concentration of NaCl in water is 174.4 g/L, which is below the solubility value of 378 g/L indicating an undersaturated solution. This supports the prediction that the fluctuation in FBRM counts is due to the formation of the HCl salt of PABA and not the NaCl salt.

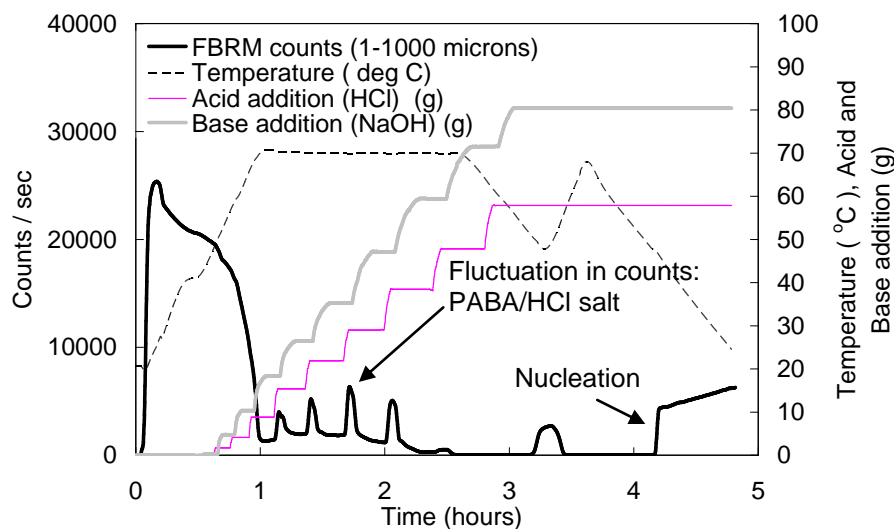


Figure 9.17 FBRM results for the cooling crystallization of PABA from ethanol at pH=5.6

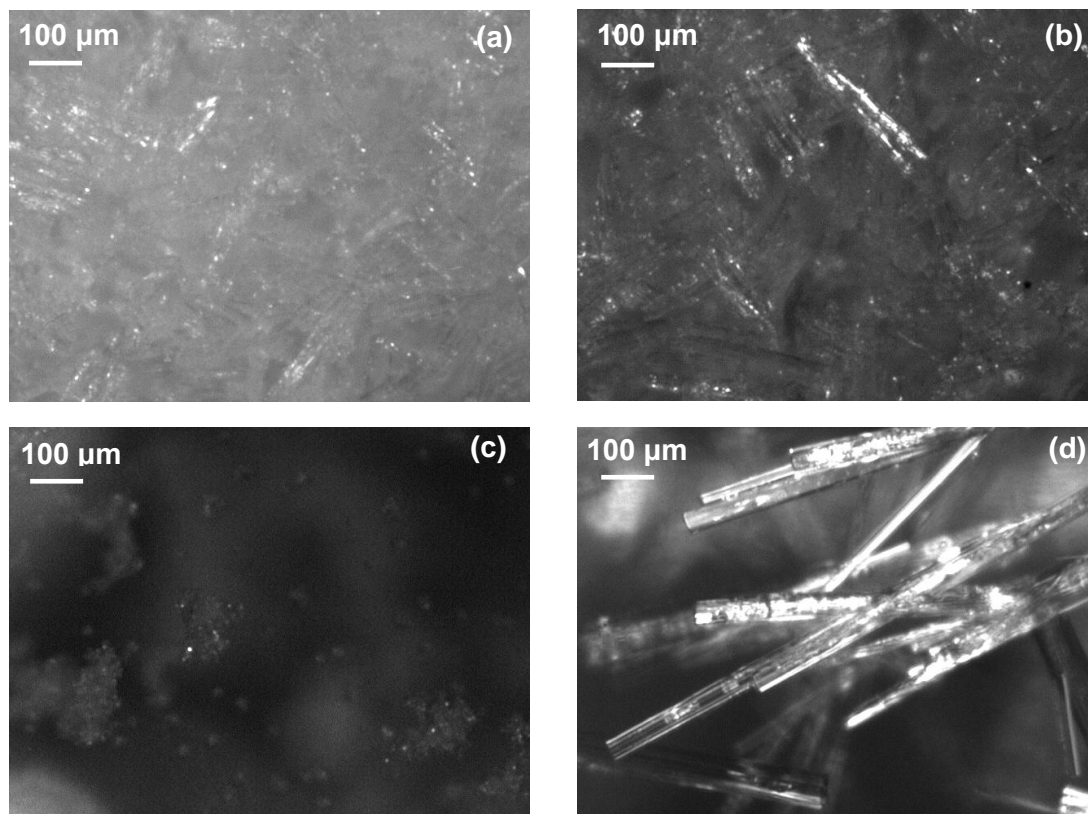


Figure 9.18. PVM images of crystals during different stages of the crystallization experiment for PABA in ethanol at set point pH=5 showing (a) raw material form of PABA (needle morphology), (b) dissolution of needles during heating phase, (c) salt formation at temperature 70 °C and (d) nucleation at pH=5

Crystal samples are removed from the process stream after nucleation at pH=5.6 and analysed using a range of solid state techniques including the optical microscope and XRPD. Optical microscope images of the crystals are shown in Figure 9.19. The image shows large needles of size greater than 400 μm, which are similar to the image shown in Figure 9.18 (d).

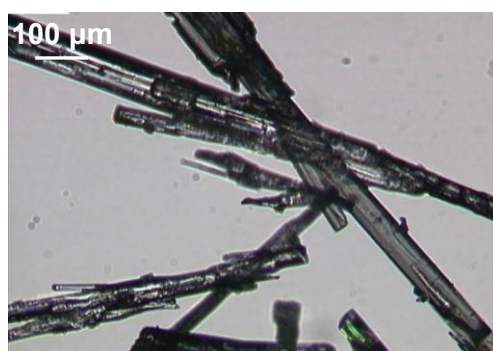


Figure 9.19. Optical microscope images of crystals nucleated from ethanol solution at pH=5.6

Figure 9.20 shows the XRPD patterns for the sample nucleated from ethanol at pH=5.6 and the raw material form of PABA (alpha). Both patterns are similar indicating the formation of this form.

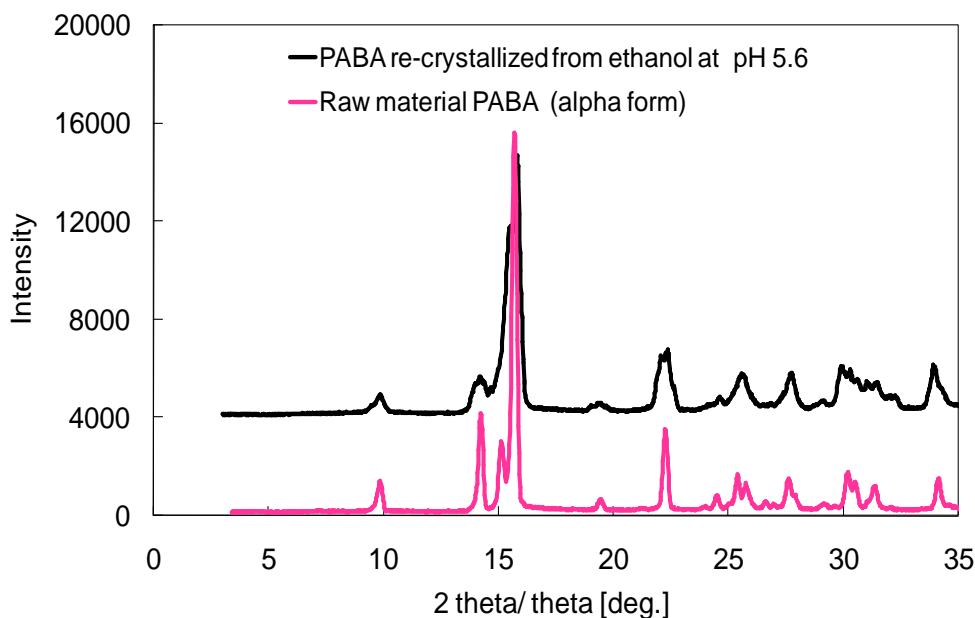


Figure 9.20. XRPD patterns for PABA re-crystallized from ethanol at pH=5.6 and the raw material form of PABA (alpha). Intensities are shifted for clearer plotting

Solid state analytical techniques provided evidence that the alpha form of PABA nucleates from ethanol solution at pH=5.6. Using a combination of PAT tools including the FBRM and PVM probe to monitor the crystallization process provided additional information to understanding the process. The starting solvent is pure ethanol but as diluted forms of acid and base are added to solution this results in a water/ethanol mixture. Due to this reason and as the pH is above a value of 3 this reduces the likelihood of the formation of a salt.

Cooling crystallization experiments for the model system PABA were performed at different conditions of pH and solvent choice. A combination of PAT and SSA techniques were used to monitor the crystallization process and to characterise the crystal product. Single nucleation events were detected with the FBRM probe and the PVM provided images of crystals during the process. SSA of the crystals provided evidence that the alpha form of PABA nucleated from water at pH range 2.5-5.9 indicating that this is not a suitable solvent for crystallizing the salt. Cooling

crystallization of PABA from ethanol at pH of 5.9 also produced that alpha form indicating that the pH must be low (below 3) for salt production.

9.6 Application of PAT tools for monitoring the pH mediated crystallization of mixtures of PABA and the HCl salt

PAT tools including the use of the FBRM, PVM and ATR-UV/Vis spectrometry are used to monitor the cooling crystallization of PABA from an ethanol solution at pH=2.5. Excess moles of PABA are added to solution compared with the moles of HCl acid. UV/Vis data shows a peak absorbance for the HCl salt of PABA at 295 nm and for PABA (alpha form) at 301 nm as shown in Figure 9.21. FBRM and UV/Vis results for the cooling crystallization experiment are shown in Figure 9.22.

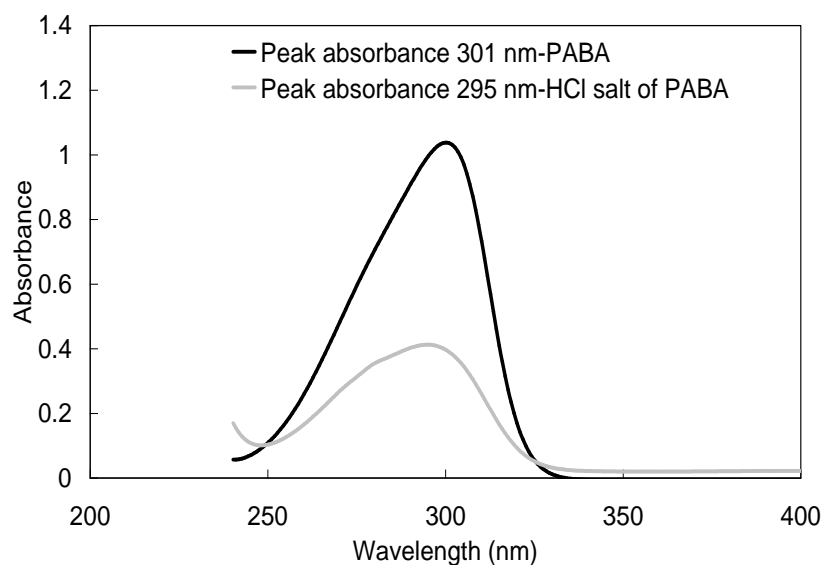


Figure 9.21. UV/Vis spectrum for PABA and the HCl salt of PABA

The sharp increase in both FBRM signal and absorbance at the start of experiment is due to the addition of solid to solution. FBRM and UV/Vis detects two dissolution events. At the moment acid (HCl) is added, the crystals dissolve as shown by a sharp decrease in the FBRM signal and sharp increase followed by a sharp decrease in absorbance at wavelength range 294-301 nm (see point (1) on Figure 9.22). The increase in absorbance is due to the PABA dissolving. As acid is added to the solution this reacts with PABA to form the salt which has a lower absorbance within the

wavelength range 295-301 nm compared to PABA causing the absorbance to decrease during acid addition. This prediction is supported with PVM images which show a change in morphology from needles to rod shape during the first dissolution event as shown in Figure 9.23 (a) and (b). Sodium hydroxide (NaOH) is added at point (2) on Figure 9.22 to dissolve all the crystals forming a clear solution of pH=2.5. The system is then cooled down at a ramp rate of 0.6 °C/min. Two nucleation events were detected by the FBRM probe showing a gradual increase in counts followed by a sharp increase in counts. The first nucleation event is due to the formation of the HCl salt of PABA and the second nucleation event is due to the formation of PABA as there was not enough acid in solution for all of the PABA to react to form the salt. During the first nucleation event the absorbance should decrease but it increases. This is thought to be due to a combination of crystals sticking to the probe window as water is present in solution and the temperature decreasing having a greater effect on the absorbance than the crystal form that nucleates from solution. A significant decrease in absorbance was detected during the second nucleation event, which is justified due to PABA absorbing to a larger extent compared to the salt within wavelengths of range 295-301 nm. PVM images of the crystals during the two nucleation events are shown in Figure 9.23 which support the prediction based on the FBRM results. Rod shape crystals form from the first nucleation event as shown in Figure 9.23 (c) and needles form during the second nucleation event as shown in Figure 9.23 (d).

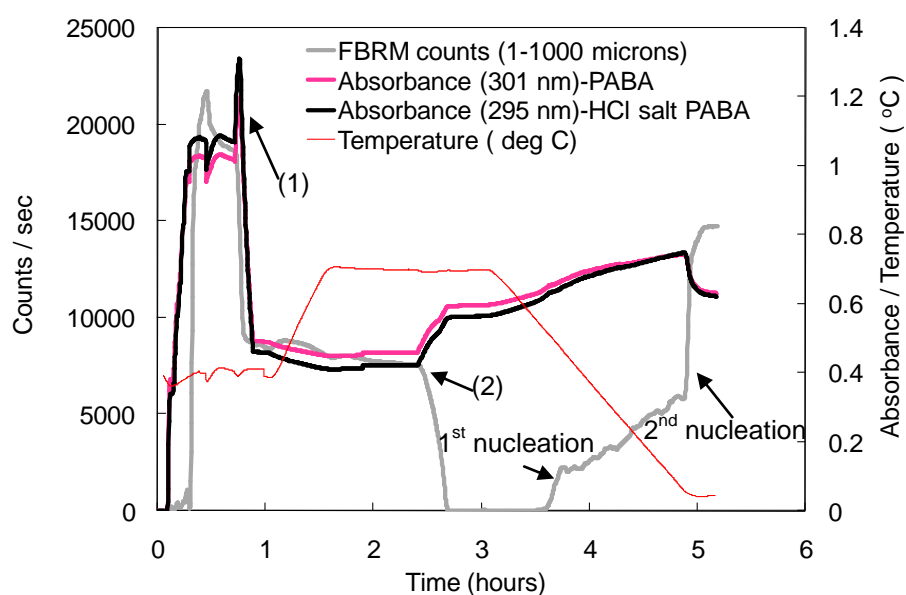


Figure 9.22. FBRM and UV/Vis results for the cooling crystallization of PABA from ethanol at pH=2.5 in which the moles of PABA is greater than HCl acid

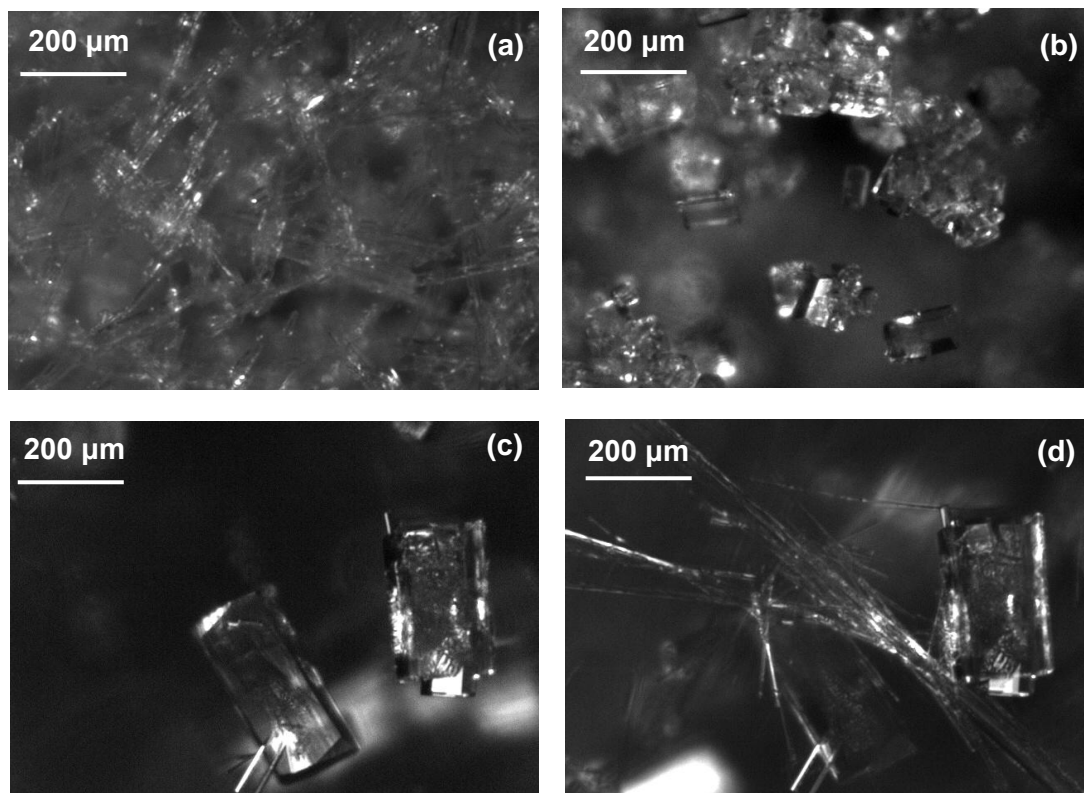


Figure 9.23. PVM images of (a) raw material PABA, (b) salt formation during the 1st dissolution event, (c) salt formation during the 1st nucleation event and (d) mixture of salt and PABA for the 2nd nucleation event

The morphology of the crystal samples obtained after the first and second nucleation events are viewed using the optical and scanning electron microscope. Figure 9.24 (a) shows the optical microscope image of the crystals obtained from the first nucleation event. The morphology of the crystals is rod shaped with longest dimension greater than 200 μm. The crystals are fine particles, which are pink in colour with a sparkling tint as shown in Figure B1 of appendix B. Optical microscope images of the crystals obtained after the second nucleation event are shown in Figure 9.24 (b). The morphology of the crystals is similar to the alpha form of PABA with needles of size greater than 300 μm. The clear difference between the morphology of the two crystal samples indicates the formation of two different forms. The hydro-chloride salt of PABA shows a rod shape while the alpha form of PABA has needle morphology. Figures 9.24 (c) and (d) show SEM images of a mixture of the salt (rod shape with a hexagonal face) and the alpha form of PABA (needles) which is present on the surface of the salt.

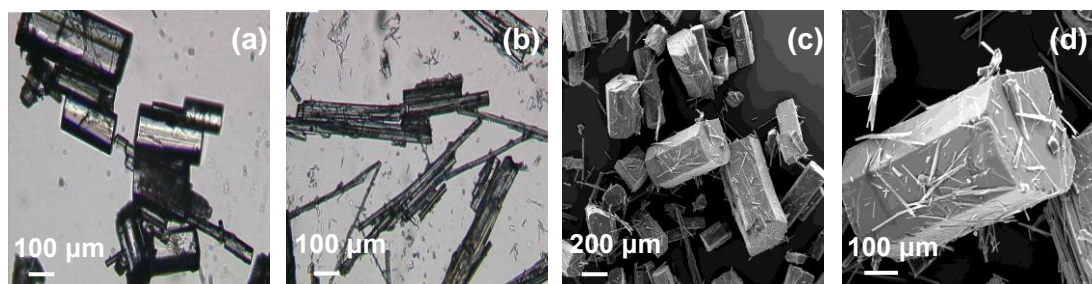


Figure 9.24. Microscope images of (a) hydro-chloride salt of PABA, (b) alpha form of PABA and scanning electron microscope images of (c, d) mixture of hydro-chloride salt of PABA and PABA (alpha form)

XRPD patterns for the sample from the first nucleation event and the salt are very similar as shown in Figure 9.25 (a). This provides evidence that the HCl salt of PABA nucleates from the first nucleation event. XRPD patterns for the sample from the second nucleation event and the raw material form of PABA (alpha) are shown in Figure 9.25 (b). The two nucleation events as shown in the FBRM results in Figure 9.22 are thought to be due to a polymorphic transformation or the nucleation of a second form resulting in a mixture of two forms. The second sample was taken from the process stream at the end of the process when the FBRM counts remained constant. The XRPD pattern for the second sample and the raw material form of PABA are not identical. The XRPD for the second sample shows peaks at angles of 9 and 14-15 which are characteristic for the alpha forms of PABA and peaks at angles of 27-29 which are characteristic of the HCl salt of PABA. This indicates that a mixture of salt and PABA (alpha form) crystallize from the second nucleation event, which confirms that the two nucleation events as shown in the FBRM results are due to the nucleation of two different forms and not a polymorphic transformation.

Two repeats of DSC results for samples at the end of the second nucleation event are shown in Figure 9.26. Two endothermic peaks appear at 187 and 194 °C. The first peak at 187 °C is the melting of PABA (alpha form) and the second peak at 194 °C is thought to be due to the salt melting/dissolving in the melt. The third peak at 210 °C is exothermic which is thought to be due to re-crystallization of a compound from the melt which has a higher melting point than the range used in the DSC results, therefore no melting point is detected at high temperatures. The DSC results clearly

indicate that after the second nucleation event there is a mixture of salt and PABA providing further evidence that the two nucleation events are due to the nucleation of two separate forms and not a polymorphic transformation.

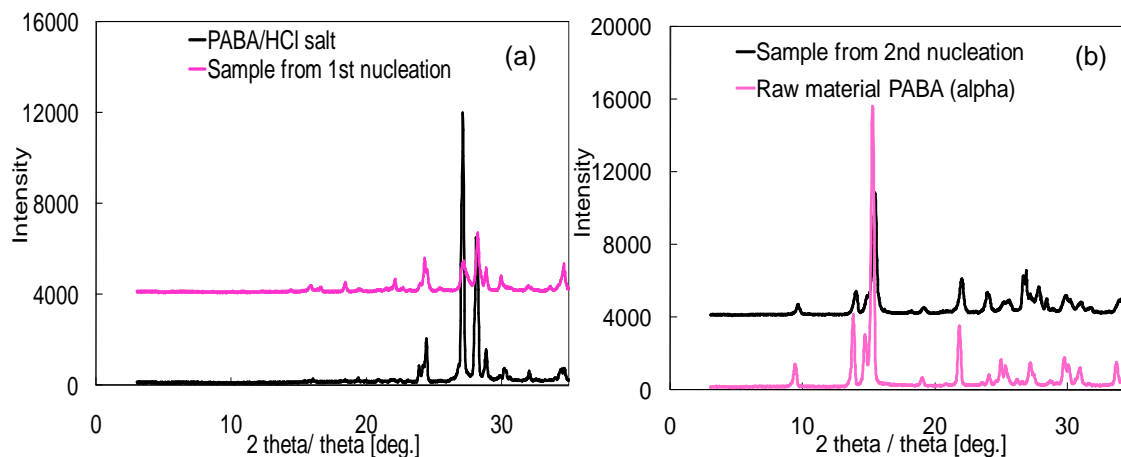


Figure 9.25 XRPD patterns of (a) sample from 1st nucleation and HCl salt of PABA and (b) sample from 2nd nucleation and raw material PABA. Intensities shifted for clearer plotting

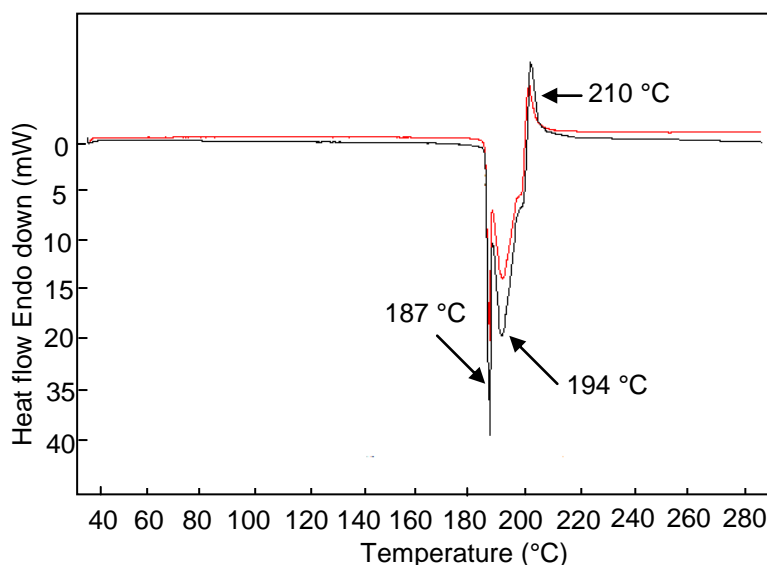


Figure 9.26 DSC results for the sample nucleated from the second nucleation event during cooling crystallization of PABA from ethanol at pH=2.5

A combination of the FBRM, PVM, ATR-UV/Vis and pH probe was used to monitor the cooling crystallization of PABA from ethanol at pH=2.5. The moles of PABA

(raw material) were in excess compared to the moles of HCl acid added. FBRM probe detected two nucleation events which were originally thought to be due to a polymorphic transformation. This statement was supported with the use of PVM images which shows a change in morphology during the two nucleation events. A range of SSA techniques were used to characterise the crystal product after the first and second nucleation events. Results showed supporting evidence that the salt nucleated from the first event and then the raw material (alpha) PABA nucleated from the second nucleation event. The two nucleation events were not due to a polymorphic transformation but the nucleation of two different crystal forms resulting in an impure product. These results show the importance of using a combination of PAT tools and SSA techniques in order to improve process understanding. PAT tools provide the conditions for which different forms crystallize from solution. This information can be use to design a robust process during scale up and prevent the crystallization of an impure product.

9.7 Conclusions

Combining PAT tools with SSA techniques provided the experimental conditions in which salts are most likely to crystallize from solution. PVM captures images of the crystals during the crystallization process which provides additional supportive information in identifying the nucleation of different crystal forms/salts. Salts do not form when using water as a solvent at pH values in the range 2.6-5.9 or in ethanol at pH values above 3. The HCl salt of PABA nucleated from ethanol at low pH value of 2.5. FBRM detected two nucleation events which were originally thought to be due to a polymorphic transformation. However the SSA of crystal samples provided evidence that two different forms nucleated resulting in an impure product. These tools prevent misinterpretation of results and provide the experimental conditions to prevent the crystallization of an impure product, saving both time and money. PAT tools and SSA techniques also were used to discover a new polymorphic form of MABA. At room temperature the stable (raw material) form has a melting point of 170 °C and the meta-stable form has a melting point of 177 °C. The two polymorphs are enantiotropic related with a transition temperature of 157 °C.

Chapter 10. Conclusions and future work

10.1 Conclusions

The aim of this research project is to apply a Quality-by-design (QbD) approach involving the use of PAT tools combined with SSA techniques to increase process understanding and knowledge for the design of robust crystallization processes. Within this section the conclusions about how PAT can be generally employed to understand how changes in the crystallization behaviour occur will be discussed and the conclusions of each chapter will be discussed together with how the key findings benefit industry. A summary table of all the compounds crystallized including new undiscovered forms and under what conditions nucleation occurred will be included in the conclusions.

PAT tools are very useful for detecting changes occurring during the crystallization process, which could be a polymorphic transformation or the crystallization of an impure product. Combining a range of PAT tools to monitor the crystallization process provides additional supportive information to understand the process and prevents the misinterpretation of results, saving both time and money.

The PVM probe is a useful tool for detecting changes in morphology of the crystals, which could indicate a polymorphic transformation or the crystallization of a impure product. This tool can identify the experimental conditions to produce crystals with the desired morphology, which will prevent problems in downstream processing such as long filtration times. The FBRM probe has many statistics that can be used to monitor the crystallization process including total counts, fine counts, coarse counts, mean chord length and median. The fine counts, coarse counts and mean chord length are useful statistics for monitoring changes in morphology during the crystallization process, which could be a polymorphic transformation. Both the FBRM and turbidity probe are tools used for detecting the solubility (clear) points, nucleation (cloud) points and meta-stable zone width (MSZW) measurements required for robust scale-up of the crystallization process. Both these tools have shown small differences in these

measurements. The turbidity probe provides less information about the process than the FBRM probe because it does not contain the additional statistics but the cost of the probe is cheaper and it provides good accurate results.

There are benefits of using a combination of PAT tools, including the FBRM probe and ATR-UV/Vis spectrometer, to monitor the crystallization process. The FBRM probe may detect a fluctuation in counts (increase or decrease). This could be interpreted as sedimentation of crystals due to insufficient mixing, crystals sticking to vessel/probe walls, nucleation or a polymorphic transformation. If the ATR-UV/Vis probe detects a decrease in absorbance then this provides supporting evidence of nucleation or a polymorphic transformation. Combining these tools prevents the misinterpretation of results, saving both time and money. However within this research it must be noted that water was found to be not a suitable solvent to use for the ATR-UV/Vis as crystals stick to the probe and therefore result in an increase in absorbance during nucleation, which can lead to misinterpretation of results.

Cooling crystallization experiments were performed using the model system sodium benzoate in water. The PAT tool used for monitoring the crystallization process is the FBRM probe. This tool detected a fluctuation in counts above a temperature of 65 °C. Similar results were observed in different size vessels ranging from 750 to 1 L and using different ramp (cooling) rates of 0.5, 0.3 and 0.1 °C/min. The repeatability of the results provided supporting evidence that the fluctuation in counts detected by the FBRM could be a polymorphic transformation. As hydrates tend to be stable at lower temperatures and anhydrides tend to be stable at higher temperatures the fluctuation at 65 °C is thought to be a polymorphic transformation from hydrate to the anhydrate form. Solid state characterisation of the crystals using a range of SSA techniques including optical microscopy, SEM, HSM, XRPD, DSC, TGA, DVS, NMR and IR spectroscopy confirmed the formation of a new undiscovered channel hydrate of sodium benzoate with molecular ratio SB to water of 1:0.28. This research highlights the usefulness of the FBRM probe in detecting polymorphic transformations and the importance of a combination of SSA techniques for the discovery of new polymorphs. Discovery of polymorphs earlier on in development can prevent late stage failures.

Polymorphic transformations and new polymorphic forms were also discovered during the antisolvent crystallization experiments using the model system sodium benzoate in an IPA/water mixture. PAT tools used for monitoring the crystallization process include the FBRM probe, turbidity probe and ATR-UV/Vis spectrometer. Both the FBRM and turbidity probe detected a change occurring during the crystallization process once the volume ratio of IPA/water reached a value of 4:1. ATR-UV/Vis confirmed the change to be due to a polymorphic transformation and provided evidence that both solvent composition and kinetics had an influence on the behaviour of the system. Solid state characterisation of the crystals using a range of SSA techniques including SEM, XRPD, HT-XRPD, DSC, TGA, IR and NMR spectroscopy, confirmed the formation of a new undiscovered channel solvate. A combined DSC and HSM approach lead to the discovery of a new higher melting polymorphic form of sodium benzoate. This research reinforces the usefulness of using a combination of PAT tools including the FBRM, turbidity probe and ATR-UV/Vis in detecting polymorphic transformations during the crystallization process. The antisolvent crystallization experiments illustrated for the first time the capability of the ATR-UV/Vis instrument to detect polymorphic transformations. These results also demonstrate the importance of using a range of SSA techniques to discover new forms of crystalline compound.

A combination of PAT tools and SSA techniques has also been used to investigate the problem of crusting (solid depositing on vessel walls) occurring within crystallization vessels. Cooling crystallization experiments were performed using the model system *para*-amino benzoic acid in ethyl acetate. The FBRM probe, turbidity probe and ATR-UV/Vis spectrometer were used to monitor the crystallization process. SSA techniques including optical microscopy, XRPD and DSC were used to characterise the crystal product. The FBRM and turbidity probes detected a change occurring during the crystallization process. Repeats of the experiments using the ATR-UV/Vis confirmed that the change was due to crusting forming on vessel walls. This research highlights the importance of using a QbD approach involving the use of PAT tools and SSA techniques for gaining a deeper understanding of the crystallization process and to prevent misinterpretation of results, saving both time and money during the drug development process. This section provides the first comprehensive PAT-SSA based investigation of the important technological problem of crusting. An additional contribution to the field of knowledge highlights the need for improvement within

industrial scale vessel design, such as the use of vessels with variable jacket height, to prevent the problems of crusting.

A QbD approach was also used during cooling crystallization experiments using the model system of ABA isomers in water to determine whether a robust MSZW can be obtained at lab scale and be used for the design of scale up experiments. The PAT tools used for measuring the solubility and nucleation curves, which is required for the determination of the MSZW, included the FBRM and turbidity probe. A robust MSZW ranging from 5.5 to 20.8 °C was obtained for the model system *meta*-ABA in water, which takes into consideration variation in ramp rate, vessel size (1 mL and 1 L), agitator type and speed. This robust MSZW can then be used to design scale up experiments, increasing the likelihood of producing a quality product. The nucleation kinetics was determined for the ABA isomers corresponding to different vessel sizes and mixing conditions. The results shows that nucleation orders vary for different crystallization set-ups involving different size vessels and mixing conditions, highlighting that crystallization models containing nucleation parameters are only valid for a specific crystallization set-up. Therefore model based design and scale-up of crystallization processes must be used carefully and more detailed mechanistic models, which take into consideration the effect of mixing need to be designed to improve the generality and applicability of crystallization models.

An alternative method used for designing a crystallization process to produce a quality product is through pH controlled polymorphic crystallization experiments, which were performed using the model systems *meta/para*-ABA in water and ethanol. A combination of 5 PAT tools was used in a single vessel to monitor the cooling crystallization process. PAT tools used include FBRM, ATR-UV/Vis, PVM, pH and a temperature probe. PAT tools detected a change occurring during the crystallization process, due to the formation of two products resulting in an impure product, confirmed by SSA methods. These results reinforce that by using a QbD approach it can increase process understanding, preventing the misinterpretation of results. This approach enables better design of the crystallization process, preventing failed batches. Various parameters including solvent, pH of solution, strength and type of acid were varied to investigate the best conditions to produce pure salts. Cooling, evaporation and precipitation methods were used to produce salts. Results showed that water solution at

all pH values and an ethanol solution above a pH value of 3 are not suitable conditions to produce salts. Strength and acid type (mono, di and tri-protic) had no effect on the formation of salts but the di and tri-protic acids resulted in salt crystals precipitating from solution forming agglomerates, which is undesirable. PVM images showed that salt crystals improve the morphology of the crystals compared to the polymorphs. Solvent and variation in mixing conditions were found to affect the morphology of the salt crystals. Careful selection of design parameters is important for producing crystals of the desired morphology so as to prevent problems in downstream processing. Solid state characterisation of salts with the use of XRPD showed that by replacing different size ions within the same polymorph results in a change in structure of the salt. Salts containing the sodium and potassium ions have a high tendency to form hydrates. This research highlights that different salt crystals of the same compound have different structures and hence different physico-chemical properties. Therefore salt selection is important to consider when designing the crystallization process to ensure a quality product.

The overall thesis presents research work that has contributed towards the field of knowledge of using a QbD approach involving the use of PAT tools and SSA techniques to design more robust crystallization processes. Key discoveries and new insights have shown that a QbD approach can overcome some of the problems that pharmaceutical industries face using PAT tools and confirmed with SSA techniques. New polymorphs were discovered during the crystallization process, which can prevent late stage failures and therefore reduce costs. The benefits of using a QbD approach, which increases process understanding and knowledge, has been shown to prevent the misinterpretation of results, speed up the crystallization process by highlighting key parameters that affect the quality of the product and identifies the experimental conditions to produce quality products. Results show the need for improvement within industrial vessel design and that the design of scale-up experiments involving the use of robust MSZW values obtained at lab scale can increase the likelihood of producing a quality product. These research findings show that a QbD approach can improve the quality of a product, prevent failed batches, speed up the time from drug discovery to market and reduce the costs of producing innovative medicines. This ultimately will improve profits by reducing essential costs of medicines and can have significant impact on our society by making new drugs available quicker and at a lower cost.

A summary table of all the crystal forms nucleated and isolated within this PhD thesis work including undiscovered new forms and the conditions of nucleation are listed in Table 10.1.

Table 10.1. Summary of results for crystals forms produced during PhD thesis and experimental conditions

Chapter	Crystal form	Method of crystallization	Conditions of nucleation
4	Sodium benzoate (SB) channel hydrate. (New undiscovered)	Cooling	water
5	SB channel solvate. (New undiscovered)	Anti-solvent	IPA/water volume ratio of 2:1
5	SB channel hydrate	Anti-solvent	IPA/water volume ratio of 4:1
5	Higher melting polymorphic form of SB at temperatures above 437 °C (melting point of anhydrous form)	-	DSC and hot stage microscopy analysis
8	HCl salt of MABA	Cooling	Ethanol at pH 2.5
8	HBr salt of MABA	Cooling	Ethanol at pH 1.5
8	HCl salt of PABA	Cooling	Ethanol at pH 2.5
8	HBr salt of PABA	Cooling	Ethanol at pH 1
8	H ₂ SO ₄ salt of PABA	Precipitation	Ethanol at pH 1.2
8	H ₃ PO ₄ salt of PABA	Precipitation	Ethanol at pH 3.3
8	Sodium salt of PABA (hydrates)	Evaporation	Ethanol at pH 10.7
8	Potassium salt of PABA (hydrates)	Evaporation	Ethanol at pH 8.1
9	Anhydrous alpha form of PABA	pH swing and cooling	Water at pH range 2.5 to 5.9 and ethanol at pH 5.9
9	Anhydrous form of MABA	Cooling	Water at pH 3 and ethanol at pH 4.1

10.2 Recommendation for future work

Recommendations for future work based on the research results presented in this thesis are mentioned in the following points:

- a) In the studies using the model systems of sodium benzoate in water and a water/IPA mixture (Chapter 4 and 5), PABA in ethyl acetate (Chapter 6) and PABA in a water/ethanol mixture (Chapter 9), crystallization experiments were performed using a range of PAT tools to monitor the process. PAT tools used include FRBM, PVM turbidity probe and ATR-UV/Vis spectrometer. In all cases the PAT tools detected a change occurring during the crystallization process, which was originally thought to be due to a polymorphic transformation. However in some cases after SSA of the crystal product this was found not to be the case. An additional PAT tool that would be recommended to monitor the crystallization process is the *in-situ* Raman probe. This technique will show a different spectrum for each polymorphic form and can be used to detect polymorphic transformation during the process. By using the Raman probe it would provide additional information that would prevent misinterpretation of results and speed up the time taken to design a robust crystallization process for the production of quality crystals.
- b) The problem of crusting (solid depositing on vessel walls) occurring during the crystallization process was identified during lab scale experiments with the use of PAT tools and SSA techniques. Crusting is a significant industrial problem since it can lead to large batch-to batch variation in product quality due to accidental seeding, formation of large lumps. Additionally the product can be contaminated through solvent inclusion as due to degradation because of overheating of the solid deposited on the wall of the vessel. A suggestion of future research would involve the design of pilot and industrial size rigs with variable jacket height vessels or an alternative design that will eliminate the problems of crusting. Novel jacket designs could be developed and a crystallization system with automated jacket height adjustment based on level measurement in the vessel would be designed. Improved design of

crystallization rigs would increase the likelihood of producing a quality product and prevent failed batches.

- c) Robust MSZW values were obtained at the lab scale for the model system *meta*-ABA in water. This robust MSZW takes into consideration variations in ramp rate, vessel size (1 mL and 1 L), agitator speed and type. Further research would involve the design of scale-up crystallization experiments (pilot plant and industrial scale) in which a supersaturation profile is followed within the robust MSZW region using a feedback loop for obtaining quality crystals with consistent properties. Additionally robust experimental design approaches could be used to determine the boundaries of the robust operating zone with a particular confidence interval, which would guarantee with a given probability, the consistency of certain product properties.
- d) The nucleation order, which is a parameter used within crystallization models was found to vary within different crystallization set-ups including variable vessel size and mixing conditions. A suggestion for further research would involve the design of mechanistic models, which take into consideration the effect of mixing in the mechanisms. These developed models can improve the generality and applicability of crystallization models and can be used for the model-based design and optimisation of the crystallization processes.
- e) Experiments involving MSZW measurements have been used to determine nucleation orders for the isomers *meta* and *para*-ABA. Further experiments involving MSZW measurements would be required to determine the nucleation order for the isomer *ortho*-ABA within the same crystallization set-up (vessel size and mixing conditions). Obtaining the nucleation order of all three isomers of ABA within the same crystallization set-up will provide new knowledge on how positional isomers influence the nucleation mechanism, and on whether crystallization models containing nucleation orders apply only to a particular isomer. This information could contribute towards better understanding of the nucleation mechanism and improving the future design of crystallization models.

References

Aaltonen, J., Heinanen, P., Peltonen, L., Kortejarvi, H., Tanninen, V.P., Christiansen, L., Hirvonen, J., Yliruusi, J. and Rantanen, J., 2006. In situ measurement of solvent-mediated phase transformations during dissolution testing. *Journal of Pharmaceutical Sciences*, **95**(12), 2730-2737.

Aamir, E., Nagy, Z.K and Rielly, C.D., 2010. Optimal seed recipe design for crystal size distribution control for batch cooling crystallization processes. *Chemical Engineering Science*, **65** (11), 3602-3614.

Abu Bakar, M.R., Nagy, Z.K. and Rielly, C.D., 2010. A combined approach of differential scanning calorimetry and hot-stage microscopy with image analysis in the investigation of sulfathiazole polymorphism. *Journal of Thermal Analysis and Calorimetry*, **99**(2), 609-619.

Abu Bakar, M.R., Nagy, Z.K., Saleemi, A.N. and Rielly, C.D., 2009a. The impact of direct nucleation control on crystal size distribution in pharmaceutical crystallization processes. *Crystal Growth & Design*, **9**(3), 1378-1384.

Abu Bakar, M.R., Nagy, Z.K. and Rielly, C.D., 2009b. Seeded batch cooling crystallization with temperature cycling for the control of size uniformity and polymorphic purity of sulfathiazole crystals. *Organic Process Research & Development*, **13**(6), 1343-1356.

Allen, F.H., 2002. The Cambridge structural database: a quarter of a million crystal structures and rising. *Acta Crystallographica Section B*, **58**, (3), 380-388

Arora, S.K., Sundaral.M, Dancz, J.S., Stanford, R.H. and Marsh, R.E., 1973. Crystal and molecular-structure of 3-aminobenzoic acid hydrochloride. *Acta Crystallographica Section B-Structural Science*, **B 29**, 1849-1855.

Athimoolam, S. and Natarajan, S., 2006. Hydrogen-bonding motifs in 4-carboxyphenylammonium nitrate and perchlorate monohydrate, and in bis(4-carboxyphenylammonium) sulfate. *Acta Crystallographica Section C-Crystal Structure Communications*, **62**, O612-O617.

- Atkinson, J. and Hibbert, C., 2001. *Chemistry*. Heinemann, Oxford.
- Bakeev, K.A., 2005. *Process analytical technology*. Blackwell Publishing Ltd,.
- Barrett, P. and Glennon, B., 2002. Characterizing the metastable zone width and solubility curve using lasentec FBRM and PVM. *Chemical Engineering Research & Design*, **80**(A7), 799-805.
- Barrett, P. and Glennon, B., 1999. In-line FBRM monitoring of particle size in dilute agitated suspensions. *Particle & Particle Systems Characterization*, **16**(5), 207-211.
- Bechtloff, B., Nordhoff, S. and Ulrich, J., 2001. Pseudopolymorphs in industrial use. *Crystal Research and Technology*, **36**(12), 1315-1328.
- Beckmann, W., 2000. Seeding the desired polymorph: background, possibilities, limitations, and case studies. *Organic Process Research & Development*, **4**(5), 372-383.
- Benali-Cherif, N., Direm, A., Allouche, F. and Soudani, K., 2007. Hydrogen bonding in 4-carboxyanilinium dihydrogenphosphate. *Acta Crystallographica Section E-Structure Reports Online*, **63**, O2272-O2274.
- Bernstein, J., Davey, R.J. and Henck, J.O., 1999. Concomitant polymorphs. *Angewandte Chemie-International Edition*, **38**(23), 3441-3461.
- Bernstein, J., 2002. *Polymorphism in Molecular Crystals*; Oxford University Press Inc., New York.
- Billot, P., Couty, M., and Hosek, P., 2010. Application of ATR-UV Spectroscopy for Monitoring the Crystallization of UV Absorbing and Nonabsorbing Molecules. *Organic Process Research and Development*, **14**(3), 511-523.
- Birch, M., Fussell, S.J., Higginson, P.D., McDowall, N. and Marziano, I., 2005. Towards a PAT-based strategy for crystallization development. *Organic Process Research & Development*, **9**(3), 360-364.
- Bravais, A. 1866, *Etudes Cristallographiques* (Paris: Gauthier Villars).

Breithaupt, J., 1990. *Understanding physics for advanced level*. Second edn. Stanley Thornes (Publishers) Ltd, Cheltenham.

Braatz, R.D., Fujiwara, M., Ma, D.L., Togkalidou, T. and Tafti, D.K., 2002. Simulation and new sensor technologies for industrial crystallization: A review. *International Journal of Modern Physics B*, **16**(1-2), 346-353.

Braatz, R.D., 2002 Advanced control of crystallization processes. *Annual Review in Control*. **26**, 87-99

Braun, D.E., Kahlenberg, V., Gelbrich, T., Ludescher, J. and Griesser, U.J., 2008. Solid state characterisation of four solvates of R-cinacalcet hydrochloride. *Crystengcomm*, **10**(11), 1617-1625.

Brittain, H.G., 1999. *Polymorphism in pharmaceutical solids*. Marcel Dekker, Inc., New York.

Bugay, D.E., 2001. Characterization of the solid-state: spectroscopic techniques. *Advanced Drug Delivery Reviews*, **48**(1), 43-65.

Burger, A. and Ramberger, R., 1979. Polymorphism of pharmaceuticals and other molecular-crystals .1. Theory of thermodynamic rules. *Mikrochimica acta*, **2**(3-4), 259-271.

Byrn, S.R. 1982. *Solid-state chemistry of drugs*. Published by Academic Press.

Caillet, A., Puel, F. and Fevotte, G., 2008. Quantitative in situ monitoring of citric acid phase transition in water using Raman spectroscopy. *Chemical Engineering and Processing*, **47**(3), 377-382.

Chemburkar, S.R., Bauer, J., Deming, K., Spiwek, H., Patel, K., Morris, J., Henry, R., Spanton, S., Dziki, W., Porter, W., Quick, J., Bauer, P., Donaubauer, J., Narayanan, B.A., Soldani, M., Riley, D. and McFarland, K., 2000. Dealing with the impact of ritonavir polymorphs on the late stages of bulk drug process development. *Organic Process Research & Development*, **4**(5), 413-417.

Chen, J.X., Yuan, J.S., Ulrich, J.C. and Wang, J.K., 2009. Online measurement of hydrocortisone particles and improvement of the crystallization process. *Chemical Engineering & Technology*, **32**(7), 1073-1077.

Chew, J.W., Black, S.N., Chow, P.S. and Tan, R.B.H., 2007. Comparison between open-loop temperature control and closed-loop supersaturation control for cooling crystallization of glycine. *Industrial & Engineering Chemistry Research*, **46**(3), 830-838.

Chianese, A., Diberardino, F. and Jones, A.G., 1993. On the effect of secondary nucleation on the crystal size distribution from a seeded batch crystallizer. *Chemical Engineering Science*, **48**(3), 551-560.

Cincic, D. and Kaitner, B., 2008a. Hydrogen bonding in the bromide salts of 4-aminobenzoic acid and 4-aminoacetophenone. *Acta Crystallographica Section C-Crystal Structure Communications*, **64**, O226-O229.

Cincic, D. and Kaitner, B., 2008b. Hydrogen-bonding motifs in 3-carboxyanilinium bromide and iodide. *Acta Crystallographica Section C-Crystal Structure Communications*, **64**, O101-O104.

Colapietro, M. and Domenicano, A., 1980. Structural studies of benzene-derivatives .7. structure of para-aminobenzoic acid hydrochloride. *Acta Crystallographica Section B-Structural Science*, **36**, 354-358.

Collins, A.N., Sheldrake, G.N. and Crosby, J., 1997. *Chirality in industry II*. John Wiley & Sons Ltd.

Cote, A., Zhou, G. and Stanik, M., 2009. A novel crystallization methodology to ensure isolation of the most stable crystal form. *Organic Process Research & Development*, **13**(6), 1276-1283.

Crystal Structure (2010). Available at:

http://en.wikipedia.org/wiki/Crystal_structure#The_Bravais_lattices (Accessed: 3rd September 2010).

Davey, R. and Garside, J., 2000. *From molecules to crystallizers (An introduction to crystallization)*. Oxford University Press Inc., United States.

Davey, R.J., 2003. Pizzas, polymorphs and pills. *Chemical Communications*, (13), 1463-1467.

Davey, R.J., Blagden, N., Potts, G.D. and Docherty, R., 1997. Polymorphism in molecular crystals: Stabilization of a metastable form by conformational mimicry. *Journal of the American Chemical Society*, **119**(7), 1767-1772.

David, P.A., Roginski, R., Doherty, S. and Moe, J., 2004. The impact of process analytical technology in pharmaceutical chemical process development. *Journal of Process Analytical Chemistry*, **9**(1), 1-5.

Desikan, S., Parsons, R.L., Davis, W.P., Ward, J.E., Marshall, W.J. and Toma, P.H., 2005. Process development challenges to accommodate a late-appearing stable polymorph: A case study on the polymorphism and crystallization of a fast-track drug development compound. *Organic Process Research & Development*, **9**(6), 933-942.

Dharmayat, S., De Anda, J.C., Hammond, R.B., Lai, X.J., Roberts, K.J. and Wang, X.Z., 2006. Polymorphic transformation of L-glutamic acid monitored using combined on-line video microscopy and X-ray diffraction. *Journal of Crystal Growth*, **294**(1), 35-40.

Doki, N., Seki, H., Takano, K., Asatani, H., Yokota, M. and Kubota, N., 2004. Process control of seeded batch cooling crystallization of the metastable alpha-form glycine using an in-situ ATR-FTIR spectrometer and an in-situ FBRM particle counter. *Crystal Growth & Design*, **4**(5), 949-953.

Donnay, J.D.H and Harker, D. 1937, *Am. Mineral.* **22**, 463.

Doyle, W.M. and Tran, L., 1999. Analysis of strongly absorbing chromophores by UV/visible ATR spectroscopy. *Spectroscopy*, **14**(4), 46-54.

Federsel, H.J., 2009. Chemical Process Research and Development in the 21st Century: Challenges, Strategies, and Solutions from a Pharmaceutical Industry Perspective. *Accounts of Chemical Research*, **42**(5), 671-680.

Ferrari, E.S., Davey, R.J., Cross, W.I., Gillon, A.L. and Towler, C.S., 2003. Crystallization in polymorphic systems: The solution-mediated transformation beta to alpha glycine. *Crystal Growth & Design*, **3**(1), 53-60.

Fevotte, G., 2007. In situ raman spectroscopy for in-line control of pharmaceutical crystallization and solids elaboration processes: A review. *Chemical Engineering Research & Design*, **85**(A7), 906-920.

Fevotte, G., 2002. New perspectives for the on-line monitoring of pharmaceutical crystallization processes using in situ infrared spectroscopy. *International Journal of Pharmaceutics*, **241**(2), 263-278.

Florence A.T., and Attwood D., 1981. *Physicochemical principles of pharmacy*. The Macmillan Press LTD.

Fontana, M.G., 1987. *Corrosion engineering*. Third edn. McGraw-Hill, Inc., Singapore.

Forbes, R.T., York, P., Fawcett, V. and Shields, L., 1992. Physicochemical properties of salts of p-aminosalicylic acid .1. Correlation of crystal-structure and hydrate stability. *Pharmaceutical Research*, **9**(11), 1428-1435.

Fox, M. A.; Whitesell, J. K., 1997. *Core Organic Chemistry*; Jones and Bartlett Publishers Inc.

Friedel, G., 1907. *Bull. Soc. Franc. Mineral.*, **30**, 326.

Fujiwara, M., Chow, P.S., Ma, D.L. and Braatz, R.D., 2002. Paracetamol crystallization using laser backscattering and ATR-FTIR spectroscopy: Metastability, agglomeration, and control. *Crystal Growth & Design*, **2**(5), 363-370.

Fujiwara, M., Nagy, Z.K., Chew, J.W. and Braatz, R.D., 2005. First-principles and direct design approaches for the control of pharmaceutical crystallization. *Journal of Process Control*, **15**(5), 493-504.

Garside, Mersmann and Nyvlt., 2002. *Measurement of crystal growth and nucleation rates*. 2nd edn. IChemE.

- Gillon, A.L., Feeder, N., Davey, R.J. and Storey, R., 2003. Hydration in molecular crystals - A Cambridge structural database analysis. *Crystal Growth & Design*, **3**(5), 663-673.
- Gillon, A.L., Steele, G., Nagy, Z.K., Makwana, N. and Rielly, C.D., 2006. PAT investigations into the crystallization of caffeine. Proceedings of the 13th International Workshop on Industrial Crystallization (BIWIC); Netherlands, September 13-15th, 35-42.
- Giron, D., 1995. Thermal-analysis and calorimetric methods in the characterization of polymorphs and solvates. *Thermochimica Acta*, **248**, 1-59.
- Giron, D., 2003. Monitoring of polymorphism-from detection to quantification. *Engineering in Life Sciences*, **3**(3), 103-112.
- Goldhill, J., 2010. Advances in drug discovery. Hope for an Alzheimer's breakthrough remains despite Dimebon's failure., <http://leaddiscovery.blogspot.com/2010/03/hope-for-alzheimers-breakthrough.html>. Accessed on 10th August 2010.
- Gracin, S. and Rasmuson, A.C., 2004. Polymorphism and crystallization of p-aminobenzoic acid. *Crystal Growth & Design*, **4**(5), 1013-1023.
- Gracin, S., Uusi-Penttila, M. and Rasmuson, A.C., 2005. Influence of ultrasound on the nucleation of polymorphs of p-aminobenzoic acid. *Crystal Growth & Design*, **5**(5), 1787-1794.
- Greaves, D., Boxall, J., Mulligan, J., Montesi, A., Creek, J., Sloan, E.D. and Koh, C.A., 2008. Measuring the particle size of a known distribution using the focused beam reflectance measurement technique. *Chemical Engineering Science*, **63**(22), 5410-5419.
- Gron, H., Borissova, A. and Roberts, K.J., 2003. In-process ATR-FTIR spectroscopy for closed-loop supersaturation control of a batch crystallizer producing monosodium glutamate crystals of defined size. *Industrial & Engineering Chemistry Research*, **42**(1), 198-206.

- Gu, C.H., Young, V. and Grant, D.J.W., 2001. Polymorph screening: Influence of solvents on the rate of solvent-mediated polymorphic transformation. *Journal of Pharmaceutical Sciences*, **90**(11), 1878-1890.
- Harris, R.K., 2007. Applications of solid-state NMR to pharmaceutical polymorphism and related matters. *Journal of Pharmacy and Pharmacology*, **59**(2), 225-239.
- Harris, R.K., 2006. NMR studies of organic polymorphs & solvates. *Analyst*, **131**(3), 351-373.
- Haynes, D.A., Jones, W. and Motherwell, W.D.S., 2005. Occurrence of pharmaceutically acceptable anions and cations in the Cambridge structural database. *Journal of Pharmaceutical Sciences*, **94**(10), 2111-2120.
- He, Y.G., Wu, C.Y. and Kong, W., 2005. A theoretical and experimental study of water complexes of m-aminobenzoic acid MABA center dot(H₂O)(n) (n = 1 and 2). *Journal of Physical Chemistry a*, **109**(5), 748-753.
- Hermanto, M.W., Chiu, M.S. and Braatz, R.D., 2009. Nonlinear model predictive control for the polymorphic transformation of L-glutamic acid crystals. *AICHE Journal*, **55**(10), 2631-2645.
- Hermanto, M.W., Chiu, M.S., Woo, X.Y. and Braatz, R.D., 2007. Robust optimal control of polymorphic transformation in batch crystallization. *AICHE Journal*, **53**, 2643-2650.
- Hermanto, M.W., Chow, P.S. and Tan, R.B.H., 2010. Implementation of focused beam reflectance measurement (FBRM) in antisolvent crystallization to achieve consistent product quality. *Crystal Growth & Design*, **10**(8), 3668-3674.
- Hilfiker, R., 2006. *Polymorphism in the Pharmaceutical Industry*. First edn. WILEY-VCH, Germany.
- Hill, G. And Holman, J., 2000. *Chemistry in Context*. Fifth edition. Nelson (publishers), Surrey.

- Hojjati, H. and Rohani, S., 2005. Cooling and seeding effect on supersaturation and final crystal size distribution (CSD) of ammonium sulphate in a batch crystallizer. *Chemical Engineering and Processing*, **44**(9), 949-957.
- Howard, K.S., Nagy, Z.K., Saha, B., Robertson, A.L. and Steele, G., 2009a. Combined PAT-solid state analytical approach for the detection and study of sodium benzoate hydrate. *Organic Process Research & Development*, **13**(3), 590-597.
- Howard, K.S., Nagy, Z.K., Saha, B., Robertson, A.L., Steele, G. and Martin, D., 2009b. A process analytical technology based investigation of the polymorphic transformations during the antisolvent crystallization of sodium benzoate from IPA/water mixture. *Crystal Growth & Design*, **9**(9), 3964-3975.
- Infantes, L., Fabian, L. and Motherwell, W.D.S., 2007. Organic crystal hydrates: what are the important factors for formation. *CrystEngComm*, **9** (1), 65-71.
- Jiang, S.F., ter Horst, J.H. and Jansens, P.J., 2008. Concomitant polymorphism of o-aminobenzoic acid in antisolvent crystallization. *Crystal Growth & Design*, **8**, 37-43.
- Jones, A.G., 2002. *Crystallization Process Systems*. Butterworth Heinemann, Oxford.
- Jones, H.P., Davey, R.J. and Cox, B.G., 2005. Crystallization of a salt of a weak organic acid and base: Solubility relations, supersaturation control and polymorphic behavior. *Journal of Physical Chemistry B*, **109** (11), 5273-5278.
- Kail, N., Marquardt, W. and Briesen, H., 2009. Process analysis by means of focused beam reflectance measurements. *Industrial & Engineering Chemistry Research*, **48**(6), 2936-2946.
- Karabas, I., Orkoula, M.G. and Kontoyannis, C.G., 2007. Analysis and stability of polymorphs in tablets: The case of Risperidone. *Talanta*, **71**(3), 1382-1386.
- Karpinski, P.H., 2006. Polymorphism of active pharmaceutical ingredients. *Chemical Engineering & Technology*, **29**(2), 233-237.

- Kennedy, A.R., Okoth, M.O., Sheen, D.B., Sherwood, J.N., Teat, S.J. and Vrcelj, R.M., 2003. Cephalexin: a channel hydrate. *Acta Crystallographica Section C-Crystal Structure Communications*, **59**, O650-O652.
- Khankari, R.K. and Grant, D.J.W., 1995. Pharmaceutical hydrates. *Thermochimica Acta*, **248**, 61-79.
- Kitamura, M. and Sugimoto, M., 2003. Anti-solvent crystallization and transformation of thiazole-derivative polymorphs - I: effect of addition rate and initial concentrations. *Journal of Crystal Growth*, **257**(1-2), 177-184.
- Kobayashi, R., Fujimaki, Y., Ukita, T. and Hiyama, Y., 2006. Monitoring of solvent-mediated polymorphic transitions using in situ analysis tools. *Organic Process Research & Development*, **10**(6), 1219-1226.
- Kubota, N., 2008. A new interpretation of metastable zone widths measured for unseeded solutions. *Journal of Crystal Growth*, **310**(3), 629-634.
- Kumar, T.L., Vishweshwar, P., Babu, J.M. and Vyas, K., 2009. Salts of hydrates of imiquimod, an immune response modifier. *Crystal Growth & Design*, **9**(11), 4822-4829.
- Lester, C., Lubey, G., Dicks, M., Andol, G., Vaughn, D., Cambron, R.T., Poiesz, K. and Redman-Furey, N., 2006. Dehydration of risedronate hemi-pentahydrate: Analytical and physical characterization. *Journal of Pharmaceutical Sciences*, **95**(12), 2631-2644.
- Leung, S.S., Padden, B.E., Munson, E.J. and Grant, D.J.W., 1998. Hydration and Dehydration Behavior of Aspartame Hemihydrate. *Journal of Pharmaceutical Sciences*, **87**(4), 508-513.
- Li, Y., Chow, P.S., Tan, R.B.H. and Black, S.N., 2008. Effect of water activity on the transformation between hydrate and anhydrate of carbamazepine. *Organic Process Research & Development*, **12**(2), 264-270.
- Li, M.Z., White, G., Wilkinson, D. and Roberts, K.J., 2005. Scale up study of retreat curve impeller stirred tanks using LDA measurements and CFD simulation. *Chemical Engineering Journal*, **108**, 81-90.

Liang, K.P., White, G., Wilkinson, D., Ford, L.J., Roberts, K.J. and Wood, W.M.L., 2004. An examination into the effect of stirrer material and agitation rate on the nucleation of L-glutamic acid batch crystallized from supersaturated aqueous solutions. *Crystal Growth & Design*, **4**(5), 1039-1044.

Lin, S.W., Ng, K.M. and Wibowo, C., 2007. Integrative approach for polymorphic crystallization process synthesis. *Industrial & Engineering Chemistry Research*, **46**(2), 518-529.

Lu, Y.H. and Ching, C.B., 2006. Study on the metastable zone width of ketoprofen. *Chirality*, **18**(4), 239-244.

Lu, Q.L., Yang, G. and Gu, H., 2005. Phase quantification of two chlorothalonil polymorphs by X-ray powder diffraction. *Analytica Chimica Acta*, **538**(1-2), 291-296.

Lung-Somarriba, B.L.M., Moscosa-Santillan, M., Porte, C. and Delacroix, A., 2004. Effect of seeded surface area on crystal size distribution in glycine batch cooling crystallization: a seeding methodology. *Journal of Crystal Growth*, **270**(3-4), 624-632.

Macrae, C.F., Bruno, I.J, Chisholm, J.A., Edgington, P.R., McCabe, P., Pidcock, E., Rodriguez-Monge, L., Taylor, R., Streek, J. and Wood, P.A., 2008. Mercury CSD 2.0- new features for the visualization and investigation of crystal structures. *Journal of Applied Crystallography*, **41** (2), 466-470.

Matthews, H.B., Miller, S.M. and Rawlings, J.B., 1996. Model identification for crystallization: Theory and experimental verification. *Powder Technology*, **88**(3), 227-235.

Meadhra, R.O., Kramer, H.J.M. and vanRosmalen, G.M., 1996. Crystallization kinetics of pentaerythritol. *Journal of Crystal Growth*, **166**(1-4), 1046-1052.

Mersmann, A. and Bartosch, K., 1998. How to predict the metastable zone width. *Journal of Crystal Growth*, **183**(1-2), 240-250.

Mineralogy Database (2010). Available at: <http://webmineral.com/>. (Accessed: 3rd September 2010).

Minerals by name (2010). Available at: <http://www.galleries.com/minerals/by-name.htm>. (Accessed: 3rd September 2010).

Muller, M., Meier, U., Wieckhusen, D., Beck, R., Pfeffer-Hennig, S. and Schneeberger, R., 2006. Process development strategy to ascertain reproducible API polymorph manufacture. *Crystal Growth & Design*, **6**(4), 946-954.

Mullin, J.M., 2001. *Crystallization*. Fourth edn. Butterworth Heinemann, Oxford.

Myerson, A.S., 2002. *Handbook of Industrial crystallization*. Second edn. Butterworth Heinemann, United States.

Nagy, Z.K., Gillon, A.L., Steele, G., Makwana, N. and Rielly, C.D., 2007. Using process analytical technology for in situ monitoring of the polymorphic transformation of organic compounds. Proceedings of the 8th International Symposium on Dynamics & Control of Process Systems (DYCOPS); Cancun, June 6-8, 2007; International Federation of Automatic Control: Laxenburg, Austria, 2007; **3**, 133-138.

Nagy, Z.K., Fujiwara, M. and Braatz, R.D., 2008a. Modelling and control of combined cooling and antisolvent crystallization processes. *Journal of Process Control*, **18**(9), 856-864.

Nagy, Z.K., Chew, J.W., Fujiwara, M. and Braatz, R.D., 2008b. Comparative performance of concentration and temperature controlled batch crystallizations. *Journal of Process Control*, **18**(3-4), 399-407.

Nagy, Z.K., Fujiwara, M., Woo, X.Y. and Braatz, R.D., 2008c. Determination of the kinetic parameters for the crystallization of paracetamol from water using metastable zone width experiments. *Industrial & Engineering Chemistry Research*, **47**(4), 1245-1252.

Nagy, Z.K., 2009. Model based robust control approach for batch crystallization product design. *Computers & Chemical Engineering*, **33**(10), 1685-1691.

Nyvt, J., 1968. Kinetics of nucleation in solutions. *Journal of Crystal Growth*, **3**(4), 377-383.

O'Grady, D., Barrett, M., Casey, E. and Glennon, B., 2007. The effect of mixing on the metastable zone width and nucleation kinetics in the anti-solvent crystallization of benzoic acid. *Chemical Engineering Research & Design*, **85**(A7), 945-952.

Ojala, W.H. and Etter, M.C. 1992. Polymorphism in anthranilic acid: A reexamination of the phase transitions. *Journal of the American Chemical Society*. **114**(26), 10288-10293.

Ono, T., Kramer, H.J.M., ter Horst, J.H. and Jansens, P.J., 2004. Process modeling of the polymorphic transformation of L-glutamic acid. *Crystal Growth & Design*, **4**(6), 1161-1167.

Ostwald W., 1897. Studien UÈber Die Bildung und Umwandlung Fester KoÈrper. *Z Physik Chem.*, **22**, 289-330.

O'Sullivan, B., Barrett, P., Hsiao, G., Carr, A. and Glennon, B., 2003. In situ monitoring of polymorphic transitions. *Organic Process Research & Development*, **7**(6), 977-982.

O'Sullivan, B. and Glennon, B., 2005. Application of in situ FBRM and ATR-FTIR to the monitoring of the polymorphic transformation of D-mannitol. *Organic Process Research & Development*, **9**(6), 884-889.

Parsons, A.R., Black, S.N. and Colling, R., 2003. Automated measurements of metastable zones for pharmaceutical compounds. *Trans IChemE*, **81**(Part A), 700-704.

Perry, R.H and Green, D.W. 1998. *Perry's Chemical Engineer's Handbook*. Seventh Edition.; McGraw-Hill.

Pirttimaki, J. and Laine, E., 1994. The Transformation of Anhydrate and Hydrate Forms of Caffeine at 100-Percent Rh and 0-Percent Rh. *European Journal of Pharmaceutical Sciences*, **1**(4), 203-208.

Pudipeddi, M. and Serajuddin, A.T.M., 2005. Trends in solubility of polymorphs. *Journal of Pharmaceutical Sciences*, **94**(5), 929-939.

Rajeshwar, K and Secco, E.A., 1976. Phase transformation studies on anthranilic acid by thermal analysis, infrared absorption, and X-ray diffraction methods, *The Canadian Journal of Chemical Engineering*, **54**, 2509.

Rao, C.N.R., 1961. *Ultra-Violet and Visible Spectroscopy*. Published by Butterworth and Co. Ltd.

Read, E.K., Shah, R.B., Riley, B.S., Park, J.T., Brorson, K.A. and Rathore, A.S., 2010. Process Analytical Technology (PAT) for Biopharmaceutical Products: Part II. Concepts and Applications. *Biotechnology and Bioengineering*, **105**(2), 285-295.

Reddy, L.S., Bethune, S.J., Kampf, J.W. and Rodriguez-Hornedo, N., 2009. Cocrystals and Salts of Gabapentin: pH dependent cocrystal stability and solubility. *Crystal Growth & Design*, **9**(1), 378-385.

Redman-Furey, N., Dicks, M., Bigalow-Kern, A., Cambron, R.T., Lubey, G., Lester, C. and Vaughn, D., 2005. Structural and analytical characterization of three hydrates and an anhydrate form of risedronate. *Journal of Pharmaceutical Sciences*, **94**(4), 893-911.

Reutzel-Edens, S.M., 2006. Achieving polymorph selectivity in the crystallization of pharmaceutical solids: Basic considerations and recent advances. *Current opinion in Drug Discovery & Development*, **9**(6), 806-815.

Reutzel-Edens, S.M., Bush, J.K., Magee, P.A., Stephenson, G.A. and Byrn, S.R., 2003. Anhydrides and hydrates of olanzapine: Crystallization, solid-state characterization, and structural relationships. *Crystal Growth & Design*, **3** (6), 897-907.

Rielly, C.D., Habib, M. and Sherlock, J.P., 2007. Flow and mixing characteristics of a retreat curve impeller in a conical-based vessel. *Chemical Engineering Research & Design*, **85**(A7), 953-962.

Roberts, S.N.C., Williams, A.C., Grimsey, I.M. and Booth, S.W., 2002. Quantitative analysis of mannitol polymorphs. X-ray powder diffractometry - exploring preferred orientation effects. *Journal of Pharmaceutical and Biomedical Analysis*, **28**(6), 1149-1159.

Rocco, W.L., Morphet, C. and Laughlin, S.M., 1995. Solid-State Characterization of zanoterone. *International Journal of Pharmaceutics*, **122**(1-2), 17-25.

Rotich, M.K., Glass, B.D. and Brown, M.E., 2001. Thermal studies on some substituted aminobenzoic acids. *Journal of Thermal Analysis and Calorimetry*, **64**(2), 681-688.

- Salas-Cimingo, G., 1968a. *C.R. Acad. Sci., Ser C (Chim)*, 267, 1304.
- Salas-Cimingo, G., 1968b. *C.R. Acad. Sci., Ser C (Chim)*, 267, 1402.
- Schachter, A.D. and Ramoni, M.F. 2007. From the analyst's couch: Clinical forecasting in drug development. *Nature Reviews Drug Discovery*, **6**, 107-108.
- Scholl, J., Bonalumi, D., Vicum, L., Mazzotti, M. and Muller, M., 2006. In situ monitoring and modeling of the solvent-mediated polymorphic transformation of L-glutamic acid. *Crystal Growth & Design*, **6**(4), 881-891.
- Seok, Y.J., Yang, K.S. and Kang, S.O., 1995. A simple spectrophotometric determination of dissociation-constants of organic-compounds. *Analytica Chimica Acta*, **306** (2-3), 351-356.
- Simon, L.L., Nagy, Z.K. and Hungerbuhler, K., 2009. Endoscopy-based in situ bulk video imaging of batch crystallization processes. *Organic Process Research & Development*, **13**(6), 1254-1261.
- Sistare, F., Berry, L.S.P. and Mojica, C.A., 2005. Process analytical technology: An investment in process knowledge. *Organic Process Research & Development*, **9**(3), 332-336.
- Smith, E.B., 1990. *Basic chemical thermodynamics*. Fourth edn. Oxford University Press, New York.
- Stephenson, G.A. and Diseroad, B.A., 2000. Structural relationship and desolvation behavior of cromolyn, cefazolin and fenopropfen sodium hydrates. *International Journal of Pharmaceutics*, **198** (2), 167-177.
- Stephenson, G.A., Forbes, R.A. and Reutzel-Edens, S.M., 2001. Characterization of the solid state: quantitative issues. *Advanced Drug Delivery Reviews*, **48**(1), 67-90.
- Stephen, H. and Stephen, T., 1963. *Solubilities of inorganic and organic compounds*. Vol 1. Binary Systems. Part 1 and 2. Pergamon Press Ltd.

- Sternitzke, C., 2010. Knowledge sources, patent protection, and commercialization of pharmaceutical innovations. *Research Policy*, **39**(6), 810-821.
- Stuart, B.; George, B.; McIntyre, P., 1998. *Modern Infrared Spectroscopy*; John Wiley and Sons Ltd.
- Svard, M., Nordstrom, F.L., Jasnobulka, T. and Rasmuson, A.C., 2010. Thermodynamics and nucleation kinetics of m-aminobenzoic acid polymorphs. *Crystal Growth & Design*, **10**(1), 195-204.
- Swislocka, R., Samsonowicz, M., Regulska, E. and Lewandowski, W., 2006. Molecular structure of 4-aminobenzoic acid salts with alkali metals. *Journal of Molecular Structure*, **792**, 227-238.
- Tadayyon, A. and Rohani, S., 1998. Determination of particle size distribution by Par-Tec (R) 100: Modeling and experimental results. *Particle & Particle Systems Characterization*, **15**(3), 127-135.
- Thompson, D.R., Kougoulos, E., Jones, A.G. and Wood-Kaczmar, M.W., 2005. Solute concentration measurement of an important organic compound using ATR-UV spectroscopy. *Journal of Crystal Growth*, **276**(1-2), 230-236.
- Threlfall, T., 2003. Structural and thermodynamic explanations of Ostwald's rule. *Organic Process Research & Development*, **7**, 1017-1027.
- Threlfall, T.L. and Chalmers, J.M., 2007. *Applications of Vibrational Spectroscopy in Pharmaceutical Research and Development*. John Wiley & Sons. Ltd.
- Tian, F., Qu, H., Louhi-Kultanen, M. and Rantanen, J., 2010. Crystallization of a polymorphic hydrate system. *Journal of Pharmaceutical Sciences*, **99** (2), 753-763.
- Towler, C.S., Davey, R.J., Lancaster, R.W. and Price, C.J., 2004. Impact of molecular speciation on crystal nucleation in polymorphic systems: The conundrum of gamma glycine and molecular 'self poisoning'. *Journal of the American Chemical Society*, **126** (41), 13347-13353.

- Trifkovic, M., Sheikhzadeh, M. and Rohani, S., 2009. Determination of metastable zone width for combined anti-solvent/cooling crystallization. *Journal of Crystal Growth*, **311**(14), 3640-3650.
- Van Der Heijden, A.E.D.M., Van Der Eerden, J.P. and Van Rosmalen, G.M., 1994. The secondary nucleation rate: A physical model. *Chemical Engineering Science*, **49**(18), 3103-3113.
- Variankaval, N., Lee, C., Xu, J., Calabria, R., Tsou, N. and Ball, R., 2007. Water activity-mediated control of crystalline phases of an active pharmaceutical ingredient. *Organic Process Research & Development*, **11**(2), 229-236.
- Varshney, D.B., Kumar, S., Shalaev, E.Y., Sundaramurthi, P., Kang, S.W., Gatlin, L.A. and Suryanarayanan, R., 2007. Glycine crystallization in frozen and freeze-dried systems: Effect of pH and buffer concentration. *Pharmaceutical Research*, **24**, 593-604.
- Vippagunta, S.R., Brittain, H.G. and Grant, D.J.W., 2001. Crystalline solids. *Advanced Drug Delivery Reviews*, **48**(1), 3-26.
- Wang, X.Z., De Anda, J.C. and Roberts, K.J., 2007. Real-time measurement of the growth rates of individual crystal facets using imaging and image analysis - A feasibility study on needle-shaped crystals of L-glutamic acid. *Chemical Engineering Research & Design*, **85**(A7), 921-927.
- Woo, X.Y., Nagy, Z.K., Tan, R.B.H. and Braatz, R.D., 2009. Adaptive concentration control of cooling and antisolvent crystallization with laser backscattering measurement. *Crystal Growth & Design*, **9**(1), 182-191.
- Wu, H.Q. and Khan, M.A., 2010. Quality-by-Design (QbD): An Integrated Process Analytical Technology (PAT) Approach for Real-Time Monitoring and Mapping the State of a Pharmaceutical Coprecipitation Process. *Journal of Pharmaceutical Sciences*, **99**(3), 1516-1534.
- Yang, X., Wang, X.J. and Ching, C.B., 2009. In situ monitoring of solid-state transition of p-aminobenzoic acid polymorphs using Raman spectroscopy. *Journal of Raman Spectroscopy*, **40**(8), 870-875.

- Yi, Y.J. and Myerson, A.S., 2006. Laboratory scale batch crystallization and the role of vessel size. *Chemical Engineering Research & Design*, **84**(A8), 721-728.
- Yu, L.X., 2008. Pharmaceutical quality by design: Product and process development, understanding, and control. *Pharmaceutical research*, **25**(10), 2463-2463.
- Yu, Z.Q., Chow, P.S. and Tan, R.B.H., 2008. Interpretation of focused beam reflectance measurement (FBRM) data via simulated crystallization. *Organic Process Research & Development*, **12**(4), 646-654.
- Yu, Z.Q., Chew, J.W., Chow, P.S. and Tan, R.B.H., 2007. Recent advances in crystallization control: an industrial perspective. *Chemical Engineering Research and Design*, **85**(A7), 893-905.
- Yu, L.X., Lionberger, R.A., Raw, A.S., D'Costa, R., Wu, H.Q. and Hussain, A.S., 2004. Applications of process analytical technology to crystallization processes. *Advanced Drug Delivery Reviews*, **56**(3), 349-369.
- Zencirci, N., Gelbrich, T., Kahlenberg, V. and Griesser, U.J., 2009. Crystallization of metastable polymorphs of phenobarbital by isomorphic seeding. *Crystal Growth & Design*, **9**(8), 3444-3456.
- Zhou, G.X., Fujiwara, M., Woo, X.Y., Rusli, E., Tung, H.H., Starbuck, C., Davidson, O., Ge, Z.H. and Braatz, R.D., 2006. Direct design of pharmaceutical antisolvent crystallization through concentration control. *Crystal Growth & Design*, **6**(4), 892-898.
- Zhu, H.J., Yuen, C.M. and Grant, D.J.W., 1996. Influence of water activity in organic solvent plus water mixtures on the nature of the crystallizing drug phase .1. Theophylline. *International Journal of Pharmaceutics*, **135**(1-2), 151-160.

Appendix A. Avantium Crystal 16 equipment



Figure (A1) Picture of the Avantium Crystal 16 equipment.

Appendix B. Pictures of salt crystals produced within Chapter 8 of thesis

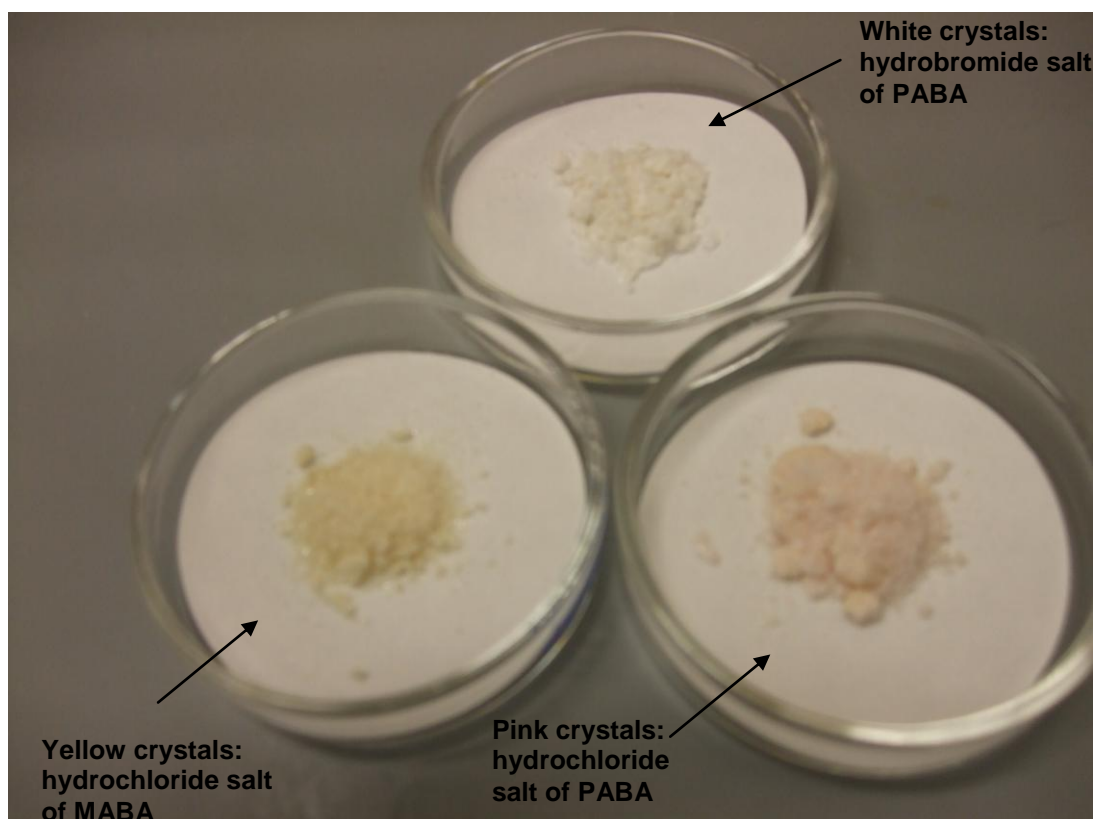


Figure B1 Picture of different colour salt crystals of PABA and MABA produced during cooling crystallization experiments.

Appendix C. Turbidity (solubility) results for sodium benzoate in organic solvents

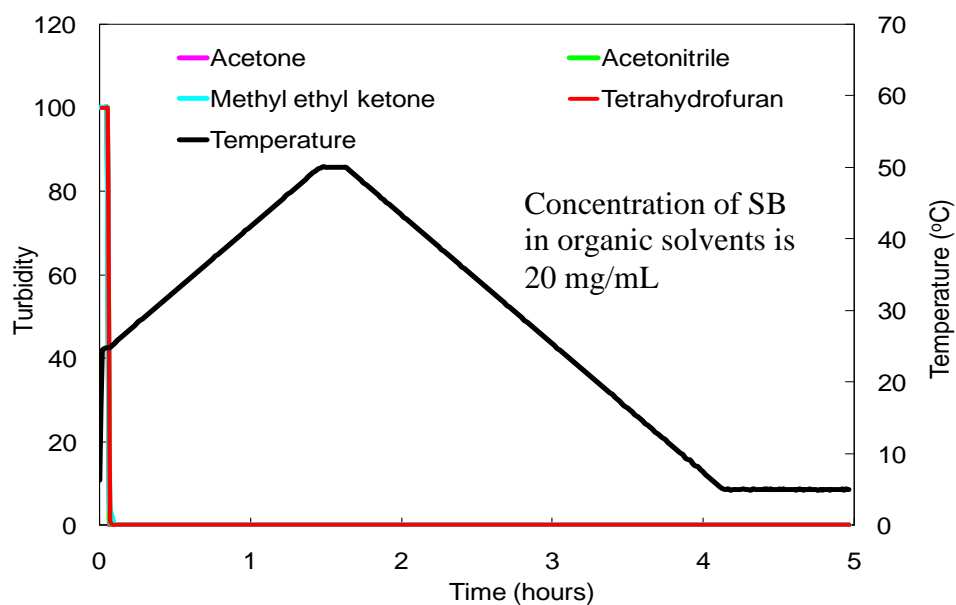


Figure (C1) Turbidity (solubility) results for sodium benzoate (SB) in acetone, acetonitrile, methyl ethyl ketone and tetrahydrofuran

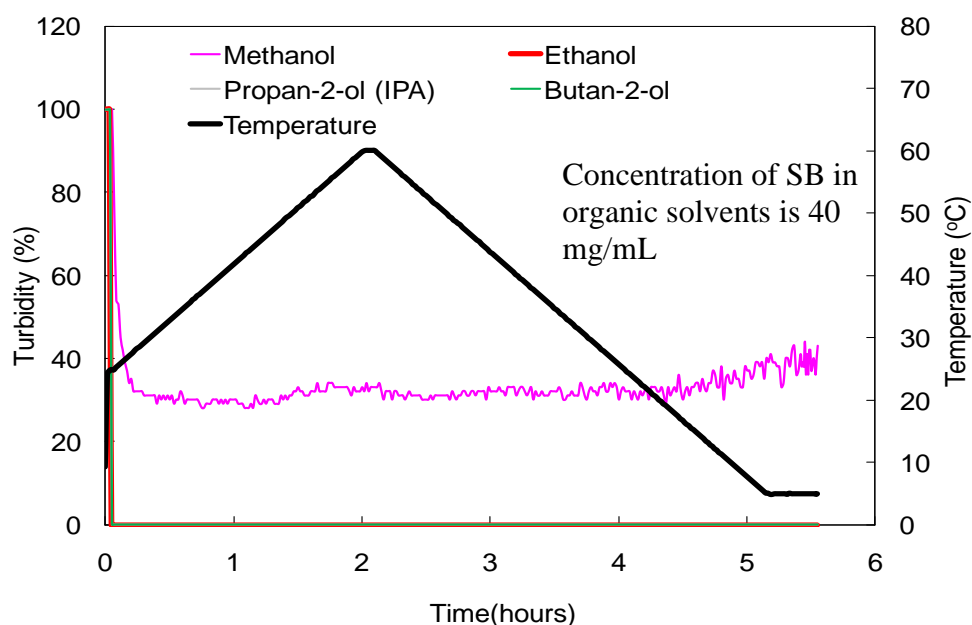


Figure (C2) Turbidity (solubility) results for sodium benzoate (SB) in methanol, ethanol, propan-2-ol (IPA) and butan-2-ol

Figures (C1 and C2) show the turbidity results for sodium benzoate in organic solvents including methanol, ethanol, propan-2-ol (IPA), butan-2-ol, acetone, acetonitrile, methyl ethyl ketone and tetrahydrofuran. A turbidity value of 100% represents a clear solution and a turbidity value of 0% represents a cloudy solution. For all organic solvents except methanol the turbidity value remains at zero % during both heating and cooling phases indicating that the solubility of sodium benzoate in organic solvents is very low.

Appendix D. Solubility graphs for *para*- and *meta*-amino benzoic acid in water obtained from the Literature

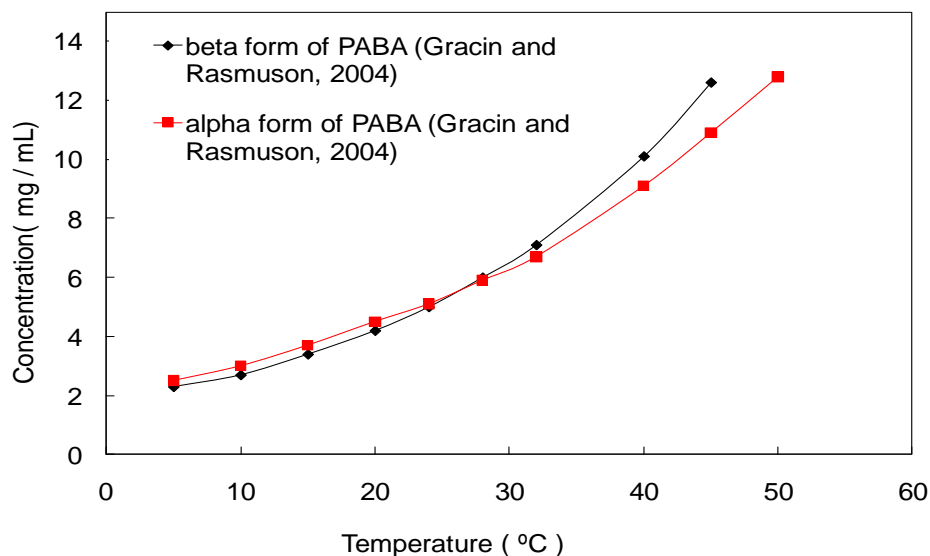


Figure (D1) Solubility data for the two forms (alpha and beta) of *para*-amino benzoic acid in water. Data obtained from the literature (Gracin and Rasmuson) using a gravimetric method.

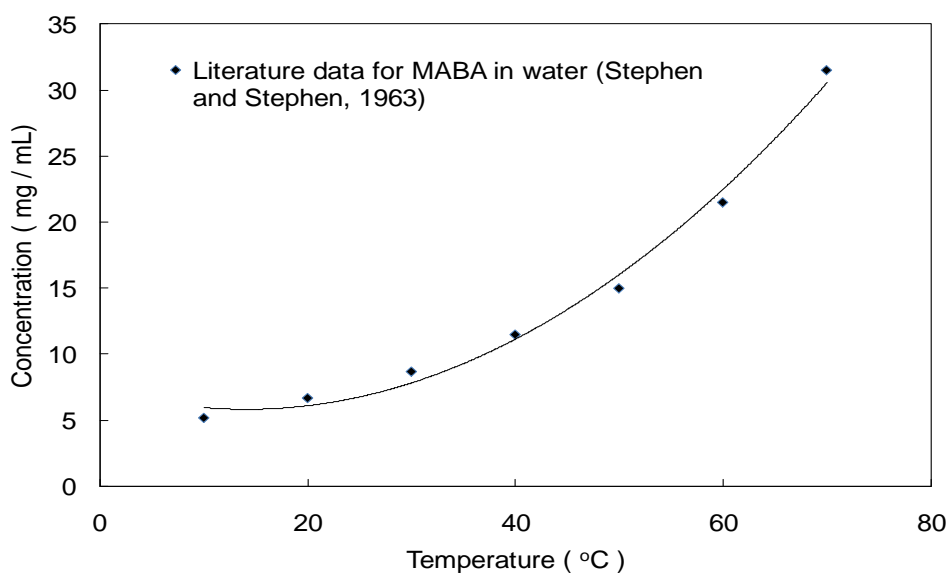


Figure (D2) Solubility data for *meta*-amino benzoic acid in water. Data obtained from the literature (Stephen and Stephen, 1963).

Appendix E. TGA and DVS calculations on the molecular ratio of sodium benzoate in water and the sodium and potassium salts of PABA (see chapters 4, 5 and 8)

A sample TGA calculation (based on results from Chapter 4) for the molecular ratio of sodium benzoate to water is shown below. For the TGA results based on the 1 mL scale for sodium benzoate that re-crystallized from water the initially sample weight was 26.497 mg (dry weight and solvent). During the heating phase from 25 to 250 °C there is a 3.166% weight decrease. This is assumed to be loss of water from the internal structure of the crystal. Therefore the amount of water lost from the sample is:

$$\left(\frac{3.166}{100}\right) \times 26.497 = 0.84 \text{mg} .$$

The amount of anhydrate form of sodium benzoate present is:

$$26.497 - 0.84 = 25.66 \text{mg} .$$

The molar ratio of sodium benzoate to water is calculated using the following formula:

$$\text{Moles} = \text{mass/molar mass.} \tag{E1}$$

The molar mass of sodium benzoate is 144.11 and for water is 18.01. From these values the molar ratio is calculated as shown below:

$$\text{Sodium benzoate (SB) to water: } \frac{25.66}{144.11} : \frac{0.8388}{18.01}$$

Molar ratio of SB: water: 0.178: 0.0465

Molar ratio of SB: water: 1: 0.26

The same method of calculation was applied for the DVS results except the initial weight of solid for TGA analysis is that of the hydrate or solvate (anhydrous (dry) weight and solvent) and the initial weight of solid for DVS analysis is that of the anhydrous (dry) form.

Appendix F. Calculation on the concentration of sodium chloride in water during a pH controlled cooling crystallization experiment of PABA in water (See Figure 9.17 within Chapter 9)

Key stages in these calculations are as follows:

- 1) Calculation on the amount of sodium chloride and water formed
- 2) Calculation on how much water is added from 5M hydrochloric acid (HCl) and 5M sodium hydroxide (NaOH) solution
- 3) Sum the total amount of water formed and added during crystallization process
- 4) Concentration calculation of NaCl is mass of NaCl / volume of water

Stage 1 Calculation on the amount of sodium chloride and water formed

Basic information:

- Total amount of HCl acid added = 21.27g
- Total amount of NaOH added= 26.4g
- Density of NaOH is 1.5g/mL
- Density of HCl is 1.18g/mL
- Density of water 1 g/mL
- Molarity of NaOH and NaCl is 5.
- Molar mass of NaCl is 58.44 g/mol
- Molar mass of water is 18 g/mol

The moles of NaOH formed is calculated using the following equations:

$$\text{Density } (D) = \frac{\text{mass } (m)}{\text{volume } (v)} \quad (\text{F1})$$

$$1.5 = \frac{26.4}{v} \quad v = 0.0176 \text{ L}$$

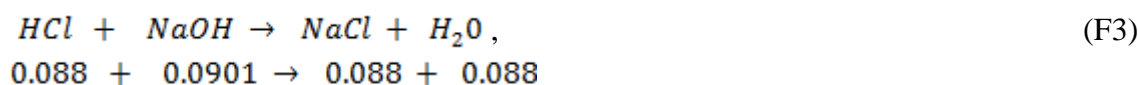
$$\text{Molarity} = \frac{\text{moles } (n)}{\text{volume } (v)} \quad (\text{F2})$$

$$5 = \frac{n}{0.0176} \quad n(\text{NaOH}) = 0.088 \text{ moles}$$

The same method is used for calculating the moles of HCl acid formed

Moles of HCl formed is 0.090

Reaction equation shows a 1 mole ratio:



Mass of sodium chloride (NaCl) formed is calculated using the following equation:

$$\text{Mass (m)} = \text{moles} \times \text{molar mass} \quad (\text{F4})$$

$$m \text{ of sodium chloride formed} = 0.088 \times 58.44 = 5.14\text{g}$$

$$\text{Mass of water formed} = 0.088 \times 18 = 1.584\text{g}$$

Volume of water formed is calculated using equation B1 = **0.001584 L**

Stage 2 Calculation on how much water is added from 5M hydrochloric acid (HCl) and 5M sodium hydroxide (NaOH) solution

Within a 1 L solution of 5M HCl there is 506g of HCl and 571g of water

Total mass of HCl and water in 1 L solution is 1077g

Percentage of HCl is $(506/1077) \times 100 = 47\%$

Percentage of water is $(571/1077) \times 100 = 53\%$

Amount of 5M HCl solution added to process is 21.27g. Therefore the **amount of water added** from the HCl solution is:

$$21.27 \times \frac{53}{100} = 11.27\text{g}$$

Within a 1 L solution of 5M NaOH there is 425.3g of NaOH and 716.5g of water

Total mass of NaOH and water in 1 L solution is 1141.8g

Percentage of NaOH is $(425.3/1141.8) \times 100 = 37.2\%$

Percentage of water is $(716.5/1141.8) \times 100 = 62.7\%$

Amount of 5M NaOH solution added to process is 26.4g. Therefore the **amount of water added** from the NaOH solution is:

$$26.4 \times \frac{62.7}{100} = 16.6 \text{ g}$$

Stage 3 Sum the total amount of water formed and added during crystallization process

Water formed = 0.001584 L

Water added = 11.27 + 16.6 = 27.9g = 0.0279 L

Total water (formed and added) = **0.02948 L**

Stage 4 Concentration calculation of NaCl is mass of NaCl / volume of water

mass of sodium chloride formed = 5.14g

Volume of water (formed and added) = 0.02948 L

$$\text{Concentration} = \frac{\text{mass}}{\text{volume}} \tag{F5}$$

Concentration of sodium chloride in water = $5.14/0.02948 = 174.4\text{g/L}$

Appendix G . Derivation of pH-solubility equations (This derivation can be obtained from Florence and Attwood, 1981) (see Chapter 8)

Basic information

- Total saturation solubility of the drug is S
- Solubility of the undissociated species is S_o
- $S = S_o +$ (concentration of ionised species)

First derivation based on acidic drugs.

Acidic drugs are less soluble in acidic solutions than alkaline solutions. The acidic drug is represented as HA.

The dissociation of the acid in water can be written as:



and the dissociation constant is given by

$$K_a = \frac{[H_3O^+][A^-]}{[HA]} \quad (G2)$$

Rearranging Equation (G2) and substituting S_o for $[HA]$

$$\frac{K_a}{[H_3O^+]} = \frac{[A^-]}{S_o} \quad (G3)$$

Concentration of ionised species is

$$[A^-] = S - S_o \quad (G4)$$

Substitution of Equation (G4) into (G3) gives the following:

$$\frac{K_a}{[H_3O^+]} = \frac{S - S_o}{S_o} \quad (G5)$$

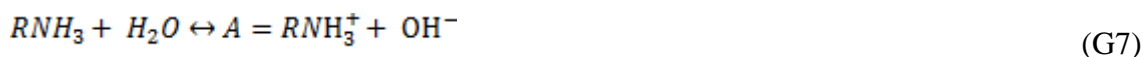
Taking logarithms of both sides of Equation (G5) gives the following:

$$pH - pK_a = \log \left\{ \frac{S - S_o}{S_o} \right\} \quad (G6)$$

Equation (G6) is used at pH values above the iso-electric point.

Second derivation based on basic drugs

Basic drugs are more soluble in acidic solution. The basic drug is represented as RNH₂. The dissociation of the base in water is shown in the following Equation (G7):



The dissociation constant is given by

$$K_b = \frac{[RNH_3^+][OH^-]}{[RNH_2]} \quad (G8)$$

Equilibrium constant (K_w) for water is given by the following Equation:

$$K_w = K_a K_b = [H^+][OH^-] \quad (G9)$$

Rearranging Equation (G9) gives the following:

$$K_b = \frac{[H^+][OH^-]}{[K_a]} \quad (G10)$$

Substituting Equation (G10) into (G8) and rearranging gives the following:

$$\frac{[H^+]}{K_a} = \frac{[RNH_3^+]}{[RNH_2]} \quad (G11)$$

Substituting $S_o = RNH_2$ and $S - S_o = RNH_3^+$ into Equation (G11) gives:

$$\frac{[H^+]}{K_a} = \frac{[S - S_o]}{[S_o]} \quad (G12)$$

Taking logarithms

$$pK_a - pH = \log\left\{\frac{S - S_o}{S_o}\right\} \quad (G13)$$

Equation (G13) is used at pH values below the iso-electric point.

List of Publications

Journal papers

K. S. Howard, Z. K. Nagy, B. Saha, A. L. Robertson and G. Steele. Combined PAT-solid state analytical approach for the detection and study of sodium benzoate hydrate. *Organic Process Research and Development*, 2009, 13 (3), 590-597.

K. S. Howard, Z. K. Nagy, B. Saha, A. L. Robertson, G. Steele and D. Martin. A process analytical technology based investigation of the polymorphic transformations during the anti-solvent crystallization of sodium benzoate from IPA/water mixture. *Crystal Growth and Design*, 2009, 9 (9), 3964-3975.

K. S. Howard, Z. K. Nagy, B. Saha, A. L. Robertson and G. Steele. Application of PAT tools for the identification of crusting problems within crystallization processes (in process)

K. S. Howard, Z. K. Nagy, B. Saha, A. L. Robertson and G. Steele. Crystallization and characterisation of salts o, m, p-amino benzoic acid isomers (in process)

K. S. Howard, Z. K. Nagy, B. Saha, A. L. Robertson and G. Steele. pH controlled polymorphic crystallization (in process)

Proceeding papers (Peer-reviewed)

K. S. Howard, Z. K. Nagy, B. Saha, A. L. Robertson and G. Steele, "Application of PAT tools for the monitoring of pH controlled crystallization of zwitterionic compounds", in Proc. of 16th International Workshop on Industrial Crystallization (BIWIC 2009), Lappeenranta, Finland, September 9-11, 2009.

K. S. Howard, Z. K. Nagy, B. Saha, A. L. Robertson and G. Steele, "A process analytical technology based investigation of the batch crystallization of sodium benzoate and *para*-amino benzoic acid", in Proc. of 15th International Workshop on Industrial Crystallization (BIWIC 2008), Magdeburg, Germany, September 10-12, 2008.

K. S. Howard, Z. K. Nagy, B. Saha, A. L. Robertson and G. Steele, "Combined PAT-solid state analytical approach for the detection and study of sodium benzoate hydrate", in Proc. of 17th International Symposium on Industrial Crystallization (ISIC17), Maastricht, The Netherlands, September 14-17, 2008.

Abstracts

K. S. Howard, Z. K. Nagy, B. Saha, A. L. Robertson and G. Steele, Combined process analytical technology and solid state analytical approach for the discovery of new forms of crystalline compounds, at the 40th British Association for Crystal Growth (BACG) Annual Conference 2009, Bristol, United Kingdom, September 7-8, 2009.

K. S. Howard, Z. K. Nagy, B. Saha, A. L. Robertson and G. Steele, New methodology using process analytical technology (PAT) for designing crystals of high quality and purity, at the British Association for Crystal Growth (BACG) Conference 2008, Loughborough, United Kingdom, September 8-9, 2008.

K. S. Howard, Z. K. Nagy, B. Saha, A. L. Robertson and G. Steele, Experimental investigation of the cooling and anti-solvent crystallization of sodium benzoate, at the British Association for Crystal Growth (BACG) and Irish Association for Crystal Growth (IACG) Conference 2007, Dublin, Ireland, September 3-4, 2007.

Presentations

Oral presentations

K. S. Howard, Z. K. Nagy, B. Saha, A. L. Robertson and G. Steele, Application of Process Analytical Technology for the design, separation and production of quality crystals, part of the IChemE Fluid Separation Subject Group (FSSG) event taken place at BP, Sunbury-on-Thames, 4th June, 2010. This presentation won first prize.

K. S. Howard, Z. K. Nagy, B. Saha, A. L. Robertson and G. Steele, PAT tools to monitor and control the crystallization of pharmaceuticals, part of the 2009-2010 Postgraduate Research (PGR) seminar competition taken place within the Chemical Engineering department at Loughborough University. This presentation won first prize.

K. S. Howard, Z. K. Nagy, B. Saha, A. L. Robertson and G. Steele, Application of Process Analytical Technology for the design, separation and production of quality crystals, part of the IChemE Fluid Separation Subject Group (FSSG) event taken place at GSK, Stevenage, 30th May, 2008.

K. S. Howard, Z. K. Nagy, B. Saha, A. L. Robertson and G. Steele, Experimental investigation of the cooling and anti-solvent crystallization of sodium benzoate, at the British Association for Crystal Growth (BACG) and Irish Association for Crystal Growth (IACG) Conference 2007, Dublin, Ireland, September 3-4, 2007.

Poster presentations

K. S. Howard, Z. K. Nagy, B. Saha, A. L. Robertson and G. Steele, Application of PAT tools for the monitoring of the pH crystallization of zwitterionic compounds, in Proc. of 16th International Workshop on Industrial Crystallization (BIWIC 2009), Lappeenranta, Finland, September 9-11, 2009.

K. S. Howard, Z. K. Nagy, B. Saha, A. L. Robertson and G. Steele, Application of PAT tools for the monitoring of the pH crystallization of zwitterionic compounds, at the 40th British Association for Crystal Growth (BACG) Annual Conference 2009, Bristol, United Kingdom, September 7-8, 2009.

K. S. Howard, Z. K. Nagy, B. Saha, A. L. Robertson and G. Steele, Process analytical technology (PAT) on the crystallization of the three isomers of amino benzoic acid, at the British Association for Crystal Growth (BACG) Conference 2008, Loughborough, United Kingdom, September 8-9, 2008.

K. S. Howard, Z. K. Nagy, B. Saha, A. L. Robertson and G. Steele, PAT for the detection of polymorphic transformations and the discovery of new forms of crystalline compound, in Proc. of 15th International Workshop on Industrial Crystallization (BIWIC 2008), Magdeburg, Germany, September 10-12, 2008.

K. S. Howard, Z. K. Nagy, B. Saha, A. L. Robertson and G. Steele, Combined PAT-solid state analytical approach for the detection and study of sodium benzoate hydrate, in Proc. of 17th International Symposium on Industrial Crystallization (ISIC17), Maastricht, The Netherlands, September 14-17, 2008.

K. S. Howard, Z. K. Nagy, B. Saha, A. L. Robertson and G. Steele, Delivery of safe pharmaceutical products with the use of process analytical technology, at the Institute of Chemical Engineers United Kingdom (IChemE) global forum, ChemEng08, Birmingham, United Kingdom, October 28-30, 2008.

K. S. Howard, Z. K. Nagy, B. Saha, A. L. Robertson and G. Steele, Effect of mixing in different vessel sizes on the crystallization of pharmaceutical products, part of the IChemE Mixing conference taken place at GSK, Stevenage, 3rd April, 2008.

Loughborough Graduate School Poster Competition 2008. Title of poster: "Crystallization of Pharmaceuticals". The poster won second prize.